

Sliding Mode Techniques for Automotive Vehicle Dynamics

Thesis submitted for the degree of

Doctor of Philosophy

at the University of Leicester

by

Roderick G. Hebden M.Phys./Eur., Sheffield
Control and Instrumentation Research Group
Engineering Department
University of Leicester
UK

UMI Number: U187209

All rights reserved

INFORMATION TO ALL USERS

The quality of this reproduction is dependent upon the quality of the copy submitted.

In the unlikely event that the author did not send a complete manuscript and there are missing pages, these will be noted. Also, if material had to be removed, a note will indicate the deletion.



UMI U187209

Published by ProQuest LLC 2013. Copyright in the Dissertation held by the Author.
Microform Edition © ProQuest LLC.

All rights reserved. This work is protected against
unauthorized copying under Title 17, United States Code.



ProQuest LLC
789 East Eisenhower Parkway
P.O. Box 1346
Ann Arbor, MI 48106-1346

Abstract

This thesis describes the use of sliding mode methods for automotive vehicle dynamics applications. Specifically, automotive stability during harsh split- μ braking and vehicle ‘mode’ detection are considered. Numerous control techniques, including full state-feedback sliding mode control, have addressed the split- μ braking manoeuvre. The controllers presented in this thesis extend previous work by using only certain measured outputs. These controllers work in conjunction with an anti-lock braking system (ABS) to provide safe, effective braking through steer-by-wire. Two strategies are presented, each using two measured outputs (yaw rate and lateral deviation) and front road wheel steering angle as the sole input. The first scheme estimates two further states by employing a sliding mode observer. It benefits from sliding mode robustness properties, and is demonstrated by simulation on a nonlinear model to be robust to large variations in tyre stiffness. The second scheme consists of a compensator-based, sliding mode controller. This controller, tested under the same conditions as the first, does not perform as well as the observer-based controller from a robustness perspective, but it produces a closed-loop system of lower order, which may be advantageous from an implementation perspective. Potentially dangerous vehicle scenarios, such as severe understeer, oversteer and split- μ braking, are currently detected using a large combination of measurements, seeking to estimate vehicle states robustly. In this thesis, a simpler approach is adopted, which, rather than estimating all the vehicle states, looks for ‘signature differences’ between the behaviour of an ideal linear vehicle model and the actual measured behaviour, in terms of vehicle yaw moments and lateral forces. A novel sliding mode estimation technique is used to predict potentially dangerous scenarios early. The scheme is flexible and could be used as part of a supervisory scheme, optimally engaging existing control systems. All of the schemes proposed have been tested using a detailed nonlinear vehicle model to demonstrate their effectiveness.

Acknowledgements

First, and foremost, I would like to thank my two supervisors, Dr Christopher Edwards and Prof. Sarah Spurgeon, for giving me the opportunity to carry out the research that has led to this thesis. Their help and guidance have been invaluable in accomplishing this work.

I am also deeply grateful to the Engineering and Physical Sciences Research Council (EPSRC) and TRW Conekt for their financial support. I would also like to thank those at TRW Conekt whose direction and expertise in the field of vehicle dynamics control has proven indispensable for this project, specific thanks go to Dr. Jim Farrelly and the Active Chassis Control group, Dr. Pete Scotson and Dr. Dong Sun.

I wish to express heartfelt thanks to all the staff and students at the University of Leicester Engineering Department, particularly the Control and Instrumentation Group, who made me welcome, and offered help and friendship during my time at the department. I would like to thank Prof. Ian Postlethwaite (Head of Department during my time at Leicester), Dr. Sarah Blaney (nee Gatley), Dr. Anita Boardman, Drs. Richard and Elisabeth Cooper, Dr. Fernando Schlindwein, Dr. Guido Hermann, Dr. Khalid Khan, Abhishek Kumar, Dr. Ridwan Kureeman, Nai-One Lai, Dr. Steve Lister, Dr. Edwin Tan, Dr. Richard Thomas, Ercument Turkoglu, Dr. Matt Turner, Paul Williams, and the staff of the departmental office.

I would also like to thank my whole family for their unending support and understanding throughout my various studies: my parents for attempting (though always in vain) to understand why on earth I would put myself through all this rather than just go and get a 'normal' job; my siblings and their respective spouses for their encouragement and bafflement by equal measure; my in-laws in the US for humouring me when I send them my technical papers to read; and my Gran for being proud of me whatever.

Warm thanks and appreciation go to Holy Trinity Church, for their love and prayers, and for making my wife, Anna, and I feel at home in Leicester over the duration of my research. In particular, I'd like to thank Dave and Jenny Ridge who have selflessly taken us under their wing, pastoring us, and bringing us so far along on our journey. I'd also like to thank Roger Morgan, and all the members of the cell groups we've been involved with.

*To Anna,
for standing by me with unwavering confidence and appreciation,
giving up so much of our time for my studies,
and giving me more love and support than I could ever ask for.*

Contents

1	Introduction	1
1.1	Introduction	1
1.1.1	Control and measured output signals	3
1.1.2	Vehicle scenario prediction measured signals	5
1.2	Thesis Structure	5
2	Overview of Vehicle Dynamics	8
2.1	Introduction	8
2.2	Vehicle Geometry	8
2.3	Tyre Properties/Forces	10
2.3.1	Lateral/Cornering Characteristics	12
2.3.2	Longitudinal Characteristics	15
2.3.3	Combined Braking and Cornering	17
2.4	Vehicle Steering & Handling	17
2.4.1	Neutral Steer Vehicle	18
2.4.2	Understeer	19
2.4.3	Oversteer and Dynamic Oversteer	19
2.4.4	Understeer versus Oversteer	20

<i>Contents</i>	vii
2.5 Split- μ Braking	21
2.5.1 Anti-lock Braking Systems (ABS)	21
2.5.2 Braking Manoeuvre	22
2.6 Conclusions	23
3 Mathematical Modelling of a Generic Automobile	24
3.1 Introduction	24
3.2 Vehicle Modelling Background	24
3.3 Four-Wheel Model with Nonlinear Tyres	25
3.4 Tyre Modelling	28
3.4.1 Dugoff Tyre Model	29
3.5 ABS Model	36
3.6 Bicycle Model	37
3.6.1 Theoretical Model	38
3.7 Conclusions	41
4 Introduction to Sliding Mode	42
4.1 Introduction	42
4.2 Controller Design	43
4.2.1 Example: The bicycle model	43
4.2.2 Ideal sliding motion	45
4.2.3 Enlarging sliding region	52
4.2.4 Robustness to matched uncertainty	52
4.2.5 Equivalent control	55
4.2.6 Increasing rate at which switching surface is attained	56

Contents	viii
4.2.7 Pseudo-sliding	58
4.3 MIMO Systems	61
4.3.1 Design Methods	65
4.3.2 Multivariable <i>unit vector</i> control law	67
4.4 Observers and Observer Design	68
4.4.1 State Estimation	68
4.4.2 Examples of Sliding Mode Observers	69
4.5 Conclusions	73
5 Split-μ Braking with Observer-Based Control	74
5.1 Introduction	74
5.1.1 Approach	74
5.2 Sliding Mode Control System	75
5.2.1 Obtaining a Linear Numerical Model	75
5.2.2 Controller Structure	81
5.2.3 Observer Structure	82
5.2.4 Controller Design	84
5.2.5 Observer Design	85
5.3 Simulation of Vehicle System in a Split- μ Braking Manoeuvre with Observer- Based Sliding Mode Control Scheme	85
5.3.1 Simulation Results	86
5.3.2 Further Robustness Testing	86
5.4 Conclusions	89
6 Split-μ Braking with Compensator-based Control	94
6.1 Introduction	94

6.2	Problem Formulation	95
6.3	Preliminaries	96
6.4	Hyperplane Design	98
6.5	Control Law Development	100
6.5.1	Control Structure	102
6.6	A compensator based existence problem	104
6.6.1	Compensator design	104
6.7	Simulation of Vehicle System in a Split- μ Braking Manoeuvre with Compensator-Based Sliding Mode Control Scheme	107
6.7.1	Simulation Results	107
6.7.2	Further Robustness Testing	109
6.7.3	Comparison of observer-based and compensator-based controllers	111
6.8	Conclusions	113
7	Vehicle Scenario Prediction Using Sliding Mode	115
7.1	Introduction	115
7.2	The Scenario Detection Problem	116
7.3	Model Co-ordinates Issues	117
7.4	Sliding Mode Unexpected Input Estimator	119
7.5	Scenario Detection	121
7.5.1	Understeer	123
7.5.2	Steady-State Oversteer	128
7.5.3	Further Oversteer Testing	133
7.5.4	Split- μ Braking	137
7.5.5	Summary of Detection Results	142

7.6	Vehicle Scenario Prediction	143
7.7	Output Measurement Noise	147
7.7.1	Vehicle Scenario Prediction Simulation Results	148
7.7.2	Discussion of Scenario Prediction Algorithm Results	149
7.8	Conclusions	156
8	Conclusions and Future Work	157
8.1	Summary	157
8.2	Contributions	158
8.2.1	Observer-based Control Scheme	158
8.2.2	Compensator-based Control Scheme	159
8.2.3	Vehicle Scenario Prediction Scheme	159
8.3	Further Work	160
8.3.1	Modelling Improvements	160
8.3.2	Controller Design Issues	161
8.3.3	Scenario Prediction Issues	162
A	Glossary	163
B	Notation	168
B.1	Table of Constants	168
B.2	Table of Coefficients	168

Chapter 1

Introduction

1.1 Introduction

One of the main areas of research being undertaken in the automotive industry is that of vehicle chassis control, seeking to improve handling performance, ride comfort and traction/braking performance [2]. The principle aims of this research include improvements in vehicle safety, steerability/manoeuvrability, increased passenger comfort and reduced driver workload. Over the years, improvements have come about through mechanical developments which act passively, such as suspension systems and passive rear-wheel steering [46]. More recently, active control systems have come into play, including anti-lock braking systems, which have quickly become an integral part of modern passenger vehicles, adding greatly to user safety. Electronic power-assisted steering has made a significant reduction to driver workload. These systems are all developed for use by the public and, as such, must provide increased safety as well as functionality, whilst remaining cheap to produce and implement on mass production vehicles. The level of research into vehicle systems shows no sign of slowing down in the long term, and automatic control systems are an increasingly important part of that research.

Automatic control systems are systems which work to perform a given function, usually the control of a physical variable, such as position, speed, temperature, pressure and so on. A subset of these control systems, termed closed-loop control systems, use information taken from the system being controlled in order to determine the control action. For example, a central heating thermostat measures the temperature inside a house, and fires up the boiler

only if the temperature is too low. Systems which do not have this information feedback are termed open-loop systems. An example of a simple open-loop control system is a kitchen stove, which takes no measurement of the temperature of the food being cooked, and requires human interference to watch the process and increase or reduce the heat, as necessary, closing the loop manually. Automotive vehicles, too, have been engineered to include control systems. Traditionally, vehicle braking systems were open-loop - when the brake pedal was depressed, the brake pressure would simply increase until the wheel eventually stopped rotating or the driver released the brake. In practice, this resulted in either the vehicle coming to rest, or, if the driver applied the brakes incorrectly, the wheels locking whilst the vehicle continued to move, resulting in the vehicle skidding along the surface of the road. ABS allowed engineers to prevent the wheels from locking by measuring wheel speeds and increasing, maintaining, or decreasing brake pressure automatically [14].

In fact, control systems have been applied to a wide variety of automotive vehicle dynamics applications, including braking [45, 118], traction [11], suspension systems [81, 117], longitudinal control for *platooning*, stability control [25], steering [2, 67, 91, 103, 122, 125], and work has been carried out into integrating some of these systems [9, 94, 101]. The past two decades have seen large advances in the electronic control of various vehicle chassis components, so that, now, most of the major vehicle chassis components have some type of controller available to them [9]. Anti-lock braking systems and Traction Control Systems (TCS) are now standard in the industry. Furthermore, as control systems become more integrated, making use of shared sensor and actuator hardware, as well as a single control processor module for the control of several subsystems, manufacturing costs can be further reduced [94].

Like control systems in many other applications, those used for vehicle dynamics control are often safety critical, and must undergo rigorous testing and evaluation before they can be put onto passenger vehicles. Also, these control systems must be designed using mathematical vehicle models which only approximate true vehicle behaviour, and, inevitably, exclude some plant nonlinearities, and the variation of system parameters which may occur through use and misuse of vehicles. For these two reasons, it is advantageous to consider advanced robust control systems, which are able to maintain good performance even in the presence of such modelling uncertainties and parameter variations. As automotive manufacturers design production

vehicles to be driven for many years, covering distances of 100 000 miles or more, robustness to plant model mismatches and parameter variation is essential to the design of a vehicle system. Consequently, a great deal of research is detailed in the literature which aims to apply various so-called robust control techniques to these applications [5, 7, 8, 62, 72, 77, 104, 121]. Unlike these techniques, the sliding mode control methodology has the unique property of the total invariance to a certain type of plant-model discrepancy, known as *matched uncertainty*. Also, sliding mode ideas have recently been explored for signal reconstruction and parameter estimation [35, 49] - advances which will be applied to automotive problems in Chapter 7.

Sliding mode techniques - a special case of Variable Structure Control Systems (VSCS) - have been successfully applied to numerous and varied applications due to their inherent performance robustness in the presence of modelling uncertainties and disturbances [31, 114]. Variable Structure Controllers are composed of feedback control laws, along with a decision rule. This decision rule is known as the switching function, as it is used to switch between control laws, depending upon where the system is to be found in the state space. Sliding mode techniques have been applied to many of the automotive vehicle dynamics systems mentioned earlier, such as braking [23], platooning [44, 89], vehicle stability [69], steering [51, 78, 93, 123, 124], and wheel-slip control [21]. It is amongst this body of research, applying sliding mode methods to automotive vehicle dynamics problems, that the work contained in this thesis is set. Specifically, using sliding mode methods for vehicle steering and stability augmentation applications, as well as for vehicle dynamics estimation and supervision.

1.1.1 Control and measured output signals

One possible approach to the control problems addressed in this thesis is to utilize 4-wheel steering (4WS) to improve directional control by accelerating the build-up of lateral tyre forces at the rear axle [25], either by full steer-by-wire [4, 67, 78, 88, 93, 103], rear wheel steer-by-wire with driver controlled front wheels [72], or by the use of additional steering angle inputs to the front and/or rear road wheels [3, 91]. However, 4WS vehicles have not made a great impact on the marketplace. The benefits have so far failed to conclusively outweigh the added complexity and cost of their introduction to production cars. For this reason, active rear wheel

steering has been deliberately avoided in this work. In the vehicle lateral plane, there are essentially four possible control signals to choose from - these are front wheel steering angle, rear wheel steering angle, front wheel differential brake pressure and rear wheel differential brake pressure [110]. In the above discussion, the use of rear wheel steering has already been ruled out. Furthermore, in order to make this study of practical use to the automotive industry, the choice has been made to include a simple ABS in the vehicle model, which will be responsible for the distribution of brake pressure, thus ruling out two more control signal possibilities. The front road-wheel steering angle now remains the sole control signal. The control may be implemented as steer-by-wire.

The control schemes presented will use just two measured outputs. Firstly, vehicle yaw rate, which may be obtained from an appropriately mounted gyro. The second measured signal is the vehicle lateral deviation, which is the variable that the controllers will seek to regulate. The yaw rate The lateral deviation signal may be obtained by calculating the vehicle position relative to road lane markings. The sensing may be robustly performed, as in many other studies, using a forward-looking mono or stereo real-time vision system. One such system, presented by researchers at the University of Michigan [68] detects lane markings using images from a single vehicle mounted camera. The authors claim to detect lane markings remarkably well from a variety of road images, and experimental results are presented which demonstrate the algorithm's performance using images with solid and dashed lines, along with varying light, shadowing and occlusion. A stereo vision system produced at the University of Parma, Italy [17], detects firstly the lane markings with one camera, and then free-space ahead of the vehicle using the stereo images. Its robustness is demonstrated in a variety of conditions on both extra-urban roads and freeways. More recently, researchers working with DaimlerChrysler [86] presented a lane recognition system which attempts to recognize lanes in an environment where lane boundaries are not necessarily present. Such a system takes the vehicle vision field toward capabilities beyond what is required for the application presented in this paper, by seeking to detect road lanes and driving corridors in difficult environments, such as alongside rows of parked cars, at intersections, and in heavy traffic, where road markings are only temporarily visible. Other vision system literature includes [10, 50, 61, 90, 92].

1.1.2 Vehicle scenario prediction measured signals

In Chapter 7 the emphasis of the work changes such that the vehicle lateral deviation signal is no longer of key significance and is no longer measured. Instead, the system seeks to estimate signals associated with vehicle yaw moment, lateral force and the derivative of the lateral force. Therefore, the measured signals in this section are the yaw rate, as in the control work, and vehicle lateral acceleration, which is a conventionally measured signal.

1.2 Thesis Structure

This thesis is arranged into eight chapters and starts by discussing the vehicle dynamics and sliding mode theory background necessary to understand the work in its context. Next, a vehicle model is developed, which will be used for testing, by simulation, the various schemes presented in later chapters. The automotive problems being addressed by the work are introduced chapter by chapter, with novel sliding mode schemes proposed to address them. Finally, the work presented in this thesis is summarized in the concluding chapter, recapping the contributions of the thesis, and possible future work is discussed.

The remainder of this chapter will outline the structure of the thesis in more detail, explaining more fully the progression of the work presented.

Chapter 2 This chapter explores, in overview, various areas of vehicle dynamics which are of particular significance to the applications which this study will attempt to address. In particular, it sets out the co-ordinate systems which will be used throughout, and discusses vehicle and tyre behaviour, introducing key vehicle manoeuvres which will be important later in the thesis.

Chapter 3 This chapter draws from Chapter 2, and, considering the various mathematical vehicle models and model types existing in the literature, brings together those elements which are most suited to the specific vehicle dynamics issues which will be encountered in the thesis. Appropriate vehicle models are then developed for use in the later chapters of the thesis, for both design and testing, in simulation, of the sliding mode methods which will be exploited.

Chapter 4 This chapter then introduces and describes, by example, some concepts of Slid-

ing Mode methods, which will be combined with the theory of the preceding chapters in the applications which follow. The chapter will primarily deal with sliding mode control, before expanding to include observer design.

Chapter 5 This, the first of the results chapters, addresses a harsh, split- μ braking manoeuvre - one of the severe, and potentially dangerous, vehicle manoeuvres described in Chapter 2. The chapter employs techniques detailed in Chapter 4 to develop an observer-based sliding mode controller which seeks to maintain safety and steerability during that manoeuvre. The control scheme presented is also tested for robustness in the presence of parameter variations. The results of this Chapter have been presented at an international conference [55] and published in a peer-reviewed journal [56].

Chapter 6 This chapter addresses the same application as Chapter 5, but uses a novel compensator-based sliding mode controller, which has no observer interpretation. This control scheme benefits from lower order closed-loop dynamics which may be advantageous from a practical, implementation perspective. Preliminary results have been published in a peer-reviewed journal [34]. This control scheme is tested for robustness under the same conditions as the scheme presented in the previous chapter.

Chapter 7 In this chapter, the scope and ambition of the study is broadened by examining, not only the split- μ braking manoeuvre tackled in Chapters 5 & 6, but also further vehicle scenarios which arise in potentially dangerous vehicle manoeuvres, described in Chapter 2. Chapter 7 does not attempt to produce a controller (or controllers) to deal with these scenarios, but uses sliding mode observer techniques from Chapter 4 to develop a scheme which sets out to predict these severe vehicle scenarios before they have time to build up, so that appropriate controllers, like those presented in Chapters 5 & 6, amongst others, may be optimally engaged as required. The results of this chapter have been submitted for publication in a peer-reviewed journal, and have been presented, in part, at an international conference [57].

Appendix A In this appendix, a glossary of vocabulary peculiar to vehicle dynamics and control theory are explained.

Appendix B Here, the mathematical notation used in this thesis is described, for clarity. Every attempt has been made by the author to stay within the bounds of well used conventions.

However, conventions are not universal, particularly in the vehicle dynamics notation, where a choice must be made. This appendix should clarify any possible confusion between systems, and reinforce notions of control theory.

Chapter 2

Overview of Vehicle Dynamics

2.1 Introduction

The purpose of this chapter is to provide the reader with a brief introduction to some vehicle dynamics concepts necessary for a full understanding of the main body of the thesis. The chapter begins by setting out the geometry and co-ordinate systems to be used when discussing vehicle motion, and introduces some key vehicle dynamics concepts such as yaw and sideslip angles. A discussion of tyre behaviour follows, with an emphasis on the longitudinal and lateral properties of the tyre. Finally, there is a discussion of vehicle handling theory which introduces the concepts of oversteer and understeer, and the split- μ braking manoeuvre, including a brief discussion on anti-lock braking systems.

2.2 Vehicle Geometry

This study uses the ISO vehicle dynamics system, as shown in Figure 2.1. In order to fully describe the vehicle motion, it is necessary to define two axis systems, which will be referred to as the vehicle-fixed axes and the earth-fixed axes. The equations of motion are derived using the vehicle-fixed axes, whose three principal directions are denoted by xyz , the origin of which is located at the vehicle centre of gravity (see Figure 2.1). The vehicle is considered a rigid body, whose velocity is described in terms of the longitudinal, u , lateral, v , and vertical, w , velocities. Components of the acceleration vector of the vehicle, relative to the vehicle-fixed

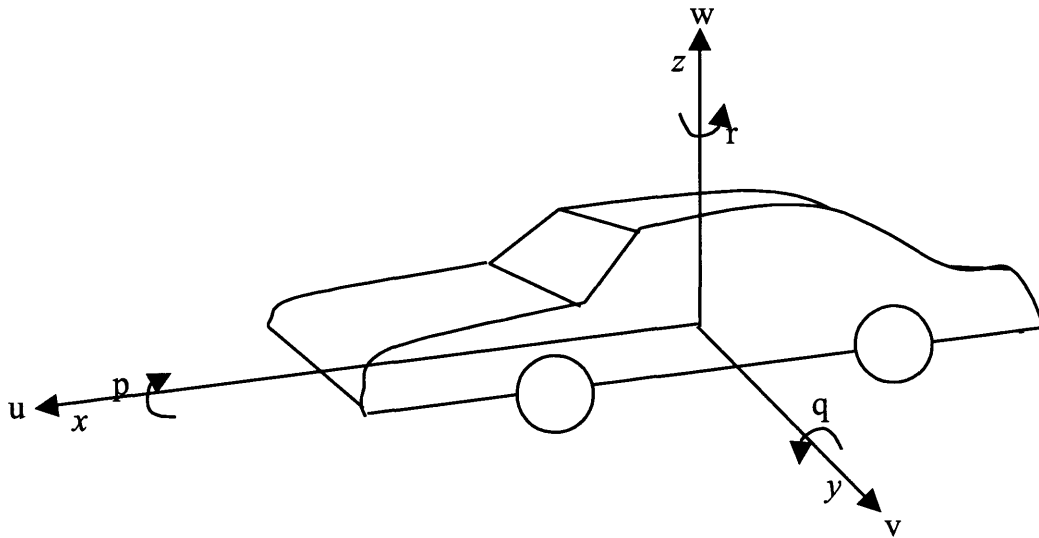


Figure 2.1: The ISO vehicle dynamics axis system

axes, which will also be discussed, are the longitudinal acceleration/deceleration, a_x , and the lateral acceleration, a_y . The axis system is right-handed, and the positive sense of rotation is clockwise when viewed, from the origin, along the positive direction of the axis with the three resolved rotation velocities given as roll rate, p , pitch rate, q , and yaw rate, r . Vehicle longitudinal and lateral forces, denoted F_x and F_y respectively, act along the vehicle x and y axes, and vehicle yaw moment, M_z , is defined as the moment tending to rotate the vehicle about the z -axis, positive clockwise when looking in the positive direction of the z -axis. The position of the vehicle is defined as the position of the origin of the vehicle-fixed axes (i.e. the vehicle centre of gravity) in an earth-fixed axis system, with principal directions denoted by XYZ , which is considered to be stationary (see Figure 2.2). The origin of the earth-fixed axes are entirely independent of the vehicle, free to be chosen at the convenience of the user at all times. The use of lower-case xyz for the vehicle-fixed system and upper-case XYZ for the earth-fixed system is a widely followed convention [1, 24, 40, 79]. In the case where vehicle pitch and roll are neglected, the vehicle body is stationary in the Z -axis, and the xy -plane lies parallel with the road at all times. In this study, the position and orientation of the earth-fixed axis system is consistently located at the starting position and orientation of the vehicle-fixed system at the beginning of each simulation, i.e. the earth-fixed axes are taken as the initial conditions of the vehicle-fixed axes.

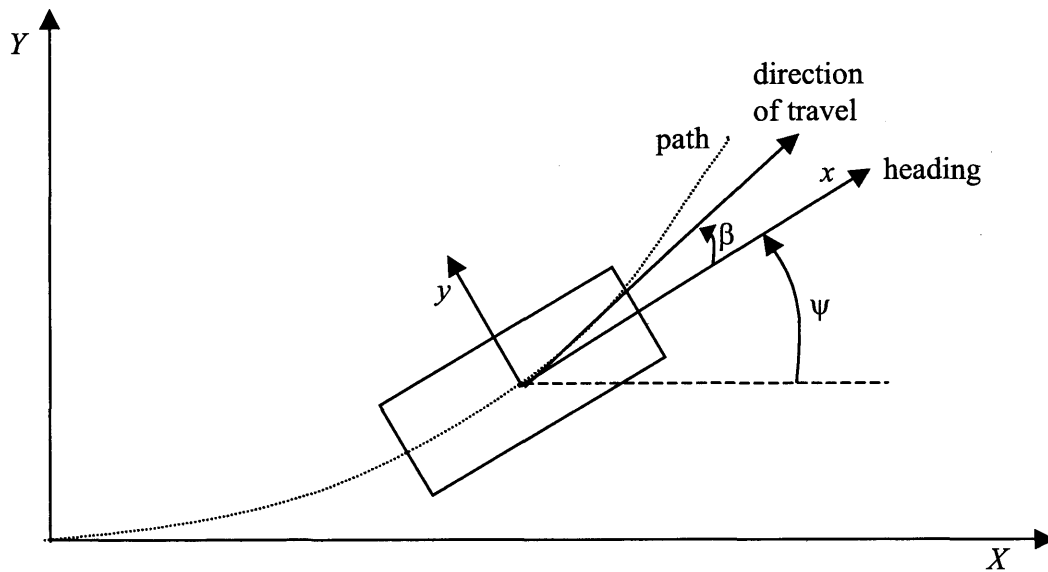


Figure 2.2: Vehicle body orientation

Figure 2.2 shows angles relating the vehicle position to the earth-fixed axes, i.e. movement over the ground. The heading angle, or yaw angle, ψ , is the integral of the yaw rate, r , and is the angle between the x -axis of the vehicle-fixed system and the X -axis of the earth-fixed system, the initial vehicle heading. Like the yaw rate, the yaw angle is positive clockwise when looking in the positive direction along the z -axis, positive anti-clockwise when viewed from above. The sideslip angle, β , is defined as the angle between the vehicle resultant velocity vector and the projected x -axis, and is also positive in the anti-clockwise direction when viewed from above¹.

2.3 Tyre Properties/Forces

It is fair to state that, with the exception of wind resistance, all of the external forces acting upon the vehicle in normal driving do so through the four tyres at the tyre/road interface. Unfortunately, the tyres are one of the least understood areas of the vehicle and the least con-

¹The sum of these two angles is known as the course angle and is usually denoted ν [46]. This angle corresponds to the angle between the velocity vector and the X -axis, and is tangential to the vehicle path. In this study, the course angle will not be discussed further, and the Greek letter, ν , will be allocated to another, unrelated, quantity.

venient for the application of sensors, although large amounts of theoretical and experimental work has been done in this area by Sakai [96, 97, 98, 99] and others [19, 26, 83]. Furthermore, vehicle tyres vary greatly in design and construction [60]. In this section, some current tyre theories will be introduced, together with the relevant terminology and conventions. Although vehicles exist with active or passive rear-wheel steering, for the discussion which follows, only the front wheels will be steerable. It is useful to consider first the Ackermann steering geometry, which sets out the proper geometry of the front road-wheel steering angles - the angles which the front wheels make with the x -axis. In order to do this, consider a vehicle travelling very slowly around a constant radius turn (see Figure 2.3). There is negligible lateral acceleration, and, so, negligible lateral forces are developed in the tyres which are assumed to roll freely. In this scenario, it can be seen that the perpendicular from each wheel must pass through a single point, otherwise the tyres will have to “fight” each other. This means that the inner and outer front road-wheel steering angles must be slightly different from each other. Taking small angles approximations:

$$\delta_{outer} \cong \frac{a + b}{R + \frac{L_t}{2}} \quad (2.1)$$

$$\delta_{inner} \cong \frac{a + b}{R - \frac{L_t}{2}} \quad (2.2)$$

In mathematical vehicle modelling, these two angles are usually approximated as the Ackermann steering angle [1]

$$\delta_A = \frac{a + b}{R} \quad (2.3)$$

which is defined as the geometric steering angle required for a car of wheelbase, $a + b$, to track a turn of radius, R , at low speeds where the external forces due to accelerations are negligible [79].

In high-speed cornering manoeuvres, when a tyre rolls quickly over a road, greater longitudinal and lateral forces are generated by a shear mechanism, due to the visco-elastic properties of the tyre rubber, and a significant amount of deformation occurs [46]. This friction coupling between the tyre and the road is brought about by surface adhesion and hysteresis, which in turn, are dependent upon the tyre ‘slipping’ to a small degree at the rear of the tyre/road interface (known as the contact patch [46]). The degree to which the tyre is deformed around the

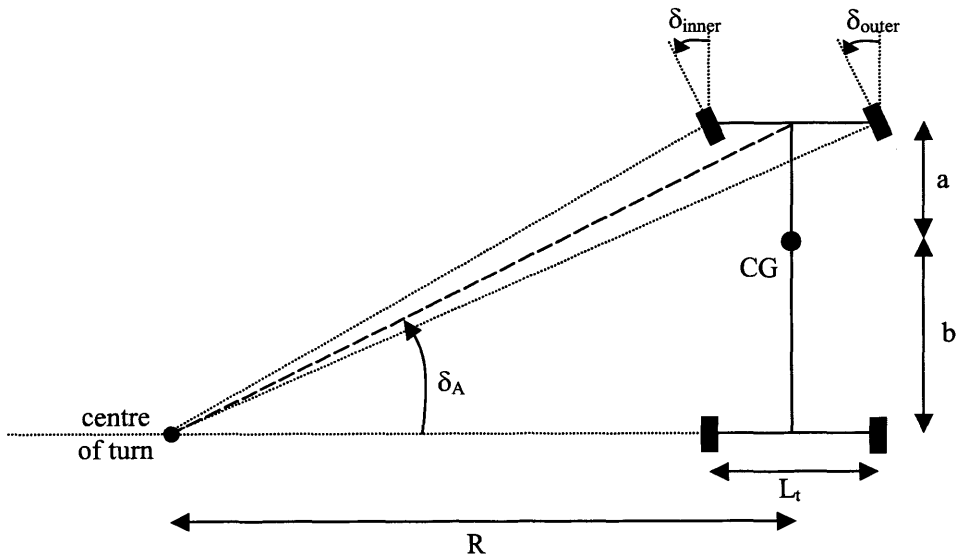


Figure 2.3: Ackermann Geometry

contact patch is characterized by two quantities: firstly, the longitudinal wheel-slip, σ , defined in Section 2.3.2; and secondly the wheel slip-angle, α , defined in Section 2.3.1. Initially, it is convenient to consider the longitudinal and lateral tyre characteristics independently.

2.3.1 Lateral/Cornering Characteristics

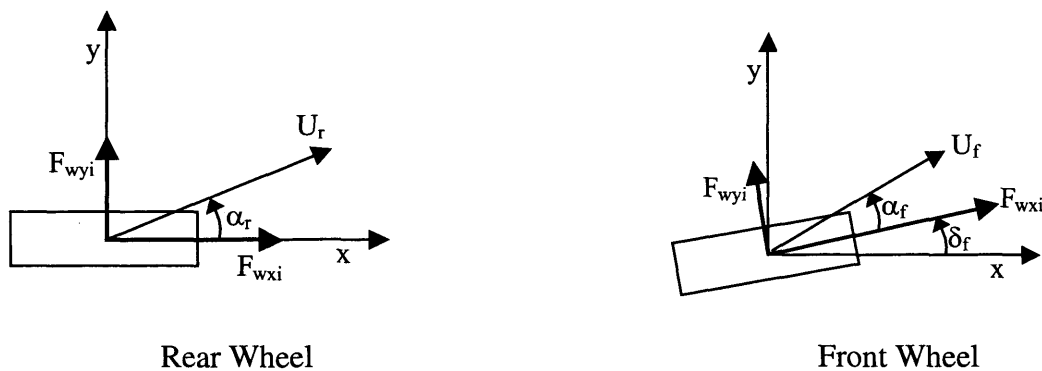


Figure 2.4: Tyre forces, velocities and slip-angles at front and rear wheels

The tyres must develop lateral forces to produce lateral acceleration, and these forces are generated by the adoption of slip-angles at the tyres. A wheel slip-angle is the angle between the wheel heading (the direction in which the wheel is pointing) and the wheel direction of travel. Individual tyre forces are shown, for a front and rear wheel, in Figure 2.4. The front

wheel is subject to the road-wheel steering angle, δ_f . The angle, δ_f , is usually modelled to be a linear scaling of the steering wheel angle (or hand-wheel steering angle), and the simplification of having δ_f equal on both front wheels is usually made. Whilst δ_f is shown relative to the vehicle axis system, the tyre forces and velocities are shown resolved parallel and perpendicular to the individual wheel heading. In each case, the wheel slip-angle is shown, which is defined for a rear wheel, α_r , and a front wheel, α_f , by:

$$\tan \alpha_r = \frac{v_r}{u_r} \quad \tan \alpha_f = \frac{v_f}{u_f} - \delta_f \quad (2.4)$$

where u_r, v_r and u_f, v_f are the longitudinal and lateral velocities of a rear and a front wheel, respectively, resolved parallel and perpendicular to the individual wheel heading (Figure 2.4).

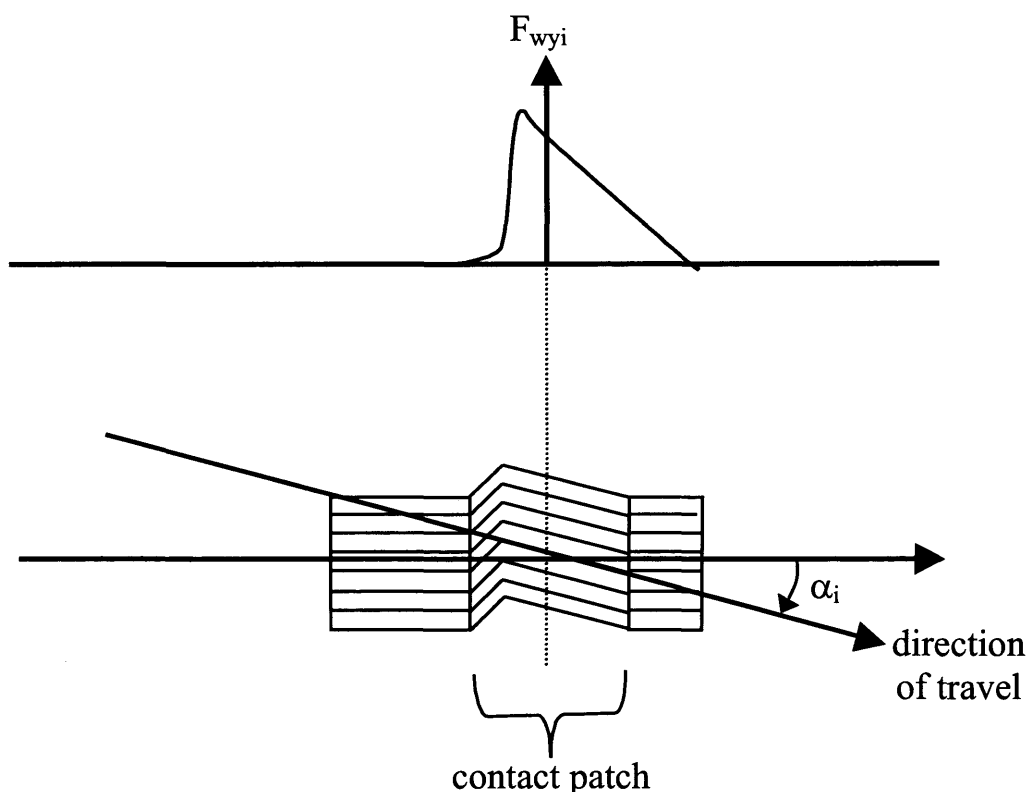


Figure 2.5: Rolling tyre deformation under a lateral force

In vehicle cornering manoeuvres, it is necessary for the tyre to generate a lateral force. Tyre lateral forces depend primarily upon the lateral slip, or slip-angle α , defined in Equation (2.4). This is illustrated simply in Figure 2.5. It can be seen from this figure how the slip-angle

develops in the tyre. As an element of the tyre enters the contact patch, it is initially undeflected from the tyre's centreline and does not exert a lateral force on the tyre. However, as the tyre rolls along the surface, this element remains stationary while the wheel is displaced laterally. Thus the tyre element builds up a sideways deflection relative to the wheel, so generating a lateral force on the tyre. This deflection increases up to the point where the lateral force exceeds the tyre/road friction force holding the tyre element stationary. At this point, lateral slip occurs as the element slides over the road surface to return to the wheel centreline [46].

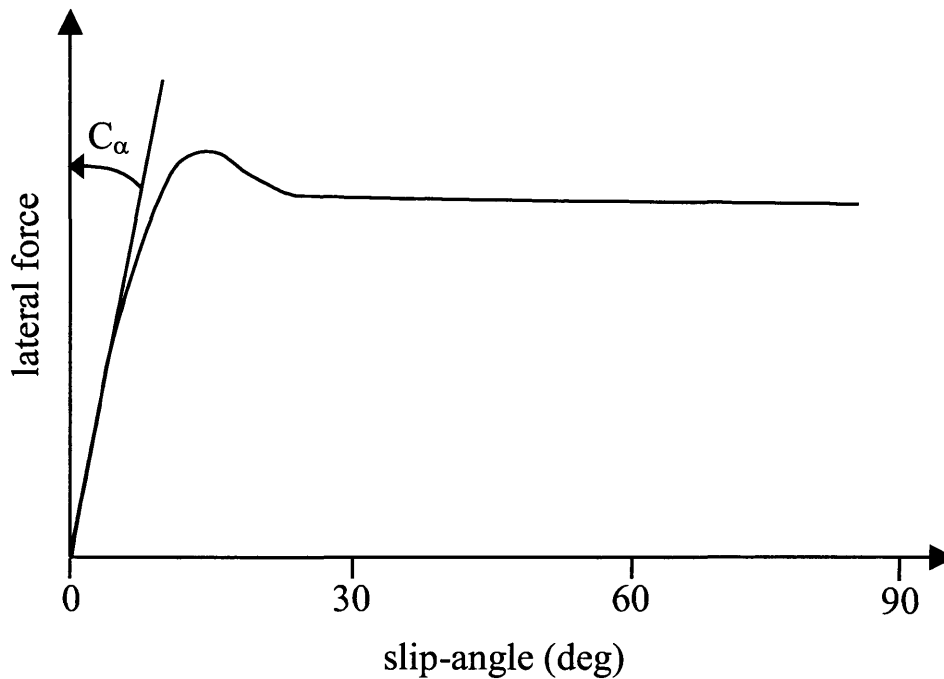


Figure 2.6: Lateral force versus slip-angle

The resistance of the contact patch of the tyre to deformation is known as the cornering stiffness, C_α , which may be defined as the cornering force, F_{wy} , developed per degree of slip-angle, α , generated, so that:

$$F_{wy} = C_\alpha \alpha \quad (2.5)$$

which means that the cornering stiffness of a tyre is given by the gradient of the cornering force to slip-angle curve normally, along its linear region [60]. A typical plot of tyre lateral force behaviour, with zero longitudinal wheel-slip, is shown in Figure 2.6, which is characterized in the steady-state (constant load and slip-angle) [46]. As the slip-angle increases, the

lateral force initially increases rapidly, before levelling out, and often (as in this plot) tends to diminish. The initial slope defines the characteristic tyre cornering stiffness coefficient, C_α at the particular vertical load.

2.3.2 Longitudinal Characteristics

Upon application of a tractive or braking torque, an amount of longitudinal wheel-slip is generated. This longitudinal slip is also sometimes known as deformation slip, and, under steady-state conditions, slip can be said to be a function of tractive or braking effort [60]. In this initial discussion the slip angle will be assumed to be zero. When a forward (or tractive) torque is applied to a wheel, as in acceleration, the tyre contact patch is shifted slightly forward of the axle, so compressing the elements of the tyre entering the contact patch. These compressed elements then provide adhesion to the road surface and are bent forward relative to the tyre generating a shear stress in the forward direction which builds up as more elements enter the contact patch. As the elements approach the rear of the contact patch their load decreases, causing the shear stress to diminish and the elements to slide over the road surface and straighten out. The sliding in the contact patch causes the angular velocity of a tyre under a driving torque to be greater than that of an equivalent free-rolling tyre. Conversely, when a braking torque is applied to a wheel, the tyre contact patch is shifted toward the rear of the tyre, compressing the tyre elements behind the contact patch, and stretching those in front. The tyre elements entering the contact patch will be bent backwards, and a longitudinal shear force will build up as more of these elements enter, in this case a rearward force is felt by the tyre. At the rear of the contact patch, as the tyre becomes unloaded, the elements slip over the road surface, straightening up. The difference between the angular velocity of the driven (or braked) wheel, ω , and the the angular velocity of the free-rolling wheel, ω_0 , is used to define the longitudinal wheel-slip, which the Society of Automotive Engineers [1] define as:

$$\sigma_{SAE} = \frac{\omega - \omega_0}{\omega_0} = \frac{\omega}{\omega_0} - 1, \quad \alpha = 0 \quad (2.6)$$

which can be expressed as a fraction or a percentage. In the discussion in this section, it is easier to refer to wheel-slip in terms of a percentage. However, in the remainder of this thesis, the value will be expressed using the decimal fraction convention. In fact, a number

of variations of wheel-slip definitions are used worldwide [79], in the case of zero slip-angle, Dugoff, Fancher and Segel [26] define wheel-slip as:

$$\sigma_{DFS} = 1 - \frac{\omega}{\omega_0}, \quad \alpha = 0 \quad (2.7)$$

Typically, the longitudinal force generated by a tyre, during braking, will vary with wheel-slip as in Figure 2.7 [46]. It can be seen that following an initial positive gradient, the force peaks (usually between 25 – 50% slip), and then gradually decreases until, at 100% slip, the wheel locks. The initial slope of the graph is largely dependent upon the longitudinal stiffness of the particular tyre. In the context of modelling, this is a matter of tuning. The peak force available, however, depends upon the road/tyre friction coefficient, as can be seen by the reduced peaks of the wet and icy road plots. The vertical load can also have an impact upon the peak force available, and as the load of a vehicle is distributed asymmetrically across the front and rear wheels, this should be taken into consideration. Indeed, the concept of friction coefficient is defined physically as the ratio of the frictional force between two bodies and the normal force.

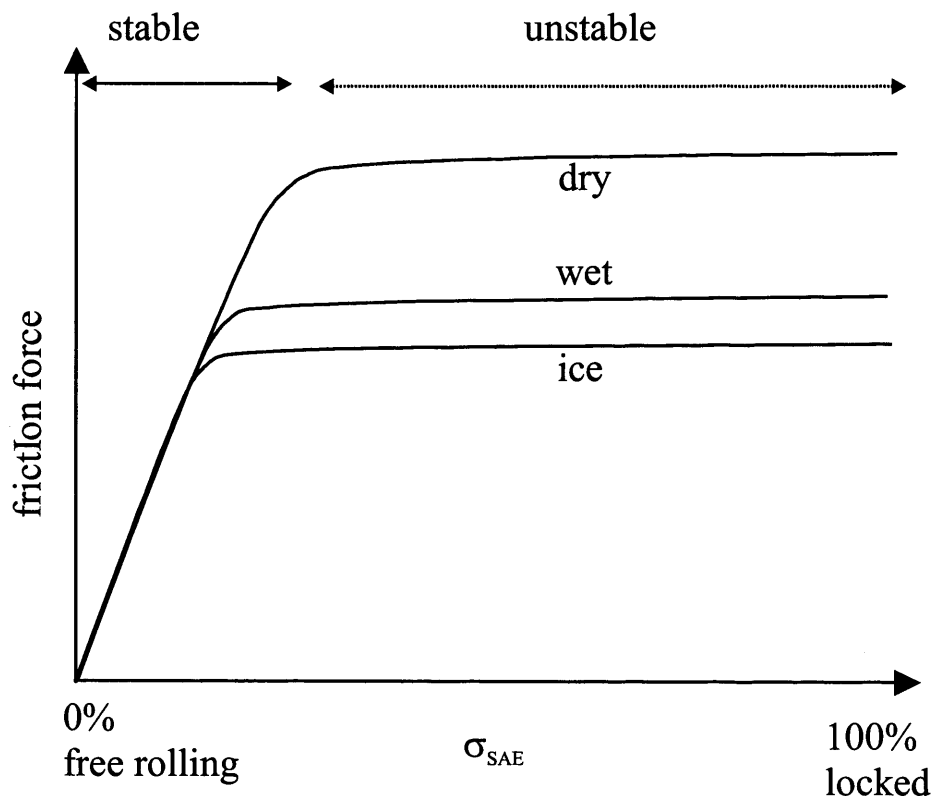


Figure 2.7: Longitudinal force versus wheel-slip

The longitudinal traction properties are of great importance in this study, as these are the properties which determine braking performance and stopping distance.

2.3.3 Combined Braking and Cornering

In many real scenarios, the tyres of a vehicle may experience both longitudinal and lateral forces simultaneously. As these forces are dependent upon the deformation of the tyre, they are not independent of each other. As the slip-angle is increased, the ability of the tyre to deform longitudinally is hindered, lowering the longitudinal wheel-slip and, so, the available longitudinal force. Conversely, an increase in wheel-slip diminishes the lateral force availability [79]. Therefore, new definitions of wheel-slip and slip-angle exist which take into account the existence of non-zero values of each other. The definitions which shall be used in this study are based upon a tyre model developed by Dugoff [26].

It is important to note that a number of factors may affect the tyre stiffness coefficients of a vehicle. These include vertical load, inflation pressure, size and width, an increase in any of which will generally result in increased cornering stiffness [46]. Tread design is also an area of great research which has a considerable affect on a tyre's behaviour at the contact patch [60].

2.4 Vehicle Steering & Handling

Later in this thesis, a system will be described which aims to detect and predict various vehicle scenarios - severe understeer, oversteer and split- μ braking. This section introduces the concepts of understeering and oversteering vehicles in steady-state and transient handling conditions. The vehicle road-wheel steering angle can be defined as:

$$\delta_f = \delta_A + K\bar{a}_y \quad (2.8)$$

where

$$\bar{a}_y = \frac{u^2}{Rg}$$

R is the radius of the turn, and δ_A is the Ackermann angle given in Equation 2.3. At low accelerations, the vehicle understeer gradient, K , is a constant and reflects the vehicle's tendency to

under or oversteer in linear or near-linear operation. For a vehicle which is neutral steer at low accelerations $K = 0$, giving $\delta_f = \delta_A$. The property of a vehicle to be nominally neutral steering, understeering or oversteering is present whether the vehicle is modelled linearly or with nonlinearities. In practice, most vehicles are designed to have a slight understeer at low lateral accelerations. However, where the vehicle lateral acceleration increases, nonlinearities in the tyres may cause the vehicle understeer gradient, K , to increase - causing terminal understeer - or become negative - causing terminal oversteer, at speeds above the critical speed.

2.4.1 Neutral Steer Vehicle

A neutral steering vehicle will, on a constant radius turn, require a constant hand- or road-wheel steering angle, equivalent to the Ackermann Angle, regardless of any increase in speed [46]. The road-wheel steering angle necessary, then, will always be prescribed by the ratio $\frac{a+b}{R}$, given in Equation (2.3). This is because, in the neutral steer vehicle, the slip-angles at the front, α_f , and rear, α_r , axles are equal, ie. $\alpha_f = \alpha_r$ and the turning moment due to the front wheels is balanced with that due to the rear wheels. Another way to understand a neutral steering car is in terms of the neutral steer point and static margin [46]. The neutral steer point is the point on the vehicle x -axis at which a pure lateral force would produce no yaw moment. In a regular rigid body, not subject to any other external forces, this point would be at the centre of gravity. However, in a car, any applied force would need to overcome the frictional forces at the front and rear tyres. By tuning the respective tyre stiffnesses at the front and rear, the neutral steer point may be shifted along the longitudinal x -axis of the vehicle. The static margin is defined as the distance at which the neutral steer point lies behind the vehicle centre of gravity. When the static margin is zero, the centre of gravity and the neutral steer point coincide, and the vehicle is said to be neutral steering. In under- and oversteering vehicles (defined formally in Sections 2.4.2-2.4.3) this is not the case, as an understeering vehicle has a positive static margin, as its neutral steer point lies behind the vehicle centre of gravity, whilst an oversteering vehicle has a negative static margin, as its neutral steer point falls ahead of the vehicle centre of gravity.

2.4.2 Understeer

An understeering vehicle turns less than the driver would expect for the given steering input [14]. That is, an understeering vehicle will, whilst performing a constant radius turn, require the steering angle to be increased with increasing speed. For an understeering vehicle, the front tyres tend to saturate before the rear, so that they require a larger increase in slip-angle to produce the same increase in lateral force [14]. The front tyres, then, have less traction, and struggle to generate sufficient lateral force, resulting in the vehicle experiencing a lower than expected yaw moment. Although understeering will not have the effect of making the vehicle become impossible for the driver to control, it does reduce the driver's ability to control the direction of travel. An understeering vehicle may seem to want to 'run wide' in a bend, with lower than expected yaw rate, and the driver may feel the need to apply a greater steer angle. In a terminal understeer manoeuvre the vehicle may carry straight on regardless of any steering efforts.

A severe understeer may be brought about by a number of factors, such as worn or incorrect front tyres, or excessive rear loading. Understeer may also be brought about by a driver attempting to turn the steering wheel too quickly approaching a bend, or commonly, a roundabout, in which case the vehicle will tend to slide to the outside of the bend or into the roundabout.

2.4.3 Oversteer and Dynamic Oversteer

Steady-State Oversteer

A vehicle is said to oversteer when it experiences a greater yaw rate than would normally be expected for a given steer angle [14]. Another definition of an oversteering vehicle is one which will, in a constant radius turn, require the steering angle to be reduced as speed is increased. Oversteer occurs when the rear tyres saturate faster than the front, so that the rear slip-angle must exceed the front slip-angle in an attempt to produce sufficient lateral force, causing the rear of the vehicle to 'slide out' [14]. As the vehicle begins to oversteer, the driver must decrease the steering angle to regain the correct yaw rate and cornering radius. In

terminal oversteer, this may result in spinning.

Modern cars are built with a slight understeer bias [14]. However, vehicles may still oversteer in a variety of circumstances. The first set of circumstances are brought about by lowered rear tyre stiffnesses - possibly due to low tyre pressures, worn tyres or reduced vertical load. The second set of circumstances, which are less well understood, are created by difficult, shifting surfaces, such as gravel, snow or sand. On such a medium, the movement of the tyre over the surface layer, is complicated by the movement of the surface itself over lower layers.

Dynamic Oversteer

In a severe oversteer manoeuvre, there is the danger that a driver may over-correct, turning the wheel too harshly in the opposite direction. This can quickly lead to a 'fish-tail' manoeuvre whereby the rear of the vehicle swings from side to side as the driver turns the steering wheel rapidly from side to side in repeated unsuccessful attempts to regain control.

2.4.4 Understeer versus Oversteer

The key issue in determining whether a vehicle will under- or oversteer is the relative lateral forces generated at the front and rear axles, and this force balance dictates the understeer/oversteer balance of the vehicle. This balance is a design consideration, and modern passenger car manufacturers choose to produce vehicles which lightly understeer, as generally, understeer is accepted as being preferable to oversteer [14]. This is based on a number of factors. Firstly, it is thought that the behaviour of an understeering vehicle tends to feel natural in its handling as its limit is approached. Also, in a difficult manoeuvre, it is natural for the driver to instinctively apply the brakes. In an understeer situation this would lessen the severity of the the understeer by transferring more of the vehicle load to the front axle, thereby increasing the traction available at the front tyres. In an oversteer situation, sudden braking may amplify the problem by reducing the traction at the rear of the vehicle. Finally, due to the possibility of losing vehicle stability in an oversteer manoeuvre, and the general belief that it is safer to collide with another object whilst travelling forwards (i.e. in line with the greater protection from crumple zones etc.), understeer is considered the safer option.

Nominally, the tendency of a vehicle to under- or oversteer is prescribed by its stability margin,

which is defined as $bC_{\alpha r} - aC_{\alpha f}$ [22], where $C_{\alpha f}$ and $C_{\alpha r}$ are the total tyre stiffnesses at the front and rear axles respectively. In the case where $|aC_{\alpha f}| = |bC_{\alpha r}|$, the vehicle is said to be neutral steering. Whereas, if $|aC_{\alpha f}| < |bC_{\alpha r}|$, then the vehicle is understeering, and for an oversteering vehicle, $|aC_{\alpha f}| > |bC_{\alpha r}|$.

2.5 Split- μ Braking

The split- μ surface is commonly used for testing vehicle braking and steering [5, 7, 78, 91, 122]. This is a surface where there is a difference in road/tyre friction coefficient (μ) between the right and the left sides of the vehicle. This can occur when driving over a patch of water, snow or ice. It is necessary, in order to discuss the behaviour of a vehicle in a split- μ manoeuvre, to first briefly introduce the action of anti-lock braking systems, which are now included in the majority of modern passenger vehicles.

2.5.1 Anti-lock Braking Systems (ABS)

Anti-lock braking systems (ABS) are closed-loop control devices designed to prevent wheel-lock during braking, thus retaining greater stability and steerability. Physically, an ABS comprises a hydraulic modulator, a wheel speed sensor and an electronic control unit (ECU), acting as a closed-loop control device, integrated within the braking system [14]. In a severe braking manoeuvre, the brake pressure increases rapidly, leading to an increase in longitudinal slip. As wheel-slip increases it reaches a limit between stable and unstable regions [14] (see Figure 2.7). In the stable region, the longitudinal slip is mostly due to deformation, whereas in the unstable region, the wheel tends towards skidding. Upon entering the unstable region, it is not possible for the wheel to generate any more braking force on the road, despite further increases in brake pressure (see Figure 2.7). Excess braking torque causes a rapid wheel deceleration, locking the wheel. ABS systems are designed to act so as to take into account disturbances, such as variations in tyre-road adhesion, due to changes in the road surface; wheel and axle vibration caused by road surface irregularities; and inconsistent wheel sizes (e.g. when a spare tyre is fitted).

The ABS associated with a wheel measures the wheel angular velocity and compares it with an estimate of the vehicle body velocity, which is taken using the average angular velocity of the three fastest-spinning wheels. From this, the wheel-slip is estimated. If the wheel starts to lock, the sudden increase in wheel deceleration and wheel-slip are detected. The desired wheel-slip for any tyre varies with the road/tyre coefficient of friction, μ_i , and this must be estimated by the ABS. When the wheel-slip reaches an excessive value, the ABS controller will stop, or reverse the brake pressure build-up until the danger of wheel-lock has passed. As the wheel-slip decreases, the ABS allows the brake pressure build-up to resume. Hence, to maintain maximum braking force, the wheel is kept in the required slip range by a combination of brake pressure build-up, reduction and holding phases.

ABS system variations exist which have various merits based on vehicle type, functionality and cost [14]. The variants may be separated into systems with two, three or four control channels. The fewer the channels, the fewer the sensors, and the lower the cost of manufacture. However, the 2-channel systems, particularly, have functional limitations, and often experience individual wheel-locking, and lower deceleration rates. The 4-channel systems have the advantage of being able to control the rear wheels using a principle known as select-low. This strategy improves stability at the rear of the vehicle as both wheels are subjected to the same brake pressure, corresponding to the wheel experiencing the lowest coefficient of friction. Advances in ABS systems continue to be made [11, 87], and research into new methods of tyre parameter estimation [53, 63] and ABS control is great [21, 23, 118, 121].

2.5.2 Braking Manoeuvre

In split- μ braking, when a vehicle brakes hard on such a surface, there is less traction available on the low friction (or low- μ) side of the vehicle. If a driver attempts to brake hard on such a surface, the wheels on the low- μ side of the vehicle will start to lock. The ABS will, therefore, reduce the braking torque on these wheels in order to prevent skidding. Consequently, a lower braking torque will build up on the low- μ side of the vehicle compared with the high- μ side. The asymmetric braking so produced, has the potential to generate a yawing motion together with a significant lateral deviation. Consequently, depending on the yaw rate generated, either

both the rear wheels may end up on the low- μ surface - if the yaw rate is high - and the car will spin, or the vehicle may veer - if the yaw rate is lower.

2.6 Conclusions

This chapter has described the co-ordinate systems which will be used throughout the thesis. Some vehicle dynamics ideas have been covered, with particular emphasis upon tyre properties. The driving scenarios described in this chapter will be used later for studies associated with the sliding mode controllers and estimators proposed later in the thesis. The next chapter uses the ideas discussed here in order to develop a suitable mathematical model of a generic passenger car, which will be used to test the efficacy of the schemes developed in the later chapters of this thesis.

Chapter 3

Mathematical Modelling of a Generic Automobile

3.1 Introduction

In order to test the ideas for novel control schemes and scenario detection systems that are the main contributions of this thesis, a suitable vehicle model must be developed which reproduces vehicle behaviour in the various scenarios in a sufficiently realistic way. In Section 3.2, some background to vehicle modelling is discussed, and in Section 3.3 a suitable model is described. The development of a vehicle model necessitates a discussion of tyre modelling. A detailed description of the one used in the vehicle simulation is given in Section 3.4. Finally, the split- μ braking scenario encountered later in this thesis requires the inclusion of a simple anti-lock braking system (ABS) model within the simulation. A description of this is found in Section 3.5. Finally, in Section 3.6, a lower order vehicle model, known as the bicycle model, is described in some detail, as this model will also be a useful tool in later chapters of the thesis.

3.2 Vehicle Modelling Background

There are many models, of varying complexity and focus, in use relating to automotive systems. Of these, a significant proportion are designed with an application to lateral control in mind. As early as 1956, a 3 degree-of-freedom model was developed by Segel [102], which described vehicle yaw, lateral and roll motion. Work has subsequently been carried out by a number of researchers who succeeded, by neglecting roll, to produce a simplified vehicle

model, known as the bicycle model. The name for this model comes about because the two front wheels are considered together as a single entity, and likewise, the two rear wheels. The states of this system are usually defined as sideslip angle, β , and yaw rate, r , with either just the front road-wheel steering angle, δ_f , or front and rear road-wheel steering angles used as system inputs. The bicycle model has become a popular choice for lateral control applications, especially for lane-changing manoeuvres, where, typically, a vehicle maintains its longitudinal velocity but follows a lateral trajectory, and platooning [48, 62, 89], whereby the car attempts to follow a preceding vehicle.

More complicated vehicle models have been developed [74] involving additional degrees-of-freedom, in terms of pitch [9] and roll [93] motion, and these have been used particularly where suspension modelling has been required. Quarter-car models are also used [81, 117] when the effects of suspension on tyre forces have been of primary interest. Work has also been carried out to model driver behaviour [75]. When dealing with lateral control in the presence of disturbances such as split- μ surfaces in a braking manoeuvre, it is essential to employ a four wheel model, as it allows each of the four wheels to act according to the friction coefficient it experiences. The effects of suspension in four-wheel models are variously included (eg. [91]), or avoided (eg. [122]). In this thesis, the model which has been developed neglects pitch and roll, as these factors are of only secondary importance in the manoeuvres to be studied, are not necessary to explain vehicle performance [40], and do not justify the added complexity of the modelling and analysis associated with their inclusion. The vehicle is therefore considered a rigid body, without suspension effects.

The model presented in the following section is realized using Matlab (v.5.3, R11.1), with Simulink (v.3), software. Matlab has been used for the design of the control and estimation schemes described later in this thesis. All simulations have been run in this environment using a variable step, Dormand-Prince solver routine.

3.3 Four-Wheel Model with Nonlinear Tyres

A model is presented here, based, in part, on previous work [78, 122]. Unlike the simple bicycle model, the forces which act on the vehicle are generated by four individual tyres, which

must be modelled to include nonlinear effects. This is necessary for simulations involving split- μ surfaces, as described in Section 2.5, as it allows both the inclusion of ABS units on each wheel, and manipulation of the tyre-road coefficient of friction on either side of the vehicle. The parameters for the vehicle are based on those for a generic passenger saloon. The geometry of the vehicle is given in Figure 3.1.

The lateral geometry differs slightly from that shown in Figure 2.3 in that the track-width (ie. the distance between the left and right wheels) is different at the front and rear for the vehicle. The dynamic equations governing the motion may be developed by considering the vehicle as a rigid body moving on a plane surface. Placing the origin of the vehicle-fixed axes at the centre of gravity produces three simple, classical equations of motion [40]:

$$\dot{u} = \frac{F_x}{m_v} + rv \quad (3.1)$$

$$\dot{v} = \frac{F_y}{m_v} - ru \quad (3.2)$$

$$\dot{r} = \frac{M_z}{I_z} \quad (3.3)$$

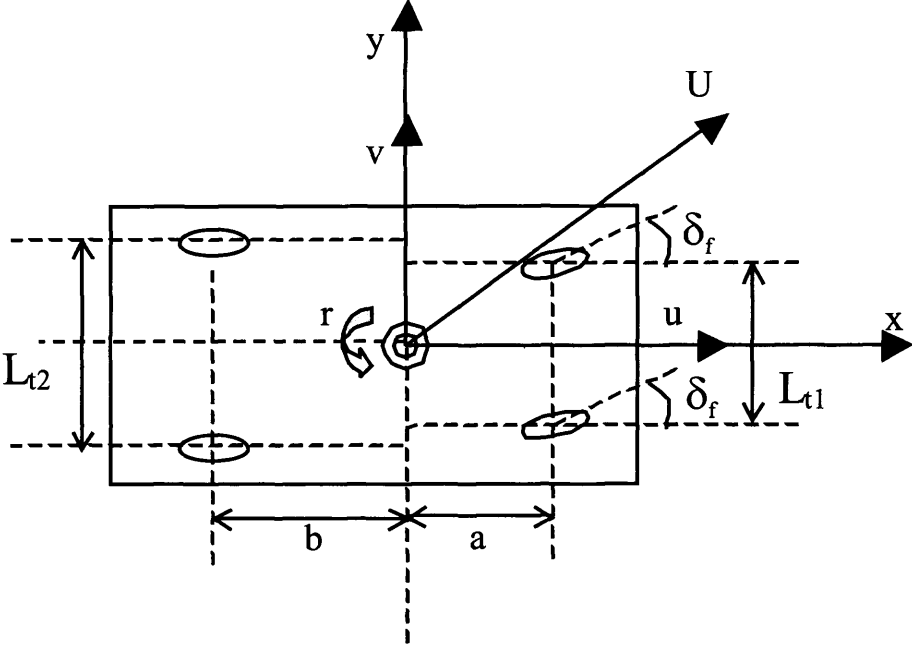
where u, v are the longitudinal and lateral velocities, in the vehicle-fixed axis system, respectively and r represents the yaw rate about the centre of gravity. These three states are given in terms of the lateral and longitudinal vehicle forces, F_x and F_y , the vehicle yaw moment, M_z , and also the total vehicle mass, m_v , and yaw moment of inertia, I_z . As each individual wheel must be modelled, it is sensible to define four further states to represent the four wheel angular velocities. These are given by:

$$\dot{\omega}_i = \frac{F_{wxi}R_t}{I_w} + \frac{T_{bi}}{I_w} \quad (3.4)$$

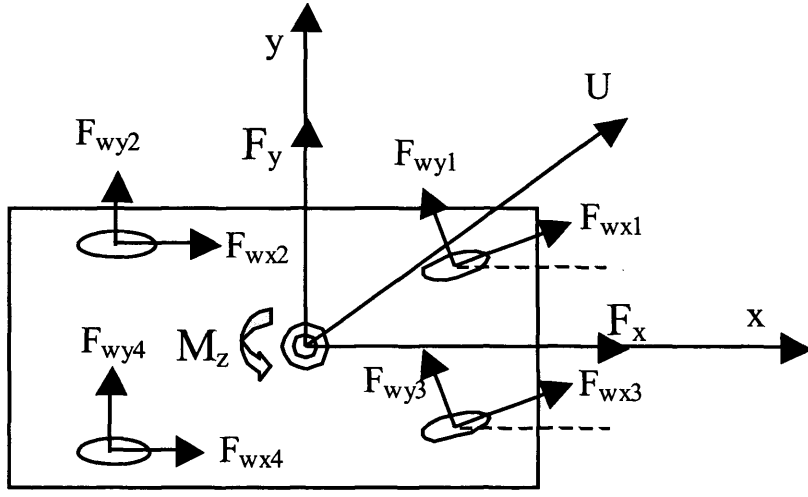
where ω_i represents the angular velocity of the i^{th} wheel, and $i = 1, 2, 3, 4$. As shown in Figure 3.1, F_{wxi} gives the tyre longitudinal force on the i^{th} wheel, and T_{bi} represents the braking torque applied at the i^{th} wheel by the associated ABS block. R_t is the wheel radius and I_w is the wheel-spin moment of inertia. For the particular problems considered in this thesis, it is also useful to add one more state: the yaw angle, ψ , which is defined simply in terms of the yaw rate:

$$\dot{\psi} = r \quad (3.5)$$

The vehicle body forces present in the first three states, from Equations (3.1)-(3.3) can be



a) Vehicle Body Kinematics



b) Vehicle Body Dynamics

Figure 3.1: Vehicle model

obtained by force balancing:

$$F_x = \frac{F_x}{F_{wx1}} = \frac{F_{wx1} \cos \delta_f - F_{wy1} \sin \delta_f + F_{wx2} + F_{wx3} \cos \delta_f - F_{wy3} \sin \delta_f + F_{wx4}}{F_{wx1} \cos \delta_f - F_{wy1} \sin \delta_f + F_{wx2} + F_{wx3} \cos \delta_f - F_{wy3} \sin \delta_f + F_{wx4}} \quad (3.6)$$

$$F_y = \frac{F_y}{F_{wy1}} = \frac{F_{wy1} \cos \delta_f + F_{wy2} + F_{wy3} \cos \delta_f + F_{wy4}}{F_{wy1} \cos \delta_f + F_{wy2} + F_{wy3} \cos \delta_f + F_{wy4}} \quad (3.7)$$

$$M_z = (a \sin \delta_f - \frac{L_{t1}}{2} \cos \delta_f) F_{wx1} - \frac{L_{t2}}{2} F_{wx2} + (a \cos \delta_f + \frac{L_{t1}}{2} \sin \delta_f) F_{wy1} - b F_{wy2} + (a \sin \delta_f + \frac{L_{t1}}{2} \cos \delta_f) F_{wx3} + \frac{L_{t2}}{2} F_{wx4} + (a \cos \delta_f - \frac{L_{t1}}{2} \sin \delta_f) F_{wy3} - b F_{wy4} \quad (3.8)$$

where δ_f represents the road-wheel steer angle (the angle of the front wheels relative to the chassis of the vehicle) and F_{wyi} gives the lateral tyre force on the i^{th} wheel. For the purposes of analysing the vehicle behaviour, it is helpful to calculate values for the vehicle trajectory in earth-fixed co-ordinate system. The origin of the earth-fixed axes - longitudinal displacement, X , and lateral deviation, Y - is placed at the initial position and orientation of the vehicle at the start of a manoeuvre. By projecting the vehicle velocities, with respect to the body fixed axes, into the earth co-ordinates:

$$\dot{X} = u \cos \psi - v \sin \psi \quad (3.9)$$

$$\dot{Y} = v \cos \psi + u \sin \psi \quad (3.10)$$

At this point it is necessary to define the tyre model used to generate the longitudinal and lateral tyre forces, F_{wxi} and F_{wyi} .

3.4 Tyre Modelling

The ongoing efforts to describe vehicle tyre behaviour have produced a number of model variations [16, 47, 96]. Researchers have followed two main strategies, attempting to produce both empirical and theoretical models. The empirical models generate tyre forces and moments using actual test data. This data is compiled by means of extensive testing of tyres at various velocities, slip-angles, etc. The advantage of this is that the model is based on real phenomena, and is thus extremely accurate. However, these models require a great deal of time to develop for each type of tyre investigated. One empirical model worth noting is the so-called Magic

Formula Tyre Model, developed by Pacejka who published studies on the effects of tyre factors on vehicle handling [83], before introducing [13] and developing [84, 85] the tyre model.

In contrast, theoretical models seek to predict tyre forces and moments based upon a mathematical description of tyre structure and deformation mechanisms. The first theoretical study [54] on the fundamentals of cornering properties of tyres was performed, and presented in German, by Fiala [43]. These models have been shown to produce good results, the main drawback being the complexity of the equations used. A significant theoretical tyre model, which has been shown to describe tyre behaviour well, has been developed by Dugoff [26].

Studies have been undertaken which compare the relative merits of various, currently used, tyre models. Interestingly, in the majority of manoeuvres, empirical and theoretical models appear comparable [54].

3.4.1 Dugoff Tyre Model

The model used here is based upon the Dugoff model [26]. The decision to use a theoretical tyre model was made for a number of reasons. The main reason was that it does not require the use of large amounts of test data and subsequent tuning and curve fitting. Secondly, the complex calculations involved can be avoided by the use of a simplified version [52, 122]. The accuracy and appropriateness of this model will be discussed in this section along with its limitations.

The components of the friction forces on each wheel are given by

$$F_{wxi} = -C_x \frac{\sigma_i}{1 - \sigma_i} f_i \quad (3.11)$$

$$F_{wyi} = -C_\alpha \frac{\tan \alpha_i}{1 - \sigma_i} f_i \quad (3.12)$$

where

$$f_i = \begin{cases} (2 - \lambda_i)\lambda_i & \text{if } \lambda_i < 1 \\ 1 & \text{if } \lambda_i \geq 1 \end{cases}$$

and

$$\lambda_i = \frac{(1 - \sigma_i)\mu_i F_{ni}}{2\sqrt{C_x^2 \sigma_i^2 + C_\alpha^2 \tan^2 \alpha_i}} \quad (3.13)$$

The four wheel normal forces, F_{ni} , are calculated as appropriate fractions of the vehicle mass, neglecting load redistribution. The wheel slip-angles

$$\tan \alpha_i = \left(\frac{(1 - \sigma_i)v_{wi}}{u_{wi}} - \delta_i \right) \quad (3.14)$$

where $\delta_i = \delta_f$ if $i = 1, 3$ and zero otherwise - as wheels 1 and 3 are located at the front of the car, wheels 2 and 4 are located at the rear (see Figure 3.1), and the model does not include rear steering. This definition of wheel slip-angle differs from that given by Equation (2.4) in that it takes into account both the road-wheel steering angle, δ_f , for the front wheels, and the effect of the longitudinal wheel-slip, σ_i . The wheel-slip values are given by

$$\sigma_i = \frac{U_{wi} - \omega_i R_t}{U_{wi}} \quad (3.15)$$

where the resultant wheel velocity

$$U_{wi} = \sqrt{u_{wi}^2 + v_{wi}^2} \quad (3.16)$$

and the individual longitudinal and lateral wheel velocities u_{wi} and v_{wi} respectively satisfy:

$$u_{w1} = u - \frac{1}{2}r L_{t1} \quad (3.17)$$

$$u_{w2} = u - \frac{1}{2}r L_{t2} \quad (3.18)$$

$$u_{w3} = u + \frac{1}{2}r L_{t1} \quad (3.19)$$

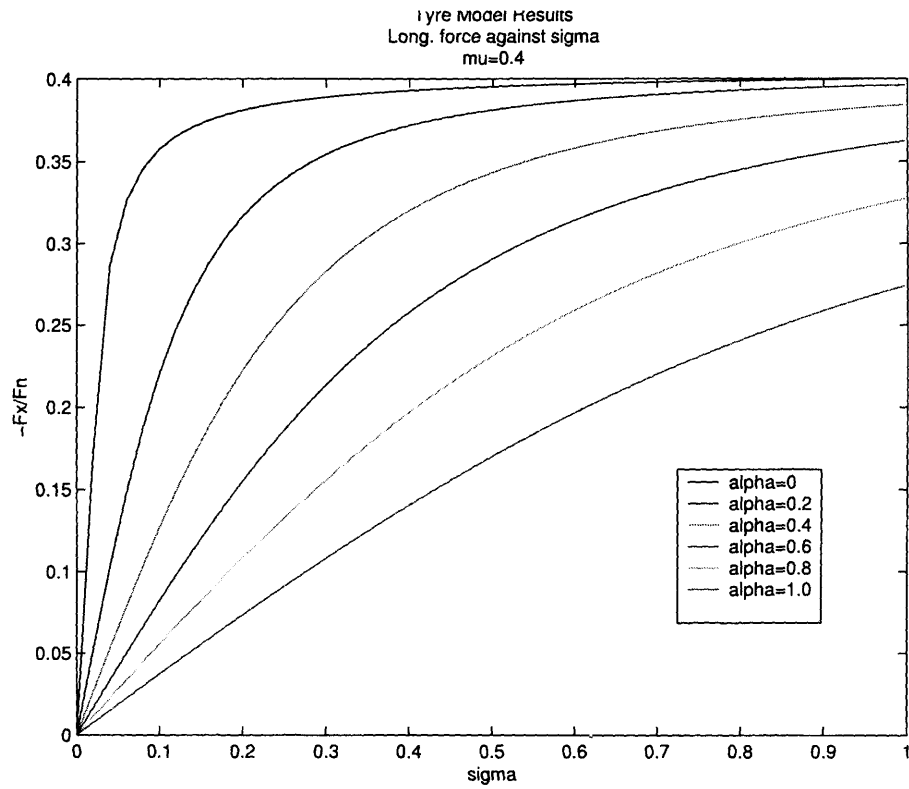
$$u_{w4} = u + \frac{1}{2}r L_{t2} \quad (3.20)$$

$$v_{w1} = v_{w3} = v + ra \quad (3.21)$$

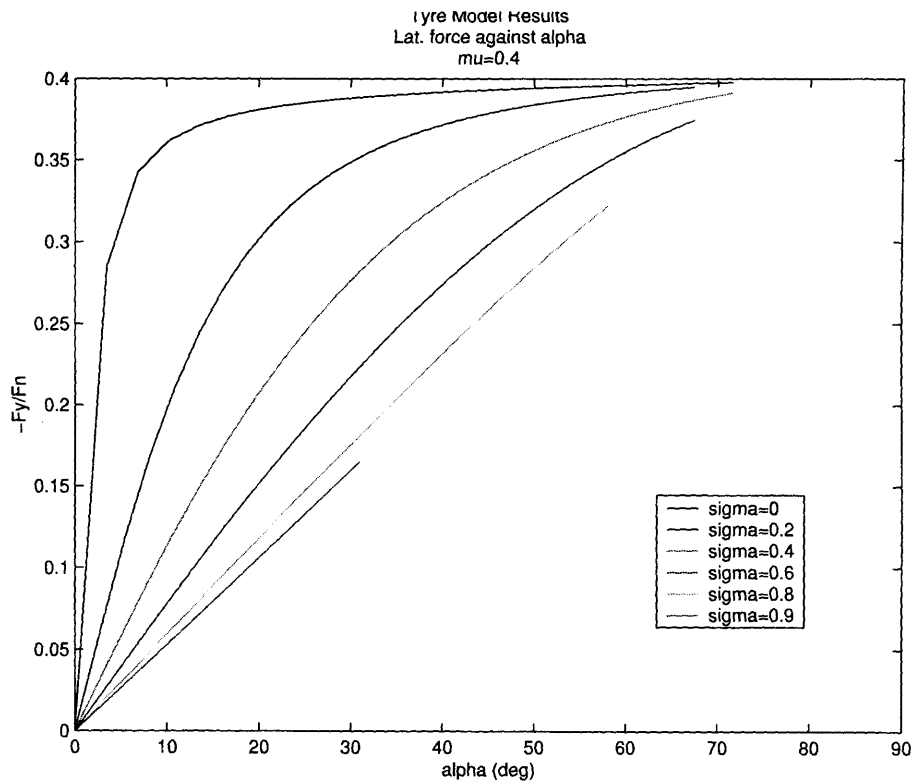
$$v_{w2} = v_{w4} = v - rb \quad (3.22)$$

where a , b , L_{t1} and L_{t2} are the vehicle dimensions as shown in Figure 3.1.

Figure 3.2 shows the behaviour of the tyre model in isolation on a surface of friction coefficient, $\mu = 0.4$, over a range of values of α and σ . These appear to be satisfactory, but for further analysis, their behaviour can be compared against that of other researchers. The results obtained by Bakker and Pacejka [13], working in a joint project involving the Volvo Car Corporation and the Delft University of Technology, can be seen in Figures 3.3(a), 3.4(a), 3.5(a), 3.6(a). In Figures 3.3(b), 3.4(b), 3.5(b), 3.6(b), an attempt to reproduce the empirical model results is made.

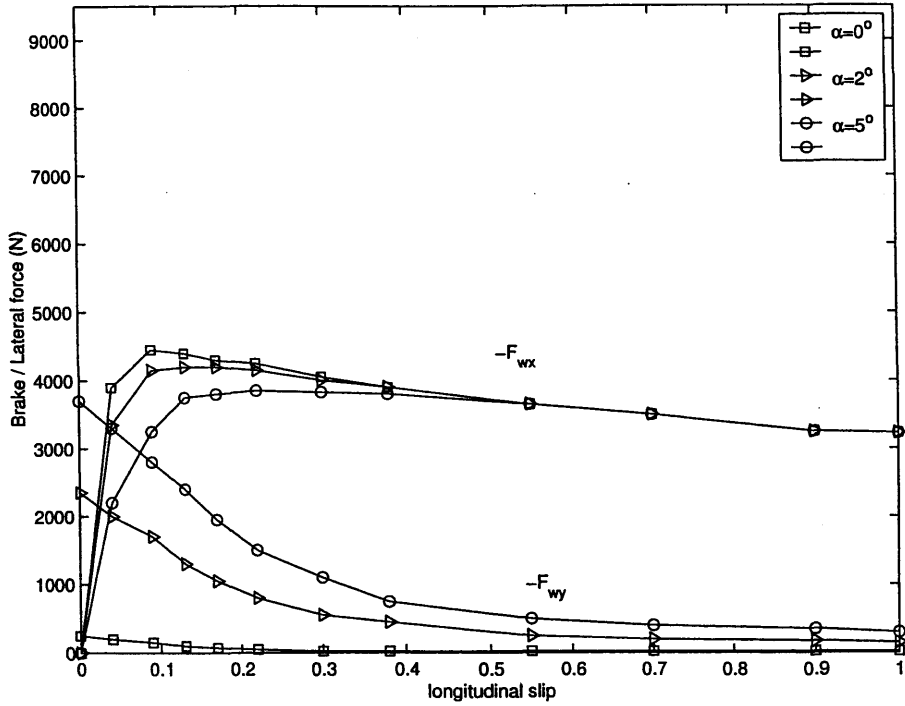


Wheel-slip (σ) versus friction coefficient

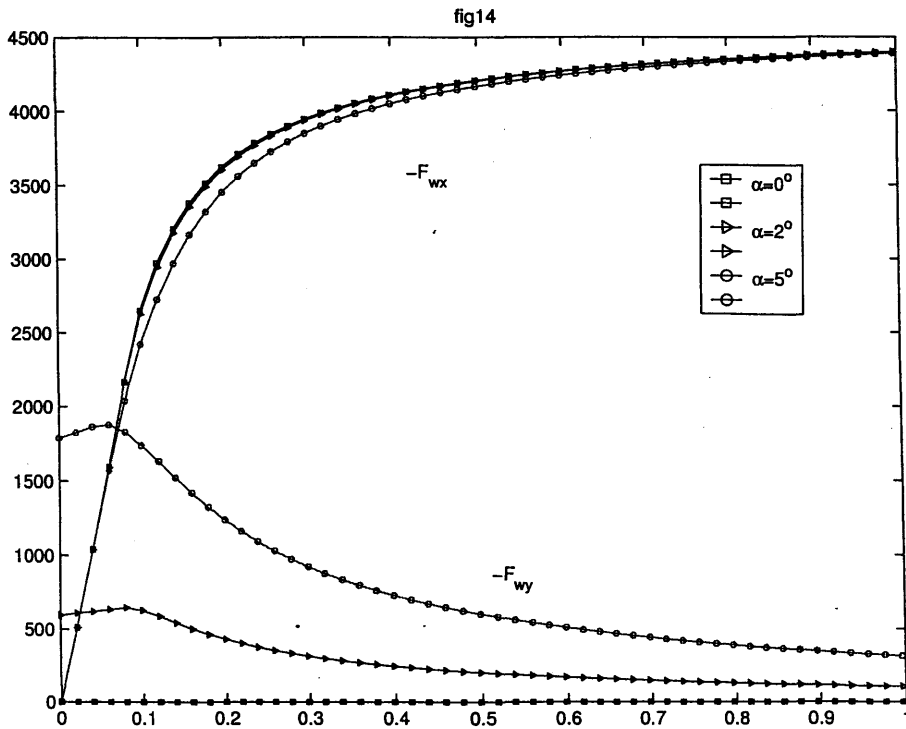


Slip-angle (α) versus friction coefficient

Figure 3.2: Dugoff tyre model

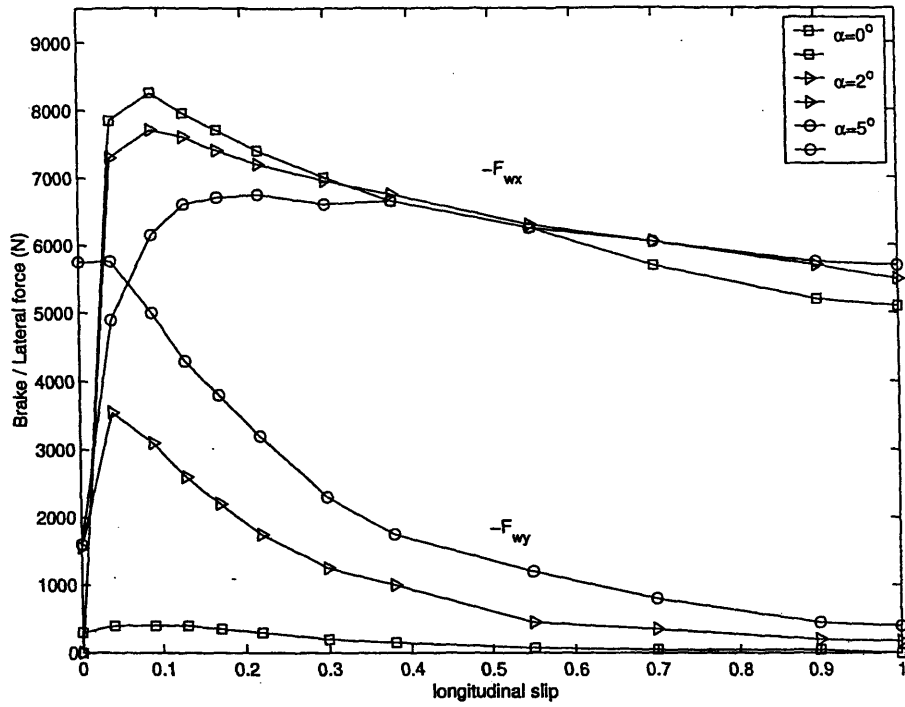


a) Pacejka

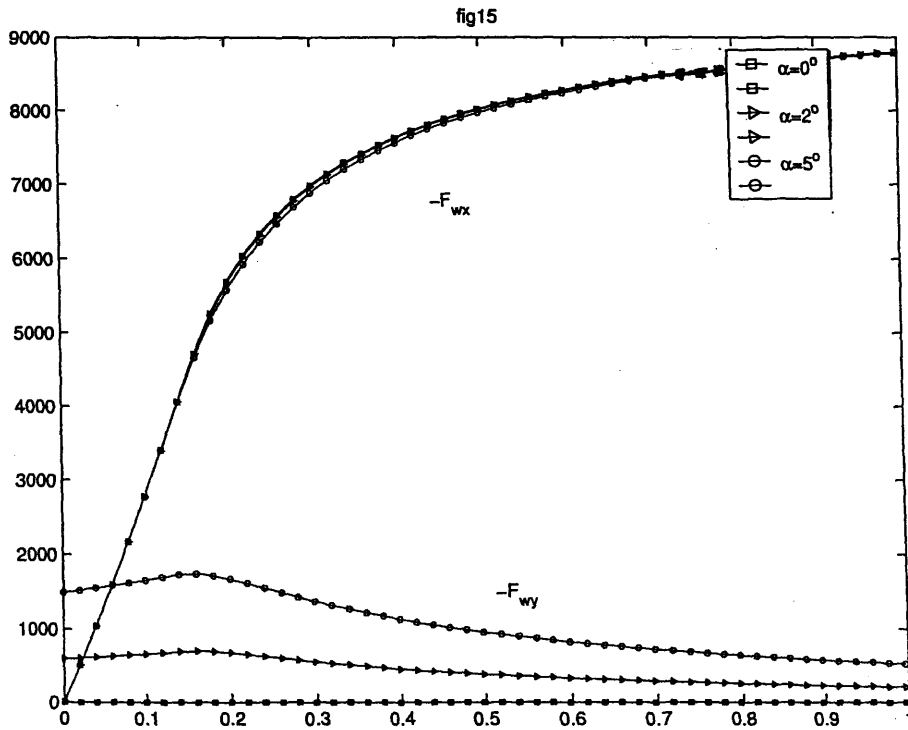


b) Dugoff

Figure 3.3: Brake force, F_{wx} , and lateral force, F_{wy} , versus longitudinal slip at different slip angles with vertical load 4kN.

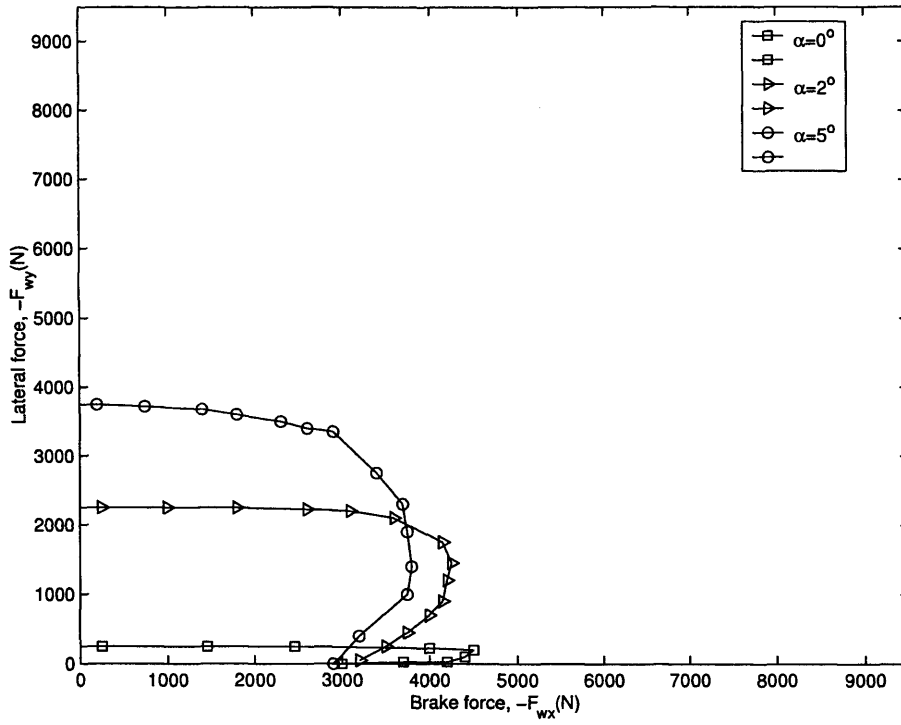


a) Pacejka

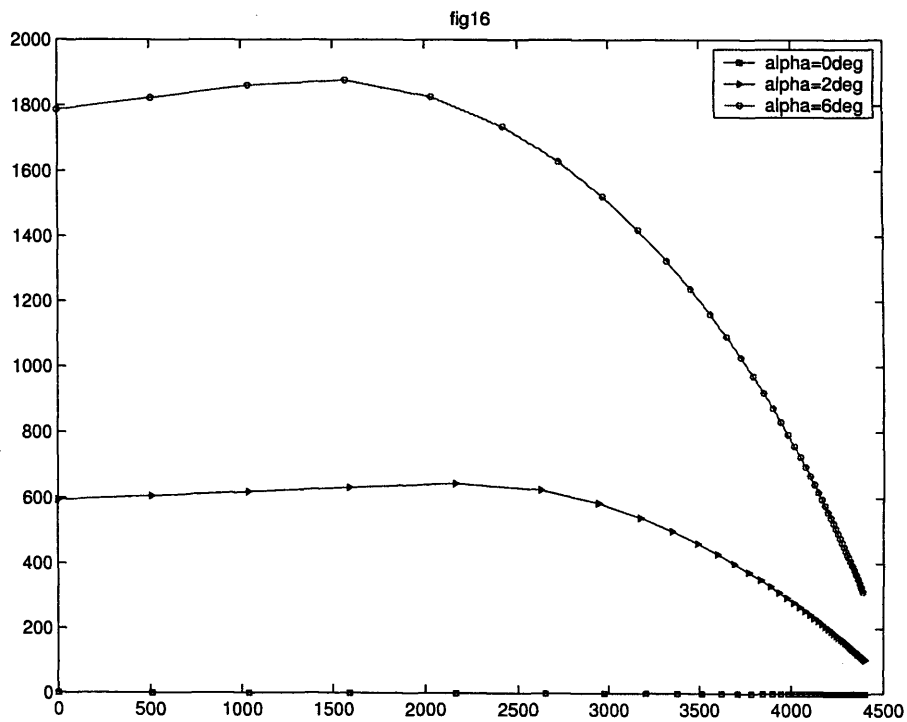


b) Dugoff

Figure 3.4: Brake force, F_{wx} , and lateral force, F_{wy} , versus longitudinal slip at different slip-angles with vertical load 8kN.

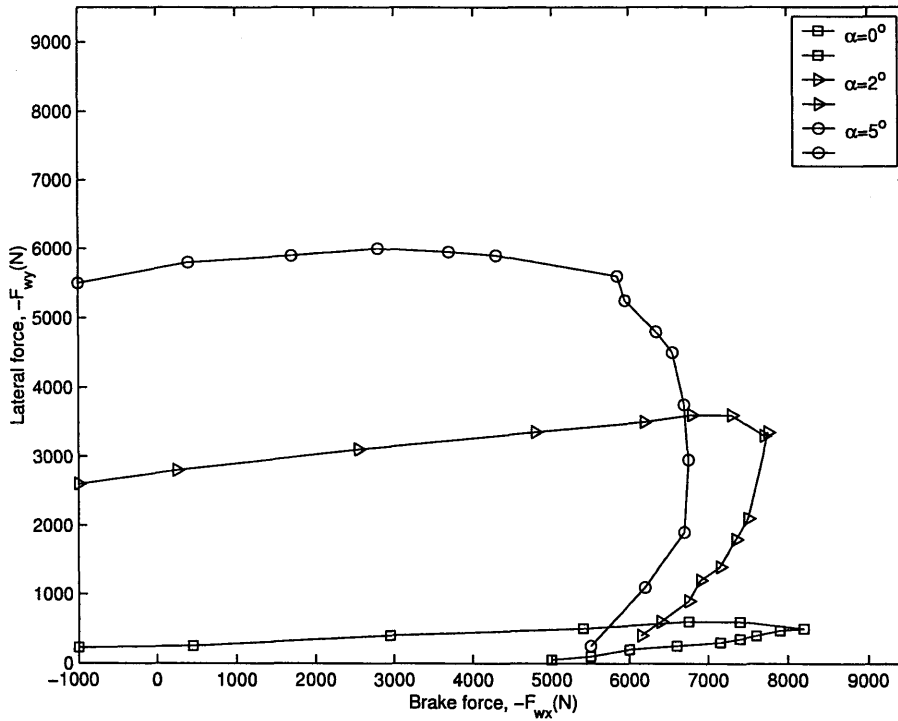


a) Pacejka

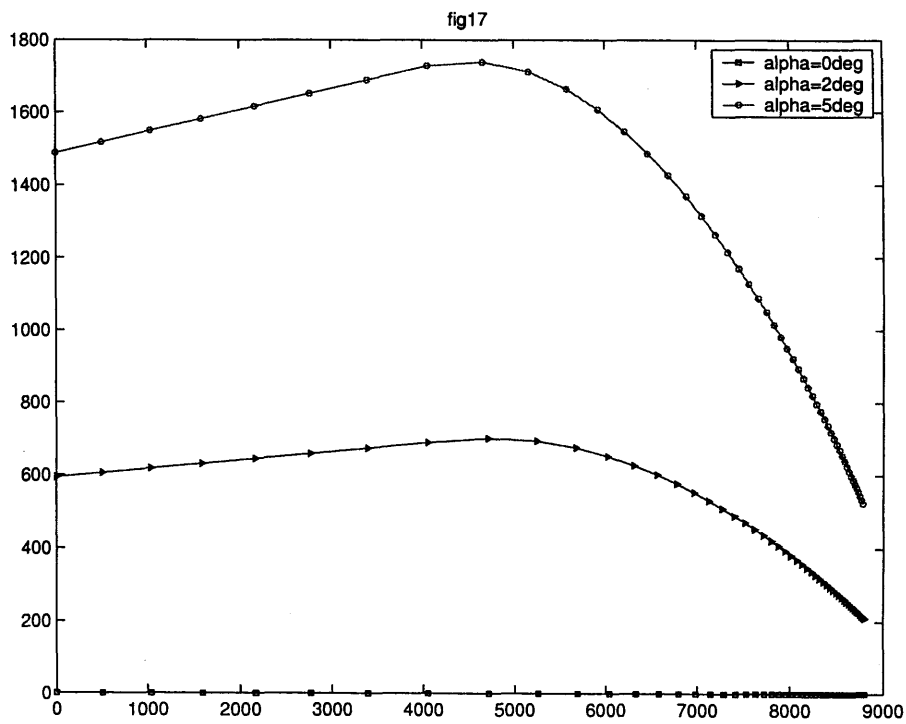


b) Dugoff

Figure 3.5: Side force, F_{wx} , and lateral force, F_{wy} , at different slip-angles with vertical load 4kN



a) Pacejka



b) Dugoff

Figure 3.6: Lateral force, F_{wy} , versus brake force, F_{wx} , at different slip-angles with vertical load 8kN

It can be seen in Figures 3.3, 3.4 that the fundamental shape, i.e. brake force versus longitudinal slip at zero slip-angle, of the theoretical tyre differs only slightly from the Pacejka tyre model. While the Pacejka tyre has a steep initial slope, peaks, and then drops off, the theoretical model has a shallower critical slope and levels off without peaking. This is not evidence of a problem with either model, rather it is merely indicative of the wide variations in tyres from different manufacturers and road surface [41].

The relative lack of variation in the plots in Figures 3.3, 3.4 are a reflection of the theoretical tyre model being less stiff than the Pacejka tyre, and this difference in stiffness is also responsible for the lower values of side force in Figures 3.3, 3.4. In Figures 3.5, 3.6, the results again describe similar trends, with magnitudes affected by the tyre stiffnesses. Also, the lack of a peak in the longitudinal force means that the theoretical model does not show the elliptical shape of the Pacejka plots. The absence of a peak in the longitudinal force signals of the Dugoff plots may present problems for 'formal' modelling of ABS, driven by instability. However, as the ABS action used in the simulations in this thesis is driven directly by the road/tyre friction coefficient, the absence of this peak should not present a problem in the simulations performed.

3.5 ABS Model

In the scenarios which will be considered in later chapters, it is necessary in the simulations that the vehicle brakes perform an "emergency stop", braking as hard as possible. In order to produce acceptable braking torques in a realistic way it is necessary to introduce an Anti-lock Braking System (ABS) into the simulation. In real vehicles, as described in Section 2.5.1, the exact working of the ABS is logic based [14], and complicated models have been developed which attempt to reproduce the braking system as a whole [45]. Here, a simple model has been produced to mimic the ABS control action.

In order to reproduce ABS signals for controller testing, an ABS block is attached to each wheel of the vehicle model during simulation, the block diagram used is shown in Figure 3.7. Each ABS block is fed the current value of road/tyre friction coefficient, μ_i , and uses look-up tables to choose appropriate values for desired slip, σ_d and half-width of a "dead-band"

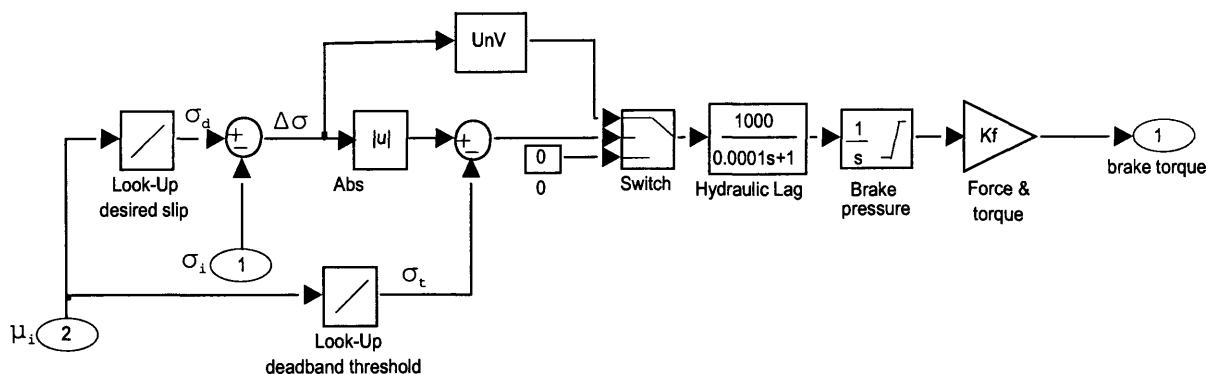


Figure 3.7: ABS Simulink Block Diagram

threshold, σ_t , around σ_d . If the actual wheel-slip falls within the dead-band, then no action is required, if it falls outside then the ABS must apply or reduce the braking torque accordingly. The desired slip is then compared with the actual wheel-slip, σ_i , to give $\Delta\sigma = \sigma_d - \sigma_i$. If $|\Delta\sigma| < \sigma_t$, then a zero signal is produced. However, if $|\Delta\sigma| > \sigma_t$, then a signal is produced in the unit vector (UnV) block $\frac{\Delta\sigma}{|\Delta\sigma|+0.01}$ which will increase or decrease the brake pressure as appropriate. This signal is then passed through a block which simulates hydraulic lag - although a gain of 1000 is used whilst for lag alone, the gain should be 1 - and then through a continuous time integrator. Finally, there is a gain, K_f , to tune the signal, accounting for asymmetric load distribution across the front and rear of the vehicle, producing a brake torque. It is important to note that whereas in this ABS model, both μ_i and σ_i are known, in a real vehicle these are signals which the ABS must estimate. However, in this work, it is not the intention to design a realistic ABS, but rather to produce sufficiently realistic ABS signals to use in simulation. Each of the front wheels have individual braking torque signals associated with them. However, the two rear wheels are controlled together, such that they follow a commonly used control strategy known as ‘selecting low’ described in Section 2.5.1.

3.6 Bicycle Model

For the purposes of control system design it is useful to produce a lower-order linear model. One way to do this is to numerically linearize the full-order nonlinear model. A second option is to derive a lower-order, parameterized, theoretical linear model. Each of these approaches

has its merits. A numerical linearization of a nonlinear model may be necessary where no suitable parameterized model exists. However, a parameterized model can be an invaluable aid to analysing closed-loop performance and robustness to parameter uncertainties. A numerical linearization, which is seen to match a theoretical parameterized model provides some confirmation of the validity of the nonlinear model from which it was obtained.

There are many examples of ‘bicycle models’ to be found in the literature [2, 44, 51] which use yaw rate, r , and sideslip angle, β , as system states. Alternatively, the states of the bicycle model may also be defined as lateral velocity, v , and yaw rate, r [76]. The justification for the use of v in some cases and β in others is based upon small angle approximations. It can be

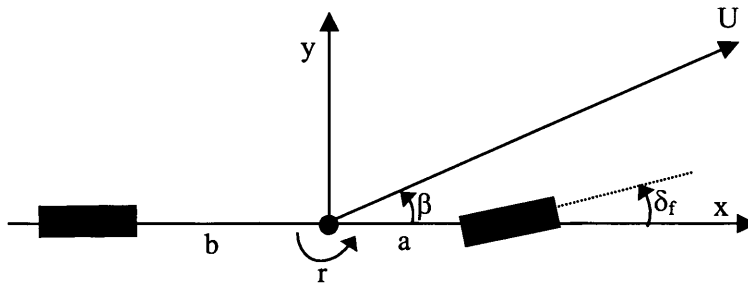


Figure 3.8: Bicycle model in terms of β , r .

seen in Figure 3.8, from the definition of lateral velocity, v , as the projection of the total speed, U , on the positive y -axis:

$$v = U \sin \beta \tag{3.23}$$

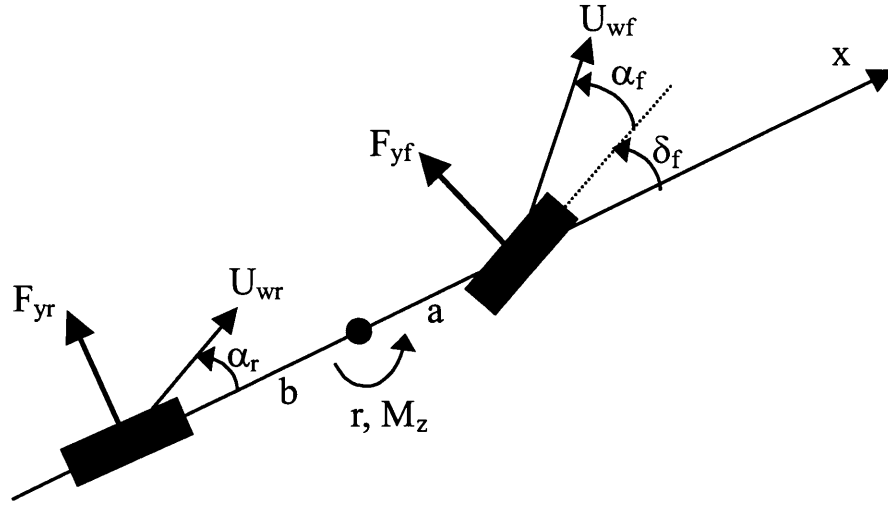
For small angles, this can be approximated to:

$$v = U\beta \tag{3.24}$$

and $U \approx u$. This shows that for small deviations, there is an approximate linear relationship between lateral velocity and sideslip.

3.6.1 Theoretical Model

A derivation of the bicycle model in terms of lateral velocity and yaw rate, as shown in Figure 3.9, is given below.

Figure 3.9: Bicycle model in terms of v, r

From Newtonian mechanics

$$\begin{aligned} I_z \dot{r} &= M_{zf} - M_{zr} \\ &= aF_{yf} - bF_{yr} \end{aligned}$$

where M_{zf} , M_{zr} are defined as the yaw moments due to the front and rear tyres respectively. While the front lateral tyre force acts at an angle of δ_f to the vehicle longitudinal x -axis, the small angle approximation, $\cos \delta_f = 1$, allows it to be considered to act exactly perpendicularly to the x -axis. The tyre lateral forces depend upon on the wheel slip-angle, α_i , in a form represented in Figure 3.2, and on the vertical load on the particular wheels. However, in the linear case the vertical force is constant and the slip angle is small. In this case only the initial gradient, the tyre stiffness $C_{\alpha i}$, at $\alpha = 0$ is required, so that the front and rear axle lateral forces are given by:

$$F_{yf} = -2C_{\alpha f}\alpha_f \quad (3.25)$$

$$F_{yr} = -2C_{\alpha r}\alpha_r \quad (3.26)$$

where $2C_{\alpha f}$, $2C_{\alpha r}$ represent the combined front and rear axle lateral tyre stiffnesses, and α_f , α_r represent tyre slip-angles at the front and rear of the vehicle, respectively. Therefore

$$I_z \dot{r} = -2aC_{\alpha f}\alpha_f + 2bC_{\alpha r}\alpha_r \quad (3.27)$$

The slip-angle, α_i is defined linearly (see Equation (2.4)) as

$$\tan \alpha_i = \frac{v_{wi}}{u_{wi}}$$

and the individual longitudinal wheel velocity is approximated as the vehicle longitudinal velocity, ie. $u_{wi} = u$. The lateral velocities are defined in Equations (3.21) and (3.22). Using the small angle approximation $\tan \alpha_i \simeq \alpha_i$, the linear expressions for the slip angles at the front, taking road-wheel steering angle into consideration, and the rear axles are

$$\alpha_f = \frac{v + ar}{u} - \delta_f \quad (3.28)$$

$$\alpha_r = \frac{v - br}{u} \quad (3.29)$$

Equation (3.27) becomes

$$\begin{aligned} I_z \dot{r} &= -2aC_{\alpha f} \left(\frac{v + ar}{u} - \delta_f \right) + 2bC_{\alpha r} \left(\frac{v - br}{u} \right) \\ \dot{r} &= \frac{2(bC_{\alpha r} - aC_{\alpha f})}{I_z u} v - \frac{2(a^2 C_{\alpha f} + b^2 C_{\alpha r})}{I_z u} r + \frac{2aC_{\alpha f}}{I_z} \delta_f \end{aligned} \quad (3.30)$$

Similarly, and given that the vehicle lateral acceleration may be given [40] by

$$a_y = \dot{v} + ur \quad (3.31)$$

then

$$\begin{aligned} m_v a_y &= F_{yf} + F_{yr} \\ m_v (\dot{v} + ur) &= -2C_{\alpha f} \alpha_f - 2C_{\alpha r} \alpha_r \\ \dot{v} &= -\frac{2(C_{\alpha f} + C_{\alpha r})}{m_v u} v + \left(\frac{2(bC_{\alpha r} - aC_{\alpha f})}{m_v u} - u \right) r + \frac{2C_{\alpha f}}{m_v} \delta_f \end{aligned} \quad (3.32)$$

The equations of motion of the two states - yaw rate, r , and lateral velocity, v - given in Equations (3.30) and (3.32) may be summarized in state space form as

$$\begin{bmatrix} \dot{r} \\ \dot{v} \end{bmatrix} = \begin{bmatrix} -\frac{2(a^2 C_{\alpha f} + b^2 C_{\alpha r})}{I_z u} & \frac{2(bC_{\alpha r} - aC_{\alpha f})}{I_z u} \\ \left(\frac{2(bC_{\alpha r} - aC_{\alpha f})}{m_v u} - u \right) & -\frac{2(C_{\alpha f} + C_{\alpha r})}{m_v u} \end{bmatrix} \begin{bmatrix} r \\ v \end{bmatrix} + \begin{bmatrix} \frac{2aC_{\alpha f}}{I_z} \\ \frac{2C_{\alpha f}}{m_v} \end{bmatrix} \delta_f \quad (3.33)$$

3.7 Conclusions

A suitable four-wheel vehicle model with nonlinear tyres has been developed in order to test the effectiveness of the controller and estimator schemes proposed later in this thesis. The vehicle model achieves a good balance between practical simplicity and realism to a level and emphasis appropriate for the scenarios to be simulated. The presence of four distinct wheels in the model facilitate the inclusion of individual ABS blocks, which is vital to the simulation of harsh split- μ braking. The vehicle model is also able to accommodate a control input to the front road-wheel or steering wheel angle. The simpler bicycle model has also been introduced as this will be useful for controller/observer design which will be described in subsequent chapters.

Chapter 4

Introduction to Sliding Mode

4.1 Introduction

This chapter seeks to introduce the reader to some Sliding Mode ideas and methods, which will be used in subsequent chapters. The area of sliding mode, which has been applied in a variety of contexts (e.g. [30, 42, 100, 111, 120]), stems from work in the field of Variable Structure Control Systems (VSCS) [65, 66]. Sliding Modes have been used in the design of robust regulators, model-reference systems, adaptive schemes, tracking systems, state observers and fault detection schemes [31]. VSCS are schemes which comprise a suite of control laws and a decision rule - known as a switching function - which determines which of the control laws is applied to the system at any particular instant. This results in a system described by a composite structure of a combination of subsystems, taking on the useful properties of the composite structures, whilst adding new useful properties of its own. In this thesis, Sliding Mode methods will be used for controller design, as well as observer design for both system state reconstruction and unknown input estimation. On one level, Sliding Mode controller and observer design are analogous, as they employ the same concepts. Therefore, whilst a discussion of observers will be included towards the end of this chapter, the more detailed motivation and description of concepts will mostly concern Sliding Mode controllers only, to avoid repetition.

4.2 Controller Design

In every control application, there exist mismatches between the model used for controller design, and the actual plant. These mismatches may arise for a number of reasons including unmodelled dynamics or variations in system parameters, or simply model approximations of complexities within the plant. Legitimate controllers should be expected to maintain good performance in the presence of such mismatches and, so, necessitate so-called robust controller design methodologies. Sliding mode control provides this robustness in two steps. A surface is first defined which prescribes an appropriate reduced order motion, termed the sliding mode or sliding motion. Subsequently, a nonlinear control law is designed which compels the system to reach and, then, remain on the surface, which is usually described as the sliding surface, or switching surface. Traditionally such a control law is discontinuous about the sliding surface [31, 114]. In order to prevent high frequency chattering (i.e. repeated crossing of the sliding surface) due to the discontinuity, a boundary region is often introduced and the controller is ‘smoothed’ [31]. The system is now constrained within the neighbourhood of the sliding surface, producing a regime often referred to as pseudo-sliding [31].

4.2.1 Example: The bicycle model

a	Front axle distance from the centre of gravity (m)	0.9130
b	Rear axle distance from the centre of gravity (m)	1.7300
$C_{\alpha f}$	Front lateral cornering stiffness for bicycle model (N/rad)	17000.0
$C_{\alpha r}$	Rear lateral cornering stiffness for bicycle model (N/rad)	17000.0
I_z	Yaw moment of inertia (kg m ²)	2550.0
m_v	Total vehicle mass (kg)	1673.0

Table 4.1: Vehicle parameter values, from [78]

In order to demonstrate the properties and strengths of sliding mode control, it is advantageous to consider a simple 2^{nd} -order model. To this end, for demonstration purposes only, the bicycle model, introduced in Section 3.6 will be used. This system has just two states: lateral velocity, v ; and yaw rate, r . The 2^{nd} -order system, using the parameters given in Table 4.1,

can, therefore, be described by:

$$\dot{x}(t) = A_b x(t) + B_b u(t) \quad (4.1)$$

where

$$A_b = \begin{bmatrix} -2.724 & -13.808 \\ 0.730 & -3.420 \end{bmatrix} \quad (4.2)$$

and

$$B_b = \begin{bmatrix} 1.355 \\ 0.812 \end{bmatrix} \quad (4.3)$$

The input $u(t)$ is the road-wheel steering angle. The eigenvalues of the system matrix are the complex conjugate pair $-3.0719 \pm 3.1560i$. As the eigenvalues lie in the left half plane, the open-loop system is seen to be stable. Most sliding mode control design methods begin by changing co-ordinates so that the system is in a suitable canonical form. If a new co-ordinate system z is introduced as

$$z = T_p x \quad (4.4)$$

where

$$T_p = \begin{bmatrix} -0.0839 & 0.1401 \\ 0.3309 & 0.6798 \end{bmatrix} \quad (4.5)$$

in the new co-ordinates, the input and output distribution matrices are now given by

$$A_p = T_p A_b T_p^{-1} = \begin{bmatrix} 0 & 1 \\ A_{21} & A_{22} \end{bmatrix} = \begin{bmatrix} 0 & 1 \\ -19.3957 & -6.1435 \end{bmatrix} \quad (4.6)$$

$$B_p = T_p B_b = \begin{bmatrix} 0 \\ B_2 \end{bmatrix} = \begin{bmatrix} 0 \\ 1 \end{bmatrix} \quad (4.7)$$

$$(4.8)$$

The key property here is the partition of the input distribution matrix. This split, into the *range space* and *null space*, of the input distribution matrix is known as regular form [114]. Equation (4.1) can now be written as

$$\dot{z}(t) = \begin{bmatrix} 0 & 1 \\ -19.3957 & -6.1435 \end{bmatrix} z(t) + \begin{bmatrix} 0 \\ 1 \end{bmatrix} u(t) \quad (4.9)$$

For generality, this system may be written

$$\dot{z}_1(t) = A_{11}z_1(t) + A_{12}z_2(t) \quad (4.10)$$

$$\dot{z}_2(t) = A_{21}z_1(t) + A_{22}z_2(t) + B_2u(t) \quad (4.11)$$

In this particular case, this system is in the so-called ‘controllable canonical form’ [82]. In the open-loop simulation presented in Figure 4.1, the initial condition is given as $z(0) = [1 \ 0]^T$, which corresponds to $v = -6.57ms^{-1}$, $r = 3.20rads^{-1}$. As is confirmed by Figure 4.1a, the system is asymptotically open-loop stable, as the system states return to the origin. This motion is shown in Figure 4.1b by means of a phase portrait. A phase portrait is simply a convenient way of analysing system behaviour for a 2nd order model, as the evolution of the system states may be clearly seen. Time does not appear explicitly, although the direction of time (if not the magnitude) may be followed along the curve, starting at the initial conditions. A controller for this system would seek to regulate the system states within a shorter space of time and without the overshoot experienced in the open-loop simulation associated with the complex conjugate pair of poles.

4.2.2 Ideal sliding motion

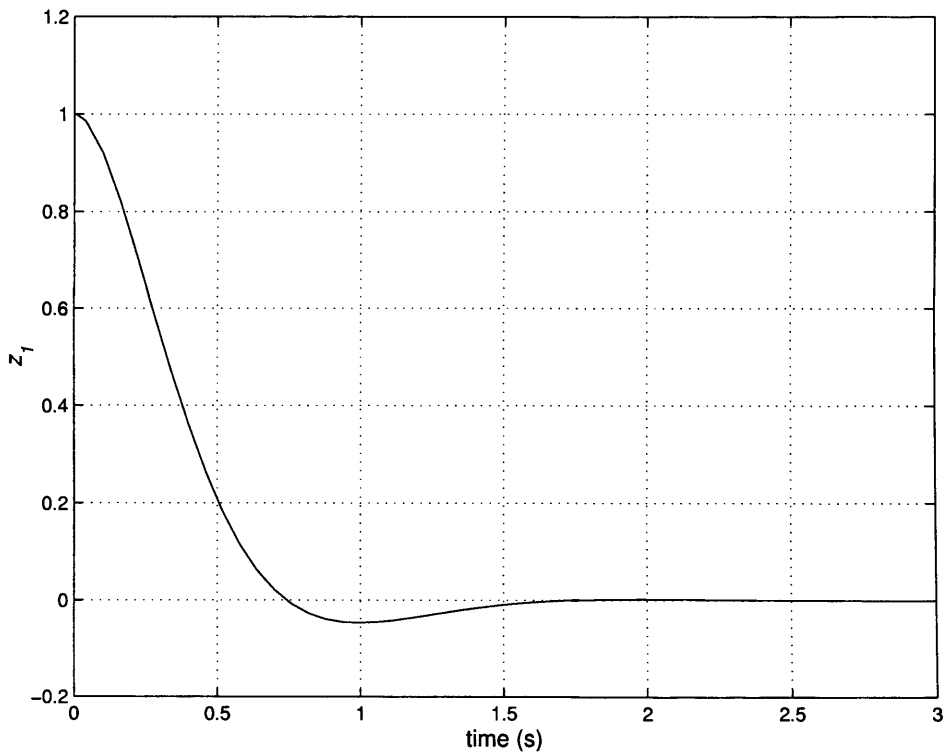
A simple example of a variable structure control law is given by

$$u(t) = -\text{sgn}(s(t)) \quad (4.12)$$

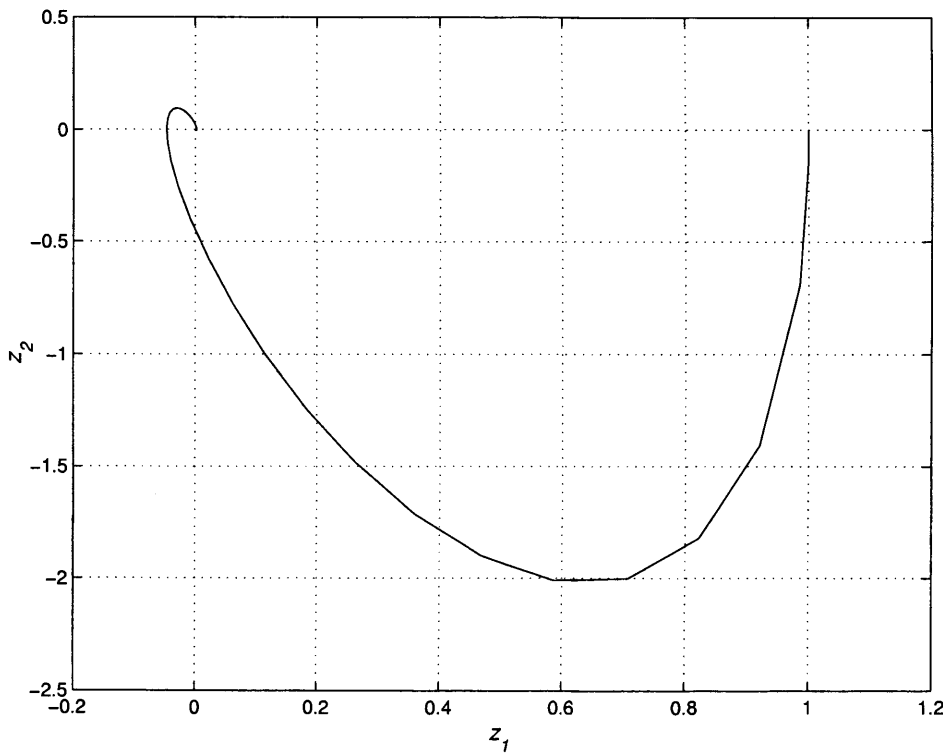
where the switching function is defined by

$$s(z) = mz_1 + z_2 \quad (4.13)$$

Note, because of the special form of Equation (4.9), $z_2 = \dot{z}_1$ and, so, (z_1, z_2) are the components of the phase portrait. The quantity m is a positive design scalar. The reason for the use of the term ‘switching function’ is clear, since the function given in Equation (4.13) is used to decide which control law is in use at any point (z_1, z_2) in the phase plane, i.e. $u = -1$ or $u = 1$. The expression in Equation(4.13) can also be conveniently expressed in matrix terms as



a) System states



b) Phase portrait

Figure 4.1: Open-loop simulation

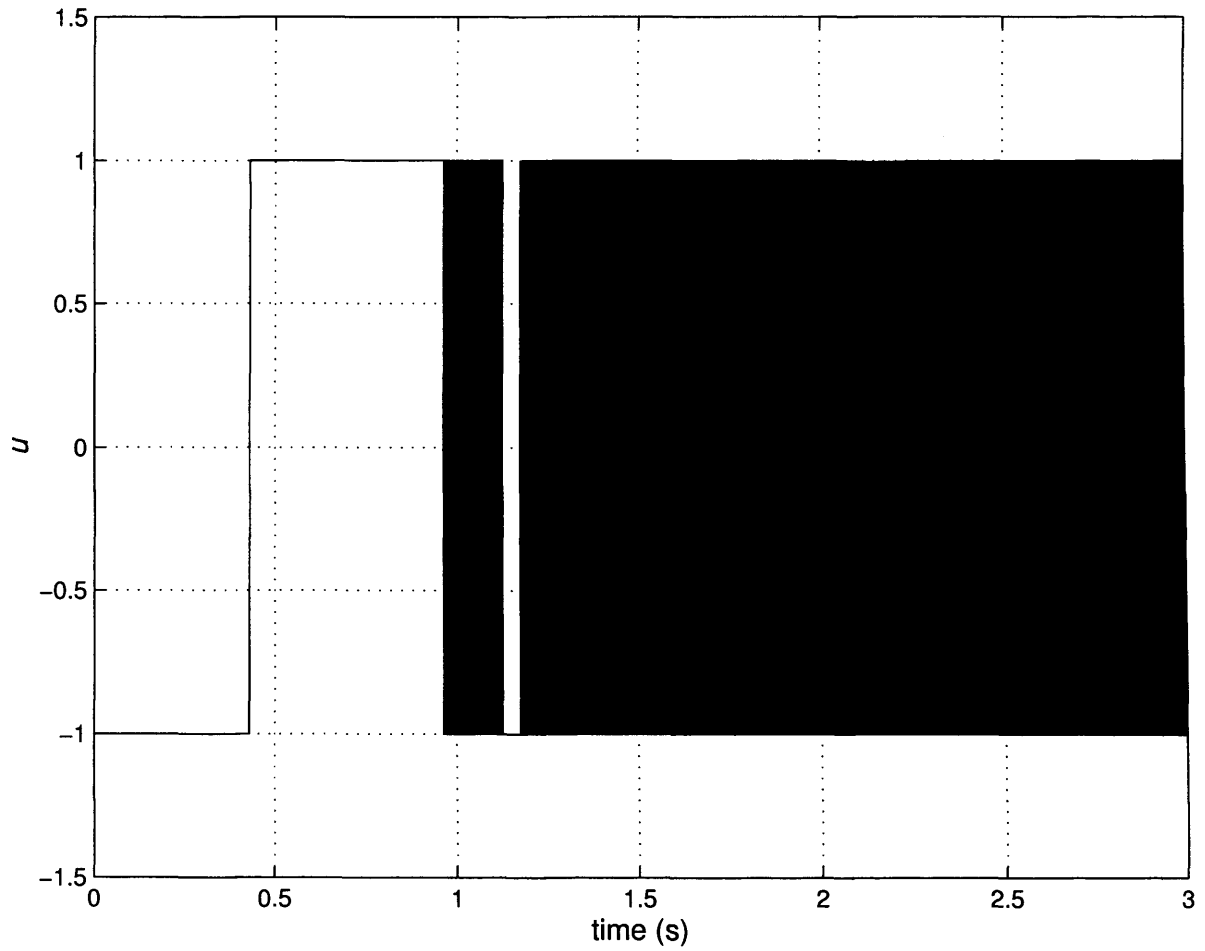
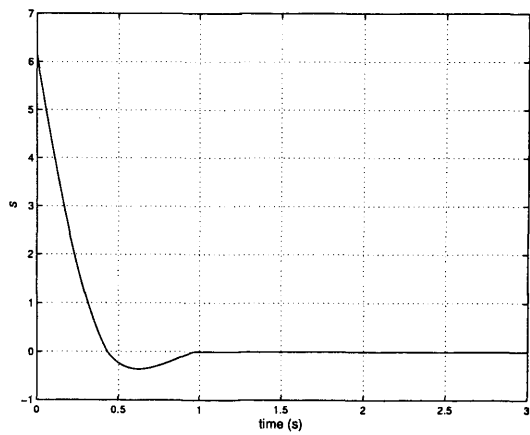
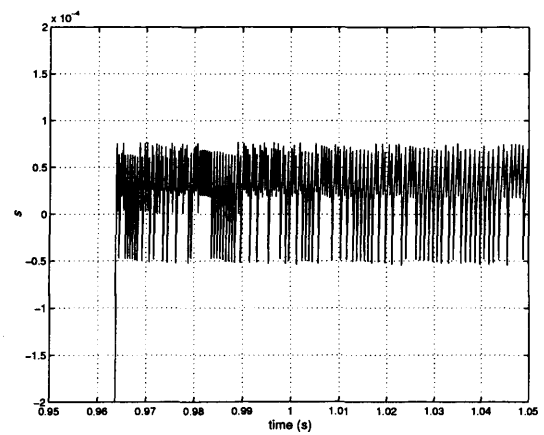


Figure 4.2: Bicycle Model with controller given by Equation (4.12) showing control signal

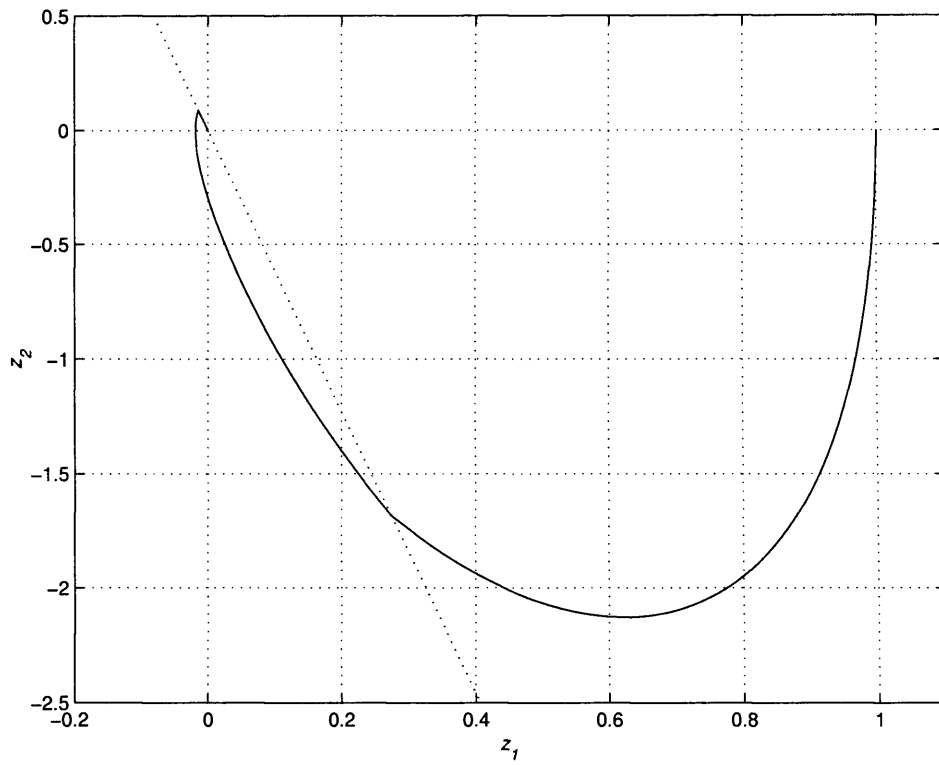


b) Switching function

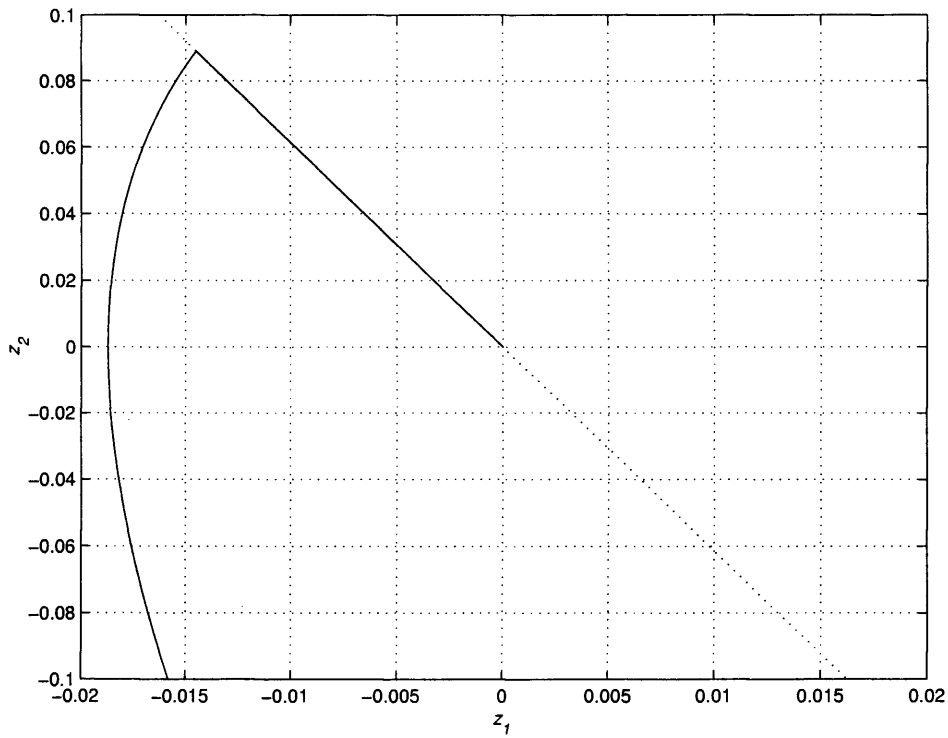


c) Close-up of b)

Figure 4.3: Bicycle Model with controller given by Equation (4.12)



a) Phase portrait



b) Close-up

Figure 4.4: Phase portrait using controller given by Equation (4.12)

$$s(z) = Sz(t) \quad (4.14)$$

where

$$S = [m \ 1] \quad (4.15)$$

In the following design, $m = -A_{22}$. This is a legitimate choice since $A_{22} = -6.1436 < 0$. For values of z_1 satisfying the inequality $|A_{21}||z_1| < 1$,

$$\begin{aligned} s\dot{s} &= s(m\dot{z}_1 + \dot{z}_2) = s(m\dot{z}_1 + A_{21}z_1 + A_{22}z_2 + u) \\ &= s(A_{21}z_1 - \text{sgn}(s)) \\ &\leq |s|(|A_{21}||z_1| - 1) < 0 \end{aligned} \quad (4.16)$$

or, equivalently

$$\lim_{s \rightarrow 0^+} \dot{s} < 0 \quad \text{and} \quad \lim_{s \rightarrow 0^-} \dot{s} > 0 \quad (4.17)$$

Consequently, when $|z_1| < 1/|A_{21}|$, the system trajectories on either side of the line

$$\mathcal{L}_s = \{(z_1, z_2) : s(z_1, z_2) = 0\} \quad (4.18)$$

point towards the line.

The expression in Equation (4.12) is used to control the presented bicycle model (producing the control signal shown in Figure 4.2) in the new (z_1, z_2) coordinates, resulting in the phase portrait given in Figure 4.4, where an initial displacement of $z(0) = [1 \ 0]^T$ is given. The dotted line represents the set of points for which $s(z_1, z_2) = 0$, in this case, a straight line through the origin of gradient $-m$.

Intuitively, high frequency switching between the two different control structures (seen in Figure 4.2) will take place as the system trajectories repeatedly cross the line \mathcal{L}_s (Figure 4.3). The high frequency switching is described as chattering. If infinite frequency switching were possible, the motion would be trapped or constrained to remain on the line \mathcal{L}_s . The motion,

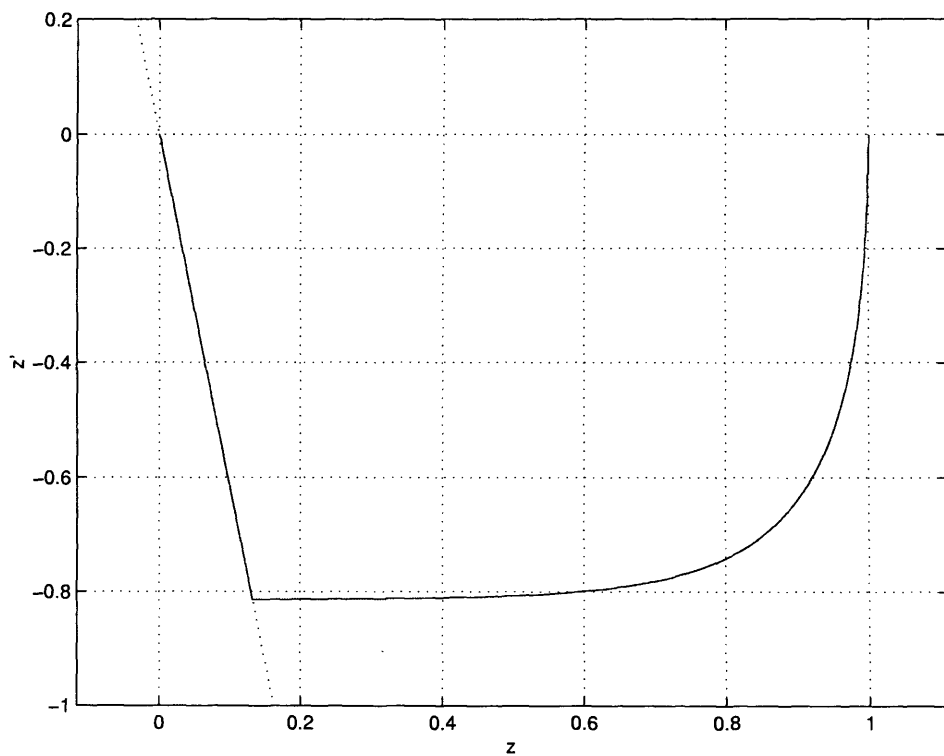
when confined to the line \mathcal{L}_s , satisfies the differential equation obtained from rearranging $s(z_1, z_2) = 0$ in Equation (4.13), namely

$$\dot{z}_1(t) = -mz_1(t) \quad (4.19)$$

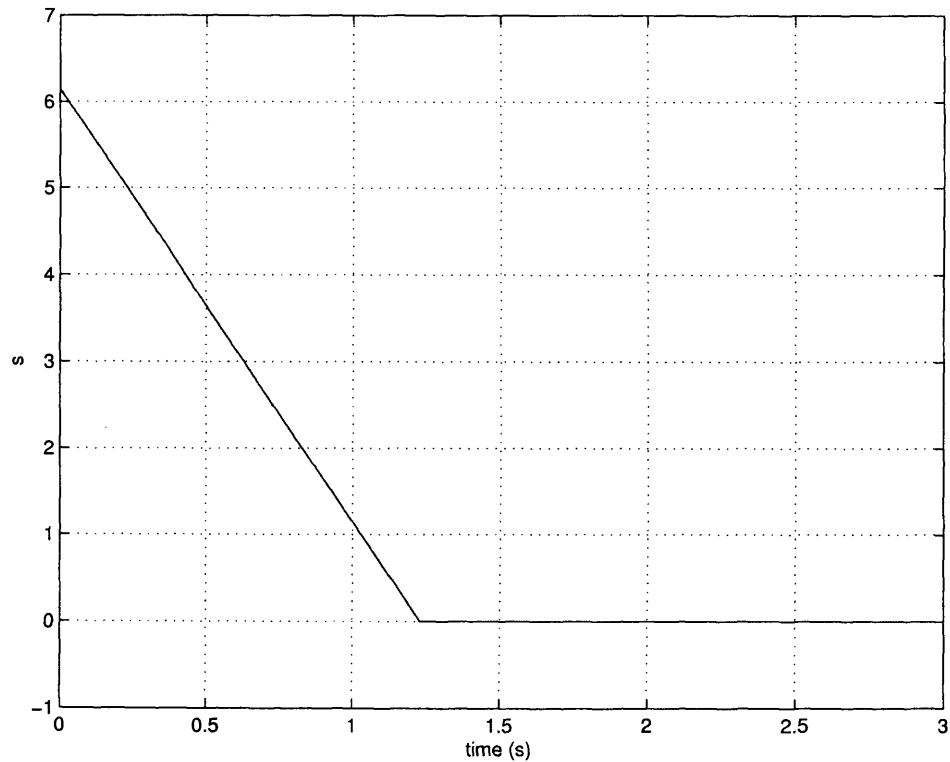
This represents a first-order decay, and the trajectories will ‘slide’ along the line \mathcal{L}_s to the origin. Such dynamical behaviour is described as an *ideal sliding mode* or an *ideal sliding motion*, and the line \mathcal{L}_s is termed the *sliding surface*. During sliding motion, the system behaves as a reduced-order system, which is apparently independent of the control. The control action, rather than prescribing the dynamic performance, ensures instead that the conditions given in Equation (4.17) are satisfied; this guarantees that $s(z_1, z_2) = 0$ is reached. The conditions in Equation (4.17) are usually written more conveniently as

$$s\dot{s} < 0 \quad (4.20)$$

which is usually referred to as the reachability condition [31]. Thus, in terms of VSCS design, the choice of the switching function, represented in this situation by the parameter m , governs the performance response; whilst the control law itself is designed to guarantee that the reachability condition is satisfied. The response shown in Figures 4.3 - 4.4 is for a very large initial displacement. It can be seen in Figure 4.3 that at approximately 0.4 seconds the trajectory intercepts the switching line \mathcal{L}_s , but insufficient control energy is available to maintain a sliding motion. The sign of the control law switches (Figure 4.2); the trajectory pierces the switching line and moves away before intercepting the line again at approximately 0.8 seconds, at which point, sliding takes place. The result is not, perhaps, surprising since the initial conditions correspond to a significant initial vehicle lateral velocity. This result agrees with the earlier result in Equations (4.16-4.20) that a sliding motion can only be guaranteed in the region of the phase plane for which the inequality $|z_1| < \frac{1}{|A_{21}|} = 0.0516$ holds.



a) Phase portrait



b) Switching function

Figure 4.5: Phase portrait and switching function, using controller given in Equation (4.21)

4.2.3 Enlarging sliding region

In order to force the system to remain on the sliding surface the first time it intercepts it, it is necessary to modify the control law. It can be considered as a problem of increasing the region in which sliding will occur to cover the entire (z_1, \dot{z}_1) plane.

Consider a new control structure

$$u(t) = l_1 z(t) + l_2 \dot{z}(t) - \rho \operatorname{sgn}(s(t)) \quad (4.21)$$

where l_1 and l_2 are scalars yet to be designed and ρ is a positive scalar which will be used as a tuning gain. In this case Equation (4.16) becomes

$$\begin{aligned} s\dot{s} &= s(m\dot{z}_1 + \ddot{z}_1) = s(A_{21}z_1 + u) \\ &= s(A_{21}z_1 + l_1 z_1 + l_2 \dot{z}_2 - \rho \operatorname{sgn}(s)) \end{aligned} \quad (4.22)$$

let $l_1 = -A_{21}$ and $l_2 = 0$, so that from Equation (4.22)

$$\begin{aligned} s\dot{s} &= s(A_{21}z - A_{21}z - \rho \operatorname{sgn}(s)) \\ &= s(-\rho \operatorname{sgn}(s)) = -\rho|s| \end{aligned} \quad (4.23)$$

By choosing $\rho > \eta$, where η is a positive design scalar, the inequality

$$s\dot{s} < -\eta|s| \quad (4.24)$$

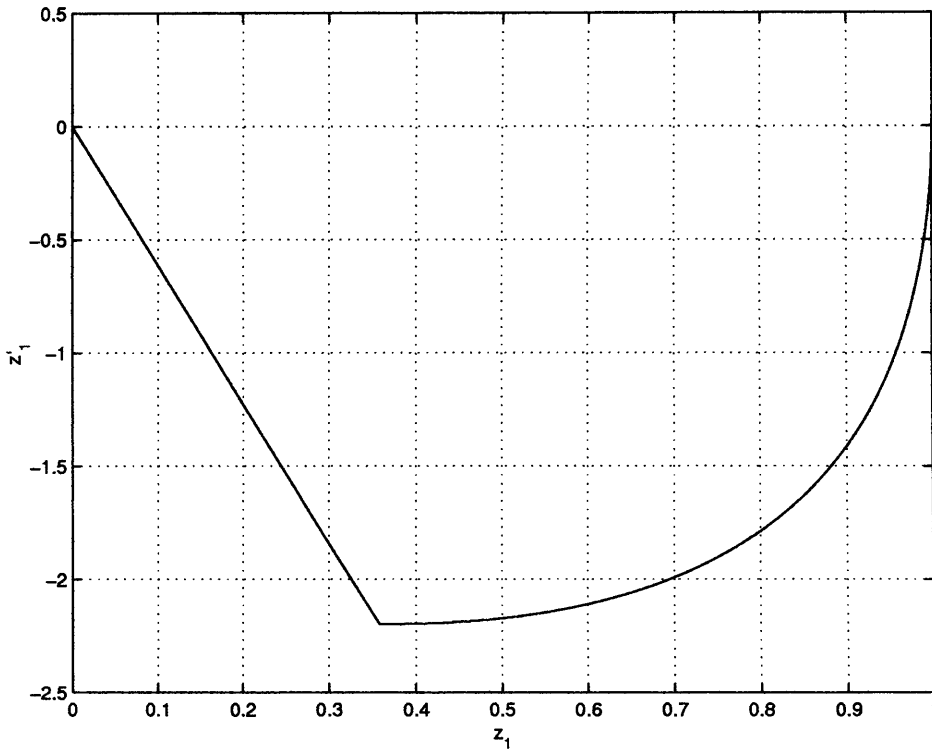
is obtained.

In the literature, this is referred to as the η -reachability condition [105, 106].

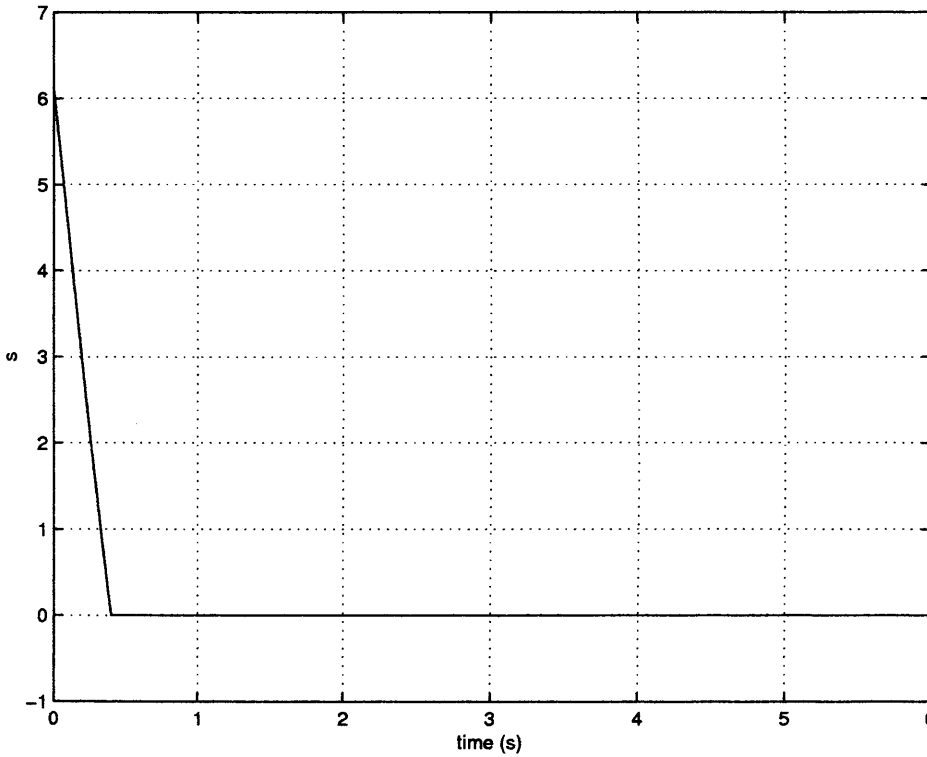
From this result, it can be seen that the condition of the inequality in Equation (4.24) is satisfied for all points on the (z_1, \dot{z}_1) plane, so that the system slides the first time it intercepts the switching surface. This can be seen in Figure 4.5. Other ways of selecting l_1 and l_2 are described in [31].

4.2.4 Robustness to matched uncertainty

As stated earlier, in most applications, there will be discrepancies between a system model and the actual plant. These may arise for many reasons, including model simplifications, or



a) Phase portrait



b) Switching function

Figure 4.6: Phase portrait and switching function with uncertainty, using controller given in Equation (4.21) and ρ from Equation (4.27)

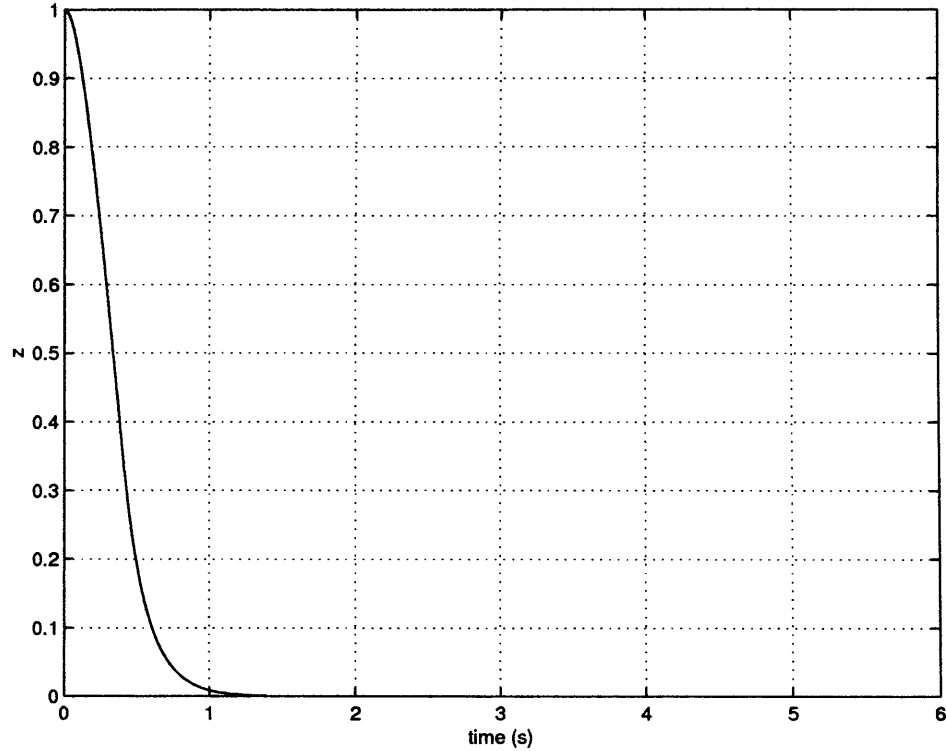


Figure 4.7: z_1 against time with controller given in Equation (4.21) and ρ Equation (4.27)

parameter variations. In the passenger vehicle presented, there is room for such discrepancy, such as variations in tyre type, and level of maintenance, or (more significantly) load variability and corresponding shifting of the vehicle centre of gravity. Consider, that the system presented in Equation (4.9) is subject to uncertainty in the range space of the input distribution matrix such that

$$A_{21} \Rightarrow A_{21} + \Delta_{21} \quad A_{22} \Rightarrow A_{22} + \Delta_{22} \quad (4.25)$$

where Δ_{21} , Δ_{22} represent some bounded uncertainty, so that Equation (4.1) can now be written as

$$\dot{z}(t) = \begin{bmatrix} 0 & 1 \\ A_{21} + \Delta_{21} & A_{22} + \Delta_{22} \end{bmatrix} z(t) + \begin{bmatrix} 0 \\ 1 \end{bmatrix} u(t) \quad (4.26)$$

Now let ρ be defined as

$$\rho = r_1|z_1| + r_2|z_2| + \eta \quad (4.27)$$

where r_1, r_2 are positive scalars designed to be greater than the bounds on the values of Δ_{21}, Δ_{22} respectively, $\eta > 0$ and $m = -A_{22}$ as before. Thus, Equation (4.22) becomes

$$\begin{aligned}
 s\dot{s} &= s(m\dot{z}_1 + \dot{z}_2) \\
 &= s(m\dot{z}_1 + (A_{21} + \Delta_{21})z_1 + (A_{22} + \Delta_{22})z_2 + u) \\
 &= s((A_{21} + \Delta_{21})z_1 + (A_{22} + \Delta_{22} - A_{22})z_2 - A_{21}z_1 - \rho \operatorname{sgn}(s)) \\
 &= s(\Delta_{21}z_1 + \Delta_{22}z_2 - \rho \operatorname{sgn}(s)) \\
 &\leq |s|(|\Delta_{21}||z_1| + |\Delta_{22}||z_2| - \rho) \\
 &\leq |s|((|\Delta_{21} - r_1||z_1| + (|\Delta_{22}| - r_2)|z_2|) - \eta|s|) \\
 &\leq -\eta|s|
 \end{aligned} \tag{4.28}$$

if $|\Delta_{21}| \leq r_1$ and $|\Delta_{22}| \leq r_2$.

Let $\Delta_{21} = 0.1|A_{21}|$, $\Delta_{22} = 0.1|A_{22}|$, but let $r_1 = 0.2|A_{21}|$, $r_2 = 0.2|A_{22}|$.

It can be seen that with a sufficiently large choice of ρ , the system can be forced to intercept and, then, remain on the sliding surface, despite the variations in A_{21}, A_{22} (see Figure 4.6). As stated earlier, once on the sliding surface, the system is forced to follow the reduced-order sliding motion described by the first-order decay in Equation (4.19), which is independent of the uncertainty. The state, z_1 is shown in Figure 4.7. From this, it can be concluded that the sliding mode controller presented is robust to bounded uncertainty in the channel of the control signal, known as *matched* uncertainty [31].

4.2.5 Equivalent control

As argued earlier, the purpose of the control action is to ensure that the trajectories are driven towards and forced to remain on the sliding surface to guarantee a sliding motion. Suppose that at time t_s the switching surface is reached, and an ideal sliding motion takes place. It follows that the switching function $s(t) = 0$ for all $t > t_s$, which in turn implies that $\dot{s} = 0$ for all $t \geq t_s$. Once sliding is attained, the control action which maintains the motion on the sliding surface is known as the *equivalent control* action [112, 114]. This is not the control signal which is actually applied to the plant but may be thought of as the control signal which

is applied 'on average'. The equivalent control also provides a useful means of capturing precisely the uncertainty or disturbance in the closed-loop system, without having any *a priori* knowledge of it, as a result of exactly cancelling it out. From Equation (4.16) it can be seen that during sliding motion

$$u_{eq} = -A_{21}z_1 \quad (4.29)$$

in this particular example.

Equivalent control: example

Consider the modified system

$$\dot{z}(t) = \begin{bmatrix} 0 & 1 \\ -19.3957 & -6.1435 \end{bmatrix} z(t) + \begin{bmatrix} 0 \\ 1 \end{bmatrix} u(t) + \begin{bmatrix} 0 \\ 1 \end{bmatrix} 0.5 \sin 20t \quad (4.30)$$

where the final *sine* term is unmodelled, whilst $\rho \geq 0.5$. Figure 4.8 shows how the equivalent control, once the closed-loop system is sliding ($t \gtrsim 0.6$), exactly cancels out the unmodelled term.

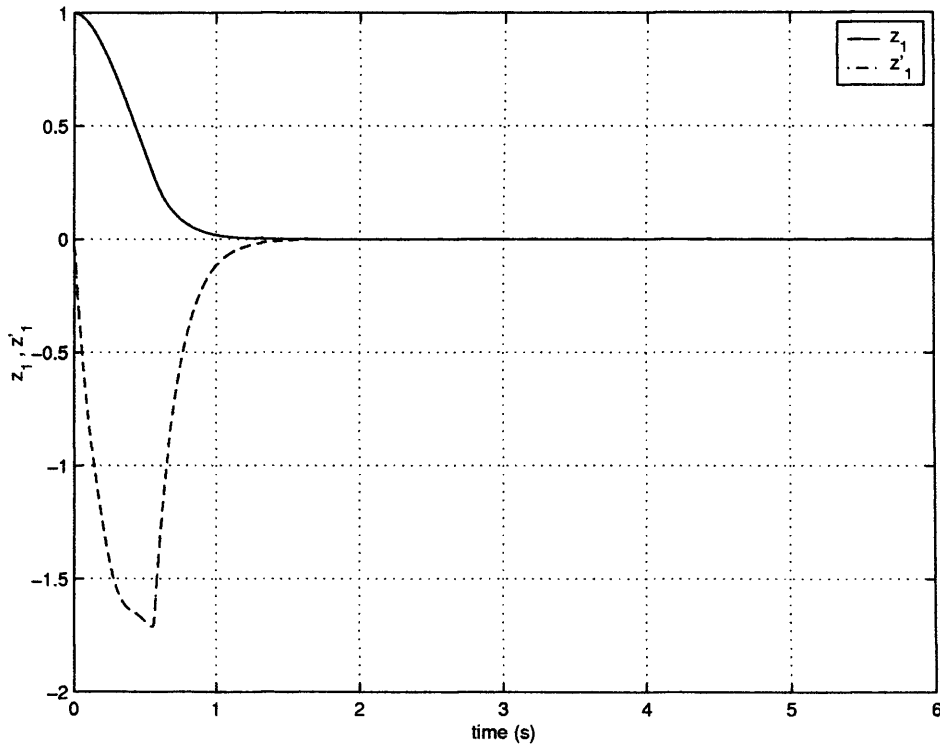
4.2.6 Increasing rate at which switching surface is attained

In the control structure used in Section 4.2.5, the value of ρ has been chosen much greater than is actually necessary to account for the matched uncertainty. Reducing it would, on the one hand be advantageous, as it would reduce the amplitude of the high-frequency switching, which would reduce the wear and tear on the plant actuators. However, a reduction in ρ , with no other adjustment, would also cause the system to take longer to reach the switching surface. For this reason, an additional term, Φ , is often introduced. Suppose the gains in Equation (4.21) are chosen as

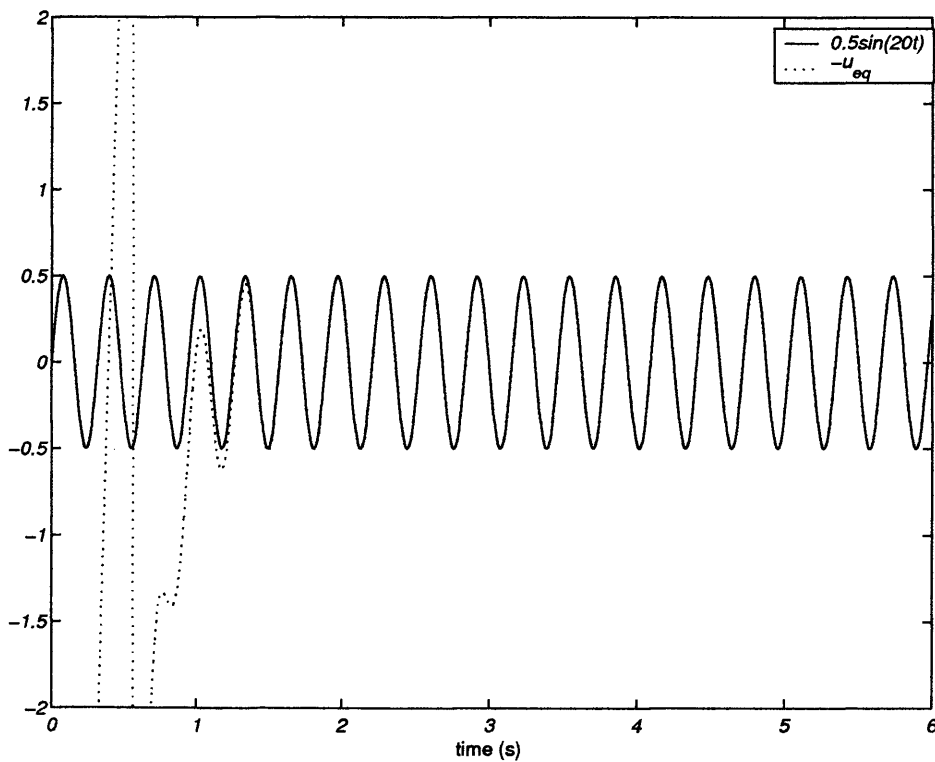
$$l_1 = -(A_{21} + \Phi m) \quad \text{and} \quad l_2 = -\Phi \quad (4.31)$$

where Φ is a positive design scalar and $m = -A_{22}$, leading to the new control law

$$u = -(A_{21} + \Phi m)z - \Phi \dot{z} - \rho \text{sgn}(s) \quad (4.32)$$



a) System states



b) Comparison of $0.5\sin(20t)$ term and the equivalent control signal

Figure 4.8: System states and equivalent control signal with unmodelled sine term, using controller given in Equation (4.21) and ρ from Equation (4.27)

Now Equation (4.16) becomes

$$\begin{aligned}
s\dot{s} &= s(m\dot{z}_1 + \dot{z}_2) = s(m\dot{z}_1 + A_{21}z_1 + A_{22}\dot{z}_1 + u) \\
&= s((A_{21} - A_{21} - \Phi m)z_1 + (A_{22} - A_{22} - \Phi)z_2 - \rho \operatorname{sgn}(s)) \\
&= s(-\Phi(mz_1 + z_2) - \rho \operatorname{sgn}(s)) \\
&= s(-\Phi s - \rho \operatorname{sgn}(s)) \\
&= -\Phi s^2 - \rho |s| \\
&\leq -\Phi s^2 - \eta |s|
\end{aligned} \tag{4.33}$$

where $\rho > \eta$, so that the η -reachability condition is established, and sliding will take place in finite time. Now, ignoring the non-linear term in Equation (4.33), it follows that

$$\frac{d}{dt}|s| \leq -\Phi |s| \tag{4.34}$$

which implies

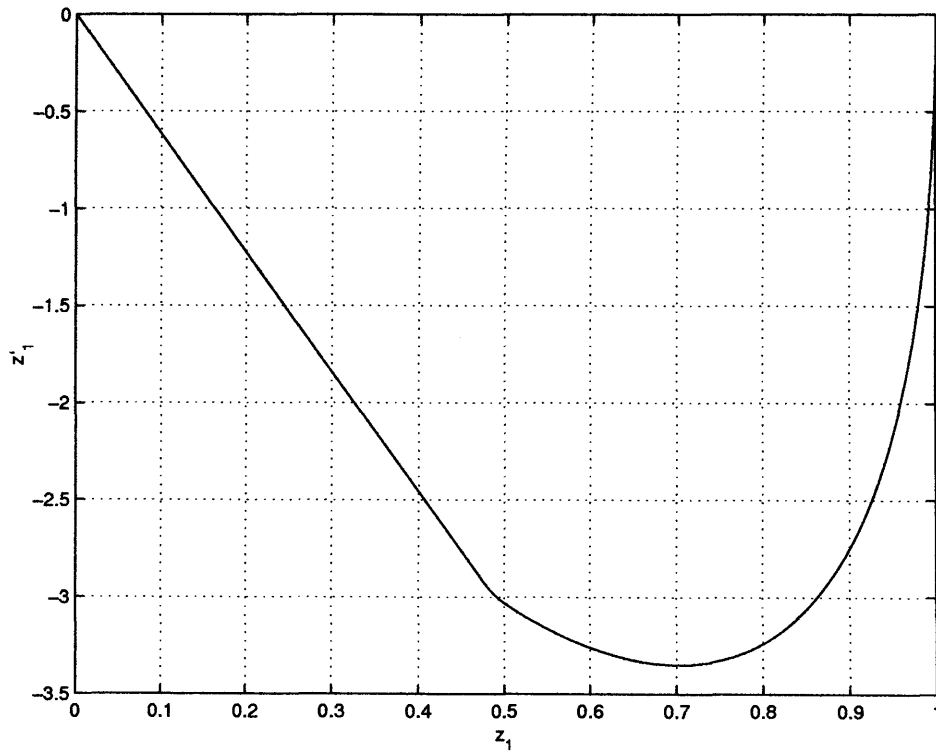
$$|s|(t) \leq |s(0)|e^{-\Phi t} \tag{4.35}$$

where $|s(0)|$ represents the initial distance of the system from the sliding surface. From this, the parameter, Φ , can be seen to affect the rate at which the sliding surface is attained. Thus, the two parameters may be tuned together. The quantity ρ may be made small, in order to reduce the amplitude of switching, whilst Φ may be chosen to determine the time taken for the system to intercept the switching surface. The time taken to attain sliding with ρ reduced so that $r_1 = 0.15|A_{21}|$, $r_2 = 0.15|A_{22}|$, while $\Phi = 10$, is shown in Figure 4.9, as is the performance of z_1 .

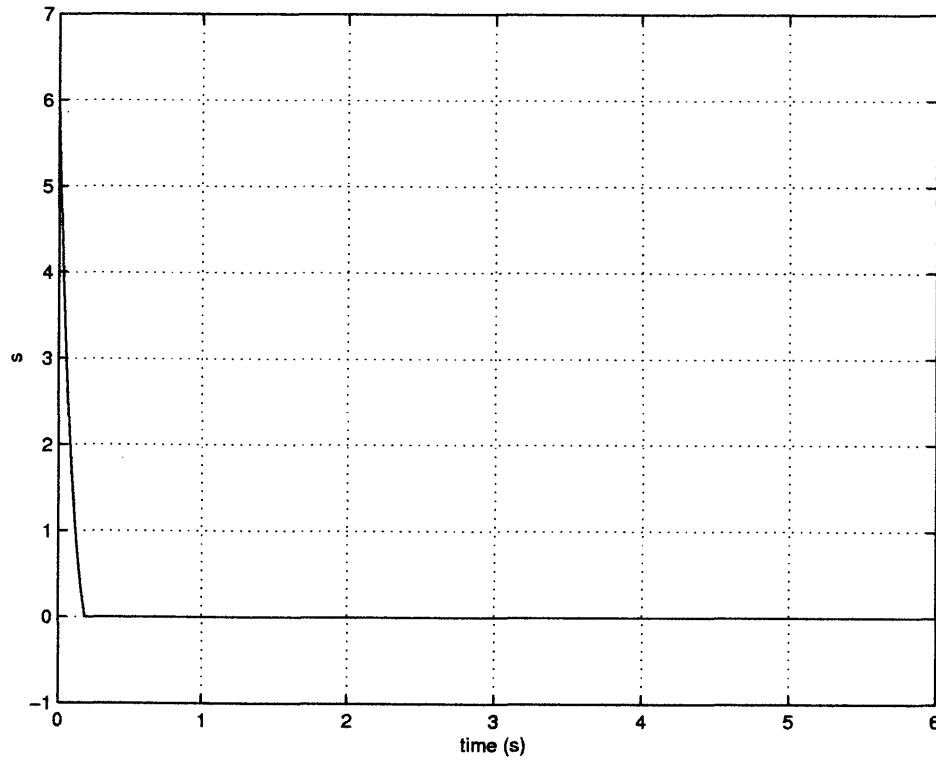
4.2.7 Pseudo-sliding

In the case of vehicle dynamics control, as in the majority of applications, a discontinuous control signal would not be considered acceptable. Such high frequency switching would have a rapid, detrimental affect upon actuators and tyres, if it were achievable at all. Therefore, it is necessary to remove this chattering. A simple way of doing this is to replace the discontinuous *signum* function with an approximation, such as the sigmoid-like function

$$\nu_\delta(s) = \frac{s}{|s| + \delta} \tag{4.36}$$

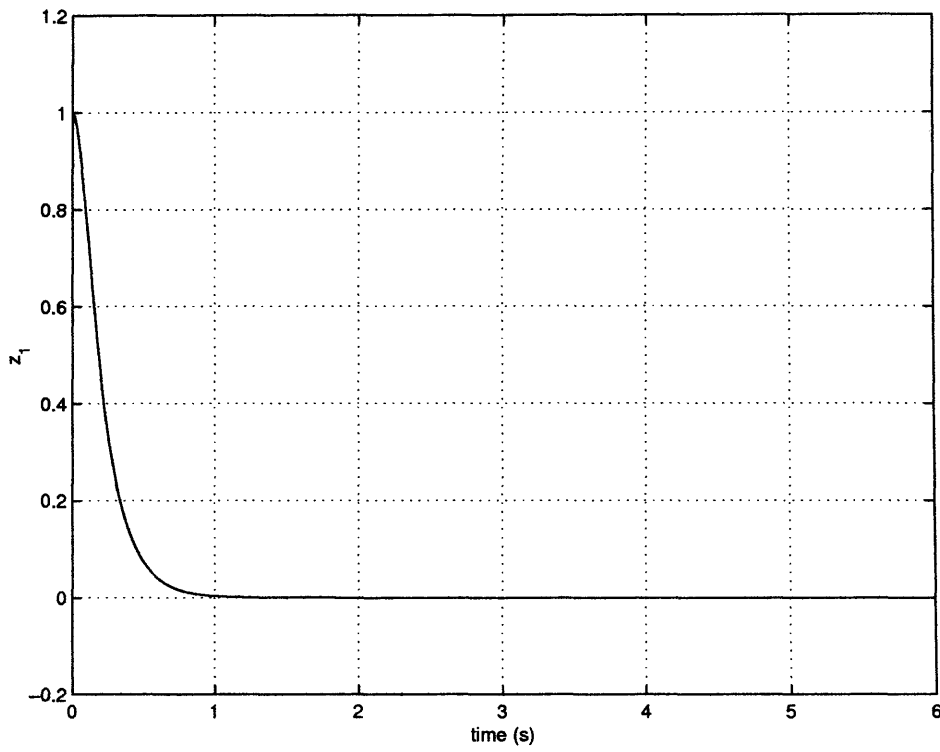


a) Phase portrait

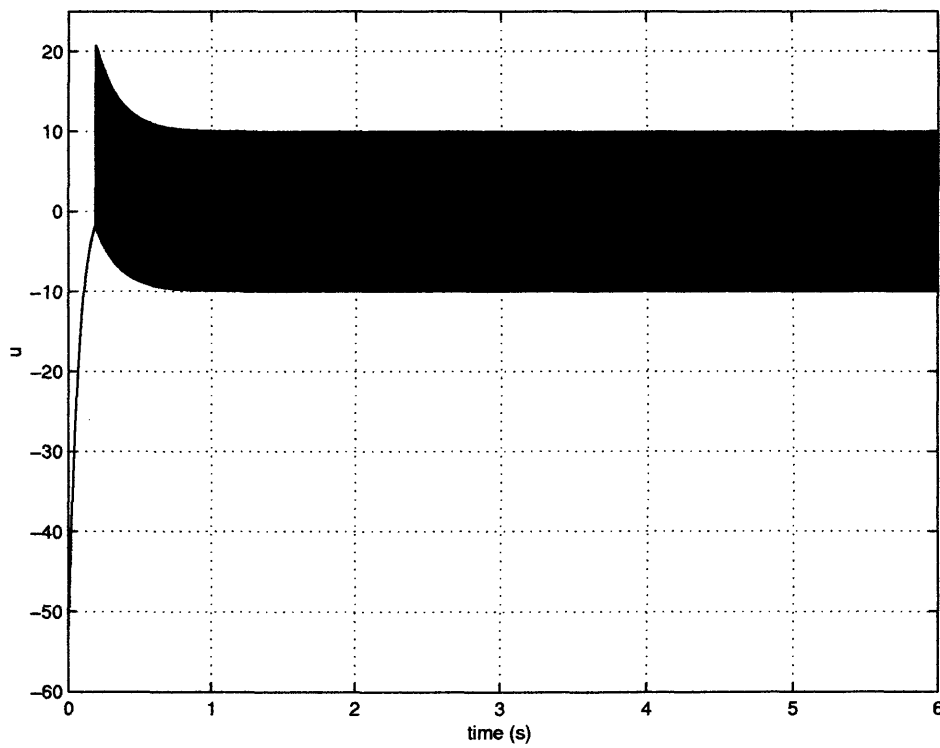


b) Switching function

Figure 4.9: Phase portrait and switching function with uncertainty, using controller given in Equation (4.32)



a) z_1



b) Control signal, u

Figure 4.10: z_1 and control signal, using controller given in Equation (4.32)

where δ is a small, positive design scalar. It can be seen that as $\delta \rightarrow 0$, so $\nu_\delta(\cdot) \rightarrow \text{sgn}(\cdot)$.

Using a value of $\delta = 0.01$, it can be seen that, while the performance of z_1 is visually identical (compare Figure 4.11a with Figure 4.10a), the control action is greatly smoothed (compare Figure 4.11b with Figure 4.10b).

As this control structure only drives the states to within a neighbourhood of the switching surface (see Figure 4.12), an ideal sliding motion can no longer be said to take place. However, the design of δ can be viewed as a trade-off between the two goals of maintaining ideal performance and ensuring a smooth control action. Furthermore, an arbitrarily close approximation to ideal sliding may be obtained by making δ small. Such a smoothed control law is often referred to as generating pseudo-sliding [31, 112].

4.3 MIMO Systems

The example shown here is a simple single-input system, which was chosen as it was useful for demonstrating the principles of sliding mode control. However, the same ideas can be relatively easily transferred into a multi-input systems context. Consider the nominal linear model of a system represented by

$$\dot{x}(t) = Ax(t) + Bu(t) \quad (4.37)$$

with n states and m inputs, where $\text{rank}(B) = m$ and (A, B) is a controllable pair. It is always possible to perform a change of coordinates

$$z(t) = T_r x(t) \quad (4.38)$$

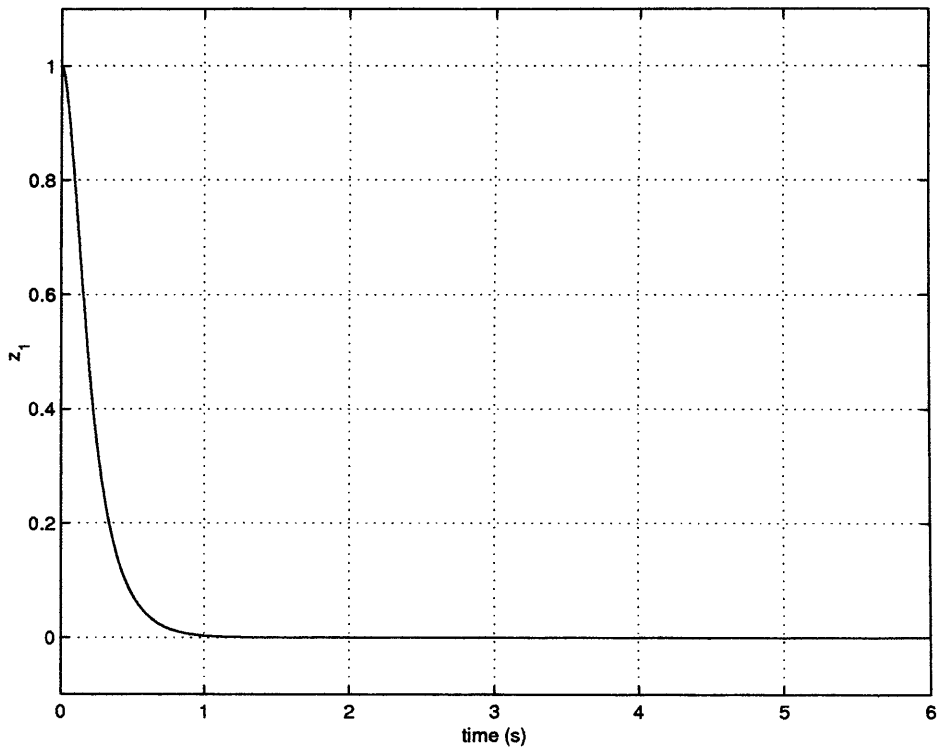
where the orthogonal matrix, T_r , is chosen such that the input distribution matrix (and the state distribution matrix) may be partitioned into the form

$$T_r A T_r^T = \begin{bmatrix} A_{11} & A_{12} \\ A_{21} & A_{22} \end{bmatrix} \quad T_r B = \begin{bmatrix} 0 \\ B_2 \end{bmatrix} \quad (4.39)$$

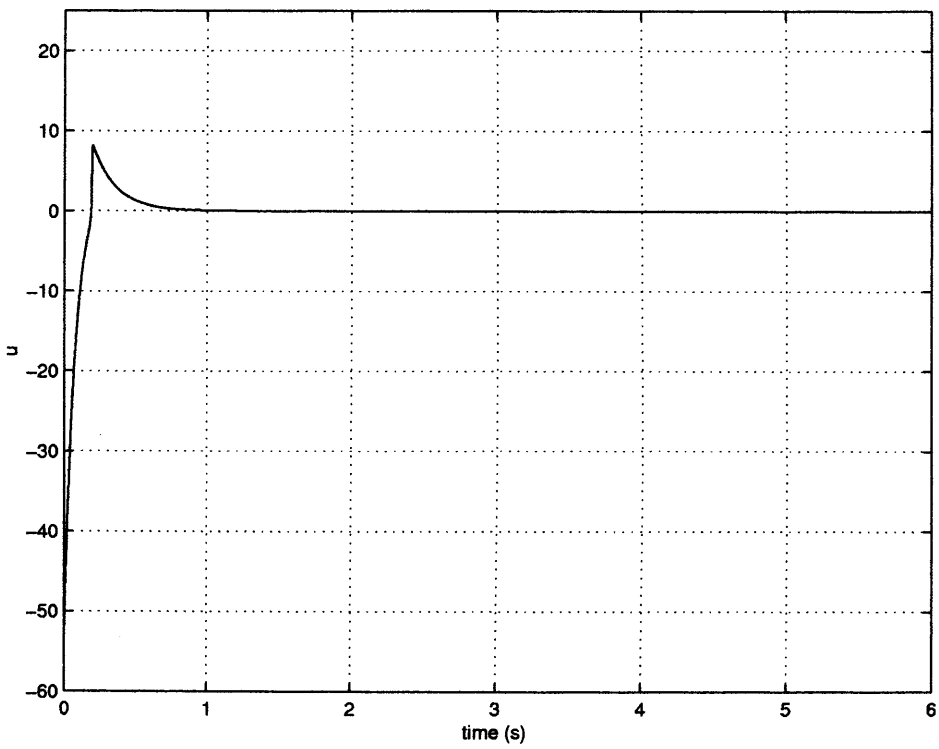
where $B_2 \in \mathbb{R}^{m \times m}$ and is nonsingular. In the new states, the system may be represented as

$$\dot{z}_1(t) = A_{11} z_1(t) + A_{12} z_2(t) \quad (4.40)$$

$$\dot{z}_2(t) = A_{21} z_1(t) + A_{22} z_2(t) + B_2 u(t) \quad (4.41)$$

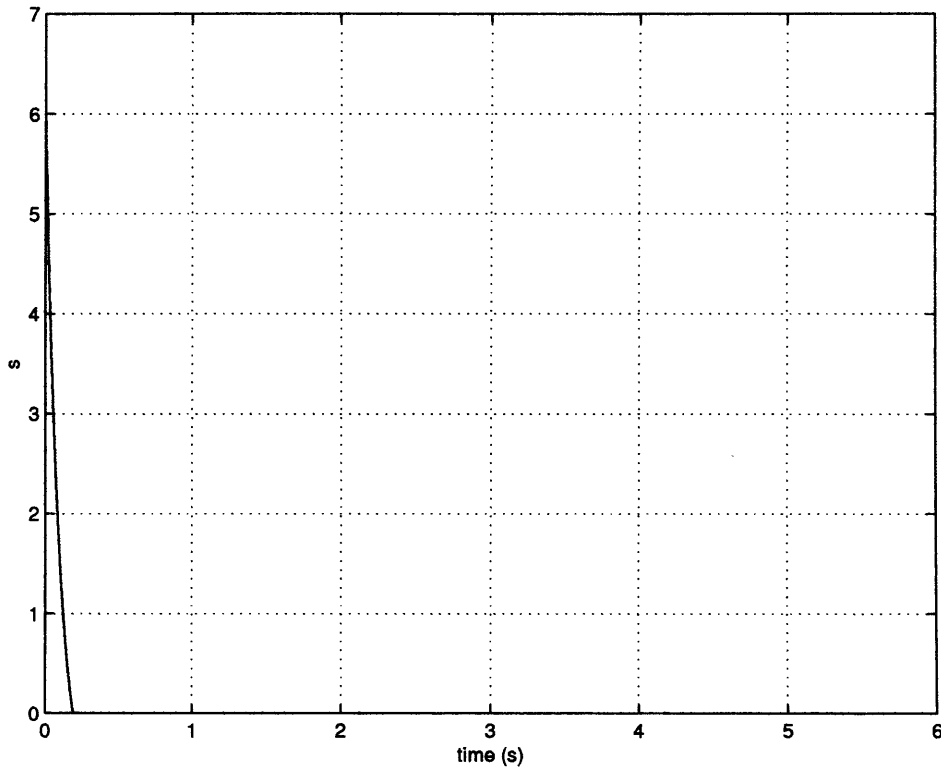


a) z_1

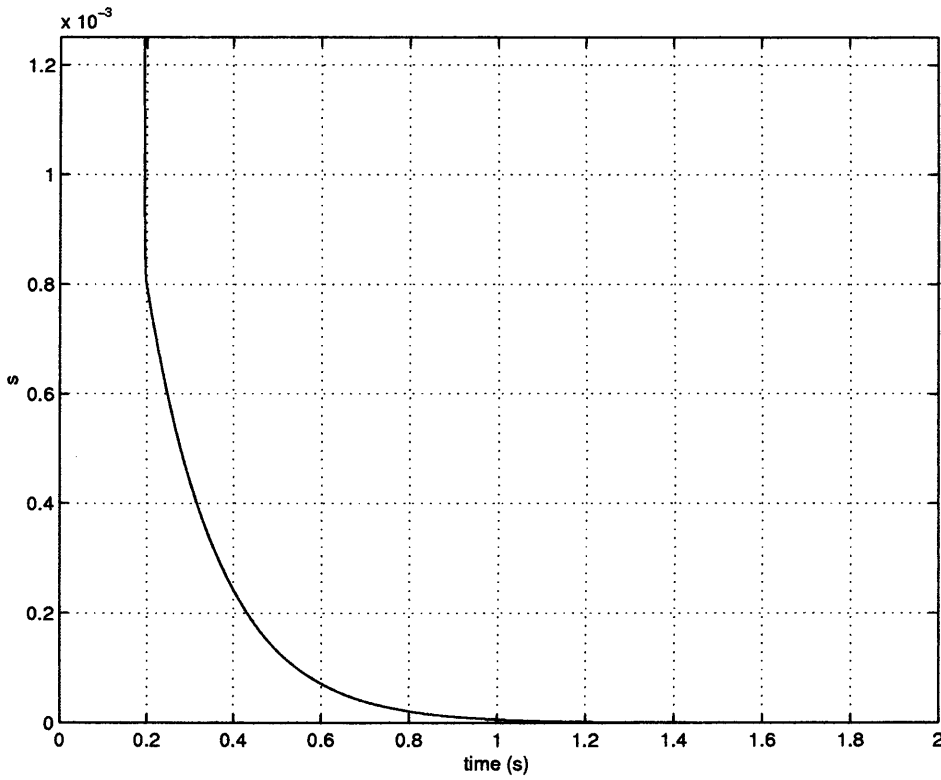


b) Control signal, u

Figure 4.11: Pseudo-sliding state z_1 and control signal against time



a) Switching function



b) Switching function close-up

Figure 4.12: Pseudo-sliding switching function

where $z_1 \in \mathbb{R}^{n-m}$ and $z_2 \in \mathbb{R}^m$. This representation is known as regular form. In this form m states are dependent on the control signals, while $n - m$ states are independent of the control signal. The system state matrix is partitioned into the *Range* space and the *Null* space, respectively.

A switching function can be defined as

$$s(t) = Sx(t) \quad (4.42)$$

which may be written in the new coordinates as

$$s(t) = S_1 z_1(t) + S_2 z_2(t) \quad (4.43)$$

where

$$ST_r^T = [S_1 \quad S_2] \quad (4.44)$$

so that SB is nonsingular. This guarantees the existence of a unique equivalent control [114]. As in the example given earlier, the switching function will be equal to zero during sliding motion, so that Equation (4.43) becomes

$$S_1 z_1(t) + S_2 z_2(t) = 0 \quad (4.45)$$

which may be re-arranged to give

$$z_2(t) = -S_2^{-1} S_1 z_1(t) \quad (4.46)$$

giving

$$z_2(t) = -M z_1(t) \quad (4.47)$$

where $M \in \mathbb{R}^{m \times (n-m)}$ is defined to be

$$M = S_2^{-1} S_1 \quad (4.48)$$

Thus, it can be seen in Equation (4.47) that the z_2 partition is linearly dependent on the z_1 partition, so that the sliding mode is now governed by Equations (4.40, 4.47). Equating these two equations for z_2 , the system is described by

$$\dot{z}_1(t) = (A_{11} - A_{12}M)z_1(t) \quad (4.49)$$

This closes the loop in Equation (4.40), acting as an $(n - m)^{th}$ order system in which z_2 has the role of a linear full-state feedback control signal. It can be shown that if the pair (A, B) is controllable, the pair (A_{11}, A_{12}) is controllable. Therefore there exists a M which will make $A_{11} - A_{12}M$ stable.

4.3.1 Design Methods

It is clear from the argument above that S_2 plays no role in the reduced order motion. However, choosing M does not uniquely determine S since there are m^2 degrees of freedom in the relationship

$$S_2M = S_1 \quad (4.50)$$

This is not really an issue in the research carried out, as it will be seen that the system has only $m = 1$ inputs. Nevertheless, the hyperplane matrix S will be determined from M by letting $S_2 = I_m$, giving

$$ST_r = [M \quad I_m] \quad (4.51)$$

so minimizing the calculation in determining S from M , and reducing the possibility of numerical errors.

The problem now becomes the design of M . One available method for the design of M is based upon a robust pole assignment approach [80, 119]. The basic idea of this method involves placing the eigenvalues of the sliding mode system arbitrarily in the complex plane by suitable choice of the matrix M . The remaining degrees of freedom available in the assignment problem are used to shape the system response using a judicious choice of eigenvector form. A second method involves the minimization of an integral cost function with quadratic integrand [115]. This method is described here more fully, as it is the method which is employed in the controller design for the vehicle model studied later. The method allows different weightings to be placed upon different elements of the state vector. Consider the problem of minimizing the quadratic performance index

$$J = \frac{1}{2} \int_{t_s}^{\infty} x(t)^T Q x(t) dt \quad (4.52)$$

where Q is a symmetric positive definite design matrix, and t_s is the time at which sliding commences. The aim is to minimize Equation (4.52) subject to the system Equation (4.37). It is assumed that the state of the system at time t_s , $x(t_s)$, is a known initial condition and is such that $x(t) \rightarrow 0$ as $t \rightarrow \infty$. The matrix Q is transformed and partitioned compatibly with z :

$$T_r Q T_r^T = \begin{bmatrix} Q_{11} & Q_{12} \\ Q_{21} & Q_{22} \end{bmatrix} \quad (4.53)$$

where $Q_{21} = Q_{12}^T$. Equation (4.52) may now be expressed as

$$J = \frac{1}{2} \int_{t_s}^{\infty} z_1^T Q_{11} z_1 + 2z_1^T Q_{12} z_2 + z_2^T Q_{22} z_2 dt \quad (4.54)$$

By defining

$$\hat{Q} = Q_{11} - Q_{12} Q_{22}^{-1} Q_{21} \quad (4.55)$$

and

$$v_q = z_2 + Q_{22}^{-1} Q_{21} z_1 \quad (4.56)$$

then Equation (4.54) becomes

$$J = \frac{1}{2} \int_{t_s}^{\infty} z_1^T \hat{Q} z_1 + v_q^T Q_{22} v_q dt \quad (4.57)$$

It is then possible to eliminate z_2 from the original constraint Equation (4.40) using Equation (4.56), giving the new constraint equation

$$\dot{z}_1(t) = \hat{A} z_1(t) + A_{12} v_q(t) \quad (4.58)$$

where

$$\hat{A} = A_{11} - A_{12} Q_{22}^{-1} Q_{21} \quad (4.59)$$

It follows that a unique positive definite solution, P_1 , is guaranteed for the Algebraic Riccati Equation which is associated with the problem defined by Equations (4.57, 4.58)

$$P_1 \hat{A} + \hat{A}^T P_1 - P_1 A_{12} Q_{22}^{-1} A_{12}^T P_1 + \hat{Q} = 0 \quad (4.60)$$

The optimal v_q minimizing Equation (4.57) is given by

$$v_q = -Q_{22}^{-1} A_{12}^T P_1 z_1 \quad (4.61)$$

This expression can be inserted into Equation (4.56) to yield

$$z_2 = -Q_{22}^{-1}(A_{12}^T P_1 + Q_{21})z_1 \quad (4.62)$$

Comparing this with Equation (4.47) yields the expression

$$M = Q_{22}^{-1}(A_{12}^T P_1 + Q_{21}) \quad (4.63)$$

As argued in Section 4.2 the design of a sliding mode control is undertaken in two steps: the selection of the switching function to define the sliding surface; and then the synthesis of a control law to induce (in finite time) a sliding mode and maintain it thereafter. Section 4.3.1 has discussed several approaches to select the sliding surface, the next section introduces a systematic method to generate an appropriate control law.

4.3.2 Multivariable *unit vector* control law

There are several approaches to the problem of developing control laws to induce a sliding motion - see [31] for example. In this subsection, one particular form is chosen. The *unit vector* control law described in this section was developed in [31] from its original incarnation by Ryan & Corless [95].

The proposed control law has two components; a linear component and a nonlinear, discontinuous component:

$$u(t) = u_l(t) + u_n(t) \quad (4.64)$$

where the linear component is given by

$$u_l = -\Lambda^{-1}(SA - \Phi S)x(t) \quad (4.65)$$

where $\Phi \in \mathbb{R}^{m \times m}$ is any stable design matrix and $\Lambda = SB$. The nonlinear component is defined to be

$$u_n(t) = -\rho(t, x)\Lambda^{-1} \frac{P_2 s(t)}{\|P_2 s(t)\|} \quad \text{for } s(t) \neq 0 \quad (4.66)$$

where $P_2 \in \mathbb{R}^{m \times m}$ is a symmetric positive definite matrix satisfying the Lyapunov equation

$$P_2 \Phi + \Phi^T P_2 = -I \quad (4.67)$$

and the scalar function $\rho(t, x)$ depends only on the magnitude of the uncertainty. The linear part involves a term which includes the nominal equivalent control $(-\Lambda^{-1}SA)$ and a linear term $(\Lambda^{-1}\Phi S(t))$ to provide asymptotic reaching of the sliding surface. As shown in Section 4.2.6 (which is just a scalar example of the generic multivariable form in (4.65)), the inclusion of this term is beneficial in terms of manipulating the rate at which sliding is attained. This control law guarantees that the switching surface is reached in finite time despite the disturbance or uncertainty, and once the sliding motion is attained, it is completely independent of the uncertainty. This control structure will be used later in Chapter 5 when developing a controller for split- μ braking.

4.4 Observers and Observer Design

4.4.1 State Estimation

It has been demonstrated that it is possible to readily determine a state feedback sliding mode control system for a controllable linear system. In practice it may not be feasible to measure all the state variables for a given system. If only a subset of state information is available, the feedback control problem must now consider a system of the form:

$$\dot{x}(t) = Ax(t) + Bu(t) \quad (4.68)$$

$$y(t) = Cx(t) \quad (4.69)$$

where $y \in \mathbb{R}^p$ denotes an available vector of output measurements. One option is to attempt to design an output feedback controller, i.e. using only the subset of states which are measurable in the control law. An alternative method to overcome problems with restricted measurements is to use a state feedback controller with a dynamic system whose purpose is to estimate the state vector. Such a dynamic system is called an *observer* [31, 73]. For the system in Equations (4.68, 4.69) a corresponding observer is defined by

$$\dot{\hat{x}}(t) = (A + LC)\hat{x}(t) + Bu(t) - Ly(t) \quad (4.70)$$

where the design matrix $L \in \mathbb{R}^{n \times p}$ is selected to ensure the eigenvalues of $A + LC$ have negative real parts, and \hat{x} is the estimated state vector. Alternatively, Equation (4.70) can be

expressed as

$$\dot{\hat{x}}(t) = A\hat{x}(t) + Bu(t) - L(Cx(t) - C\hat{x}(t)) \quad (4.71)$$

and, hence, the observer is seen to be a model of the plant, which is driven by the mismatch between the plant and observer outputs. The difference between the actual state $x(t)$ and the estimated state $\hat{x}(t)$ can be defined to be

$$e(t) = x(t) - \hat{x}(t) \quad (4.72)$$

Then it is straightforward to establish that the dynamic behaviour of the error signal is given by

$$\begin{aligned} \dot{e}(t) &= Ax(t) + Bu(t) - (A\hat{x}(t) + Bu(t) - LC(x - \hat{x})) \\ &= A(x - \hat{x}) + LC(x - \hat{x}) \\ &= (A + LC)e(t) \end{aligned} \quad (4.73)$$

As $A + LC$ is a stable matrix, it follows that the error vector will converge to zero from any initial conditions, and thus $\hat{x}(t)$ will converge to $x(t)$. Judicious choice for the poles of $A + LC$ will ensure that the error tends to zero rapidly. An observer may only need to estimate a subset of the n state variables, those which are unmeasurable. In this case the observer is called a *reduced-order observer* [31, 73]. There are a class of observers in the literature using sliding mode techniques. In this case the observer is driven by discontinuous terms which depend on $Ce(t)$. A class of sliding mode observer is described in the next subsection.

4.4.2 Examples of Sliding Mode Observers

In this section, the earliest sliding mode observer described in the literature [114] will be described and applied to the Bicycle model in Section 3.6 is used as an example. In this case it will be assumed that the yaw rate state, r , is measurable, and that an estimate of the lateral velocity state, v is sought. The system now takes the form given in Equation (4.68):

$$\dot{x}(t) = A_b x(t) + B_b u(t) \quad (4.74)$$

$$y(t) = C_b x(t) \quad (4.75)$$

where y is the measured output, r , the control signal is given by u , and $C_b = [0 \ 1]$. Now define

$$A_b = \begin{bmatrix} A_{11} & A_{12} \\ A_{21} & A_{22} \end{bmatrix} \quad (4.76)$$

$$B_b = \begin{bmatrix} B_1 \\ B_2 \end{bmatrix} \quad (4.77)$$

and let $x_1 = v$ (and $y = x_2 = r$). The nominal system can now be written as

$$\dot{x}_1 = A_{11}x_1 + A_{12}y + B_1u \quad (4.78)$$

$$\dot{y} = A_{21}x_1 + A_{22}y + B_2u \quad (4.79)$$

The observer proposed by Utkin [113] has the form

$$\dot{\hat{x}}_1 = A_{11}\hat{x}_1 + A_{12}\hat{y} + B_1u + L\nu \quad (4.80)$$

$$\dot{\hat{y}} = A_{21}\hat{x}_1 + A_{22}\hat{y} + B_2u - \nu \quad (4.81)$$

where (\hat{x}_1, \hat{y}) are the state estimates for (x_1, y) , $L \in \mathbb{R}^{(n-p) \times p}$ is a constant feedback gain matrix and the discontinuous vector, or in this case scalar, ν is defined by

$$\nu = N \operatorname{sgn}(\hat{y} - y) \text{ for } N \in \mathbb{R}_+ \quad (4.82)$$

where 'sgn' represents the signum function, as before.

The error between the estimates and the true states may be written as $e_1 = \hat{x}_1 - x_1$ and $e_y = \hat{y} - y$, and so, from Equations (4.78)-(4.81), the following error system is obtained:

$$\dot{e}_1 = A_{11}e_1 + A_{12}e_y + L\nu \quad (4.83)$$

$$\dot{e}_y = A_{21}e_1 + A_{22}e_y - \nu \quad (4.84)$$

Since the pair (A_b, C_b) is observable, the pair (A_{11}, A_{21}) is also observable [31]. As a consequence, L can be chosen to make $\lambda(A_{11} + LA_{21})$ lie in the open left half plane. Define a change of co-ordinates by

$$T_s = \begin{bmatrix} 1 & L \\ 0 & 1 \end{bmatrix} \quad (4.85)$$

and let

$$\begin{bmatrix} x'_1 \\ y \end{bmatrix} = T_s \begin{bmatrix} x_1 \\ y \end{bmatrix} \quad (4.86)$$

Then the error system, with respect to these new co-ordinates, can be written as

$$\dot{e}'_1 = A'_{11}e'_1 + A'_{12}e_y \quad (4.87)$$

$$\dot{e}_y = A_{21}e'_1 + A'_{22}e_y - \nu \quad (4.88)$$

where

$$\begin{bmatrix} A'_{11} & A'_{12} \\ A'_{21} & A'_{22} \end{bmatrix} = T_s A_b T_s^{-1} \quad (4.89)$$

and, in particular, $A'_{11} = A_{11} + LA_{21}$. It can be shown using singular perturbation theory that for large enough N , a sliding motion can be induced on the output error state in Equation (4.88). It follows that, after some time t_s , for all subsequent time, $e_y = 0$ and $\dot{e}_y = 0$. Equation (4.87) then reduces to

$$\dot{e}'_1 = A'_{11}e'_1 \quad (4.90)$$

which, by choice of L , represents a stable system and so $e'_1 \rightarrow 0$ as $t \rightarrow \infty$. Consequently, $\hat{x}_1 \rightarrow x_1$ can be constructed in the original co-ordinate system. The major practical difficulty in this approach is the selection of an appropriate gain N to induce a sliding motion in finite time.

Consider now the effect of adding a negative output error feedback term [27] to each equation of the Utkin observer in Equations (4.80)-(4.81). This results in a new error system governed by

$$\dot{e}'_1 = A'_{11}e'_1 + A'_{12}e_y - G_1e_y \quad (4.91)$$

$$\dot{e}_y = A'_{21}e'_1 + A'_{22}e_y - G_2e_y - \nu \quad (4.92)$$

By selecting $G_1 = A'_{12}$ and $G_2 = A'_{22} - A_{22}^s$, where A_{22}^s is any stable design matrix of appropriate dimension, then

$$\dot{e}'_1 = A'_{11}e'_1 \quad (4.93)$$

$$\dot{e}_y = A'_{21}e'_1 + A_{22}^s e_y - \nu \quad (4.94)$$

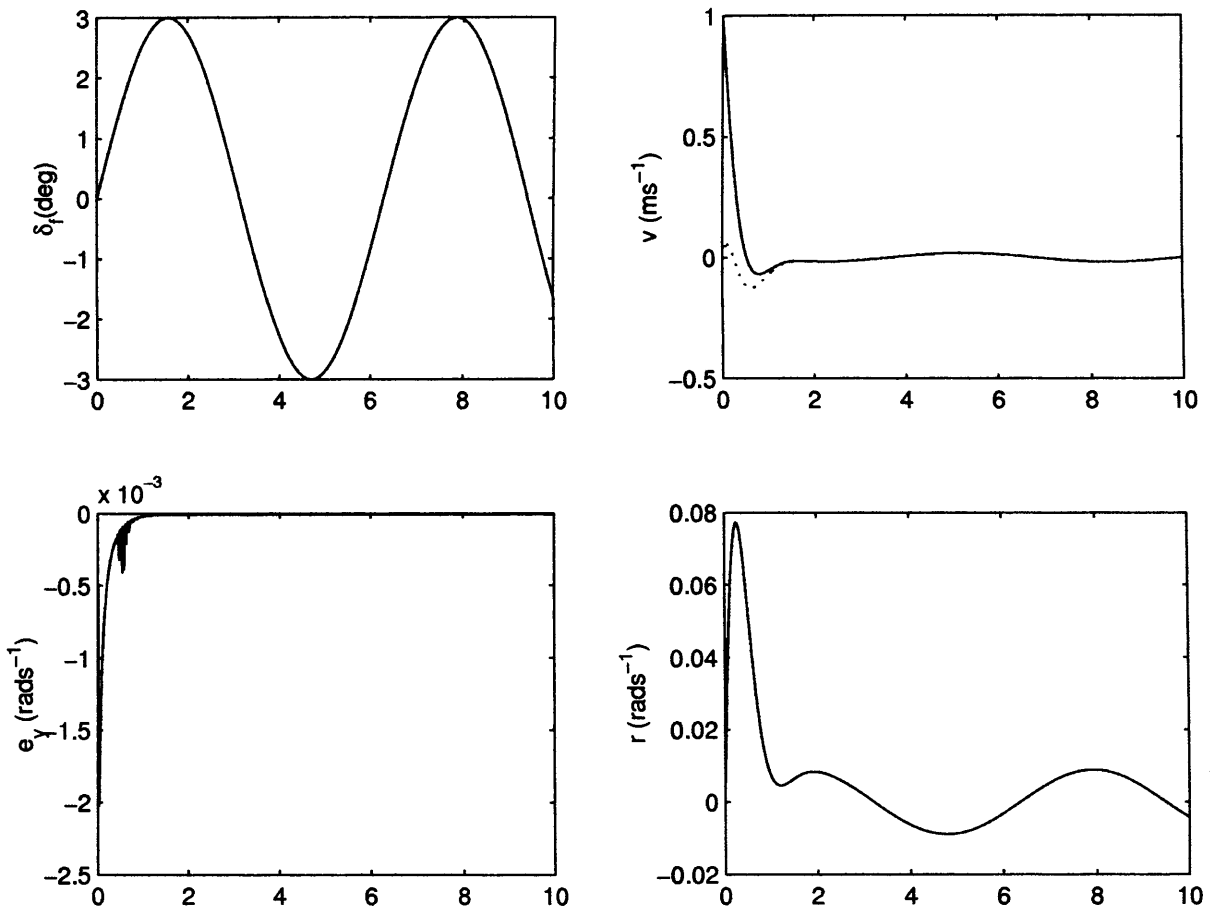


Figure 4.13: Observer example: bicycle model

so that, even if $\nu \equiv 0$, $e'_1 \rightarrow 0$ and $e_y \rightarrow 0$.

In this example, choose $L = -1.7473$, giving

$$G = \begin{bmatrix} G_1 & G_2 \end{bmatrix}^T = \begin{bmatrix} -1.7473 & -1 \end{bmatrix}^T \quad (4.95)$$

Figure 4.13 shows plots of a simulation of the bicycle model example using this observer design. The bicycle model is driven by a sinusoidal input signal (presented in top-left plot) to the front road-wheel angle, and a discrepancy has been included between the initial conditions of the plant and the observer - initial lateral velocity of the plant is $1ms^{-1}$ compared with $0ms^{-1}$ for the observer. The two states are shown on the right with the actual states given by a solid line and the observer estimated states given by a dotted line. The actual and estimated signal for the measured yaw rate output, r , are visually identical. The estimate of the lateral velocity state, v , tracks the actual lateral velocity signal at around $1s$ and is visually indistinguishable

thereafter. The output estimate error signal, e_y , is shown at the bottom-left, and is seen to quickly go to zero.

In this form, the nominal system is asymptotically stable for $\nu \equiv 0$ because the poles of the combined system are given by $\sigma(A'_{11}) \cup \sigma(A^s_{22})$ and, so, lie in the open left half complex plane. In the original Utkin observer, the switching action ν was potentially required to make the error system stable. The addition of a Luenberger type gain matrix, feeding back the output error, yields the potential to provide robustness against certain classes of uncertainty using the discontinuous portion, ν , and then to imply some information about this uncertainty.

A more sophisticated version of this observer will be used in Chapter 5 when developing a controller for split- μ braking. Again the observer will have both linear and discontinuous output error injection. In Section 5.2.3 a special choice of gain for the discontinuous injection term will be described which facilitates the analysis of the closed loop system obtained from using the observer as part of a controller/observer pair.

4.5 Conclusions

This chapter has introduced a number of concepts associated with the theory of Sliding Mode systems, including controller and observer methods, using the bicycle model as a simple two-state example. It has been shown that sliding mode techniques can, not only provide good performance, but also robustness to certain types of uncertainty, which is of great value in real applications in which plant/model mismatches may arise. These sliding mode concepts will be used in later chapters, and applied to particular vehicle dynamics problems. The next chapter (Chapter 5) uses both sliding mode control and observer techniques, demonstrated here, in a split- μ braking manoeuvre, whilst Chapter 6 uses sliding mode control techniques to produce a compensator-based controller, also in a split- μ braking manoeuvre.

Chapter 7 draws from the sliding mode observer methods, and uses them to reconstruct unknown signals in order to predict the emergence of various severe vehicle scenarios, including the split- μ braking manoeuvre investigated in Chapters 5+6.

Chapter 5

Split- μ Braking with Observer-Based Control

5.1 Introduction

In this chapter, a sliding mode observer-based controller - published with peer review [55, 56] - will be proposed which will seek to maintain a straight vehicle trajectory in the presence of asymmetric braking during a so-called split- μ manoeuvre. This is the first use of an observer-based sliding mode controller for this application available in the literature. The control scheme presented uses a minimum set of measured signals and benefits from sliding mode robustness properties.

The nonlinear model described in Chapter 3 will first be linearized numerically, to obtain a lower order model for controller/observer design purposes. The sliding mode methods presented in Chapter 4 will then be used to design a sliding mode controller and observer, designed from the linear vehicle model. Finally, open-loop and closed-loop simulations will be used to test the performance of the control scheme, using the nonlinear vehicle model described in Chapter 3. Further simulations will then be carried out to test the closed-loop robustness to certain parameter uncertainties.

5.1.1 Approach

The retention of vehicle stability and steerability in a harsh split- μ braking manoeuvre, as described in Section 2.5, may be sought via a number of different means. One approach is

to interpret the driver's hand-wheel command as a lateral acceleration and an implied yaw-rate [6, 77, 101]. In the straight-line trajectory split- μ braking scenario, this method would have a controller attempting to maintain zero yaw rate and yaw angle. However, it may be argued that maintaining a zero lateral deviation is of greater importance than zero yaw rate. Furthermore, these two goals may be mutually exclusive. This is because any steering applied by the controller or driver to counteract the yawing motion and keep the vehicle 'straight' will also cause lateral motion away from the central line. In order to prevent this, the vehicle must adopt a slight yaw angle. The controller must, therefore, allow the vehicle a transient yaw rate with which to develop the necessary yaw angle.

5.2 Sliding Mode Control System

A control scheme must now be designed which will seek to take the available outputs from the nonlinear vehicle model, described in Section 3.3, in simulation, and use them to generate a single control signal (road-wheel steering angle, δ_f) in order to minimize vehicle lateral deviation - without excessive yaw motion - in a harsh split- μ braking manoeuvre. Initially, the nonlinear model will be numerically linearized and manipulated into a more convenient form for controller design. A sliding mode controller will then be designed which will use certain states to generate an appropriate control signal. However, as not all of these outputs are assumed to be measurable, a sliding mode observer will also be designed which will use the available, measured outputs to estimate the required states, which are not measured. In the sliding mode controller used here, integral action is also introduced in order to improve the steady state tracking accuracy as well as transient performance.

5.2.1 Obtaining a Linear Numerical Model

The 8th-order nonlinear vehicle model given by Equations (3.1) - (3.22) was linearized numerically - using parameter values for a standard family saloon, given in Appendix B - about a steady-state operating point. The operating point chosen was a straight trajectory at $15ms^{-1}$ longitudinal velocity, with corresponding wheel angular velocities, zero lateral velocity, yaw rate and yaw angle, and a homogeneous road surface with friction coefficient $\mu = 0.8$. The

resulting 8th-order linear model - with states given by $[u \ v \ r \ \omega_1 \ \omega_2 \ \omega_3 \ \omega_4 \ \psi]^T$, as defined in Section 3.3 - is described by the system and input distribution matrices:

$$A = \begin{bmatrix} -4.006 & 0 & 0 & 0.319 & 0.319 & 0.319 & 0.318 & 0 \\ 0 & -2.724 & -13.808 & 0 & 0 & 0 & 0 & 0 \\ 0 & 0.730 & -4.782 & -0.150 & -0.151 & 0.150 & 0.151 & 0 \\ 313.423 & 0.000 & -225.037 & -99.668 & 0 & 0 & 0 & 0 \\ 313.423 & 0.000 & -226.291 & 0 & -99.668 & 0 & 0 & 0 \\ 313.423 & 0.000 & 225.037 & 0 & 0 & -99.668 & 0 & 0 \\ 313.423 & 0.000 & 226.291 & 0 & 0 & 0 & -99.668 & 0 \\ 0 & 0 & 1.000 & 0 & 0 & 0 & 0 & 0 \end{bmatrix} \quad (5.1)$$

and

$$B = \begin{bmatrix} 0 \\ 1.355 \\ 0.812 \\ 0 \\ 0 \\ 0 \\ 0 \\ 0 \end{bmatrix} \quad (5.2)$$

The outputs of interest are lateral velocity, v , yaw rate, r , and yaw angle, ψ . The wheel states may be altered by matrix manipulation to give the new system matrices:

$$A_d = \begin{bmatrix} -2.724 & -13.808 & 0 & 0 & 0 & 0 & 0 & 0 & 0 \\ 0.730 & -4.782 & -0.300 & -0.302 & 0 & 0 & 0 & 0 & 0 \\ 0 & -225.037 & -99.668 & 0 & 0 & 0 & 0 & 0 & 0 \\ 0 & -226.291 & 0 & -99.668 & 0 & 0 & 0 & 0 & 0 \\ 0 & 1.000 & 0 & 0 & 0 & 0 & 0 & 0 & 0 \\ 0 & 0 & 0 & 0 & 0 & -4.006 & 0.637 & 0.637 & 0 \\ 0 & 0 & 0 & 0 & 0 & 313.423 & -99.668 & 0 & 0 \\ 0 & 0 & 0 & 0 & 0 & 313.423 & 0 & -99.668 & 0 \end{bmatrix} \quad (5.3)$$

and

$$B_d = \begin{bmatrix} 1.355 \\ 0.812 \\ 0 \\ 0 \\ 0 \\ 0 \\ 0 \\ 0 \\ 0 \end{bmatrix} \quad (5.4)$$

with the new states $[v \ r \ \omega_{df} \ \omega_{dr} \ \psi \ u \ \omega_{ar} \ \omega_{af}]^T$, where ω_{af} , ω_{ar} are average front and rear wheel angular velocity states, respectively, and ω_{df} , ω_{dr} are differential front and rear wheel angular velocity states, respectively, given by:

$$\omega_{af} = \frac{\omega_1 + \omega_3}{2} \quad (5.5)$$

$$\omega_{df} = \frac{\omega_1 - \omega_3}{2} \quad (5.6)$$

$$\omega_{ar} = \frac{\omega_2 + \omega_4}{2} \quad (5.7)$$

$$\omega_{dr} = \frac{\omega_2 - \omega_4}{2} \quad (5.8)$$

It can be seen from Equation (5.3) that the final three states (u , ω_{af} , and ω_{ar}) are decoupled from the states of interest. Therefore, these states are removed to produce a 5th-order model, described by:

$$A_g = \begin{bmatrix} -2.724 & -13.808 & 0 & 0 & 0 \\ 0.730 & -4.782 & -0.300 & -0.302 & 0 \\ 0 & -225.037 & -99.668 & 0 & 0 \\ 0 & 226.291 & 0 & -99.668 & 0 \\ 0 & 1.000 & 0 & 0 & 0 \end{bmatrix} \quad (5.9)$$

and

$$B_g = \begin{bmatrix} 1.355 \\ 0.812 \\ 0 \\ 0 \\ 0 \end{bmatrix} \quad (5.10)$$

with the states $[v \ r \ \omega_{df} \ \omega_{dr} \ \psi]^T$. As the stated intention is to control the vehicle lateral deviation with respect to earth-fixed co-ordinates, it is useful to include lateral deviation as a state. From Equation (3.10), lateral deviation is approximated for small angles, at the longitudinal velocity of the linearization point. Thus, the 6th-order system, with lateral deviation, Y , as a function of lateral velocity and yaw angle, is obtained, with states $[v \ r \ \psi \ Y \ \omega_{df} \ \omega_{dr}]^T$, as:

$$A_h = \begin{bmatrix} -2.724 & -13.808 & 0 & 0 & 0 & 0 \\ 0.730 & -4.782 & 0 & 0 & -0.300 & -0.302 \\ 0 & 1.000 & 0 & 0 & 0 & 0 \\ 1.000 & 0 & 14.921 & 0 & 0 & 0 \\ 0 & -225.037 & 0 & 0 & -99.668 & 0 \\ 0 & 226.291 & 0 & 0 & 0 & -99.668 \end{bmatrix} \quad (5.11)$$

and

$$B_h = \begin{bmatrix} 1.355 \\ 0.812 \\ 0 \\ 0 \\ 0 \\ 0 \end{bmatrix} \quad (5.12)$$

From Equation (5.11) it can be seen that the remaining wheel angular velocity states appear almost decoupled from the states of interest (elements 2, 5 and 2, 6 are 'small'). Their removal may therefore be considered to further simplify the model. Without these states, the system appears as:

$$\hat{A} = \begin{bmatrix} -2.724 & -13.808 & 0 & 0 \\ 0.730 & -4.782 & 0 & 0 \\ 0 & 1.000 & 0 & 0 \\ 1.000 & 0 & 14.921 & 0 \end{bmatrix} \quad (5.13)$$

and

$$\hat{B} = \begin{bmatrix} 1.355 \\ 0.812 \\ 0 \\ 0 \end{bmatrix} \quad (5.14)$$

with states

$$\hat{x} = \begin{bmatrix} v & r & \psi & Y \end{bmatrix}^T$$

and scalar control input δ_f , the road-wheel steer angle.

The frequency-response characteristics of linear systems may be represented by logarithmic plots of the magnitude and phase angle of the sinusoidal transfer function, known as Bode diagrams. The Bode diagrams of both the 4th-order and 6th-order models, seen in Figure 5.1, are visually indistinguishable in terms of magnitude and phase over the frequencies of interest.

For the purpose of applying sliding mode control, it is useful to transform the system into regular form [114], separating the system into *null space dynamics*, which are independent

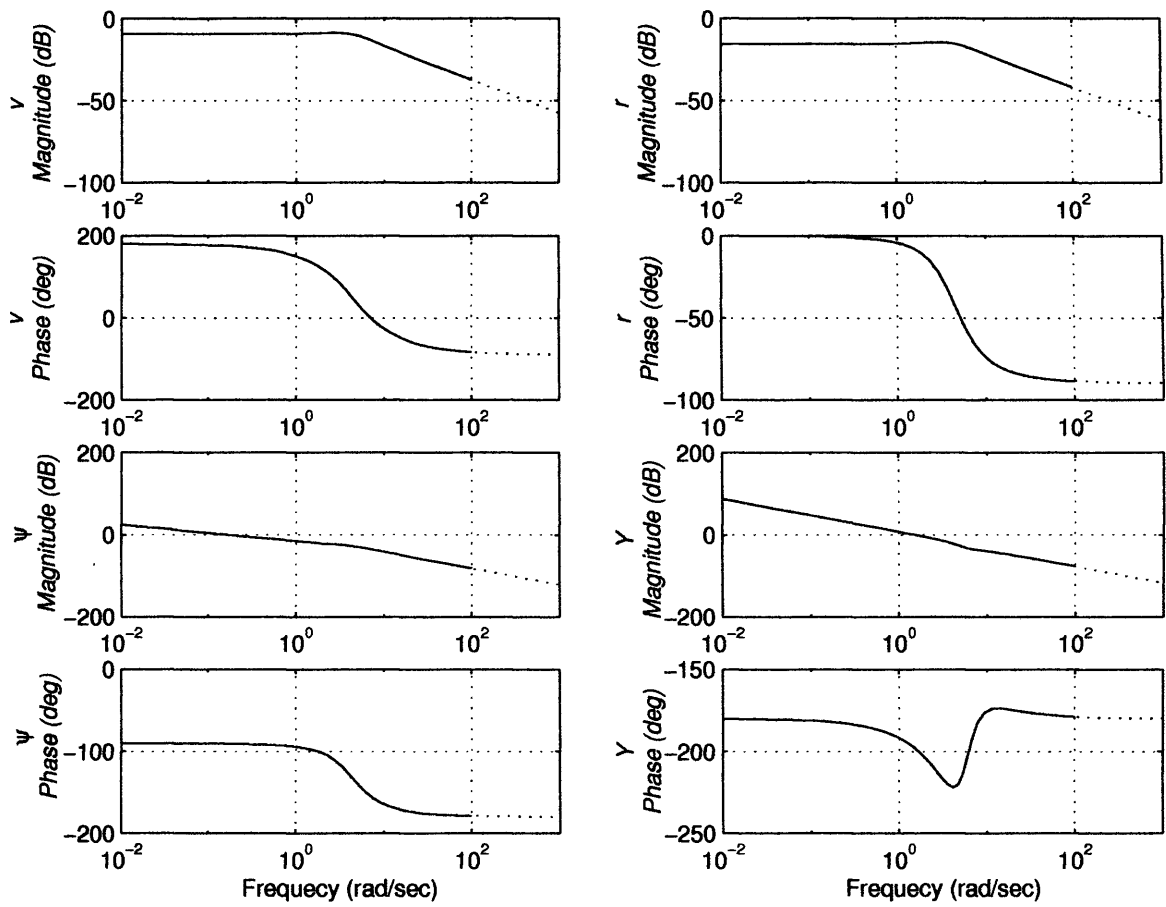


Figure 5.1: Bode diagrams of the four states of the 4th-order and 6th-order models

of the control signal, and *range space dynamics*, which coincide with the dimension of the control. Regular form, as discussed in Section 4.2, is invariably viewed as the starting point for the design of the sliding surface [31, 114]. To this end, the states were re-ordered, and the lateral velocity state altered, to remove its dependence upon the control signal. The new state is given by:

$$\bar{v} = v - \frac{B_1}{B_2}r$$

where B_1, B_2 are the first two elements of \hat{B} , in Equation (5.14). The new system is given by:

$$A_n = \begin{bmatrix} -3.9404 & 0 & 0 & -14.6916 \\ 0 & 0 & 0 & 1.0000 \\ 1.0000 & 14.9206 & 0 & 1.6695 \\ 0.7296 & 0 & 0 & -2.1991 \end{bmatrix} \quad (5.15)$$

and

$$B_n = \begin{bmatrix} 0 \\ 0 \\ 0 \\ 0.8116 \end{bmatrix} \quad (5.16)$$

with states

$$x_n = \begin{bmatrix} \bar{v} & \psi & Y & r \end{bmatrix}^T$$

In this form, the control signal now enters the system through just one channel, and any uncertainties or unmodelled dynamics occurring in this channel are said to be ‘matched’ [31, 114].

The output distribution matrix is assumed to be

$$C_n = \begin{bmatrix} 0 & 0 & 1 & 0 \\ 0 & 0 & 0 & 1 \end{bmatrix} \quad (5.17)$$

which corresponds to measuring lateral deviation and yaw rate.

5.2.2 Controller Structure

The control objective is to minimize lateral deviation; for this reason integral action has been introduced. Specifically

$$\dot{Y}_{int}(t) = Y(t) \quad (5.18)$$

Augment the states with the integral action state and define

$$\tilde{x} = \begin{bmatrix} Y_{int} \\ x_n \end{bmatrix} \quad (5.19)$$

The associated system and input distribution matrices for the augmented system are

$$\tilde{A} = \begin{bmatrix} 0 & e_3^T \\ 0 & A_n \end{bmatrix} \quad \text{and} \quad \tilde{B} = \begin{bmatrix} 0 \\ B_n \end{bmatrix} \quad (5.20)$$

where $e_3^T = [0 \ 0 \ 1 \ 0]$. A sliding surface of the form

$$S = \{\tilde{x} \in \mathbb{R}^5 : S\tilde{x} = 0\} \quad (5.21)$$

where $S \in \mathbb{R}^{1 \times 5}$ has been chosen (see Chapter 2 in [31]). The control law, which (as in Section 4.3.2), comprises both a linear component to provide asymptotic decay onto the sliding mode for the nominal system and a discontinuous component to provide robustness and convergence to the sliding mode in finite time, is then given by

$$u = -(S\tilde{B})^{-1}(S\tilde{A} - \Phi S)\tilde{x}(t) + u_n \quad (5.22)$$

where Φ is a negative design scalar and the discontinuous vector

$$u_n = \begin{cases} -\rho_c(u, y)(S\tilde{B})^{-1} \frac{S\tilde{x}}{\|S\tilde{x}\|} & \text{if } S\tilde{x} \neq 0 \\ 0 & \text{otherwise} \end{cases} \quad (5.23)$$

The positive scalar function $\rho_c(u, y)$ depends on the magnitude of the matched uncertainty. This control scheme is the special case of tracking controller in [29] when the reference signal is taken as zero. This control structure is identical to that described in Section 4.3.2 except that integral action has been incorporated to provide tracking.

5.2.3 Observer Structure

The control law described above is based on state information. In this application only a subset of the states are measurable. To overcome this a sliding mode observer will be used to estimate the states. The approach used here is based on the work of [29] and employs an observer first

introduced in [116]. The observer is a special case of the one described in Section 4.4.2. The structure of the observer is given by

$$\dot{x}_o(t) = A_n x_o(t) + B_n u(t) - GC_n e(t) + B_n \nu_o \quad (5.24)$$

where $x_o \in \mathbb{R}^4$ represents an estimate of the true states x_n , and $e = x_o - x_n$ is the state estimation error. The output error feedback gain matrix $G \in \mathbb{R}^{4 \times 2}$ is chosen so that the closed loop matrix $A_0 = A_n - GC_n$ is stable and has a positive definite Lyapunov matrix P satisfying both

$$PA_0 + A_0^T P < 0 \quad (5.25)$$

and the structural constraint

$$PB_n = C_n^T F^T \quad (5.26)$$

for some matrix $F \in \mathbb{R}^{1 \times 2}$. The discontinuous vector ν_o is given by

$$\nu_o = \begin{cases} -\rho_o(y, u) \frac{FC_n e}{\|FC_n e\|} & \text{if } FC_n e \neq 0 \\ 0 & \text{otherwise} \end{cases} \quad (5.27)$$

where $\rho_o(y, u)$ is a scalar function which bounds the matched uncertainty. The observer induces a sliding motion on

$$\mathcal{S}_o = \{ e \in \mathbb{R}^n : FC_n e = 0 \} \quad (5.28)$$

Necessary and sufficient conditions for the existence of matrices G, P and F which satisfy Equations (5.25) and (5.26) are that $\text{rank}(C_n B_n) = 1$, and that the invariant zeros of the system (A_n, B_n, C_n) lie in the open L.H.P. [29]. For the system given by Equations (5.15)-(5.17) these conditions are satisfied. The analytical solution based on a canonical form from [29] has been used here to synthesize the gains F and G . This provides precise tracking of the outputs, giving a set of states which give the output of the plant exactly.

Note that this observer is a special case of the one introduced in Section 4.4.2. Now sliding is induced on $FCe = 0$ rather than $Ce = 0$. The introduction of the matrix F provides an additional design element. How the gain through which the nonlinear switched gain is introduced is now B (which reduces the design freedom). This choice of injection gain is vital for the closed loop stability proof in [29].

5.2.4 Controller Design

To design the sliding surface for the state feedback control law the optimal quadratic approach of [115] has been employed. In this approach the cost functional

$$J = \int_{t_s}^{\infty} \tilde{x}^T(t) Q \tilde{x}(t) dt$$

is minimized, where t_s represents the time at which sliding first occurs. In the following design

$$Q = \text{diag}\{0.01, 1, 15, 1.5, 0.01\} \quad (5.29)$$

The elements of the Q matrix were chosen in order to improve damping and so remove oscillation from the yaw rate and lateral deviation. By removing oscillation from these states, it was possible to produce a control signal which acts in such a short period of time that the vehicle returns to a state in which the driver feels comfortable before having time to react to the initial disturbance. As the element of the Q matrix which proved to have the greatest effect on damping was that associated with ψ (the third state), this element was heavily weighted. Meanwhile, weighting the element associated with the lateral deviation, Y (the fourth state), actually had a negative effect on the damping, and so in choosing the weighting of this element, a trade-off was required between maintaining appropriate damping and minimizing lateral deviation. The remaining elements of the Q matrix were chosen in a similar fashion. The choice of weighting matrix in Equation (5.29) produces a sliding surface

$$S = \begin{bmatrix} -1.0000 & -1.5175 & -47.2779 & -12.5035 & -1.0000 \end{bmatrix} \quad (5.30)$$

The pole associated with the range-space dynamics $\Phi = -4$. This yields a state feedback gain of

$$L = \begin{bmatrix} -4.9288 & -16.4261 & -463.2190 & -62.8611 & -58.7245 \end{bmatrix}$$

5.2.5 Observer Design

In terms of the observer design

$$G = \begin{bmatrix} -290.0806 & -14.7110 \\ 51.5000 & 1.0000 \\ 40.0646 & 1.6695 \\ -15.0290 & 17.8037 \end{bmatrix}$$

which gives

$$\lambda(A - GC) = \{-12.0, -14.0, -18.0, -20.0\}$$

These dynamics are significantly faster than those associated with the sliding motion from Section 5.2.4. The matrix associated with the hyperplane in the state estimation error system

$$F = \begin{bmatrix} 0 & 0.0203 \end{bmatrix}$$

The nonlinear scalar gains $\rho_o = \rho_c = 20$ in the observer and state feedback switching functions. In this example, both the discontinuous terms in Equations (5.23) and (5.27) are scalar. The discontinuities have been implemented with the continuous approximation $sign(s) \approx \frac{s}{|s| + \delta}$ where δ is a small positive scalar.

5.3 Simulation of Vehicle System in a Split- μ Braking Manoeuvre with Observer-Based Sliding Mode Control Scheme

The observer-based controller design was tested by simulation on the vehicle model from Section 3.3 performing a harsh split- μ braking manoeuvre. The vehicle is initially travelling in a straight trajectory, with a longitudinal velocity of $27m.s^{-1}$ (or approximately $97kmhr^{-1}$), when it encounters a split- μ surface. This surface is (initially) symmetric about the central longitudinal axis of the car, with coefficient of friction, $\mu = 0.8$ (dry) and $\mu = 0.2$ (ice) on the left and right sides of the car respectively. The driver's desire is for the vehicle to come to a complete halt as quickly as possible, (ideally) without deviating from the original straight trajectory.

5.3.1 Simulation Results

Open loop, it can be seen from Figures 5.2 and 5.3 that the ABS allows the brake torque to rapidly ramp up to $1,140Nm$ on the front high- μ wheel, but to much lower levels on the low- μ wheels. The rear, high- μ wheel is also subject to less severe braking as the two rear wheels select-low. Immediately the car starts to yaw and veer to the left. The car veers so significantly that at $t = 1.3s$ and $t = 1.8s$ respectively, the front right and rear right wheels cross over from the low- μ to the high- μ surface. At this point, with all four wheels on the high- μ surface, the ABS allows the braking to ramp up on the remaining three wheels. However, by the time the car reaches a standstill, at $t = 5.25s$, it has recorded a peak yaw angle of around 20° and has veered a potentially disastrous $8m$ from the original road lateral position. The closed loop simulation shows a significant improvement (Figures 5.4 and 5.5). The ABS allows the braking torques to ramp up as before. However, the controller manages to stop the vehicle from developing an excessive yaw angle. Also, the lateral deviation, Y , is halted with a peak of just $1cm$ and is regulated to zero. The controller develops and maintains sufficient yaw angle as is necessary to counteract the yawing moment induced by the asymmetric ABS braking. The input signal which the controller utilizes to perform this is equivalent to a hand-wheel angle of around 60° or a steer-by-wire road-wheel angle of 4.2° , which is achievable. It can be seen from Figure 5.6 that the controller attains sliding motion and maintains it.

5.3.2 Further Robustness Testing

In the simulation results shown in the preceding section, it has been demonstrated that the controller is robust with respect to mismatches between the linear and the nonlinear models. The robustness of the controller may be demonstrated further through parameter variation. Firstly, it is sensible to vary the parameters in a way which is roughly equivalent to a real scenario. A closed-loop simulation is now undertaken in which the longitudinal and lateral tyre stiffnesses are decreased by 15%, corresponding to under-inflated tyres.

The biggest change seen in the new plots (Figures 5.7-5.9) is that the vehicle takes slightly longer to stop. This is due to the tyres being more liable to slip, leading to the ABS allowing less braking. The controller reacts in a virtually identical way as in the previous simulation,

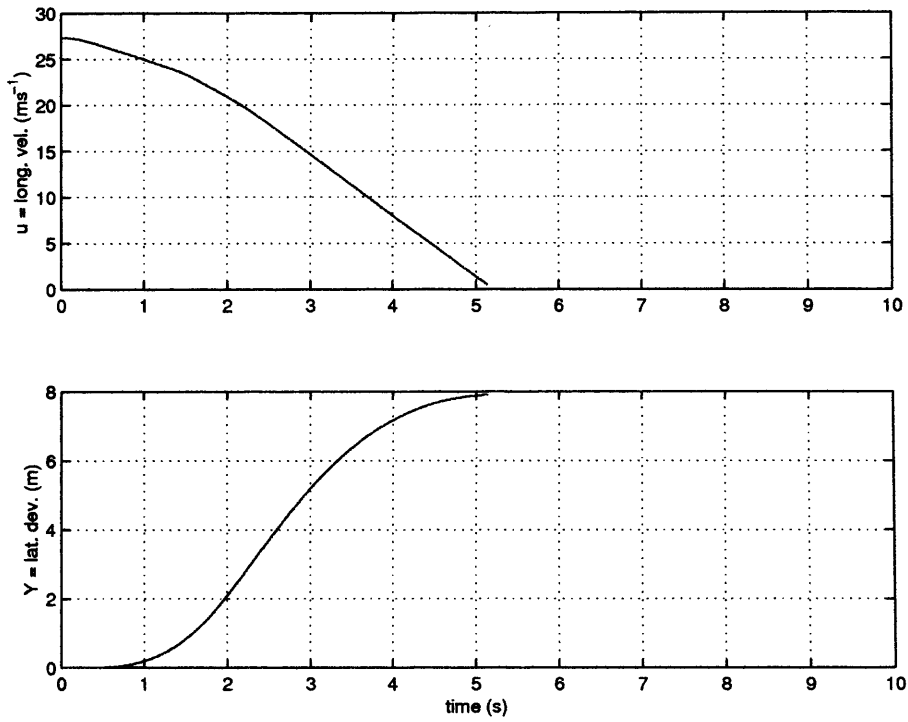


Figure 5.2: Vehicle longitudinal velocity and lateral deviation for open-loop simulation

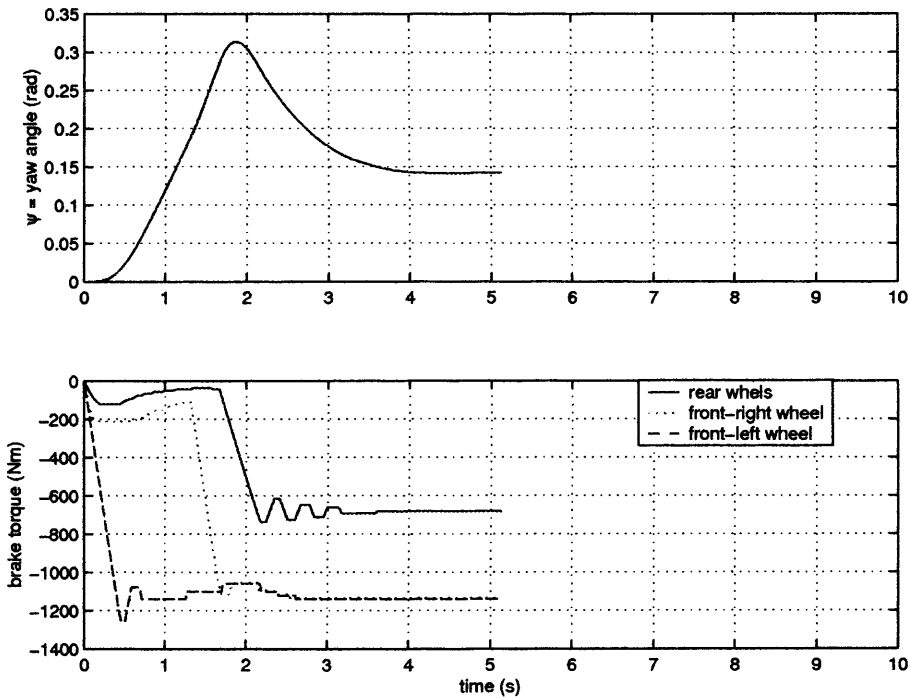


Figure 5.3: Vehicle yaw angle and braking torques for open-loop simulation

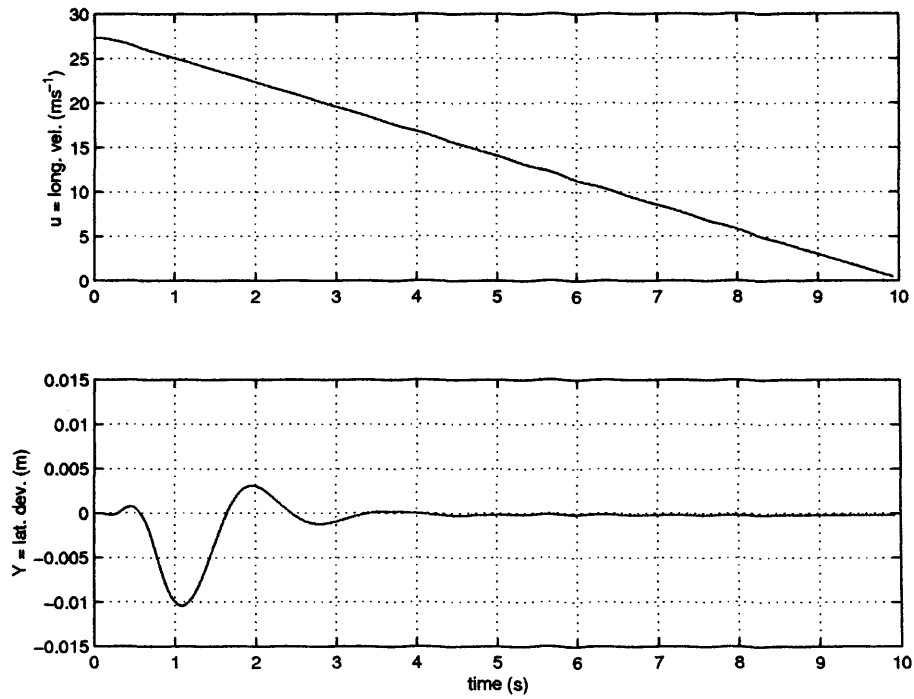


Figure 5.4: Vehicle longitudinal velocity and lateral deviation for closed-loop simulation

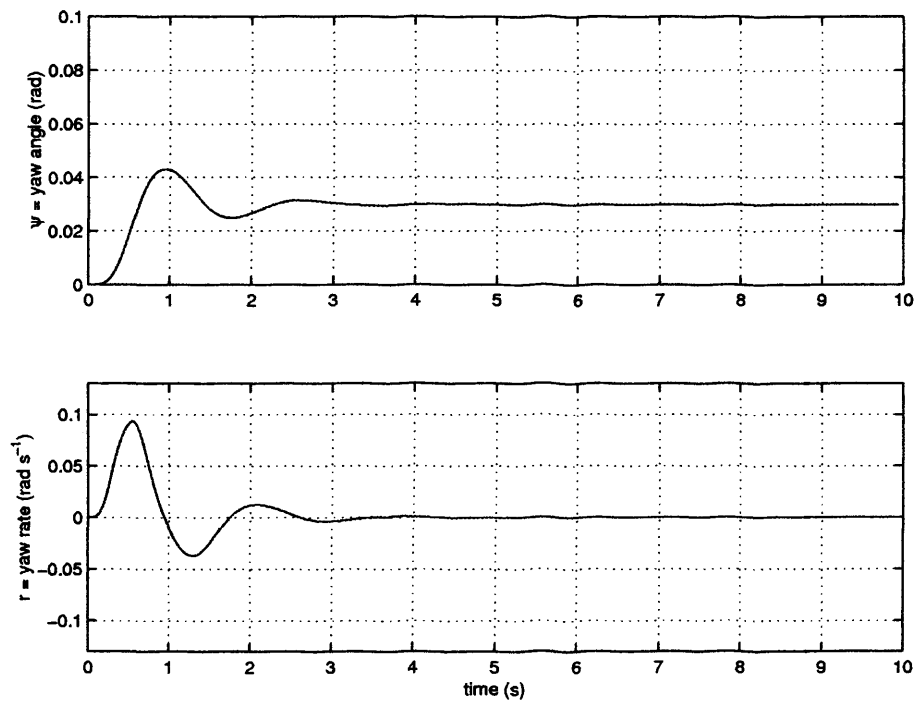


Figure 5.5: Vehicle yaw angle and yaw rate for closed-loop simulation

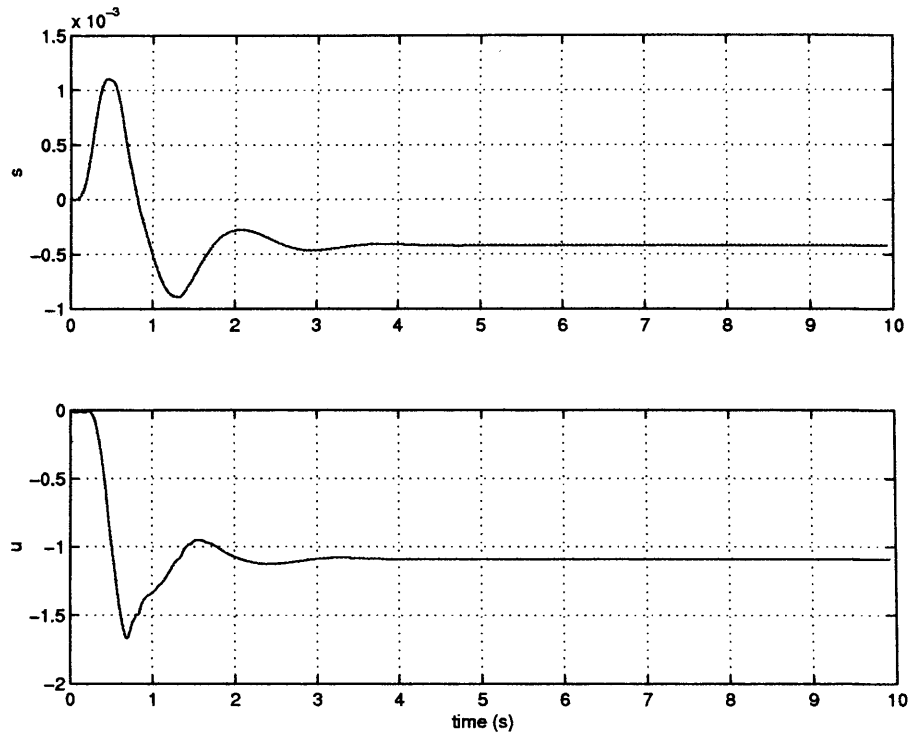


Figure 5.6: Switching function and control signal

achieving and maintaining sliding throughout. The vehicle lateral deviation is minimal, with just a small increase in the magnitude of the initial oscillation of the lateral velocity and yaw states, which are rapidly damped to a steady value. In a more severe situation, the tyre stiffness values may vary by an even greater margin. A final closed loop simulation is now performed using tyre stiffness parameters decreased by 40% of their nominal values. In Figures 5.10 and 5.11, it can be seen that in this harsh situation, whilst the damping is reduced slightly, the lateral deviation is maintained below 1.5cm . The peak in the control signal (Figure 5.12) is increased to around 7.6° road-wheel steering angle, before settling at a steady value of around 5.3° .

5.4 Conclusions

The feasibility of designing an observer-based sliding mode control system which can safely and effectively deal with a harsh split- μ braking manoeuvre has been demonstrated. This has been shown to be achievable without the need for 4WS. The controller is observer-based, and

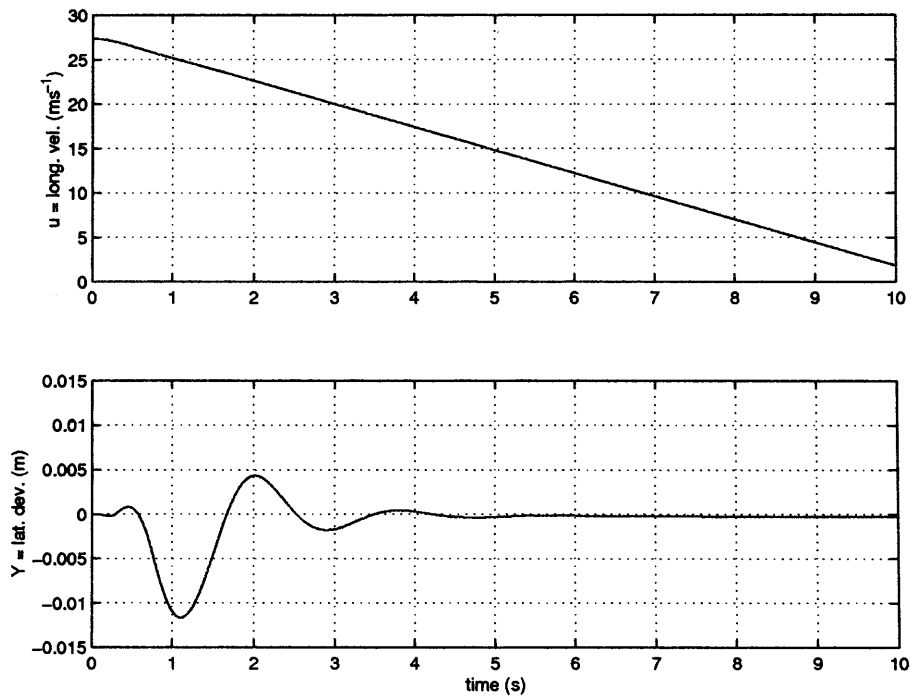


Figure 5.7: Vehicle longitudinal velocity and lateral deviation for robustness test: 15% tyre stiffness reduction

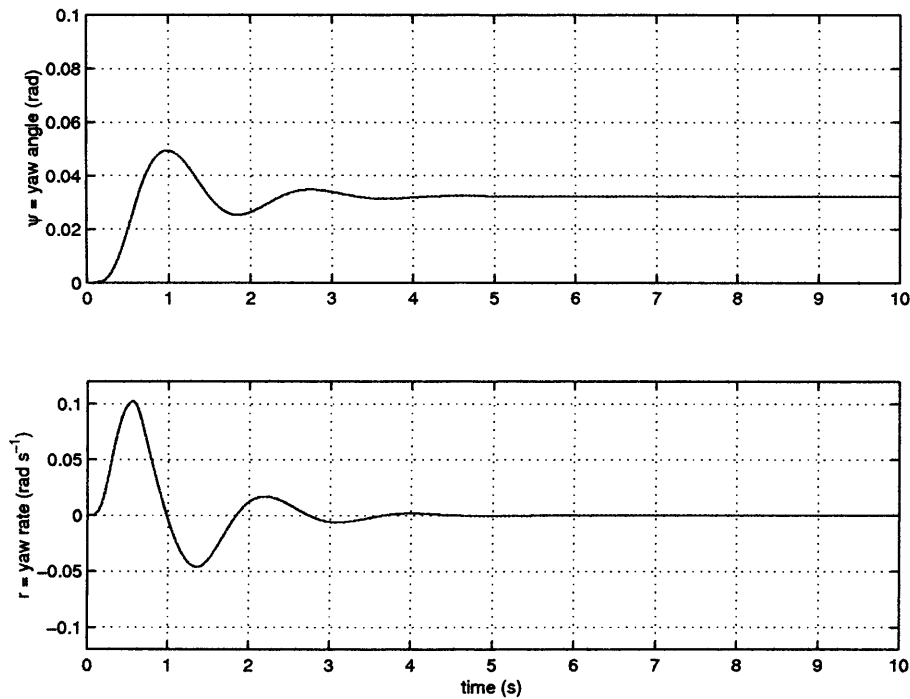


Figure 5.8: Vehicle yaw angle and yaw rate for robustness test: 15% tyre stiffness reduction

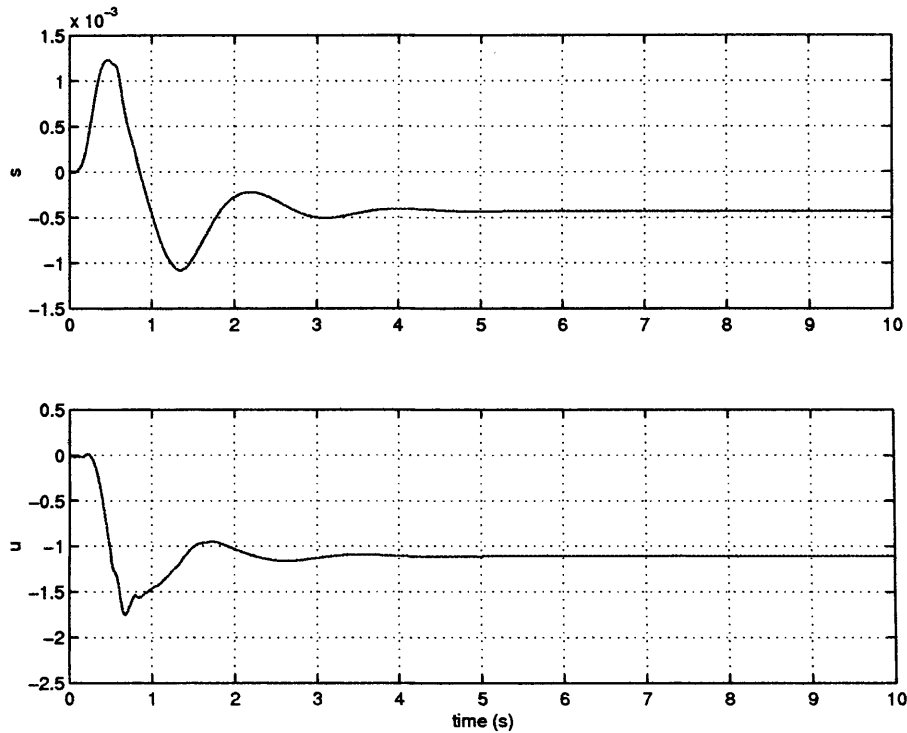


Figure 5.9: Switching function and control signal for robustness test: 15% tyre stiffness reduction

uses only two measured signals to reconstruct the state variables needed in the control law, and is, therefore, not dependent on full state-feedback. The control scheme can be used in conjunction with vision systems in development for lane detection and path following applications.

The control scheme presented here extends current work through its use of a minimum of state measurements, and its sliding mode robustness properties. Its validity is further strengthened through its testing on a nonlinear, four-wheel model, with modelled ABS units, in a harsh split- μ braking manoeuvre, and in the presence of large changes in the tyre stiffnesses. The next chapter will approach the same split- μ braking problem, but will address it using a compensator-based (rather than observer-based) control approach.

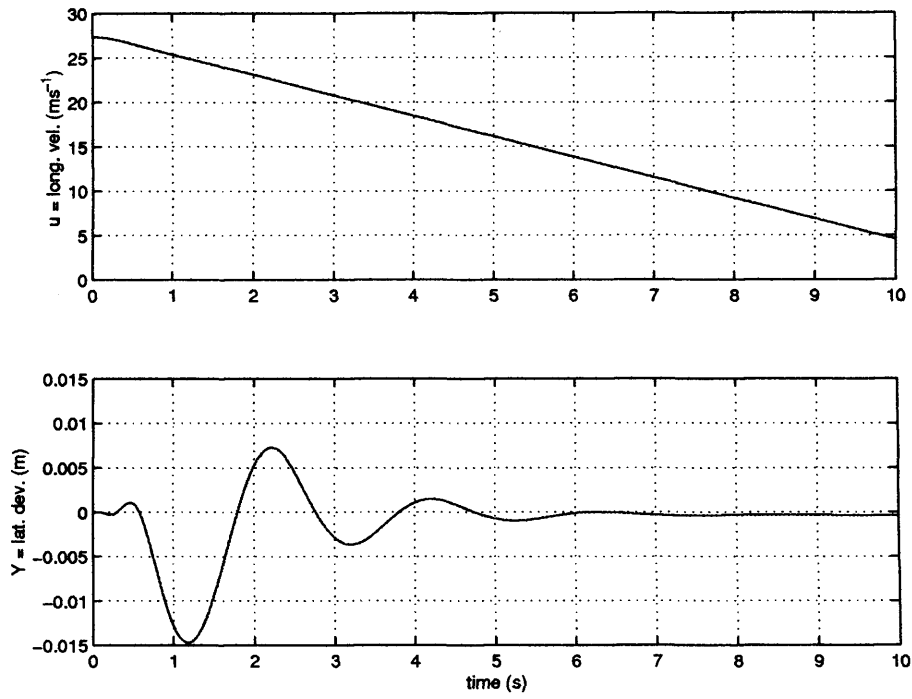


Figure 5.10: Vehicle longitudinal velocity and lateral deviation for robustness test: 40% tyre stiffness reduction

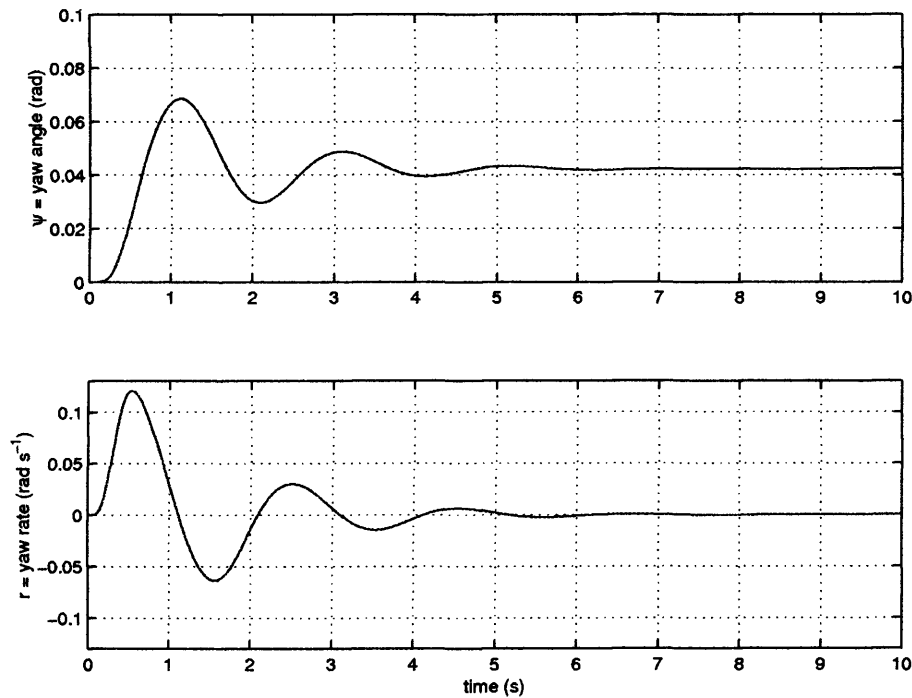


Figure 5.11: Vehicle yaw angle and yaw rate for robustness test: 40% tyre stiffness reduction

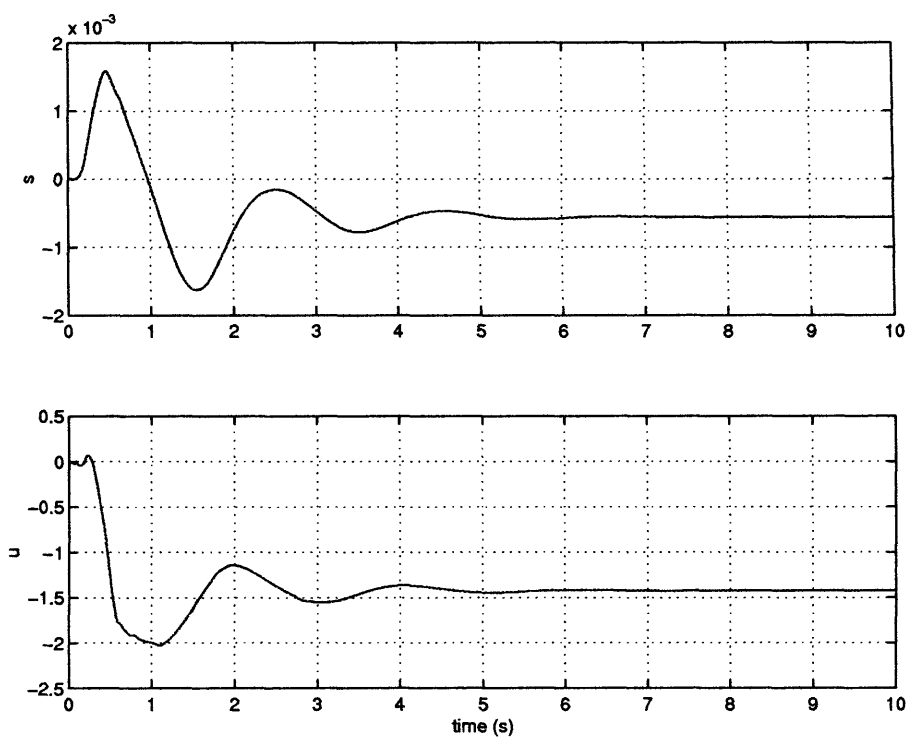


Figure 5.12: Switching function and control signal for robustness test: 40% tyre stiffness reduction

Chapter 6

Split- μ Braking with Compensator-based Control

6.1 Introduction

The previous chapter described the design of an observer-based sliding mode controller for a nonlinear vehicle model in a split- μ braking manoeuvre. The observer produced estimates of system states so that a state-feedback controller design could be used to regulate the states and keep the vehicle stable under harsh conditions.

In this chapter, the use of a novel compensator-based sliding mode controller (which does not possess an observer interpretation), which results in a closed-loop system of lower order, will be considered and implemented on the same nonlinear vehicle model (as published in [34]). Finally, closed-loop simulations will be performed to test the performance of the control scheme, using the original, nonlinear vehicle model taken from Chapter 3. Further simulations will be carried out to test the closed-loop robustness to certain parameter uncertainties. The results of these simulations will then be compared with those achieved by the observer-based control scheme in Chapter 5.

A benefit of using a compensator-based controller is that it is less complex (ie. of lower dynamical order). From a practical, implementation perspective, this could be advantageous since less computational load is placed on the micro controller which would be used to implement the scheme. Also, in the presence of unmatched uncertainty, formal analysis of the closed-loop system may be more tractable.

The development of the theory of Variable Structure Systems and, in particular the Sliding Mode phenomenon, was based on the study of differential equations (with discontinuous right hand sides) and therefore evolved within a state-space perspective. As a consequence, the design of early sliding mode controllers, as discussed in Chapter 4, assumed the availability of complete state information – or equivalently that the output of the system could be (perfectly) differentiated sufficiently often. In terms of implementing sliding mode controllers on systems of industrial relevance, the assumption of full state information availability is untenable. This has motivated research in the area of sliding mode control under the restriction that only certain measured output information is available for use in the controller or equivalently that only a certain subset of the states are available. One approach in the literature is to use the measured output information to drive an observer to estimate the unmeasured states (as discussed in Chapter 5). However, for the reasons mentioned earlier, this can have its disadvantages.

Instead, in this chapter the output feedback case will be considered when purely measured outputs are used to calculate the controller, and it will also investigate the use of low order dynamical compensators (which do not possess observer interpretations). It will be argued that whilst in the state feedback case controllers are designed to give global sliding surface reachability, such a restriction in the output feedback situation (needlessly) restricts the class of system.

6.2 Problem Formulation

Consider an uncertain dynamical system of the form

$$\begin{aligned}\dot{x}(t) &= Ax(t) + Bu(t) + f(t, x, u) \\ y(t) &= Cx(t)\end{aligned}\tag{6.1}$$

where $x \in \mathbb{R}^n$, $u \in \mathbb{R}^m$ and $y \in \mathbb{R}^p$ with $m \leq p < n$. Assume that the nominal linear system (A, B, C) is known and that the input and output matrices B and C are both of full rank. The unknown function $f : \mathbb{R}_+ \times \mathbb{R}^n \times \mathbb{R}^m \rightarrow \mathbb{R}^n$, which represents the system nonlinearities plus any model uncertainties in the system, is assumed to satisfy the matching condition

$$f(t, x, u) = B\xi(t, x, u)\tag{6.2}$$

where the bounded function $\xi : \mathbb{R}_+ \times \mathbb{R}^n \times \mathbb{R}^m \rightarrow \mathbb{R}^m$ satisfies

$$\|\xi(t, x, u)\| < k_1 \|u\| + \alpha(t, y) \quad (6.3)$$

for some known function $\alpha : \mathbb{R}_+ \times \mathbb{R}^p \rightarrow \mathbb{R}_+$ and positive constant $k_1 < 1$.

Initially the intention will be to explore when static output feedback sliding mode control can be employed. A control law will be sought which induces an ideal sliding motion on the surface

$$\mathcal{S} = \{x \in \mathbb{R}^n : FCx = 0\} \quad (6.4)$$

for some selected matrix $F \in \mathbb{R}^{m \times p}$ of the form

$$u(t) = Gy(t) - \nu_y \quad (6.5)$$

where $G \in \mathbb{R}^{m \times p}$ is a fixed gain matrix and the discontinuous vector

$$\nu_y = \begin{cases} \rho(t, y) \Lambda \frac{Fy(t)}{\|Fy(t)\|} & \text{if } Fy \neq 0 \\ 0 & \text{otherwise} \end{cases} \quad (6.6)$$

where $\rho(t, y)$ is some positive scalar function of the outputs and $\Lambda \in \mathbb{R}^{m \times m}$ is an invertible matrix. This is effectively an output feedback version of the state feedback sliding mode control laws considered by [95, 107] and described in Chapter 4.

6.3 Preliminaries

Consider the system in Equation (6.1) and assume that $p > m$ and $\text{rank}(CB) = m$. In order for a unique equivalent control to exist, the matrix $FCB \in \mathbb{R}^{m \times m}$ must have full rank. It is well known that

$$\text{rank}(FCB) \leq \min\{\text{rank}(F), \text{rank}(CB)\}$$

and so in order for FBC to have full rank both F and CB must have rank m . A necessary condition therefore for the matrix FBC to be full rank is that $\text{rank}(CB) = m$. The sliding motion will be governed by the invariant zeros of (A, B, FC) denoted by $\mathcal{Z}_{A,B,FC}$ [36]. The invariant zeros of (A, B, C) are given by

$$\mathcal{Z}_{A,B,C} = \left\{ z \in \mathbb{C} : \text{rank} \begin{bmatrix} zI - A & -B \\ C & 0 \end{bmatrix} < n + m \right\} \quad (6.7)$$

Writing

$$\begin{bmatrix} zI - A & -B \\ FC & 0 \end{bmatrix} = \begin{bmatrix} I & 0 \\ 0 & F \end{bmatrix} \begin{bmatrix} zI - A & -B \\ C & 0 \end{bmatrix}$$

it follows that if $z \in \mathcal{Z}_{A,B,C}$ then

$$\text{rank} \begin{bmatrix} zI - A & -B \\ FC & 0 \end{bmatrix} < n + m$$

which implies $z \in \mathcal{Z}_{A,B,FC}$ and therefore

$$\mathcal{Z}_{A,B,C} \subset \mathcal{Z}_{A,B,FC} \quad (6.8)$$

Two necessary system restrictions can be expressed as

A1) $\text{rank}(CB) = m$

A2) the invariant zeros $\mathcal{Z}_{A,B,C} \subset \mathbb{C}_-$.

Remarks: If a static output feedback controller as in Equations (6.5)-(6.6) is required, then A1-A2 are not sufficient. (If dynamic compensation is employed they are necessary and sufficient - this will be discussed in a later section.) Condition A1, in reality, is the most restrictive - and amounts to a constraint on the relative degree. Most systems with more outputs than inputs do not possess any invariant zeros and therefore A2 is satisfied by default. These two conditions are similar to the ones required to be satisfied to guarantee the existence of the sliding mode observer discussed in Section 5.2.3.

The first phase of the variable structure control method concerns designing a switching hyperplane so that when the system trajectories are confined to this surface, the overall dynamic behaviour of the system is stable and has some desired characteristics. This is usually referred to as the *existence problem*. In the static output feedback case this entails constructing a matrix $F \in \mathbb{R}^{m \times p}$ so that the motion on the hyperplane given by Equation (6.4) satisfies the design specifications.

The second phase - the so-called *reachability problem* - involves designing a control law to drive the states onto the sliding surface in finite time and subsequently maintain the sliding motion despite the uncertainty.

6.4 Hyperplane Design

For linear systems with no uncertainty the problem of hyperplane design using output information has been investigated by El-Khazali & DeCarlo [38, 39]. For uncertain systems Hui and Žak [64] propose an algorithm for output dependent hyperplane design based upon eigenvector methods. Edwards and Spurgeon [28] demonstrate that the hyperplane design problem is equivalent to a static output feedback problem and provide necessary and sufficient conditions in terms of the system structure for a stable reduced order motion to exist. This final method will be discussed in this subsection. All three viewpoints (not surprisingly) require A1 to be satisfied.

From a geometric viewpoint, the problem is one of finding an F so that the nonzero eigenvalues of the matrix

$$A_s := (A - B(FCB)^{-1}FCA) = (I_n - B(FCB)^{-1}FC)A$$

lie in \mathbb{C}_- . The matrix will have at least m zero eigenvalues as a result of the projection properties of $(I_n - B(FCB)^{-1}FC)$. Some of the remaining $n - m$ eigenvalues can be affected by choice of F . However, as argued earlier,

$$\mathcal{Z}_{A,B,C} \subset \{\lambda(A - B(FCB)^{-1}FCA)\} - \{0\}^m$$

The approach of [28] has much more in common with the one of [37] and relies on establishing a classical output feedback pole placement problem for a given subsystem obtained from the original state-space matrices. If condition A1 is satisfied, it can be shown [28] that there exists a coordinate system in which the triple (A, B, C) has the structure

$$A = \begin{bmatrix} A_{11} & A_{12} \\ A_{21} & A_{22} \end{bmatrix} \quad B = \begin{bmatrix} 0 \\ B_2 \end{bmatrix} \quad C = \begin{bmatrix} 0 & T \end{bmatrix} \quad (6.9)$$

where $B_2 \in \mathbb{R}^{m \times m}$ is nonsingular and $T \in \mathbb{R}^{p \times p}$ is orthogonal. Furthermore, $A_{11} \in \mathbb{R}^{(n-m) \times (n-m)}$ has the structure

$$A_{11} = \begin{bmatrix} A_{11}^o & A_{12}^o \\ 0 & \tilde{A}_{11} \end{bmatrix} \quad (6.10)$$

where the eigenvalues of $A_{11}^o \in \mathbb{R}^{r \times r}$ are the invariant zeros of the system. In addition, the pair $(\tilde{A}_{11}, \tilde{C}_1)$ where

$$\tilde{C}_1 := \begin{bmatrix} 0_{(p-m) \times (n-p-r)} & I_{p-m} \end{bmatrix} \quad (6.11)$$

is completely observable. This will be shown to be a useful standpoint from which to analyse output feedback controllers and the associated sliding motion. This differs from the canonical form used by Hui and Žak in that the output distribution matrix in Equation (6.9) has a partitioned structure and special features in the sub-block A_{11} are exposed.

Without loss of generality, the sliding surface matrix can be parameterized as

$$F := F_2 \begin{bmatrix} K & I_m \end{bmatrix} T^T \quad (6.12)$$

where $K \in \mathbb{R}^{m \times (p-m)}$ and $F_2 \in \mathbb{R}^{m \times m}$ is a nonsingular matrix [28]. Here, for simplicity, assume $F_2 = I_m$. If $[x_1^T \ x_2^T]^T$ represents a partition of the states commensurate with the system matrix in Equation (6.9), then, as argued in Section 4.3, it can be shown that during the sliding motion

$$\dot{x}_1(t) = (A_{11} - A_{12}KC_1)x_1(t) \quad (6.13)$$

where

$$C_1 := \begin{bmatrix} 0_{(p-m) \times (n-p)} & I_{p-m} \end{bmatrix} \quad (6.14)$$

This reveals the *static output feedback* nature of the hyperplane design problem. Furthermore, it can easily be shown that

$$\lambda(A_{11} - A_{12}KC_1) = \lambda(A_{11}^o) \cup \lambda(\tilde{A}_{11} - \tilde{B}_1K\tilde{C}_1)$$

where \tilde{B}_1 represents the last $n - p - r$ rows of the matrix A_{12} from Equation (6.9). It follows directly that for a stable sliding motion, the invariant zeros of the system (A, B, C) must lie in the open left half plane. It can be shown that if the pair (A, B) is completely controllable then the pair $(\tilde{A}_{11}, \tilde{B}_1)$ is completely controllable; the pair $(\tilde{A}_{11}, \tilde{C}_1)$ is completely observable by construction and thus if the triple $(\tilde{A}_{11}, \tilde{B}_1, \tilde{C}_1)$ satisfies the Kimura-Davison conditions, output feedback pole placement methods can be used to assign the poles appropriately [28].

The attractive feature of the approach of [28] is that a standard classical output feedback problem appears. Whilst solving this is still very much an on-going area of research [109], many existing software/design packages which address this problem can be employed directly.

Consider the fourth order system representing a linearization of the rigid body dynamics of a passenger vehicle, as described by Equations (5.15-5.17) in Section 5.2. The first state is an average of the lateral velocity v and yaw rate r ; the second state represents Ψ , the vehicle orientation; the third state, Y , is the lateral deviation from the intended lane position and the fourth state, r , is the yaw rate. The measured outputs are, again, the yaw rate and the lateral deviation, and the input to the system, δ_f , is the angular position of the front wheels relative to the chassis.

Notice this is already in the canonical form of Equation (6.9) and so

$$\begin{aligned} A_{11} &= \begin{bmatrix} -3.9404 & 0 & 0 \\ 0 & 0 & 0 \\ 1.0000 & 14.9206 & 0 \end{bmatrix} & A_{12} &= \begin{bmatrix} -14.6916 \\ 1.0000 \\ 1.6695 \end{bmatrix} \\ C_1 &= \begin{bmatrix} 0 & 0 & 1 \end{bmatrix} \end{aligned} \quad (6.15)$$

The so-called Kimura-Davison conditions are not met for this example since $m + p = 3 < 4 = n$. In this case $p - m = 1$ and $m = 1$ and so the hyperplane matrix can be parameterized as

$$F = \begin{bmatrix} k & 1 \end{bmatrix}$$

where k is a scalar design parameter. The sliding motion is determined by a classical root locus of the 'plant' $G_p = C_1(sI - A_{11})^{-1}A_{12}$ in series with a gain ' k ' in a unity feedback configuration. The root locus plot is given in Figure 6.1.

For a value of $k > 2.58$ all the sliding mode poles lie in \mathbb{C}_- and so this constitutes an appropriate solution to the existence problem.

6.5 Control Law Development

Having designed the surface, it is necessary to develop a controller of the form given in Equations (6.5)-(6.6) to induce and sustain a sliding motion. The quantity $\rho(t, y)$ in Equation (6.6) must upper bound the uncertainty in Equations (6.1)-(6.2) given in Equation (6.3). The key design choice is the selection of an appropriate gain G in Equation (6.5). A common design

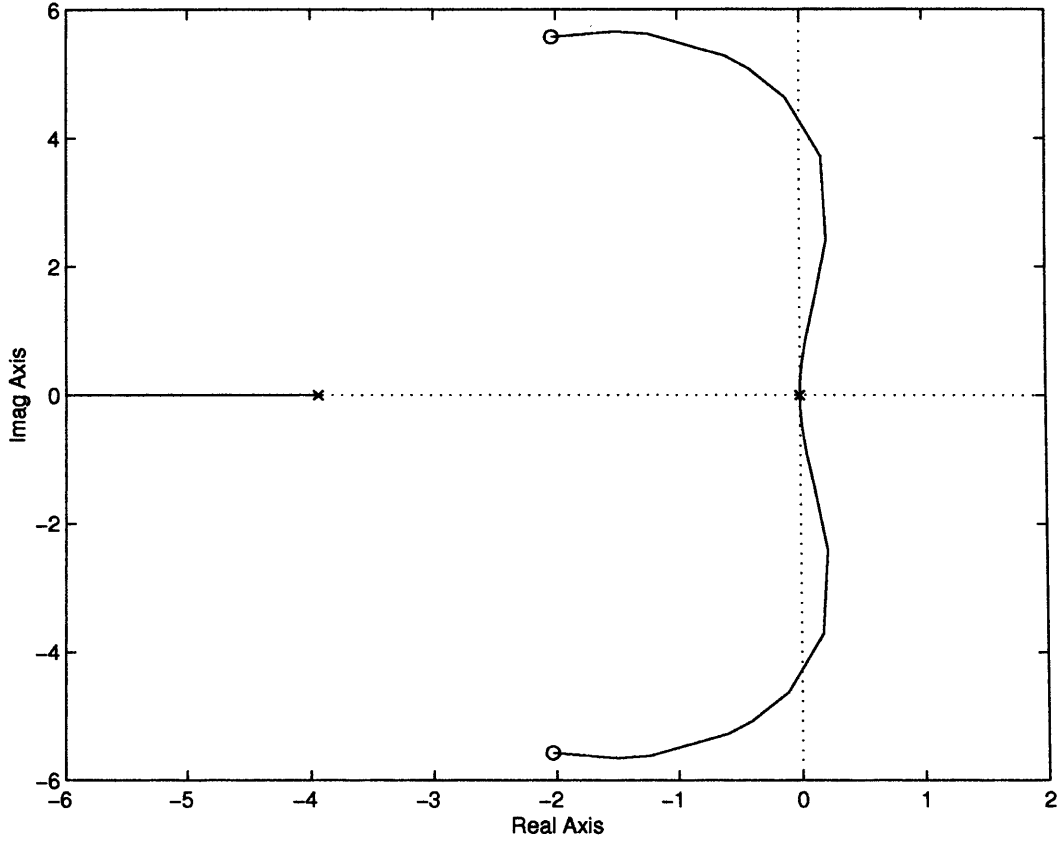


Figure 6.1: Sliding mode poles as a root locus

methodology [12, 38, 58, 59] is based on synthesizing a static output feedback gain numerically to ensure the so-called reachability condition is satisfied.

To facilitate the analysis, an additional, switching function dependent coordinate transformation will be made. Let $x \mapsto T_K x = z$ where

$$T_K := \begin{bmatrix} I_{(n-m)} & 0 \\ KC_1 & I_m \end{bmatrix} \quad (6.16)$$

with B_2 as defined in Equation (6.9) and C_1 is defined in Equation (6.14). In this new coordinate system, the system triple $(\hat{A}, \hat{B}, F\hat{C})$ has the property that

$$\hat{A} = \begin{bmatrix} \hat{A}_{11} & \hat{A}_{12} \\ \hat{A}_{21} & \hat{A}_{22} \end{bmatrix} \quad \hat{B} = \begin{bmatrix} 0 \\ B_2 \end{bmatrix} \quad F\hat{C} = \begin{bmatrix} 0 & I_m \end{bmatrix} \quad (6.17)$$

where $\hat{A}_{11} = A_{11} - A_{12}KC_1$ which is assumed to be stable by choice of K . Furthermore

$$\hat{C} = \begin{bmatrix} 0_{p \times (n-p)} & \hat{T} \end{bmatrix} \quad (6.18)$$

where

$$\hat{T} := \begin{bmatrix} (T_1 - T_2 K) & T_2 \end{bmatrix} \quad (6.19)$$

and T_1 and T_2 represent the first $p - m$ and last m columns of the matrix T from Equation (6.9). Notice that \hat{T} is nonsingular.

6.5.1 Control Structure

Several different control laws exist in the literature [12, 59, 28]. In this subsection a slightly modified canonical form will be considered in which F_2 is chosen so that $FCB = I_m$ and $B_2 = I_m$ in the coordinate system of Equation (6.17). For full details see [32]. The scaling matrix in the nonlinear component of the control law given by Equation (6.6) is given by $\Lambda = P_2^{-1}$ where $P_2 \in \mathbb{R}^{m \times m}$ is a symmetric positive definite matrix to be designed and

$$\rho(t, y) = (k_1 \|Gy(t)\| + \alpha(t, y) + \eta) / (1 - k_1) \quad (6.20)$$

with η a design scalar which will be shown to define the region in which sliding takes place.

Without loss of generality, write the feedback gain from Equation (6.5) as

$$G = \begin{bmatrix} G_1 & G_2 \end{bmatrix} \hat{T}^{-1} \quad (6.21)$$

where \hat{T} is from Equation (6.19) and $G_1 \in \mathbb{R}^{m \times (p-m)}$ and $G_2 \in \mathbb{R}^{m \times m}$. Define a symmetric positive definite block diagonal matrix

$$P := \begin{bmatrix} P_1 & 0 \\ 0 & P_2 \end{bmatrix} > 0 \quad (6.22)$$

where $P_1 \in \mathbb{R}^{(n-m) \times (n-m)}$. Then, it is proved in [33] that if it is possible to find a matrix P as in Equation (6.22), and a gain matrix G so that

$$PA_c + A_c^T P < 0 \quad (6.23)$$

where $A_c = \hat{A} - \hat{B}G\hat{C}$, then the control law will induce a sliding motion on the surface \mathcal{S} inside the domain (the sliding patch)

$$\Omega = \{(z_1, z_2) : \|z_1\| < \eta\gamma^{-1}\}$$

where $\gamma = \|P_2(\hat{A}_{21} - G_1C_1)\|$ and $z_1 \in \mathbb{R}^{(n-m)}$, $z_2 \in \mathbb{R}^m$ represent a partition of the state z .

From the point of view of control law design, a requirement is to make

$$\|P_2(\hat{A}_{21} - G_1C_1)\| \quad (6.24)$$

small to make the sliding patch Ω large.

Rather than merely guaranteeing the eigenvalues of A_c lie in the open left half plane, in [33], for a given scalar γ , the gain G (of minimum norm) is selected which places the poles of $A_c = (\hat{A} - \hat{B}G\hat{C})$ in the region

$$\mathcal{D} = \{z \in \mathbb{C} : \text{Re}(z) < h_d, |z| < r_d\} \quad (6.25)$$

such that

$$\|P_2(\hat{A}_{21} - G_1C_1)\| < \gamma, \quad P_2 > I_m \quad (6.26)$$

If $L_1 := P_2G_1$ and $L_2 := P_2G_2$, it follows that $PA_c + A_c^T P$ is affine in the parameters P_1, P_2, L_1 and L_2 , and $P_2(\hat{A}_{21} - G_1C_1)$ is affine in P_2 and L_1 [33]. It is shown in [33] that this problem can be posed as a convex optimization problem and that Linear Matrix Inequality methods [20] can be used to synthesize the gains numerically.

Remarks:

- The block diagonal structure in Equation (6.22), together with the canonical form in Equation (6.17), effectively guarantees a solution to the structural constraint $P\hat{B} = (F\hat{C})^T$, which in turn ensures the transfer function matrix $F\hat{C}(sI - \hat{A})^{-1}\hat{B}$ is strictly positive real [108].
- In terms of the problem formulation just given, if the design requirements given in terms of \mathcal{D} in Equation (6.25) are removed then a control law always exists. (In fact in [28] an ‘analytical solution’ was provided - see [28], Section 5.3).

Consider, again, the example from Section 5.2. From the root locus in Figure 6.1 it can be seen that high gain is needed to improve the damping of the dominant complex conjugate pair. With a value of $k = 100$ the sliding motion poles are governed by

$$\{-1.9241 \pm 5.6081i, -167.0320\}$$

The approach in Section 6.5.1 when $h_2 = 0$ and $r_d = 175$ gives

$$G = \begin{bmatrix} 1095.7134 & 208.2982 \end{bmatrix}$$

and

$$\lambda(A - BGC) = \{-162.0054, -12.4248, -0.3736 \pm 5.0794i\}$$

Remarks: Although from a control theory point of view this example demonstrates the theory is valid and that a static output feedback controller does exist, the resulting scheme is not practical. Here the gain G is large and the sliding motion will be governed by two quite poorly damped dominant complex eigenvalues. This motivates the consideration of compensator based output feedback sliding mode controller design.

6.6 A compensator based existence problem

So far, only the static output feedback case has been considered. In certain circumstances, the subsystem triple $(\tilde{A}_{11}, \tilde{B}_1, \tilde{C}_1)$ is known to be infeasible (it is easy to construct SISO examples to demonstrate this – see for instance [31]). In such situations, Bag et al. [12] consider the introduction of a dynamic compensator similar to that of [38]. Work by Kwan [70, 71] considers the introduction of one-dimensional compensators to facilitate the design of a control law which satisfies the reachability problem. The following sections discuss the problem in more generality.

6.6.1 Compensator design

Specifically, let

$$\dot{x}_c(t) = Hx_c(t) + Dy(t) \quad (6.27)$$

where the matrices $H \in \mathbb{R}^{q \times q}$ and $D \in \mathbb{R}^{q \times p}$ are to be determined. Define a new hyperplane in the augmented state space, formed from the plant and compensator state spaces, as

$$\mathcal{S}_c = \{(x, x_c) \in \mathbb{R}^{n+q} : F_c x_c + FCx = 0\} \quad (6.28)$$

where $F_c \in \mathbb{R}^{m \times q}$ and $F \in \mathbb{R}^{m \times p}$. Define $D_1 \in \mathbb{R}^{q \times (p-m)}$ and $D_2 \in \mathbb{R}^{q \times m}$ as

$$\begin{bmatrix} D_1 & D_2 \end{bmatrix} = DT \quad (6.29)$$

then the compensator can be written as

$$\dot{x}_c(t) = Hx_c(t) + D_1C_1x_1(t) + D_2x_2(t) \quad (6.30)$$

where C_1 is defined in Equation (6.14). Assume that a control action exists which forces and maintains motion on the hyperplane \mathcal{S}_c given in Equation (6.28). As before, in order for a unique equivalent control to exist, the square matrix F_2 must be invertible. By writing $K = F_2^{-1}F_1$ and defining $K_c = F_2^{-1}F_c$ then the system matrix governing the reduced order sliding motion, obtained by eliminating the coordinates x_2 , can be written as

$$\dot{x}_1(t) = (A_{11} - A_{12}KC_1)x_1(t) - A_{12}K_cx_c(t) \quad (6.31)$$

$$\dot{x}_c(t) = (D_1 - D_2K)C_1x_1(t) + (H - D_2K_c)x_c(t) \quad (6.32)$$

If A_{121} represents the first r rows of A_{12} then from Equation (6.10) it follows that

$$\begin{bmatrix} A_{11} - A_{12}KC_1 & -A_{12}K_c \\ (D_1 - D_2K)C_1 & H - D_2K_c \end{bmatrix} = \begin{bmatrix} A_{11}^o & A_{12}^o - A_{121}K\tilde{C}_1 & -A_{121}K_c \\ 0 & \tilde{A}_{11} - \tilde{B}_1K\tilde{C}_1 & -\tilde{B}_1K_c \\ 0 & (D_1 - D_2K)\tilde{C}_1 & H - D_2K_c \end{bmatrix}$$

As in the uncompensated case, it is necessary for the eigenvalues of A_{11}^o to have negative real parts. The design problem becomes one of selecting a compensator, represented by the matrices D_1 , D_2 and H , and a hyperplane, represented by the matrices K and K_c , so that the matrix

$$A_c = \begin{bmatrix} \tilde{A}_{11} - \tilde{B}_1K\tilde{C}_1 & -\tilde{B}_1K_c \\ (D_1 - D_2K)\tilde{C}_1 & H - D_2K_c \end{bmatrix} \quad (6.33)$$

is stable. One approach is to specifically choose $D_2 = 0$ in Equation (6.33). The resulting matrix can be viewed as the negative feedback interconnection of the 'plant' $G_p(s) = \tilde{C}_1(sI - \tilde{A}_{11})^{-1}\tilde{B}_1$ and the 'compensator'

$$K(s) = K + K_c(sI - H)^{-1}D_1 \quad (6.34)$$

(see for instance pp.66 in [126]). In certain situations it is advantageous to consider the feedback configuration in Figure 6.2 and to design a compensator $K(s)$ using any time domain/frequency domain method to yield appropriate closed-loop performance. From the state-space realization of $K(s)$ in Equation (6.34), the parameters K , K_c , D_1 and H can be identified. If

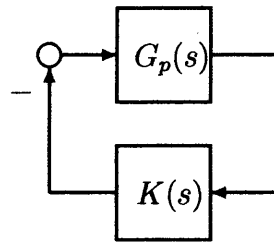


Figure 6.2: A general linear feedback configuration

the quantity $p - m$ is small, using ‘classical control’ ideas, very simple compensators may be found which give good closed-loop performance to the fictitious feedback system in Figure 6.2 which governs the sliding mode performance of the real system.

The third order ‘plant’ from Equation (6.15) has a double pole at the origin. In terms of classical control, this suggests the use of a lead-compensator. Choosing

$$K(s) = \frac{(s + 0.5)}{(s + 10)} \quad (6.35)$$

in unity feedback with $G_p(s)$ gives closed loop poles at

$$\{-12.1413, -0.9656, -1.2490 \pm 0.9718\}$$

This has improved the damping ratio of the dominant complex pair. A realization of the compensator in Equation (6.35) is $H = -10$, $D_1 = 1$, $K_c = -9.5$ and $K = 1$. Using these values and $D_2 = 0$ in the formulae in Equations (6.12) and (6.29) gives

$$F_a := \begin{bmatrix} F_c & F \end{bmatrix} = \begin{bmatrix} -11.7059 & 1.2322 & 1.2322 \end{bmatrix} \quad (6.36)$$

and

$$D = \begin{bmatrix} 1 & 0 \end{bmatrix}$$

Using these matrices, an appropriate controller to induce a sliding motion may be obtained by using the method in Section 6.5.1 on the augmented system

$$A_a = \begin{bmatrix} H & DC \\ 0 & A \end{bmatrix} \quad B_a = \begin{bmatrix} 0 \\ B \end{bmatrix} \quad C_a = \begin{bmatrix} 1 & 0 \\ 0 & C \end{bmatrix} \quad (6.37)$$

where the switching function matrix F_a is defined in Equation (6.36). Using $h_2 = -0.8$ and $r_d = 50$ gives

$$G = \begin{bmatrix} -45.9050 & 4.7749 & 0.3392 \end{bmatrix}$$

and

$$\lambda(A_a - B_a G C_a) = \{-8.6605, -3.0494 \pm 1.9424i, -0.8238 \pm 0.3124\}$$

6.7 Simulation of Vehicle System in a Split- μ Braking Manoeuvre with Compensator-Based Sliding Mode Control Scheme

Similar to the observer-based control scheme in Chapter 5, the compensator-based controller design was tested by simulation on the vehicle model performing a harsh split- μ braking manoeuvre. As before, the vehicle is initially travelling in a straight trajectory, with a longitudinal velocity of 27ms^{-1} (or approximately 97kmhr^{-1}), when it encounters a split- μ surface. This surface is (initially) symmetric about the central longitudinal axis of the car, with coefficient of friction, $\mu = 0.8$ (dry) and $\mu = 0.2$ (ice) on the left and right side of the car respectively. The driver's desire is for the vehicle to come to a complete halt as quickly as possible, (ideally) without deviating from the original straight trajectory.

Again, the steer-by-wire system will alter the front wheel position (the control input) in an effort to brake in a straight line. The key requirement is, therefore, to keep the third state, Y , in Equations (5.15)-(5.17) as near to zero as possible.

From the canonical form in Equation (6.15) the output of the fictitious system $G_p(s) = C_1(sI - A_{11})^{-1}A_{12}$ (as far as the switching function design is concerned) is, in the real system, the output of interest, Y . Because $G_p(s)$ has a double integrator characteristic no integral action is needed to achieve a steady state error of zero. Thus, the lead compensator from Section 6.6 and the associated controller can be used.

6.7.1 Simulation Results

The closed-loop simulation obtained from a fully nonlinear model is shown in Figures 6.3 and 6.4. In all of the results presented here, the results from Chapter 5 are shown, on the same axes,

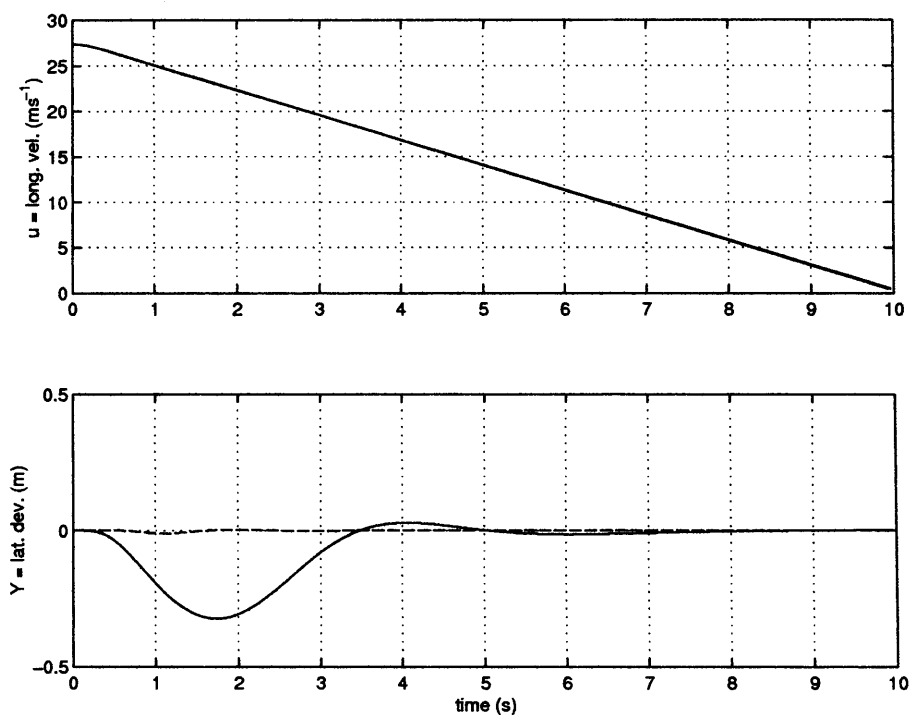


Figure 6.3: Vehicle longitudinal velocity and lateral deviation for closed-loop simulation

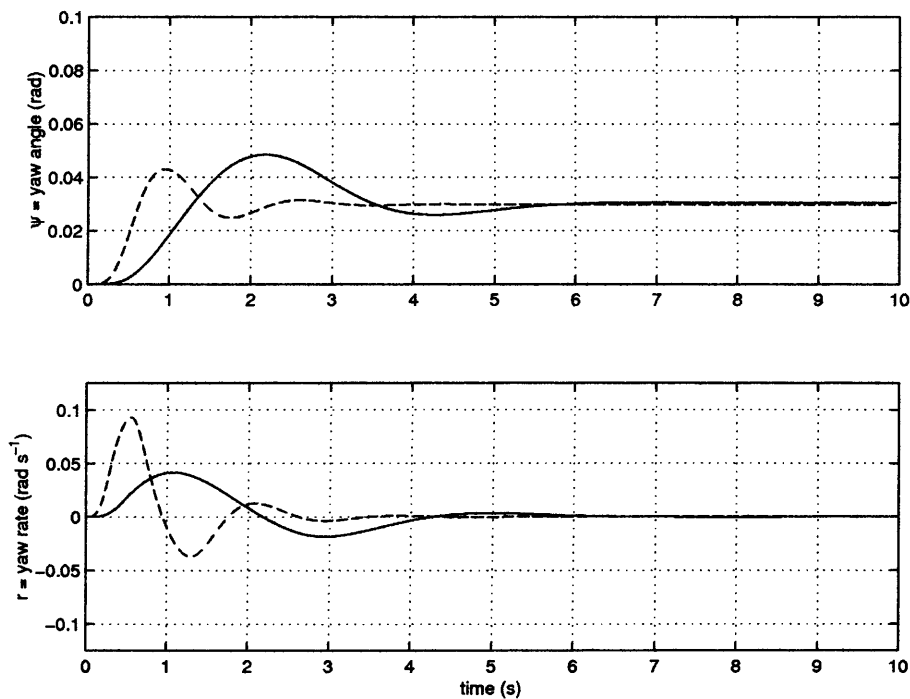


Figure 6.4: Vehicle yaw angle and yaw rate for closed-loop simulation

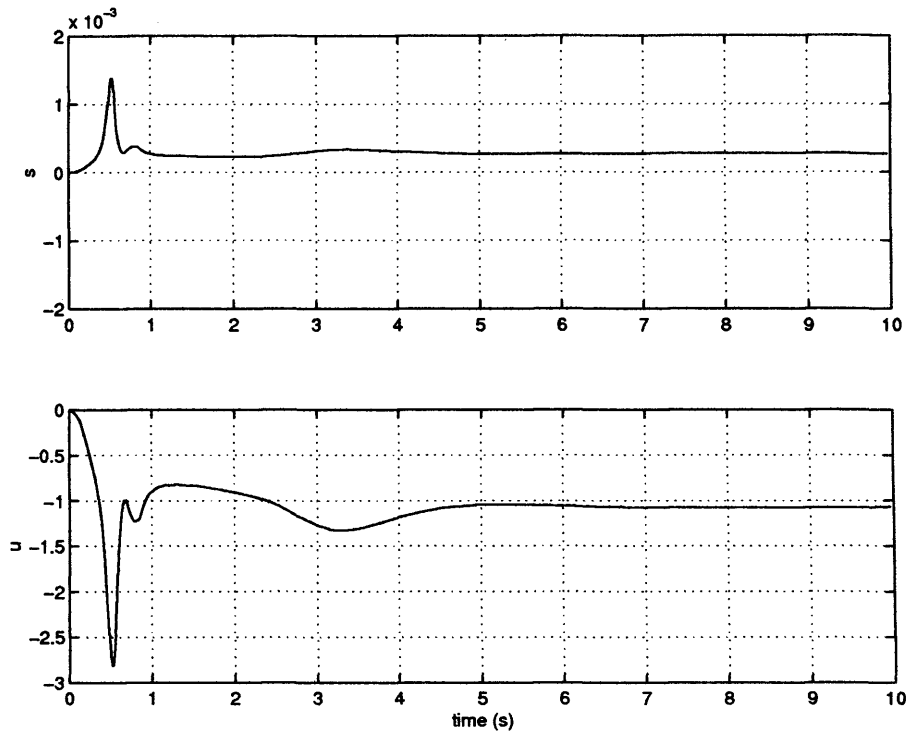


Figure 6.5: Switching function and control signal

with dashed lines. The controller manages to stop the vehicle from developing an excessive yaw angle, which peaks at around 3° . Also, the lateral deviation, Y , is halted with a peak of 32cm and is regulated to zero. The controller develops and maintains sufficient yaw angle to counteract the yawing moment induced by the asymmetric braking. The input signal which the controller utilizes to perform this is shown in Figure 6.5. This figure also demonstrates that a sliding motion is maintained throughout the manoeuvre.

6.7.2 Further Robustness Testing

In order to test the robustness of the control scheme, as in Section 5.3.2, closed-loop simulations are performed in which the longitudinal and lateral tyre stiffnesses are decreased: initially by 15% - corresponding to under-inflated tyres; then more harshly, by 40%.

The results are seen in the new plots (Figures 6.6-6.8, and Figures 6.9-6.11). The controller reacts in a similar way as in the previous simulation, achieving and maintaining sliding throughout. The peak vehicle lateral deviation increases from 35cm in the nominal case to 45cm in the

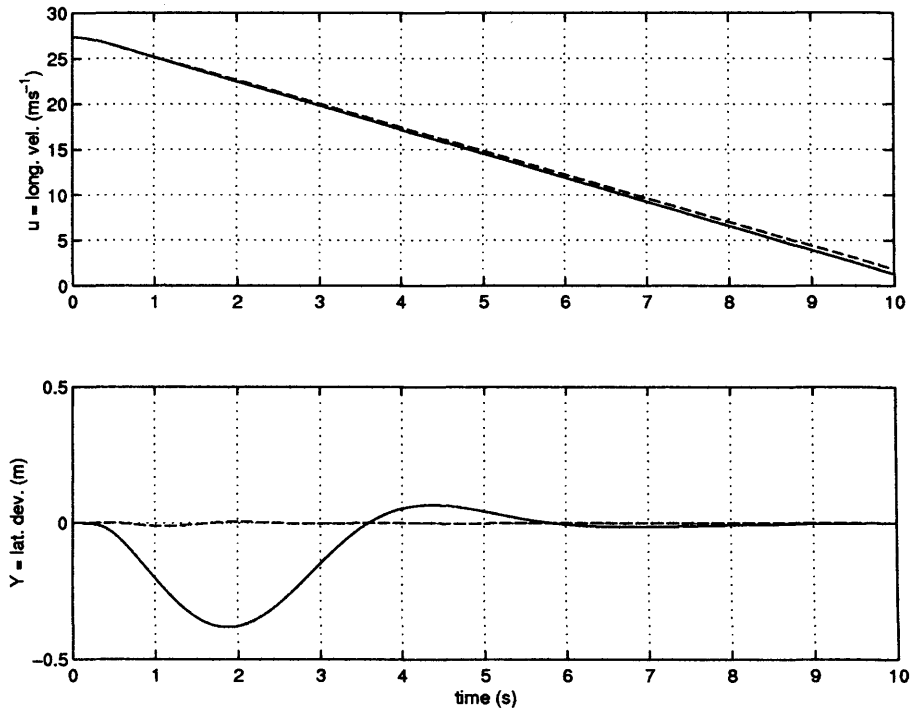


Figure 6.6: Vehicle longitudinal velocity and lateral deviation for robustness test: 15% tyre stiffness reduction

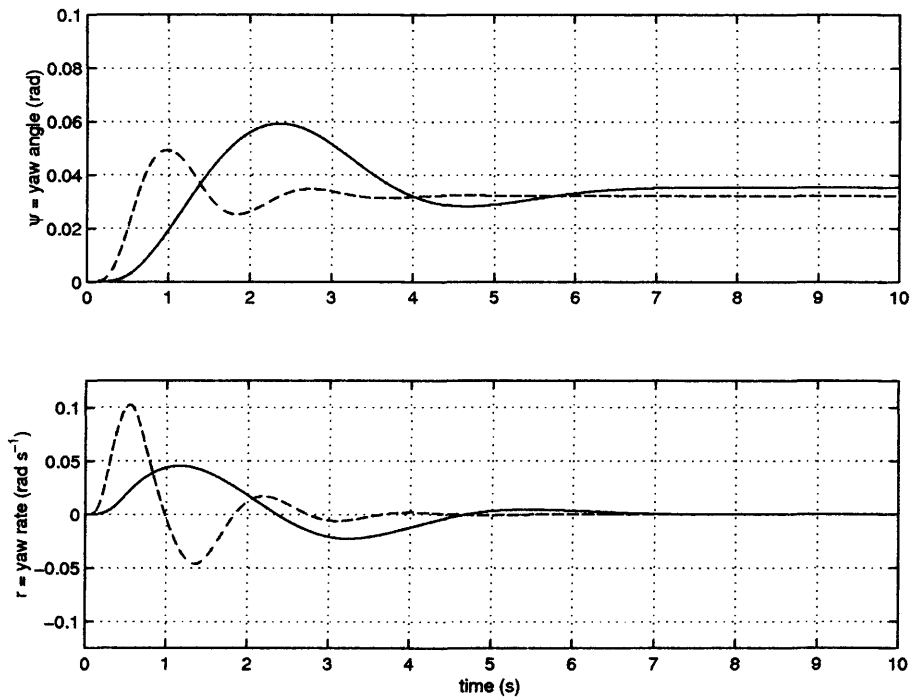


Figure 6.7: Vehicle yaw angle and yaw rate for robustness test: 15% tyre stiffness reduction

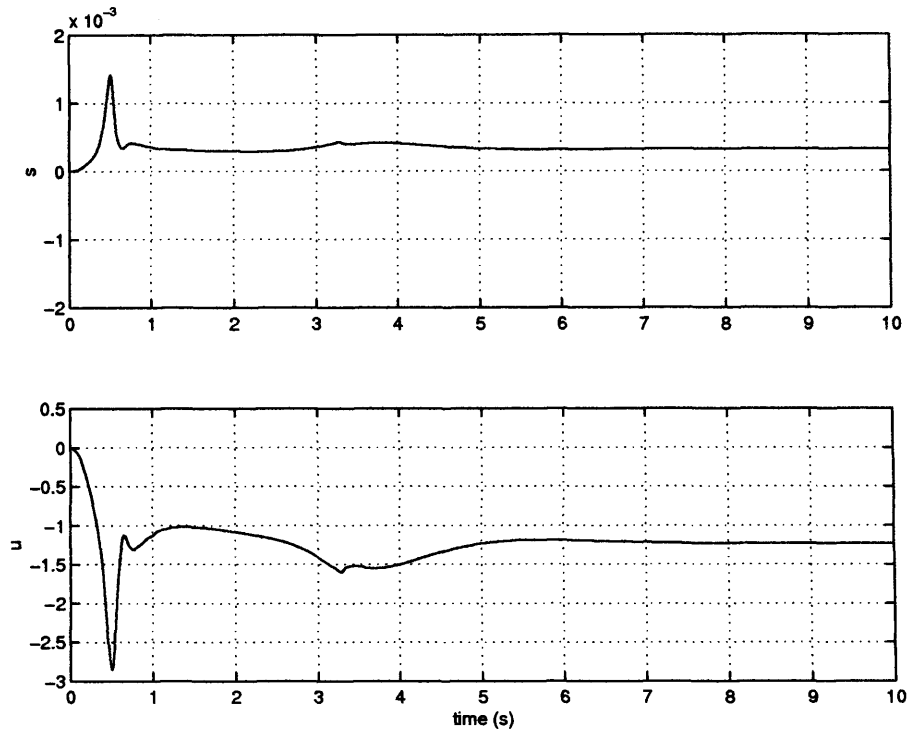


Figure 6.8: Switching function and control signal for robustness test: 15% tyre stiffness reduction

40% reduction test. Also, in the robustness tests, the closed-loop response becomes increasingly oscillatory, with the lateral velocity, yaw angle and yaw rate states all suffering decreased damping. In the case of the 40% robustness test, the settling time for the yaw rate is longer than 8 seconds.

6.7.3 Comparison of observer-based and compensator-based controllers

Comparing Figures 6.3-6.5 (which show the compensator-based control scheme response) with Figures 5.4-5.6 (which show the observer-based control scheme response), a number of clear differences can be seen. Whereas the compensator-based controller (which will be referred to as controller B, for the discussion in this section) showed a dramatic improvement relative to the open-loop simulation (Figures 5.2-5.3), it produced an inferior response to that obtained by the observer-based controller (termed controller A). The peak lateral deviation, Y , recorded using controller B was over three times the magnitude of the value whilst using controller A.

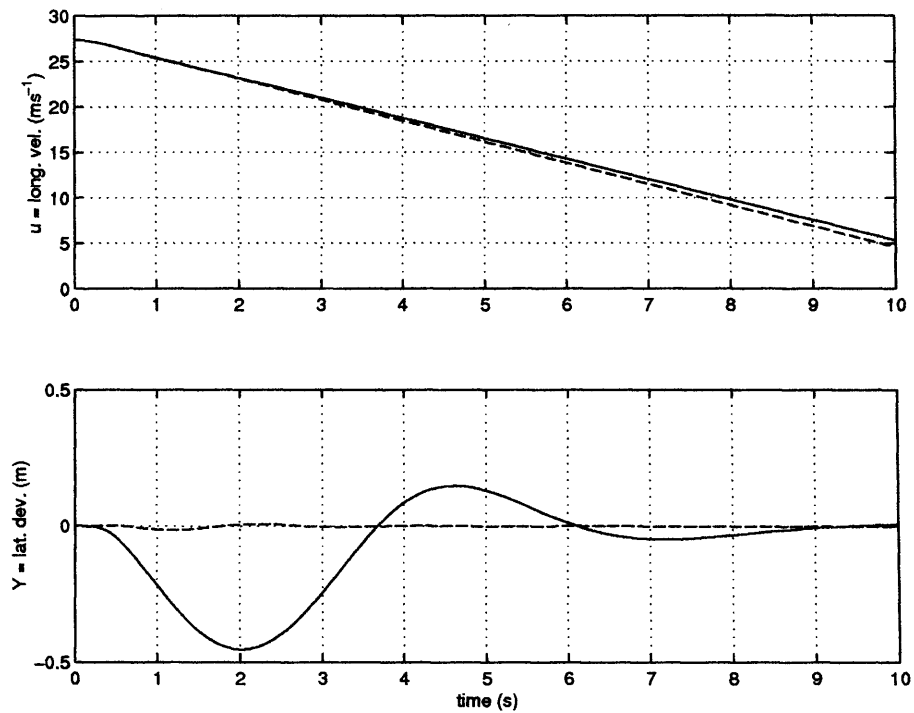


Figure 6.9: Vehicle longitudinal velocity and lateral deviation for robustness test: 40% tyre stiffness reduction

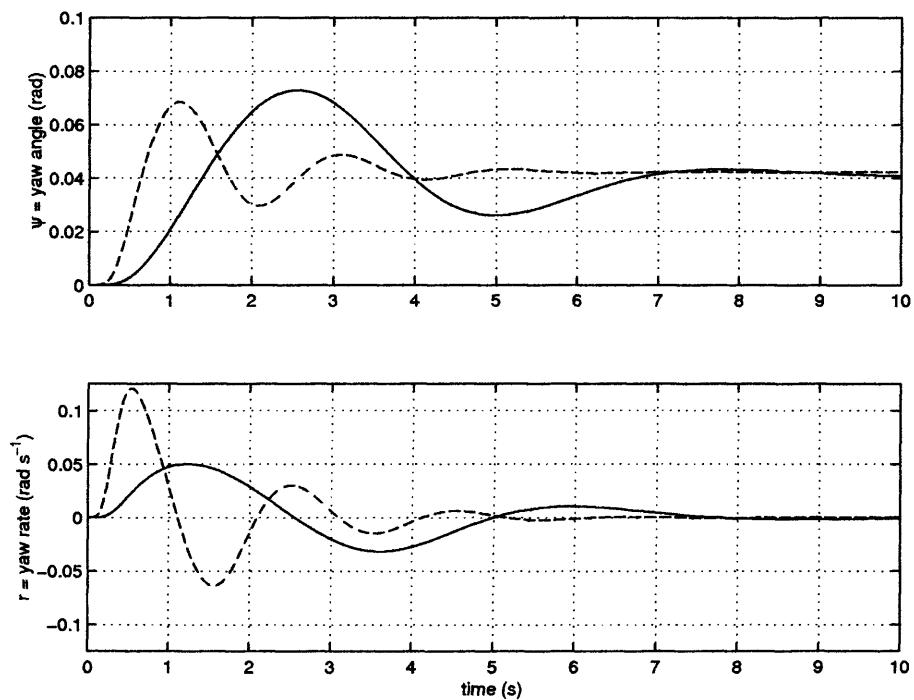


Figure 6.10: Vehicle yaw angle and yaw rate for robustness test: 40% tyre stiffness reduction

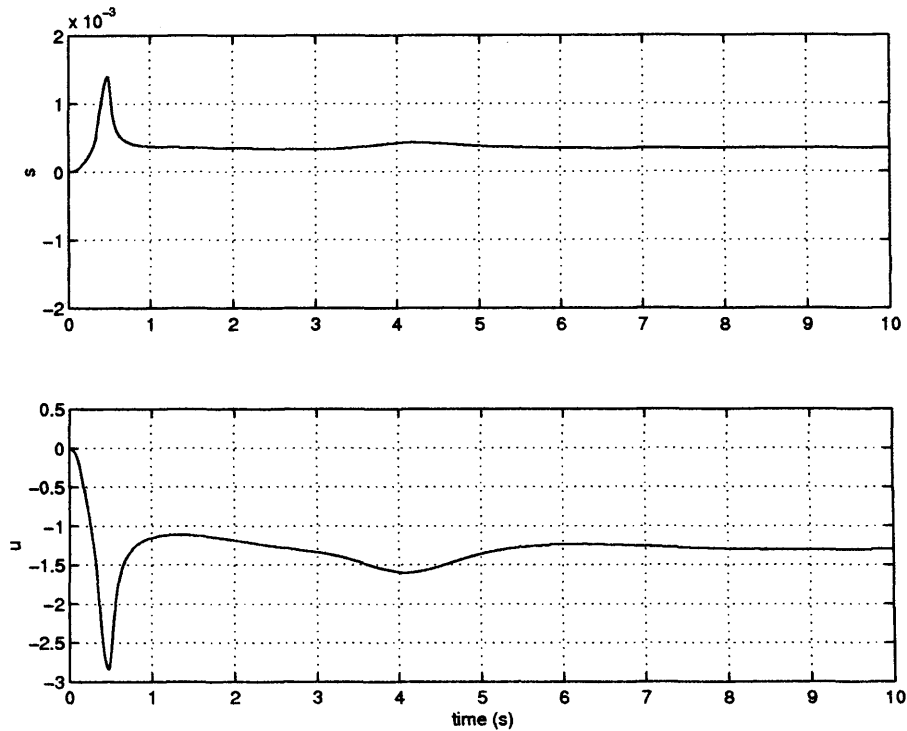


Figure 6.11: Switching function and control signal for robustness test: 40% tyre stiffness reduction

The yaw rate induced to maintain a small lateral deviation shows a far slower response for controller B, leading to a higher peak yaw angle, ψ .

More significantly, the closed-loop system incorporating controller B is far less well damped than the system using controller A, resulting in a more oscillatory response. This oscillatory response becomes increasingly exaggerated in the robustness tests. The peak yaw rate value is higher for controller A (shown in Figure 5.4) than controller B (Figure 6.3), but it is damped roughly twice as quickly.

6.8 Conclusions

This chapter has considered the use of a novel compensator-based sliding mode control scheme for an uncertain linear system representation when only output information is available to the controller. It is shown that in situations where compensators are required, appropriate system parameterizations have been constructed in order to recover the switching surface and

compensator dynamics efficiently. A novel parameterization has been proposed which enables 'classical control' ideas to be used in certain situations to synthesize the gains. A new design methodology is presented where the four elements of Equation (6.34) are chosen to design a compensator $K(s)$. A compensator-based controller has been designed for the automotive split- μ braking application, as in Chapter 5, which has been tested by simulation on the same nonlinear vehicle model, with robustness tests. The compensator-based controller has been compared with the observer-based controller in Chapter 5, and whilst it has the advantage of having closed-loop dynamics of lower order, it has been shown, in this example, to be less robust to parameter uncertainty, particularly in terms of maintaining sufficient damping.

The next chapter will deal with the problem of identification and prediction of a split- μ braking manoeuvre, as well as three further, potentially dangerous vehicle scenarios. This is useful as many different types of controller exist on current vehicles, and early prediction of potentially dangerous manoeuvres would allow the appropriate controller, such as those presented in Chapters 5 and 6, to be engaged as necessary.

Chapter 7

Vehicle Scenario Prediction Using Sliding Mode

7.1 Introduction

This chapter describes a novel scheme capable of predicting when a vehicle performing a transient manoeuvre enters a potentially dangerous scenario, such as severe oversteer, severe understeer, or split- μ braking, to distinguish between these scenarios, and to give some indication of their severity. This information could be used, in real-time, to select a control strategy appropriate to the vehicle's circumstances, such as controllers which attempt to improve ride comfort in normal driving, vehicle stability controllers which manipulate individual wheel torques to prevent a vehicle from understeering or oversteering dangerously, or controllers to facilitate safe braking on harsh split- μ surfaces.

This approach of recognizing potentially dangerous vehicle scenarios by patterns in these signals is new, and simpler than existing systems. However, the scheme identifies potential vehicle scenarios extremely early. In this chapter, a novel sliding mode estimator has been designed specifically for this application.

The scheme presented has the advantage of possessing the flexibility to be retro-fitted to systems with existing controllers, and could be used as part of a supervisory scheme, optimally engaging other control systems.

7.2 The Scenario Detection Problem

Various commercial systems now in the marketplace, such as Dynamic Stability Control (DSC - BMW, Jaguar); Electronic Stabilization Programme (ESP - Audi, Mercedes-Benz, SAAB) [15]; Vehicle Stability Control (VSC - Toyota, Lexus); and Vehicle Stability Enhancement System (VSES - TRW Automotive), use a combination of wheel speeds, ABS information, yaw rate, lateral acceleration and steer angle and seek to robustly estimate all the vehicle states. In this chapter a simpler approach will be adopted which does not attempt to explicitly estimate the states, but instead looks for ‘signature differences’ between the behaviour of an ideal linear vehicle model and the actual measured behaviour. In this way, the scheme presented here will use vehicle yaw moment, lateral force and its derivative at the outset of a steer (or split- μ) event to maximize phase advantage in the information available, and get detection of the scenario as rapidly as possible. For the remainder of this chapter, the terms ‘understeer’ and ‘oversteer’ will be used to mean ‘terminal understeer’ and ‘terminal oversteer’.

The approach taken in the work described in this chapter makes the assumption that as a vehicle starts to terminally understeer, oversteer, or enter a harsh split- μ braking manoeuvre, both *unexpected vehicle yaw moments* and *unexpected lateral forces* will arise. For each of the scenarios, these two signals can reasonably be expected to display differing characteristic signatures. These quantities are difficult to measure directly and instrumentation to do so is unlikely to be fitted to commercial vehicles. Therefore, if a scheme can be designed to reconstruct these ‘unexpected’ signals from more easily measured quantities, the vehicle scenario may be determined and an appropriate control strategy selected. In the proposed scheme, it is assumed that measurements of yaw rate, r , and lateral acceleration, a_y , are available. It is also assumed that the front road-wheel steer angle, δ_f , and its derivative, is known.

It is also significant to note that, as stated in Section 2.4, the observer is designed about a model which itself has an understeer gradient which should match that of the vehicle at low lateral accelerations. In practice this means that where there is no disparity at all between the linear and nonlinear models, it should be implied that the nonlinear model is, rather than neutral steering, slightly understeering with the same understeer gradient as the linear model.

angles at the front and rear of the vehicle respectively. Given that

$$\alpha_f = \frac{v + ar}{u} - \delta_f \quad (7.2)$$

$$\alpha_r = \frac{v - br}{u} \quad (7.3)$$

then

$$I_z \dot{r} = -2aC_{\alpha f} \left(\frac{v + ar}{u} - \delta_f \right) + 2bC_{\alpha r} \left(\frac{v - br}{u} \right) + M_{z,un} \quad (7.4)$$

and so

$$\dot{r} = \underbrace{\frac{2(bC_{\alpha r} - aC_{\alpha f})}{I_z u}}_{A_{12}} v - \underbrace{\frac{2(a^2C_{\alpha r} + b^2C_{\alpha f})}{I_z u}}_{A_{11}} r + \underbrace{\frac{2aC_{\alpha f}}{I_z}}_{B_1} \delta_f + \frac{M_{z,un}}{I_z} \quad (7.5)$$

Given that the lateral acceleration

$$a_y = \dot{v} + ur \quad (7.6)$$

then

$$m_v a_y = F_{yf} + F_{yr} + F_{y,un} \quad (7.7)$$

Substituting for a_y from Equation (7.6)

$$m_v(\dot{v} + ur) = -2C_{\alpha f}\alpha_f - 2C_{\alpha r}\alpha_r + F_{y,un} \quad (7.8)$$

and so

$$\dot{v} = -\underbrace{\frac{2(C_{\alpha f} + C_{\alpha r})}{m_v u}}_{A_{22}} v + \left(\underbrace{\frac{2(bC_{\alpha r} - aC_{\alpha f})}{m_v u}}_{A_{21}} - u \right) r + \underbrace{\frac{2C_{\alpha f}}{m_v}}_{B_2} \delta_f + \frac{F_{y,un}}{m_v} \quad (7.9)$$

For design purposes the outputs may then be described as r and a_y , where

$$a_y = A_{21}r + A_{22}v + B_2\delta_f + \frac{F_y}{m_v} \quad (7.10)$$

For the development which follows, it is convenient to establish new equations in terms of r and a_y . By re-arranging Equation (7.9) and substituting for \dot{v} from Equation (7.6) an expression for $v(r, a_y)$ is:

$$\begin{aligned} v &= \frac{1}{A_{22}} \left(\dot{v} - (A_{21} - u)r - B_2\delta_f - \frac{F_y}{m_v} \right) \\ &= \frac{1}{A_{22}} \left(-A_{21}r + a_y - B_2\delta_f - \frac{F_y}{m_v} \right) \end{aligned} \quad (7.11)$$

Substituting from Equation (7.11) into Equation (7.5) gives

$$\begin{aligned}\dot{r} &= A_{11}r + \frac{A_{12}}{A_{22}} \left(a_y - A_{21}r - B_2\delta_f - \frac{F_y}{m_v} \right) + B_1\delta_f + \frac{M_z}{I_z} \\ &= \left(A_{11} - \frac{A_{12}}{A_{22}}A_{21} \right) r + \frac{A_{12}}{A_{22}}a_y + \left(B_1 - \frac{A_{12}}{A_{22}}B_2 \right) \delta_f + \frac{M_{z,un}}{I_z} - \frac{A_{12}}{A_{22}} \frac{F_{y,un}}{m_v}\end{aligned}\quad (7.12)$$

Differentiating Equation (7.10) yields

$$\dot{a}_y = A_{21}\dot{r} + A_{22}\dot{v} + B_2\dot{\delta}_f + \frac{\dot{F}_y}{m_v}\quad (7.13)$$

then substituting from Equations (7.5) and (7.6)

$$\dot{a}_y = A_{21} \left(A_{11}r + A_{12}v + B_1\delta_f + \frac{M_z}{I_z} \right) + A_{22}(a_y - ur) + B_2\dot{\delta}_f + \frac{\dot{F}_y}{m_v}\quad (7.14)$$

which, on collecting terms, yields

$$\begin{aligned}\dot{a}_y &= \left(A_{11}A_{21} - A_{22}u - \frac{A_{12}}{A_{22}}A_{21}^2 \right) r + \left(A_{22} + \frac{A_{12}}{A_{22}}A_{21} \right) a_y \\ &\quad + A_{21} \left(B_1 - \frac{A_{12}}{A_{22}}B_2 \right) \delta_f + B_2\dot{\delta}_f + A_{21} \frac{M_{z,un}}{I_z} - \frac{A_{12}}{A_{22}}A_{21} \frac{F_{y,un}}{m_v} + \frac{\dot{F}_{y,un}}{m_v}\end{aligned}\quad (7.15)$$

7.4 Sliding Mode Unexpected Input Estimator

Sliding mode ideas will be used in order to estimate the unknown signals $\dot{F}_{y,un}$, $F_{y,un}$, $M_{z,un}$. The estimator uses two discontinuous injection signals, ν_r and ν_a , to try to force the observed states, \tilde{r} and \tilde{a}_y , to track the measured states of the system, r and a_y from Equations (7.12) and (7.15), perfectly. Specifically, the observer takes the form:

$$\dot{\tilde{r}} = \left(A_{11} - \frac{A_{12}}{A_{22}}A_{21} \right) \tilde{r} + \frac{A_{12}}{A_{22}}\tilde{a}_y + \left(B_1 - \frac{A_{12}}{A_{22}}B_2 \right) \delta_f + \nu_r\quad (7.16)$$

$$\begin{aligned}\dot{\tilde{a}}_y &= \left(A_{11}A_{21} - A_{22}u - \frac{A_{12}}{A_{22}}A_{21}^2 \right) \tilde{r} + \left(A_{22} + \frac{A_{12}}{A_{22}}A_{21} \right) \tilde{a}_y \\ &\quad + A_{21} \left(B_1 - \frac{A_{12}}{A_{22}}B_2 \right) \delta_f + B_2\dot{\delta}_f + \nu_a\end{aligned}\quad (7.17)$$

where

$$\nu_r = -\rho_r \text{sgn}e_r\quad (7.18)$$

$$\nu_a = -\rho_a \text{sgn}e_a\quad (7.19)$$

and $e_r = \tilde{r} - r$ and $e_a = \tilde{a}_y - a_y$.

The positive scalars ρ_r and ρ_a are design parameters and must be chosen large enough to induce a sliding motion on $e_r = 0$ and $e_a = 0$.

From Equations (7.12) and (7.16) the error in the yaw rate estimation, e_r may be written as:

$$\begin{aligned} \dot{e}_r &= \dot{\tilde{r}} - \dot{r} \\ &= \left(A_{11} - \frac{A_{12}}{A_{22}} A_{21} \right) (\tilde{r} - r) + \frac{A_{12}}{A_{22}} (\tilde{a}_y - a_y) + \nu_r - \left(\frac{M_{z,un}}{I_z} - \frac{A_{12}}{A_{22}} \frac{F_{y,un}}{m_v} \right) \\ &= \left(A_{11} - \frac{A_{12}}{A_{22}} A_{21} \right) e_r + \frac{A_{12}}{A_{22}} e_a + \nu_r - \frac{M_{z,un}}{I_z} + \frac{A_{12}}{A_{22}} \frac{F_{y,un}}{m_v} \end{aligned} \quad (7.20)$$

and from Equations (7.15) and (7.17)

$$\begin{aligned} \dot{e}_a &= \dot{\tilde{a}_y} - \dot{a}_y \\ &= \left(A_{11} A_{21} - \frac{A_{12}}{A_{22}} A_{21}^2 \right) (\tilde{r} - r) \\ &\quad + \left(A_{22} + \frac{A_{12}}{A_{22}} A_{21} \right) (\tilde{a}_y - a_y) + \nu_a - \left(\frac{M_{z,un}}{I_z} - \frac{A_{12}}{A_{22}} \frac{F_{y,un}}{m_v} \right) \\ &= \left(A_{11} A_{21} - A_{22} u - \frac{A_{12}}{A_{22}} A_{21}^2 \right) e_r + \left(\frac{A_{12}}{A_{22}} A_{21} \right) e_a \\ &\quad + \nu_a - A_{21} \frac{M_{z,un}}{I_z} + A_{21} \frac{A_{12}}{A_{22}} \frac{F_{y,un}}{m_v} + \frac{\dot{F}_{y,un}}{m_v} \end{aligned} \quad (7.21)$$

It can be seen that both $\dot{e}_r e_r < 0$ and $\dot{e}_a e_a < 0$ for a compact domain in the error space (e_a, e_r) which includes the origin. These inequalities constitute reachability conditions [114, 31] and so a sliding motion takes place on $e_r = e_a = 0$ in finite time. Once sliding is attained, $\dot{e}_r = \dot{e}_a = e_r = e_a = 0$, so Equations (7.20) and (7.21) become

$$0 = \bar{\nu}_r - \frac{M_{z,un}}{I_z} + \frac{A_{12}}{A_{22}} \frac{F_{y,un}}{m_v} \quad (7.22)$$

$$0 = \bar{\nu}_a - A_{21} \frac{M_{z,un}}{I_z} + A_{21} \frac{A_{12}}{A_{22}} \frac{F_{y,un}}{m_v} + \frac{\dot{F}_{y,un}}{m_v} \quad (7.23)$$

where $\bar{\nu}_r$ and $\bar{\nu}_a$ are the equivalent output error injection signals necessary to maintain sliding in the face of $F_{y,un}$ and $M_{z,un}$. These equivalent injection signals are analogous to the equivalent control signal discussed in Chapter 4. The information provided by the injection signals about the unexpected signals of interest is given by observing

$$\bar{\nu}_r = \frac{M_{z,un}}{I_z} - \frac{A_{12}}{A_{22}} \frac{F_{y,un}}{m_v} \quad (7.24)$$

$$\bar{v}_a = A_{21}\bar{v}_r + \frac{\dot{F}_{y,un}}{m_v} \quad (7.25)$$

Note that a component of the second injection signal, \bar{v}_a , is the scaled first injection signal, \bar{v}_r , and that, by subtracting this component, \bar{v}_a can be used to obtain an estimate of the unexpected signal, $\dot{F}_{y,un}$.

The first injection signal, \bar{v}_r , provides a weighted average of the unexpected signals, $M_{z,un}$ and $F_{y,un}$. As $M_{z,un}$ and $F_{y,un}$ are free to vary independently, this injection signal cannot be unravelled, without further information, to extract the two unexpected signals. However, it can be seen that, given the scalings present in Equation (7.24), the signal, \bar{v}_r , can usually be expected to be dominated by the unexpected yaw moment, $M_{z,un}$, since $\frac{A_{12}}{A_{22}} = 0.2026$ (and is independent of the forward speed u).

The two ‘unexpected’ signals which can be obtained, using this scheme, in order to attempt to determine the vehicle scenario, are \dot{F}_y and \bar{v}_r .

7.5 Scenario Detection

In this section, the various manoeuvres will be discussed in turn, each with a hypothesis outlining the characteristic signatures which might be expected from the signals of interest, according to simple vehicle dynamics arguments. Plots of the results of the particular manoeuvre simulations are then presented with explanations. Plots of the output estimation error signals and equivalent injection signals are also shown. The results of the simulations are then discussed for each manoeuvre, and compared with the hypothesis. Finally, in Section 7.5.5, the scenario detection results are summarized, and the signatures for each manoeuvre characterized.

In the simulations performed in this section, the sliding mode estimator presented in Section 7.4 will be used, employing the scalars $\rho_r = \rho_a = 100$ to be sure of maintaining sliding throughout the manoeuvres. In order to assess the accuracy of the reconstruction of the unexpected signals, it is useful to generate a comparison. As hinted at above, the unexpected signals occur whenever the system deviates from ideal linear behaviour, and so can be considered as

the nonlinear component of the total yaw moment and lateral force signals. In the non-linear model from Section 3.3, it is possible to pick out the total values for the vehicle yaw moment and lateral force, and to numerically differentiate the latter to give \dot{F}_y . The linear, ‘expected’ signals ($M_{z,l}$ and $F_{y,l}$) are calculated ‘off-line’, using the linear components of Equation (7.1) (ie. $M_{z,l} = M_{zf} - M_{zr}$) and Equation (7.9) (ie. $F_{y,l} = F_{yf} + F_{yr}$) respectively using the values of u , v and r from the simulation to calculate slip. The linear (‘expected’) signals are then subtracted from the total signals obtained from the nonlinear simulation and the remaining non-linear components are used as a comparison for the reconstructed ‘unexpected’ signals.

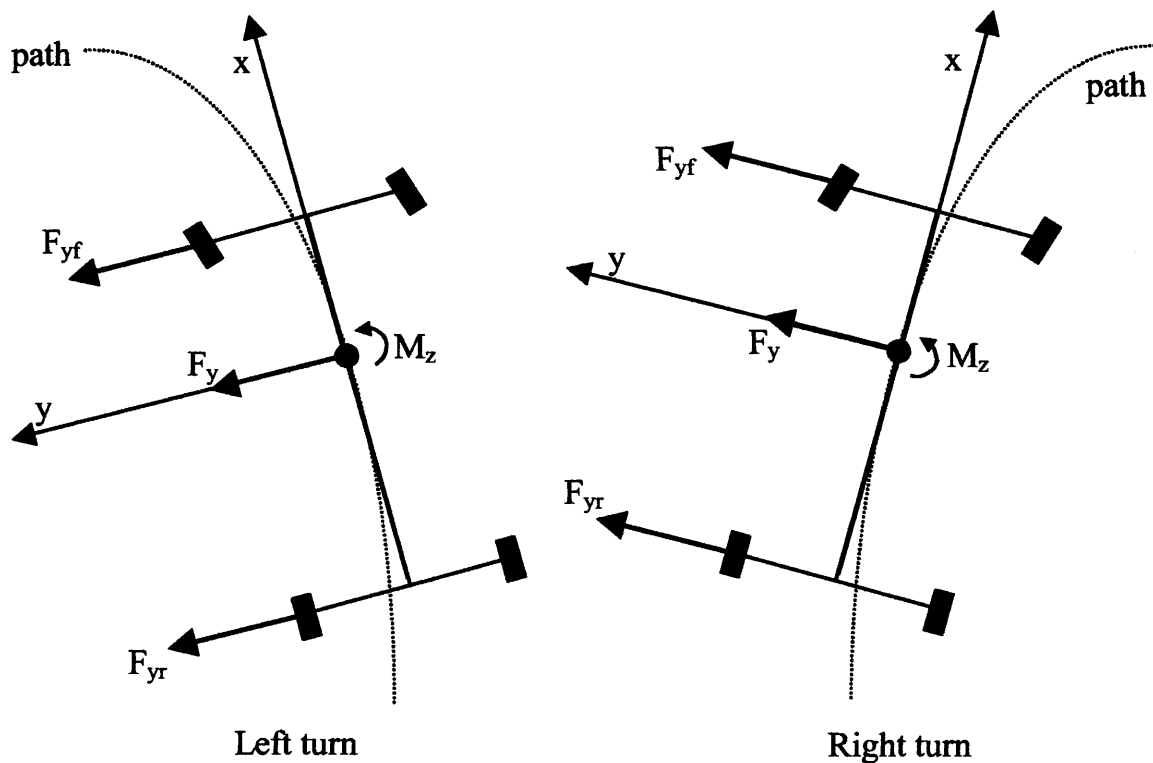


Figure 7.2: Turning geometry

Figure 7.2 shows a vehicle performing a left and a right turn, and reference to this figure will provide the basis for the scenario detection hypotheses which follow. The total lateral force, F_y , experienced by the vehicle is given, as in Equation (7.9), by

$$F_y = F_{y,l} + F_{y,un} \quad (7.26)$$

so that

$$F_{y,un} = (F_{yf} + F_{yr}) - F_{y,l} \quad (7.27)$$

Similarly, the total yaw moment (M_z) experienced by the vehicle is given by

$$M_z = M_{z,l} + M_{z,un} \quad (7.28)$$

so that

$$M_{z,un} = (aF_{yf} - bF_{yr}) - M_{z,l} \quad (7.29)$$

Of the four manoeuvres investigated, three deal with a vehicle understeering or oversteering. A vehicle which is neither understeering nor oversteering is said to be neutral steering. In this case

$$F_{yf} + F_{yr} = F_{y,l} \quad (7.30)$$

and so, from Equation (7.27)

$$F_{y,un} = 0 \quad (7.31)$$

Similarly, from Equation (7.29)

$$aF_{yf} - bF_{yr} = M_{z,l} \quad (7.32)$$

$$M_{z,un} = 0 \quad (7.33)$$

7.5.1 Understeer

Hypothesis: In an understeer manoeuvre, the actual yaw rate experienced by the vehicle is less than the yaw rate which would be expected if the vehicle were operating linearly. For this reason, it is sensible to expect that the build up of understeer would be accompanied by an ‘unexpected’ yaw moment, $M_{z,un}$, in a direction away from the turn.

In an understeer manoeuvre the front tyres saturate leading to an increase in front wheel slip-angles and increased lateral force, away from the turn, at the front of the vehicle. Therefore, an understeer manoeuvre should generate an ‘unexpected’ lateral force toward the outside of the turn, increasing as the severity of the understeer rises, and decreasing should the severity be reduced. The rate of change of lateral force - the reconstruction signal, $\dot{F}_{y,un}$ - should increase in the direction of the outside of the turn at the beginning of an understeer manoeuvre, drop

down to zero should the severity peak, and increase into the turn should the understeer die down. This can be seen by examining Figure 7.2 and Equations (7.27) and (7.29): in an understeer manoeuvre, as $|F_{yf}|$ is reduced,

$$|F_{yf} + F_{yr}| < |F_{y,l}| \quad (7.34)$$

In a left turn (as in the simulation), $F_{yf} > 0$, $F_{yr} > 0$, $F_{y,l} > 0$ and $M_{z,un} > 0$. Then from Equations (7.34) and (7.27) it follows

$$F_{y,un} < 0 \quad (7.35)$$

Also, since

$$aF_{yf} - bF_{yr} < M_{z,l} \quad (7.36)$$

from Equation (7.29)

$$M_{z,un} < 0 \quad (7.37)$$

However, in a right turn $F_{yf} < 0$, $F_{yr} < 0$ and $F_{y,l} < 0$. Then from Equations (7.34) and (7.27)

$$F_{y,un} > 0 \quad (7.38)$$

Also

$$|aF_{yf} - bF_{yr}| < |M_{z,l}| \quad (7.39)$$

and so, from Equation (7.29)

$$M_{z,un} > 0 \quad (7.40)$$

Thus, in an understeer manoeuvre, both the unexpected lateral force, and the unexpected yaw moment will always act in the opposite direction to the turn.

Understeer Results

Figure 7.3 shows an understeer manoeuvre performed on the nonlinear simulation described in Section 7.4. The first plot shows the road-wheel steering angle and results in a left turn. The second plot compares the actual yaw rate of the nonlinear model compared with the expected

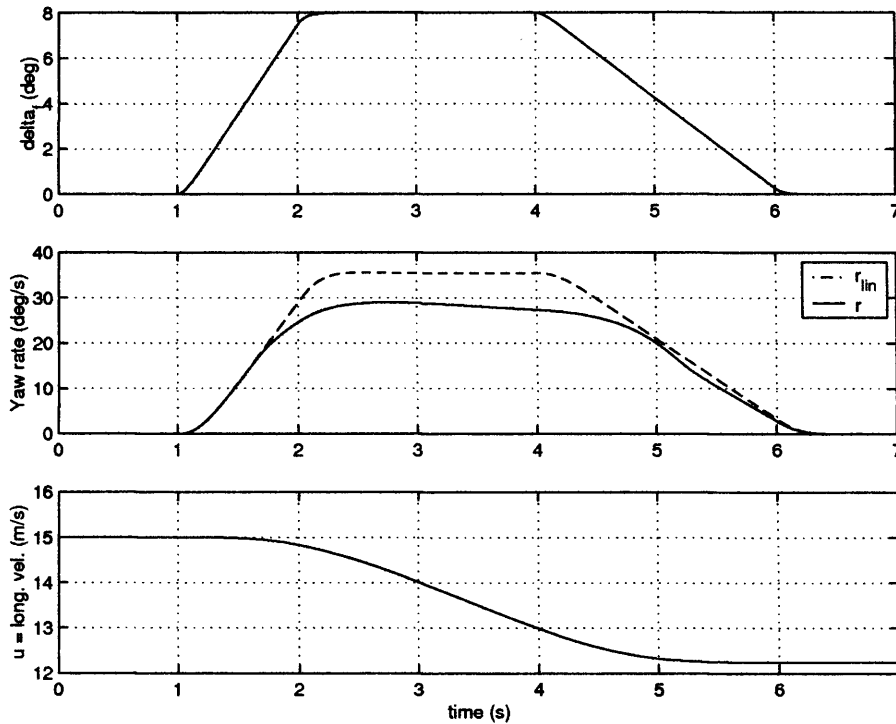


Figure 7.3: Understeer manoeuvre

yaw rate, taken from a linear model subject to the same wheel inputs. The third plot shows how the longitudinal velocity drops over the course of the simulation.

Figure 7.4 shows the output estimation error signals, e_r and e_a associated with the sliding mode observer, and it can be seen that a sliding motion is maintained throughout the simulation.

Figure 7.5 shows plots of the equivalent injection signals described in Equations (7.24) and (7.25). These are the signals the nonlinear injection terms in the observer needed to maintain sliding.

As discussed in Section 7.4, Figure 7.6 shows the ‘unexpected’ signal information, $\dot{F}_{y,un}$, and \bar{v}_r . The comparison signals (see Section 7.5) are plotted with the reconstruction signals from the estimator. In both cases, good agreement is displayed.

For easier visual analysis, the $\dot{F}_{y,un}$ signal has been integrated to give $F_{y,un}$, and this is used to calculate $M_{z,un}$ from the \bar{v}_r signal using Equation (7.25). These signals are plotted in Figure 7.7, along with the comparison signals, calculated as before. It is not expected that these signals, calculated via integration of the $\dot{F}_{y,un}$ signal, could be used in a practical application

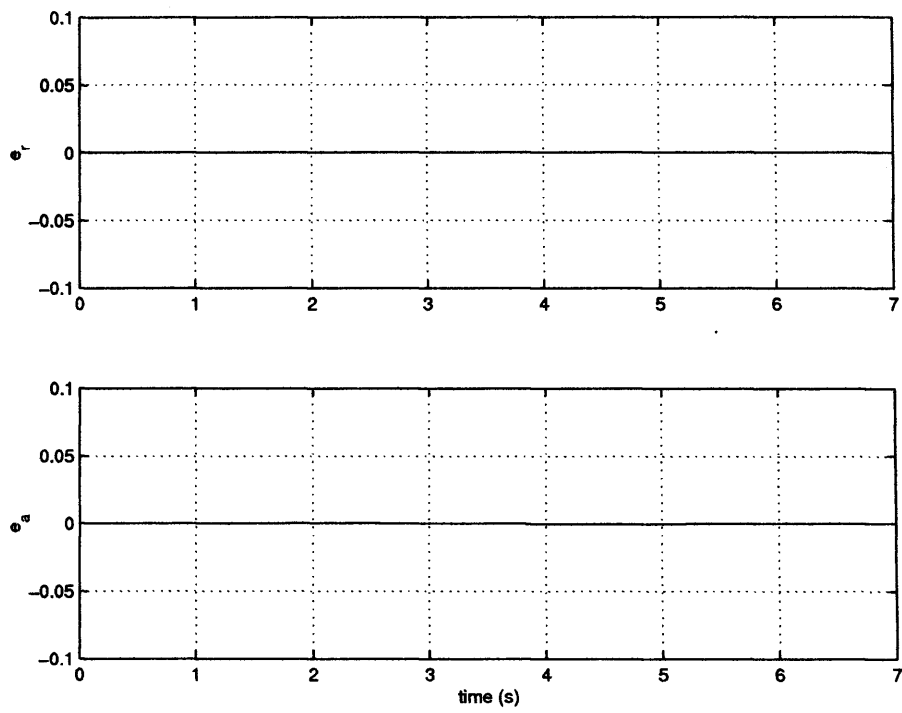


Figure 7.4: Understeer manoeuvre:- observer-state error signals

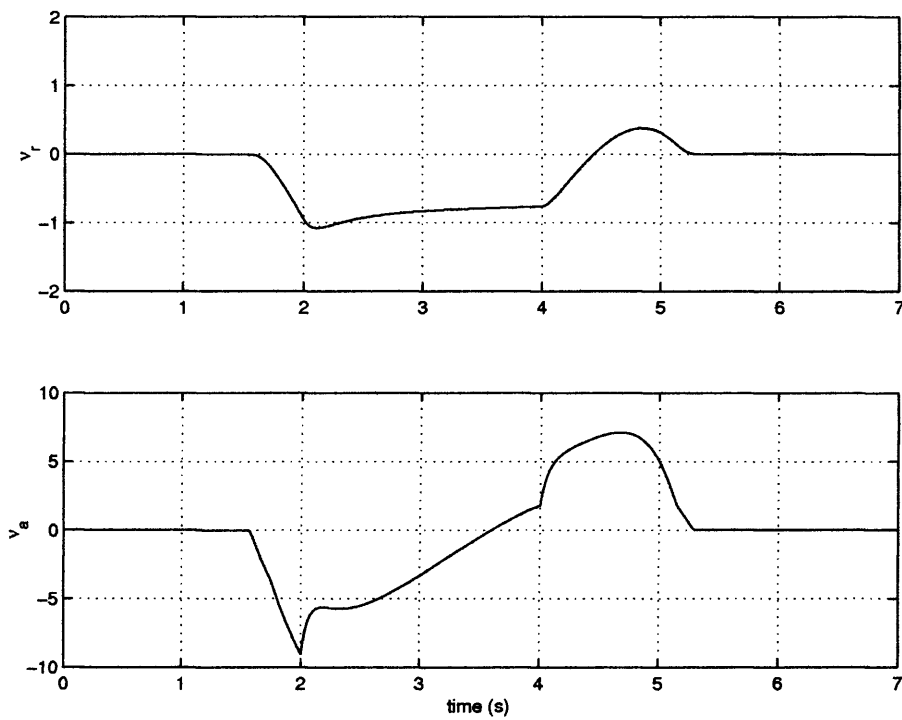


Figure 7.5: Understeer manoeuvre:- observer equivalent injection signals

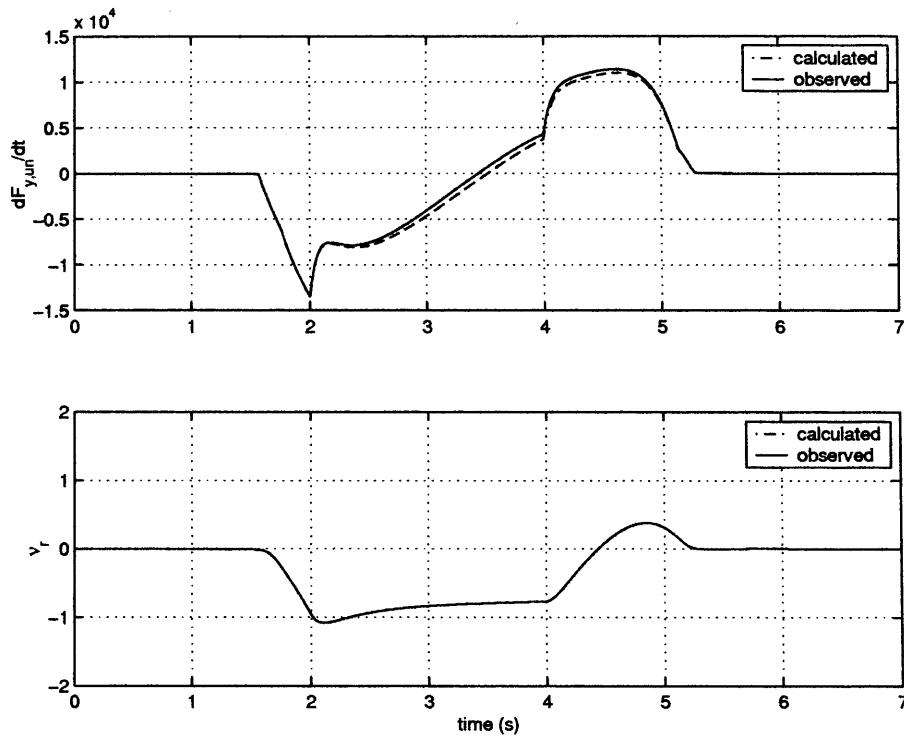


Figure 7.6: Understeer manoeuvre:- comparison of observed unexpected signals

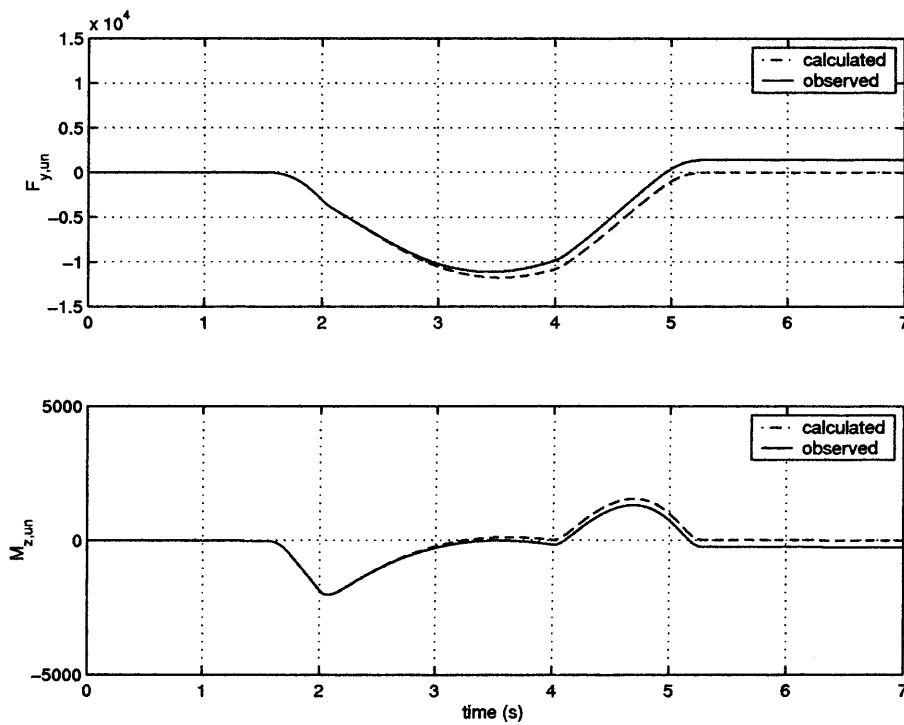


Figure 7.7: Understeer manoeuvre:- comparison of integrated observed unexpected signals

due to the problems associated with the integration of noisy signals but they are included for discussion purposes. They show the ability of the unknown input estimator to reconstruct the unexpected signals with good fidelity.

In the first half-second of the steering angle application (which begins at 1 second), the vehicle behaviour is linear, hence the yaw rate increases linearly. During this time, there are no ‘unexpected’ signals present, and none are detected. However, as soon as the vehicle begins to understeer at around 1.4s (shown in Figure 7.3) both the $\dot{F}_{y,un}$ and \bar{v}_r signals ramp down (Figure 7.6). This indicates an increasing unexpected lateral force and yaw moment - both toward the the outside of the bend. This agrees with the earlier hypothesis, which describes the understeering vehicle failing to generate the expected (+ve) yaw rate into the turn (ie. an unexpected (-ve) yaw moment), due to the front tyres having insufficient traction to generate the (+ve) lateral force necessary to make the turn (ie. an unexpected (-ve) lateral force toward the outside of the turn).

During the period in which the steering angle is maintained constant (between 2 and 4 seconds in Figure 7.3), it is straight-forward to see that the \bar{v}_r signal, dominated by the unexpected yaw moment, levels off and varies very little which may be expected as the severity of the understeer is unchanged. At the start of this period the unexpected lateral force gently peaks and falls away slightly. The corresponding derivative of this lateral force ($\dot{F}_{y,un}$), which is the quantity that is reconstructed, drops in magnitude before becoming positive.

As the steering angle is brought back to zero, so both the reconstructed signals \bar{v}_r and $\dot{F}_{y,un}$ return to zero.

7.5.2 Steady-State Oversteer

Hypothesis: In an oversteer manoeuvre, the actual yaw rate experienced by the vehicle is greater than the yaw rate which would be expected if the vehicle were operating linearly. For this reason, it is sensible to expect that the build up of oversteer would be accompanied by an additional ‘unexpected’ yaw moment, $M_{z,un}$, in the same direction as the turn.

In an oversteer manoeuvre the rear tyres saturate leading to an increase in rear wheel slip-angles and increased lateral force, away from the turn, at the rear of the vehicle. Therefore,

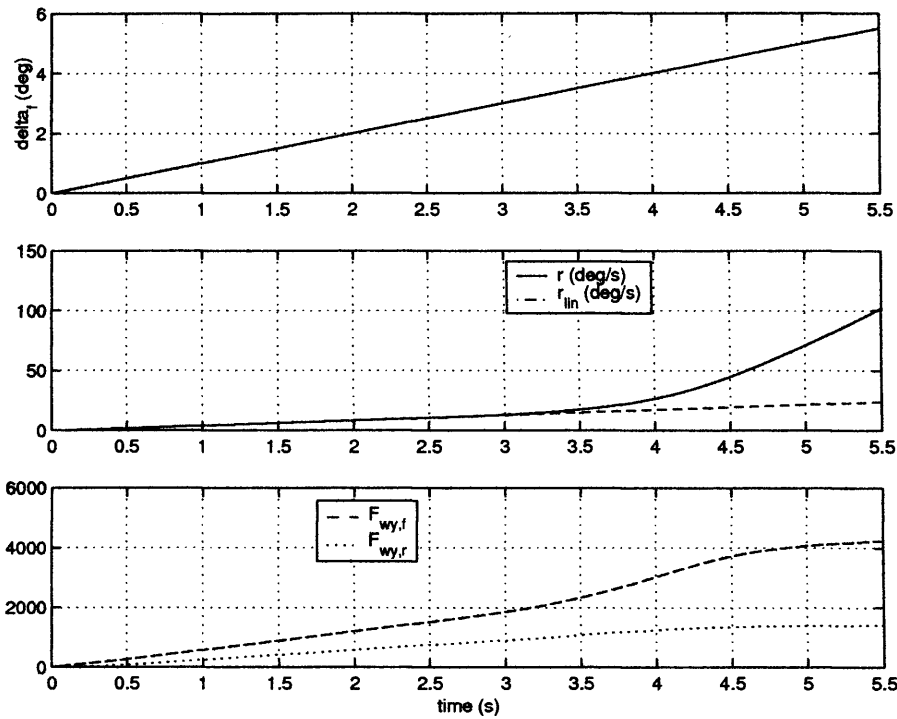


Figure 7.8: Steady-state oversteer manoeuvre

an oversteer manoeuvre should generate an ‘unexpected’ lateral force toward the outside of the turn, increasing as the severity of the oversteer rises, and decreasing should the severity be reduced. The rate of change of lateral force - the reconstruction signal, $\dot{F}_{y,un}$ - should increase in the direction of the outside of the turn at the beginning of an oversteer manoeuvre, drop down to zero should the severity peak, and increase into the turn should the oversteer reduce.

This can be seen by examining Figure 7.2 and Equations (7.27) and (7.29): in an oversteer manoeuvre, $|F_{yr}|$ is reduced and

$$|F_{yf} + F_{yr}| < |F_{y,l}| \tag{7.41}$$

In a left turn (as in the simulation), $F_{yf} > 0$, $F_{yr} > 0$, $F_{y,l} > 0$ and $M_{z,un} > 0$ The Equations (7.41) and (7.27) imply

$$F_{y,un} < 0 \tag{7.42}$$

Also

$$aF_{yf} - bF_{yr} > M_{z,l} \tag{7.43}$$

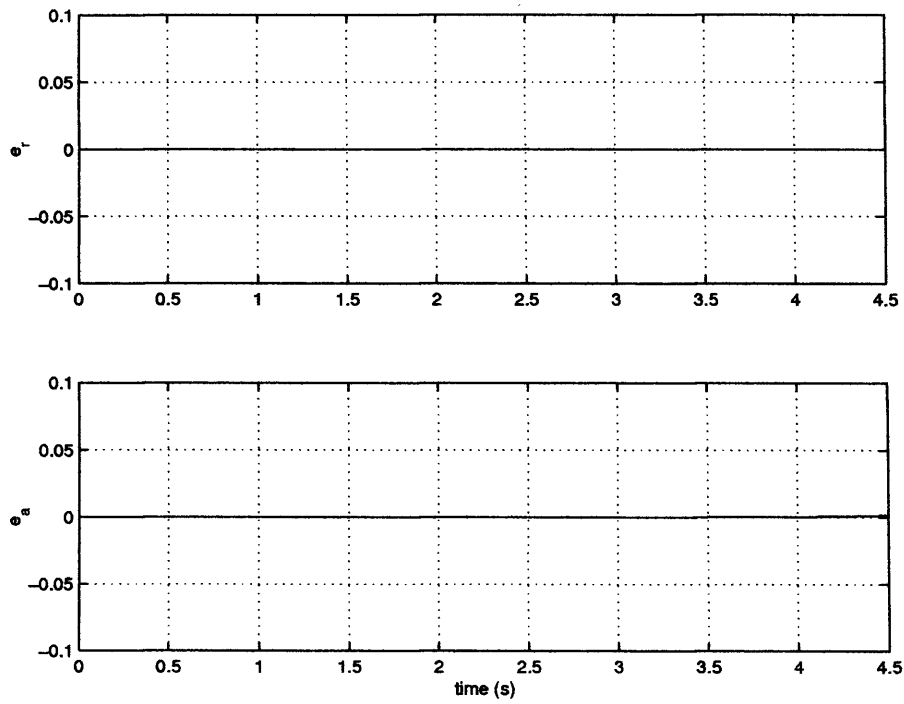


Figure 7.9: Steady-state oversteer manoeuvre:- observer-state error signals

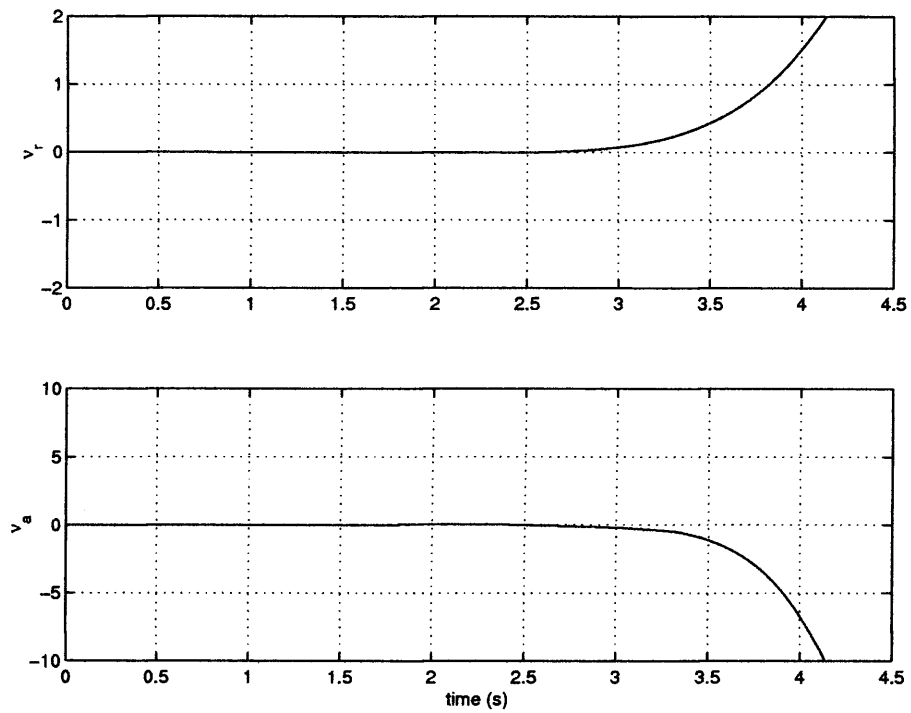


Figure 7.10: Steady-state oversteer manoeuvre:- observer equivalent injection signals

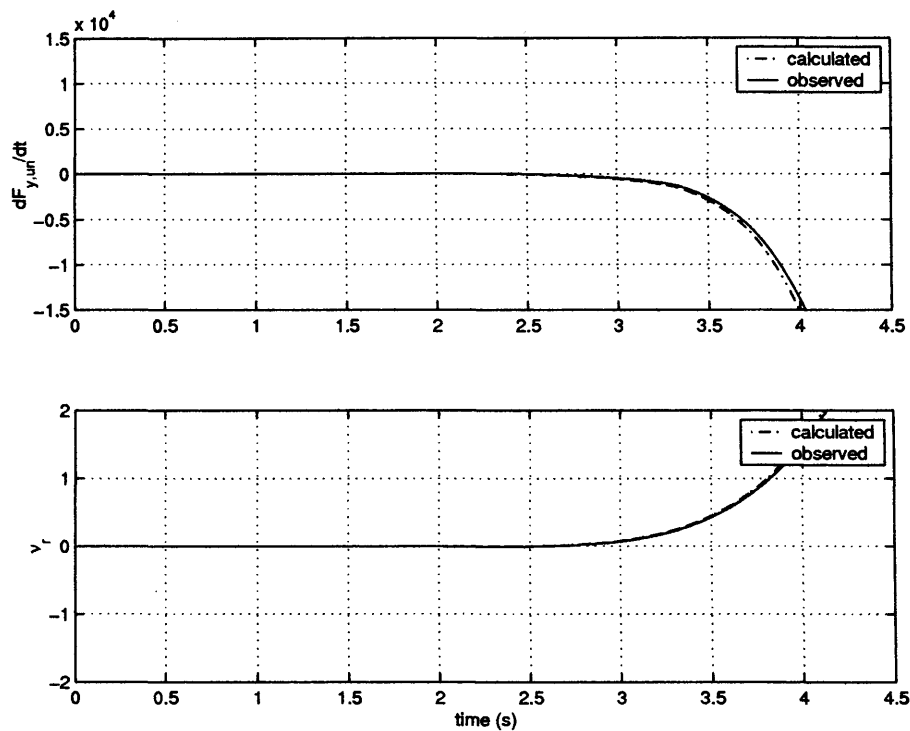


Figure 7.11: Steady-state oversteer manoeuvre:- comparison of observed unexpected signals

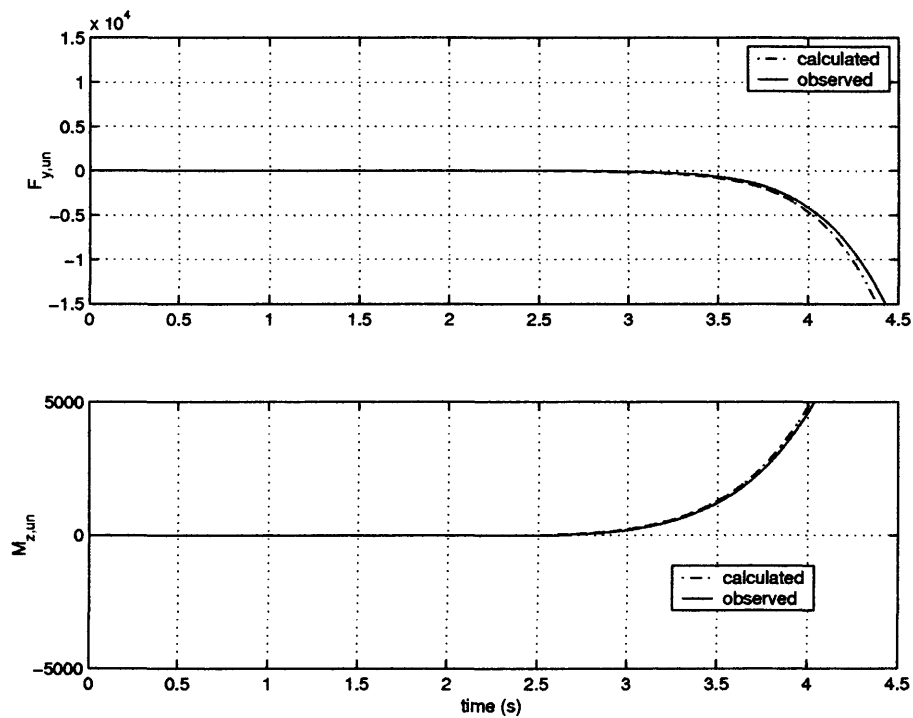


Figure 7.12: Steady-state oversteer manoeuvre:- comparison of integrated observed unexpected signals

and so, from Equation (7.29)

$$M_{z,un} > 0 \quad (7.44)$$

However, in a right turn, $F_{yf} < 0$, $F_{yr} < 0$, $F_{yl} < 0$ and $M_{z,un} < 0$. Then Equations (7.41) and (7.27) imply

$$F_{y,un} > 0 \quad (7.45)$$

Also

$$aF_{yf} - bF_{yr} < M_{z,l} \quad (7.46)$$

and so, from Equation (7.29)

$$M_{z,un} < 0 \quad (7.47)$$

Therefore, in an oversteer manoeuvre, whilst the unexpected lateral force will always act away from the turn - to the right in a left turn, and to the left in a right turn - the unexpected yaw moment will always act into the turn - to the left in a left turn, and to the right in a right turn. It is also worth noting that Equation (7.45) is identical to Equation (7.38) in the understeer discussion. This simply shows that the nonlinear model (or actual vehicle) will naturally produce lower magnitude value than the linear model due to the nonlinearity in the tyres.

Steady-State Oversteer Results

Figure 7.8 shows the steady-state oversteer manoeuvre on the nonlinear simulation of the vehicle (see Section 3.3). The first plot shows the road-wheel steering angle. The second plot shows the actual yaw rate of the nonlinear model increasing rapidly, and diverging from the expected yaw rate at around 3.5 seconds, indicating the beginning of an oversteer manoeuvre. The third plot compares the lateral forces present at a front tyre and a rear tyre. As the oversteer commences - around 3.5 seconds - the front lateral tyre force starts to increase more rapidly, whilst the rear lateral tyre force begins to saturate. Most vehicles are designed, for safety reasons, not to oversteer, but to tend to understeer slightly. In order to encourage the vehicle in the simulation to oversteer, the coefficient of friction on the two rear tyres has been dropped artificially in the simulation from 0.8 to 0.5. This has the effect of reducing the traction available to the rear tyres, increasing the rear wheel slip and reducing the rear lateral tyre

forces. Other means of inducing oversteer would be reducing rear tyre cornering stiffnesses or increasing proportion of load at the rear.

Figure 7.9 shows the output estimation error signals, e_r and e_a respectively, that are produced from the nonlinear observer. They show that sliding is maintained throughout the simulation period.

Figure 7.10 shows plots of the equivalent injection signals described in Equations (7.24) and (7.25). The vertical axis has been ‘locked’ because the signals become very large very quickly.

As discussed in Section 7.4, Figure 7.11 shows the observed ‘unexpected’ signal information, $\dot{F}_{y,un}$ and ν_r . The comparison signals (see Section 7.5) are plotted with the reconstruction signals from the estimator.

As before, for easier visual analysis, the $\dot{F}_{y,un}$ signal is integrated to give $F_{y,un}$, and this is used to calculate $M_{z,un}$ from the ν_r signal. These signals are plotted in Figure 7.12, along with the actual unexpected signals.

For the first 3 seconds of this manoeuvre, the vehicle behaves linearly, as seen by the identical yaw rate and linear yaw rate signals in Figure 7.8. During this linear region, no unexpected signals are detected. However, after 3 seconds, as the actual yaw rate diverges from the expected linear yaw rate, both the unexpected signals are seen to ramp up. Notably, in this manoeuvre, the two reconstruction signals have opposite signs. While $\bar{\nu}_r$ - dominated by the unexpected yaw moment - increases in a positive direction, $\dot{F}_{y,un}$ is negative. This agrees with the hypothesis stated earlier which predicts that as a vehicle oversteers its yaw moment, and hence $\bar{\nu}_r$, will be greater than expected and so be positive into a left turn. Meanwhile, as the rear tyres saturate and begin to slip out of the turn, so a negative lateral force, and hence a negative $\dot{F}_{y,un}$, will be generated.

7.5.3 Further Oversteer Testing

Hypothesis: This oversteer manoeuvre consists of a series of oversteer regions, each one greater than the last. The reconstruction signals would be expected to follow the same pattern witnessed in the steady-state oversteer manoeuvre. However, in this case, the reconstruction

signals of each oversteer region should be progressively greater in magnitude and should alternate in direction. As, in Section 7.5.2, in order to encourage the vehicle in the simulation to oversteer, the coefficient of friction on the two rear tyres has been dropped artificially in the simulation from 0.8 to 0.5. This has the effect of reducing the traction available to the rear tyres, increasing the rear wheel slip and reducing the rear lateral tyre forces.

Further Oversteer Results

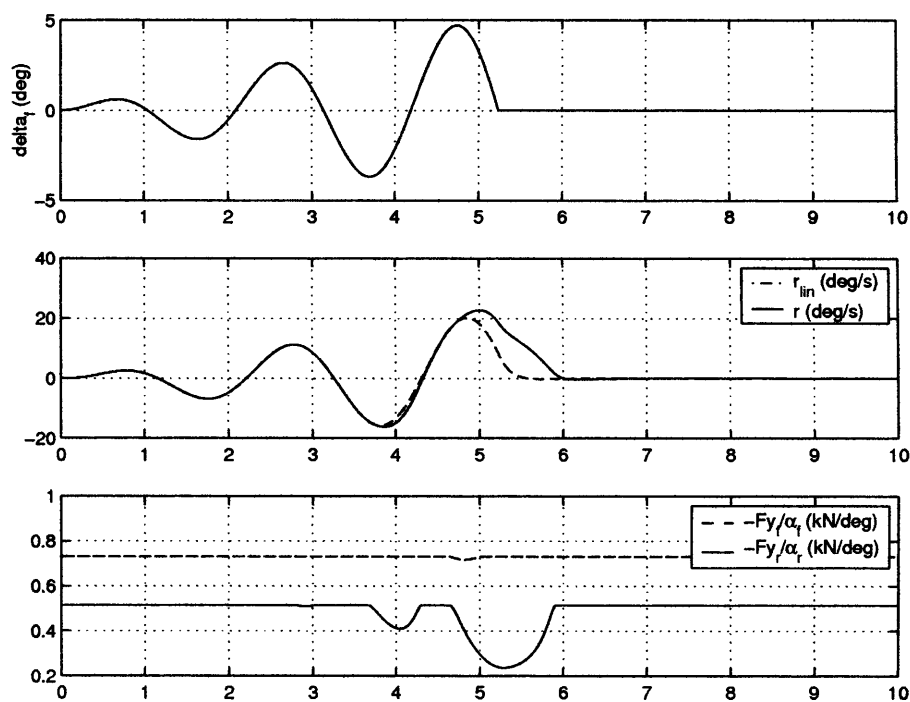


Figure 7.13: Further oversteer manoeuvre

Figure 7.13 shows the further oversteering manoeuvre. The first plot shows the road-wheel steering angle. The second plot compares the actual yaw rate of the nonlinear model with the expected yaw rate, taken from a linear model driven by the same wheel inputs. As in the steady-state case, as a region of oversteer is entered, the actual yaw-rate begins to exceed the expected yaw-rate of the linear model. Two oversteer manoeuvres are seen, one around 3.75 seconds, and a second from around 4.75 seconds. This is confirmed by the third plot which compares the tyre force achieved per degree of wheel slip-angle from a front and a rear tyre. During the oversteer regions, this value decreases at the rear tyre.

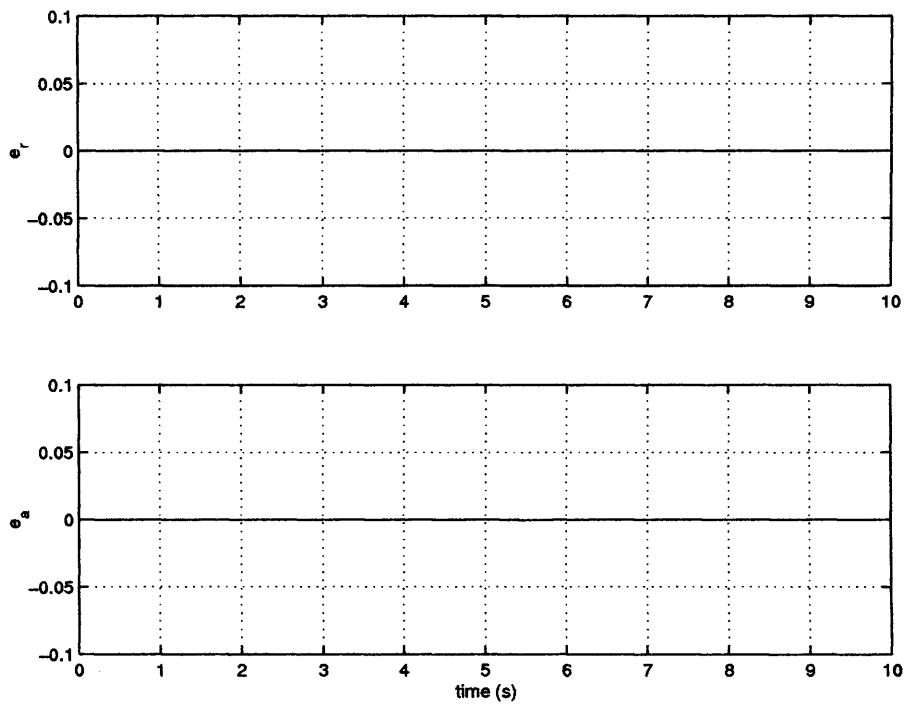


Figure 7.14: Further oversteer manoeuvre:- observer-state error signals

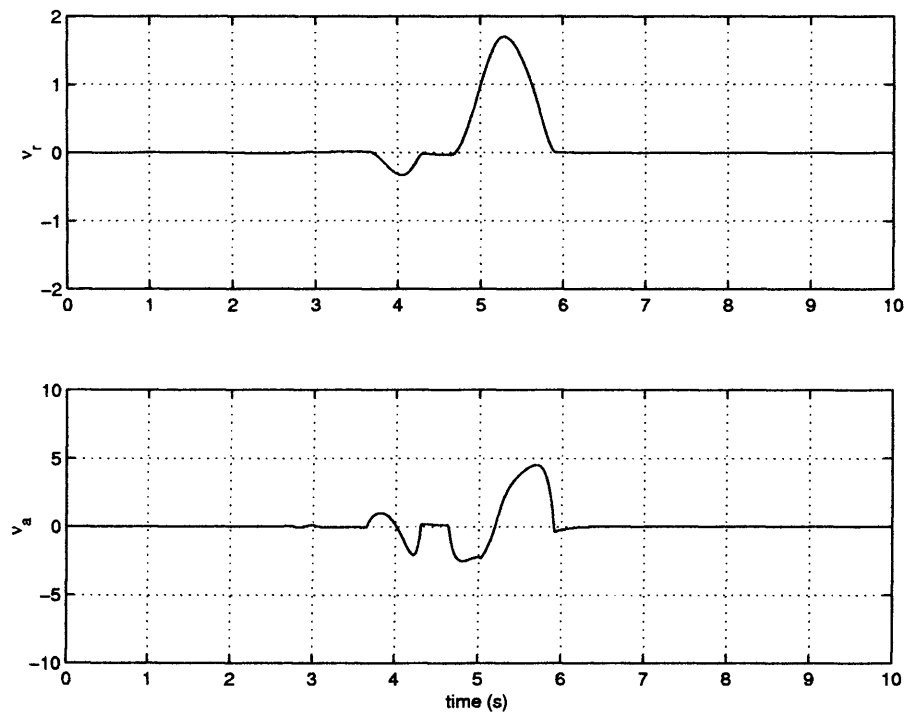


Figure 7.15: Further oversteer manoeuvre:- observer equivalent injection signals

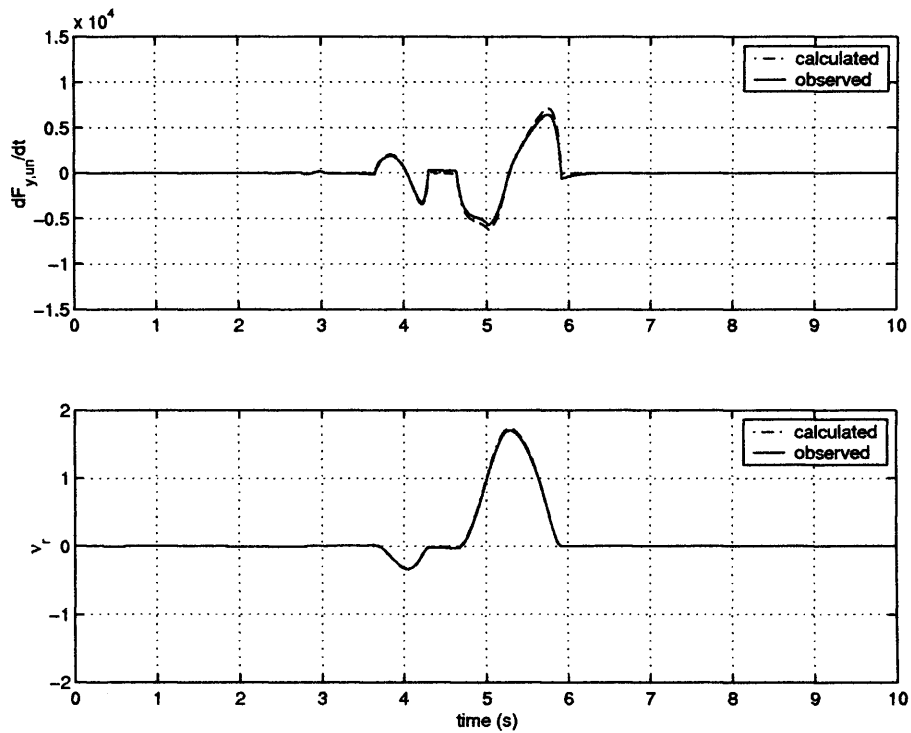


Figure 7.16: Further oversteer manoeuvre:- comparison of observed unexpected signals

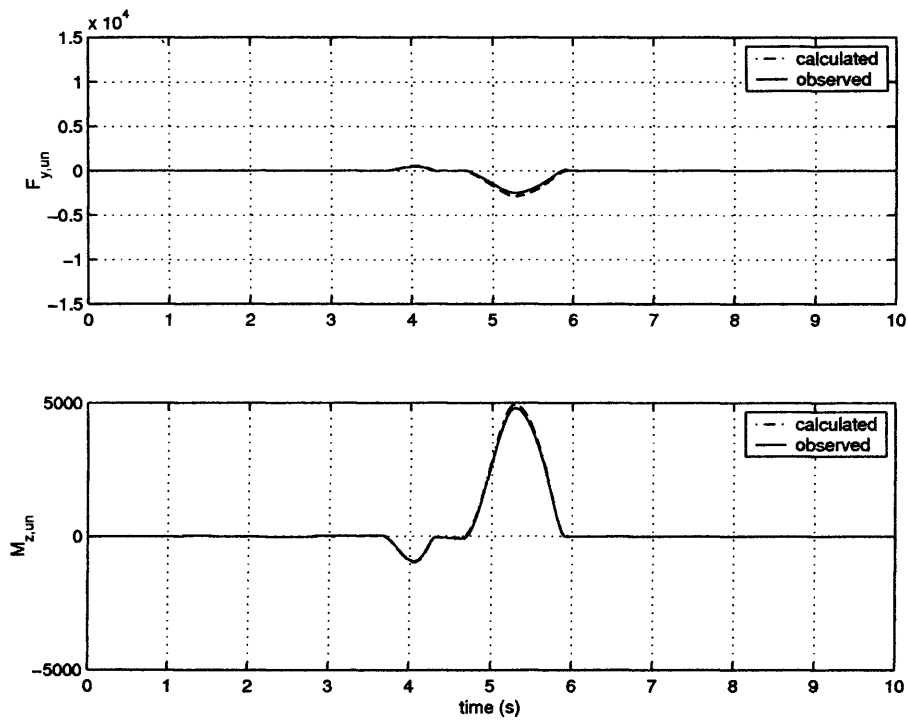


Figure 7.17: Further oversteer manoeuvre:- comparison of integrated observed unexpected signals

Figure 7.14 shows the output estimation error signals, e_r and e_a respectively, that are produced by the nonlinear observer. It shows that a sliding motion is maintained throughout the simulation. Figure 7.15 shows plots of the equivalent injection signals described in Equations (7.24) and (7.25).

As discussed in Section 7.4, Figure 7.16 shows the observed ‘unexpected’ signal information, $\dot{F}_{y,un}$, and ν_r . The comparison signals (see Section 7.5) are plotted with the reconstruction signals from the estimator. Good agreement is shown.

Again, for easier visual analysis, the $\dot{F}_{y,un}$ signal is numerically integrated to give $F_{y,un}$, and this is used to calculate $M_{z,un}$ from the ν_r signal. These signals are plotted in Figure 7.17, along with the comparison signals.

In this oversteer manoeuvre, a vehicle is simulated moving into and out of oversteer by repeated over-corrective steering inputs. It can be seen from the saturating lateral tyre forces coupled with escaping wheel slip-angles in Figure 7.13 that in the simulation there are two regions in which the vehicle is oversteering and that these two regions coincide with the two final peaks of the steering angle signal, δ_f . As in the steady-state oversteering manoeuvre, no unexpected signals are detected until the vehicle enters an oversteering region, at which point the beginning of the oversteer is marked by sudden ramping of the two reconstruction signals in opposite directions - $\bar{\nu}_r$ into the turn and $\dot{F}_{y,un}$ out of the turn. The two regions are most immediately seen in Figure 7.17 as both $M_{z,un}$ and $F_{y,un}$ increase in magnitude as the severity of the oversteer increases and then drop as the severity is reduced and the vehicle returns to linear behaviour. In the case of the $\dot{F}_{y,un}$ signal, the situation is a little more complicated as the signal (as in the understeer manoeuvre) switches sign as the unexpected lateral force reaches and drops from its maximum, however the oversteer region is still quite easily deduced.

7.5.4 Split- μ Braking

In the simulation which follows, the nonlinear vehicle model simulates a harsh ABS split- μ braking manoeuvre on surface of $\mu = 0.8, 0.2$ with zero steering angle. This is identical to the manoeuvre considered in Chapters 5 and 6. In Figure 7.18, the front high- μ wheel reaches its peak braking torque at ≈ 0.5 seconds. At 0.7s, the vehicle leaves the split- μ surface and

enters a homogeneous surface with $\mu = 0.8$. The simulation runs open-loop and the vehicle is allowed to drift toward the high- μ surface.

Hypothesis: In this scenario, it is expected that there would be an initial unexpected yaw moment - due to the asymmetric braking - with any unexpected lateral force building up more slowly, as a result of the assumed yaw angle. As the braking torque reaches a peak, the unexpected yaw moment should level off, leaving the lateral force continuing to build up. As the vehicle leaves the split- μ surface, the unexpected yaw moment should rapidly decrease as traction returns to the tyres and the braking becomes symmetrical.

Split- μ Braking Results

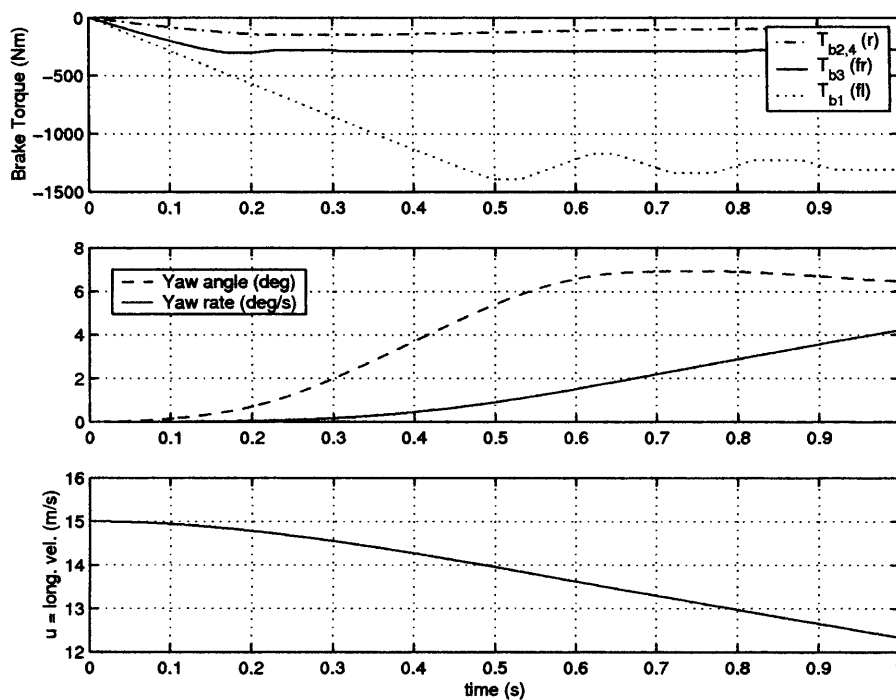


Figure 7.18: Split- μ braking manoeuvre

Figure 7.18 shows the split- μ braking manoeuvre on the nonlinear vehicle simulation. The first plot shows the four brake torques (T_{b1} - front left, T_{b2} - rear left, T_{b3} - front right, T_{b4} - rear right). The two rear brake torques coincide on the plot due to the ‘select-low’ strategy (see Section 2.5.1). The second plot shows the yaw angle and yaw rate of the vehicle and the third plot shows how the longitudinal velocity drops over the course of the simulation.

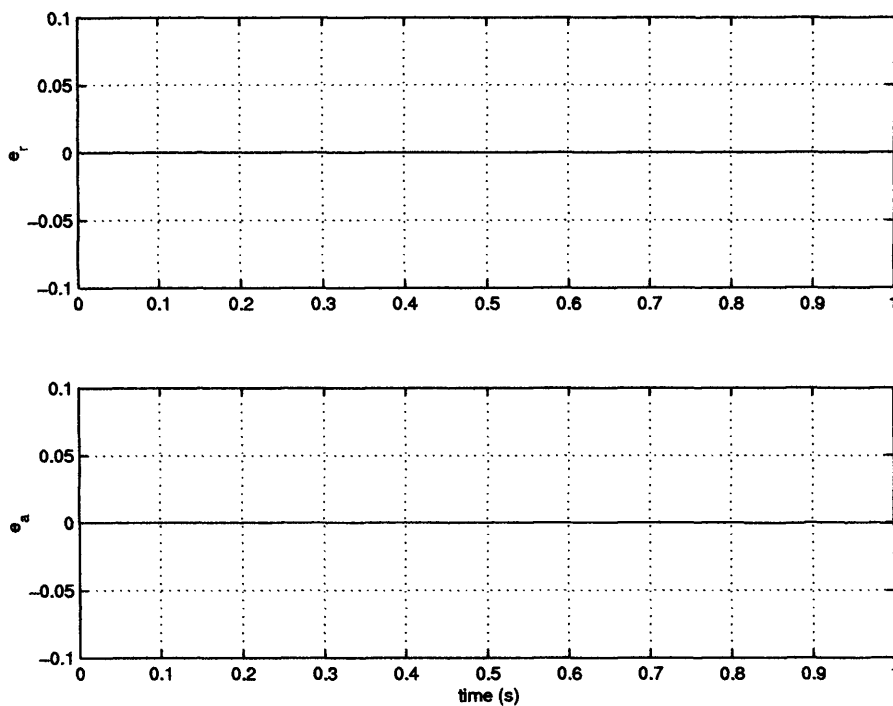


Figure 7.19: Split- μ braking manoeuvre:- observer-state error signals

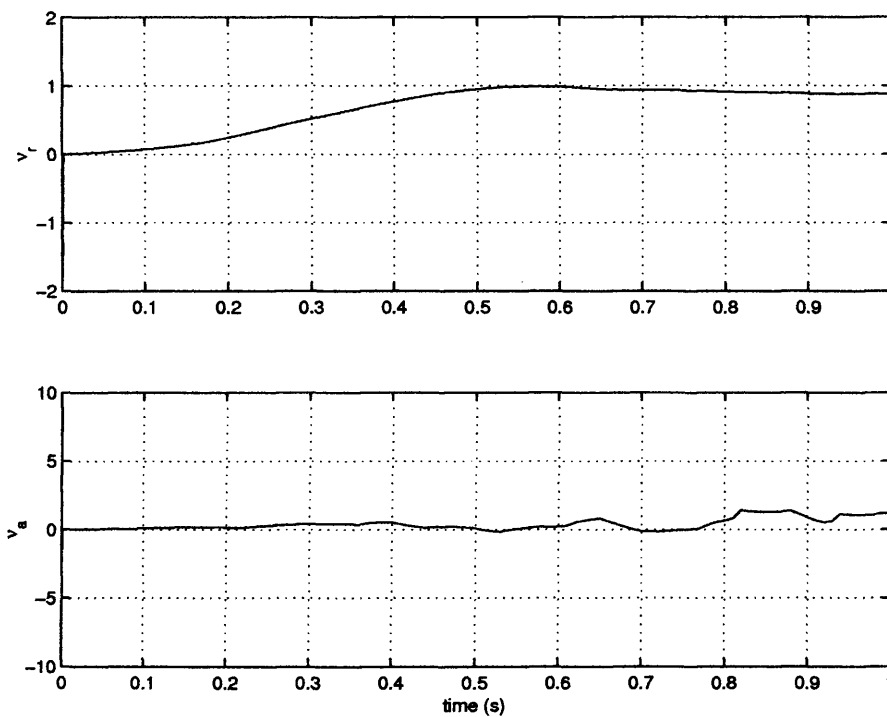


Figure 7.20: Split- μ braking manoeuvre:- observer equivalent injection signals

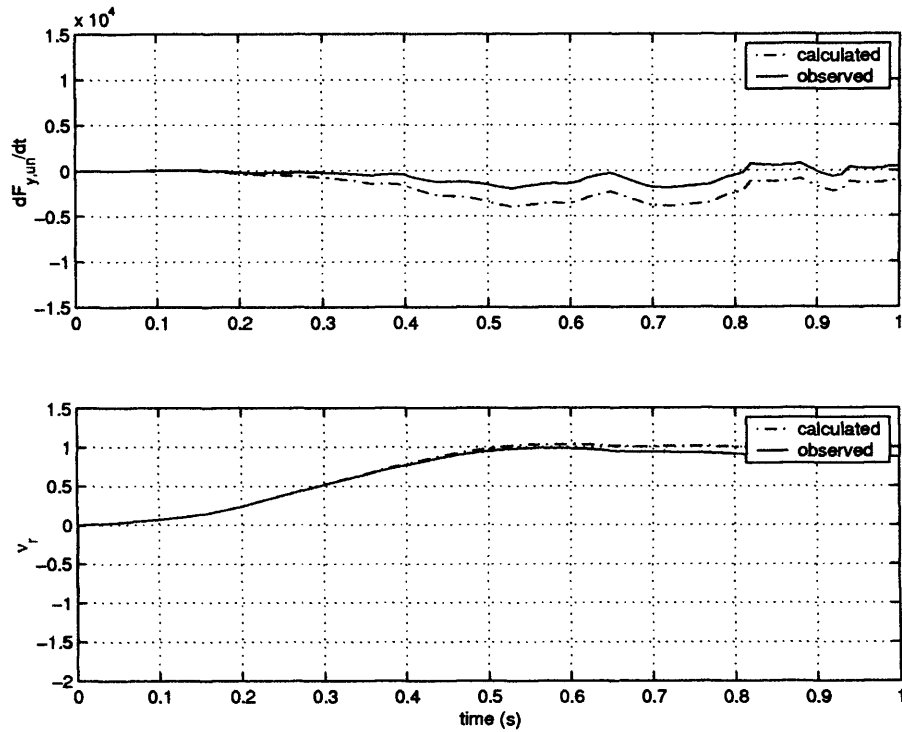


Figure 7.21: Split- μ braking manoeuvre:- comparison of observed unexpected signals

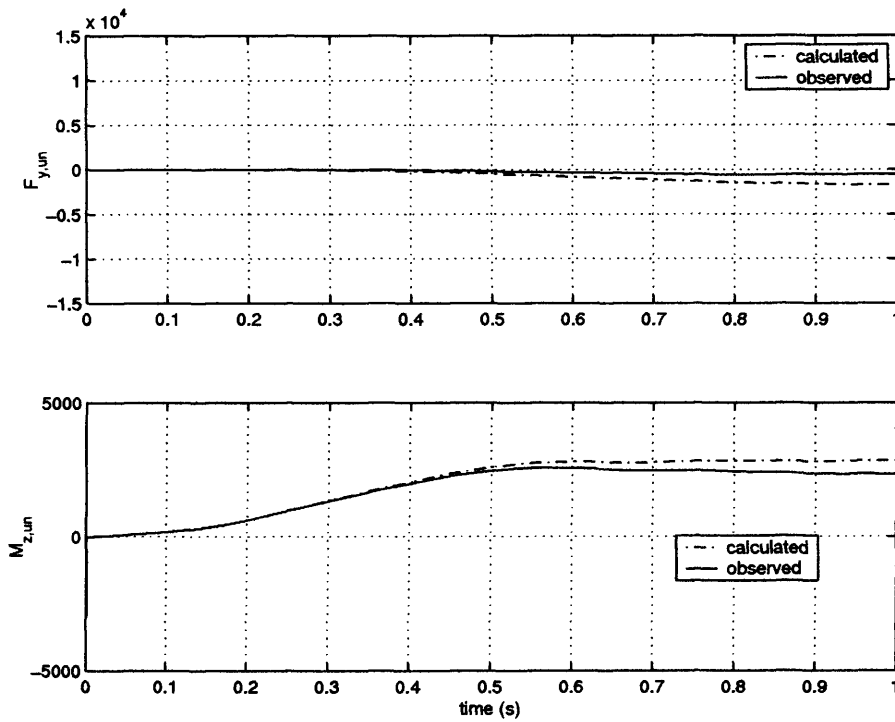


Figure 7.22: Split- μ braking manoeuvre:- comparison of integrated observed unexpected signals

Figure 7.19 shows the output estimation error signals, e_r and e_a respectively, that are produced from the nonlinear observer. They show that sliding is maintained throughout the simulation period. This is the point at which the vehicle's four wheels move suddenly onto the high- μ surface.

Figure 7.20 shows plots of the equivalent injection signals described in Equations (7.24) and (7.25).

As discussed in Section 7.4, Figure 7.21 shows the 'unexpected' signal information, $\dot{F}_{y,un}$, and $\bar{\nu}_r$. The comparison signals are plotted with the reconstruction signals from the estimator. Less faithful agreement is obtained here compared with the other scenarios.

Once more, for easier visual analysis, the $\dot{F}_{y,un}$ signal has been integrated to give $F_{y,un}$, and this is used to calculate $M_{z,un}$ from the $\bar{\nu}_r$ signal. These signals are plotted in Figure 7.22, along with the comparison signals.

As predicted, the first of the reconstruction signals (Figure 7.21) to react is $\bar{\nu}_r$ - dominated by the yaw moment - which immediately begins to ramp up as the brake torque on the high- μ side of the vehicle increases at a greater rate than that of the low- μ side. At around 0.2s the gradient of this slope increases as the braking on the low- μ tyres peaks. The $\bar{\nu}_r$ reconstruction signal continues to increase until around 0.5s - when the high- μ brake torque peaks - at which point it levels off.

In contrast, the $\dot{F}_{y,un}$ reconstruction signal remains at zero in the first 0.2s of the manoeuvre, in agreement with both the comparison signal and the prediction. At the point at which this signal does react, it follows the comparison signal in form though not in magnitude, with peaks and troughs relating to the oscillating individual brake torques.

The split- μ braking manoeuvre is characterized by an initial zero $\dot{F}_{y,un}$ reconstruction signal, while the $\bar{\nu}_r$ reconstruction signal - dominated by the yaw moment - ramps up and then levels off. The level at which the $\bar{\nu}_r$ signal reaches a maximum gives an indication of the severity of the split as it is related to the yaw moment generated by the asymmetric braking.

7.5.5 Summary of Detection Results

The first point which can be drawn from Figures 7.6-7.21 is that the sliding mode observer presented is able to reconstruct the ‘unexpected’ signals well, but with an accuracy which varies from manoeuvre to manoeuvre. In the understeer manoeuvre, the form of the reconstruction signals agrees well with the comparison signals although the magnitude does not remain accurate throughout the manoeuvre. In the two oversteer manoeuvres the reconstruction signal agrees very well with the comparison signal in form, and, in the further oversteer manoeuvre, maintains very good accuracy. In the steady-state oversteer manoeuvre, the reconstruction signal loses accuracy as the manoeuvre becomes too severe. However, by this point the vehicle stability is already lost. It is only in the split- μ braking scenario, for the $\dot{F}_{y,un}$ reconstruction signal, that accuracy, though not form, is lost. Nevertheless, in all of the manoeuvres the key features needed to interpret the signals are preserved, and even in the split- μ braking manoeuvre the severity of the manoeuvre may be assessed from the accurate \bar{v}_r reconstruction signal.

The second, and equally important observation is that the unexpected signals which can be reconstructed vary significantly between the manoeuvres. The characteristic signatures which are seen are discussed for each manoeuvre as follows:

- **Understeer:** An understeer manoeuvre may be detected by the presence of sudden increases in both the reconstruction signals *in the same direction*. As the severity of the understeer manoeuvre reaches a peak value, the \bar{v}_r signal levels off, and the $\dot{F}_{y,un}$ signal decreases and switches sign. As the region of understeer ends, both the reconstruction signals return to zero.
- **Oversteer:** An oversteer manoeuvre may be detected by the presence of sudden increases in the reconstruction signals in opposite directions. As the severity of the oversteer manoeuvre reaches a peak value, the \bar{v}_r signal levels off, and the $\dot{F}_{y,un}$ signal decreases and switches sign. As the oversteer region ends, both the reconstruction signals return to zero. The repeated oversteering in the further oversteer testing is characterized by two or more oversteer regions in succession, with the initial ramping sign of each

reconstruction signal reversing from one oversteer region to the next.

- **Split- μ Braking:** A harsh split- μ braking manoeuvre may be detected by the presence of a sudden ramping of the \bar{v}_r reconstruction signal with no initial accompanying increase in the $\dot{F}_{y,un}$ signal.

The severity of any one of the under and oversteer manoeuvres may be assessed using \bar{v}_r . The severity of a split- μ surface assessed by the peak \bar{v}_r value attained before it levels off.

7.6 Vehicle Scenario Prediction

It is clear from the results presented in the previous section that the sliding mode observer has successfully reconstructed two input signals to an overall high level of accuracy. The ‘unexpected’ input signals display distinctive signatures depending upon which manoeuvre is being performed. The reconstructed signals may also be used to obtain an indication of the severity of the particular manoeuvre being performed. However, for a scenario detection scheme to be useful, it must be able to predict the severe scenario before it becomes dangerous, so that preemptive action may be taken to avoid any danger. In the previous section the vehicle scenarios were identified using the signals obtained over the whole simulation, and so the scenario would only be identified after the event, which is obviously too late to take any preventative action. Therefore, the very first moments of each scenario must be examined, and a logical algorithm set-up, so that the first warning signs of each severe vehicle scenario may be recognized by their distinctive signatures. In the first few moments of the manoeuvre, the algorithm must make a clear, unambiguous identification of the scenario and, ideally, an indication of the potential severity.

The figures which follow (Figures 7.28-7.32) show a few seconds of each simulation at the point at which the vehicle enters a manoeuvre or vehicle scenario region. For example, Figure 7.28 shows the reconstructed signals at the point at which the vehicle first enters the understeer region of the simulation, whereas Figure 7.32 shows the the reconstructed signals at the start of the split- μ simulation, as the braking torques are first applied. These plots are taken from the simulations presented earlier in the chapter, and so can be compared with Figures 7.3-7.22.

As can be seen in Figures 7.13-7.17, in the further oversteering manoeuvre, the vehicle twice enters a region of oversteer, firstly to the right, and then to the left. The second of these two oversteer regions being significantly more severe than the first. Both of these two oversteer regions will be looked at in detail in this section, in Figures 7.30-7.31.

The method proposed for predicting the various scenarios requires the definition of appropriate thresholds for the two reconstruction signals. In order to determine suitable initial choices for these thresholds, two manoeuvres are performed which involve significant lateral dynamics whilst avoiding significant under- or oversteer. The first manoeuvre is a simple lane change manoeuvre. In this manoeuvre, the vehicle travels at the same longitudinal velocity as in the previous under- oversteer scenarios, whilst a road-wheel steering angle input is applied which causes the vehicle to move laterally between two straight trajectories. A lateral shift of around $3.65m$ is chosen - corresponding to the standard lane width specified by the UK Highways Agency [18] - and the manoeuvre lasts approximately 4 seconds. The manoeuvre can be seen in Figure 7.23, and the resulting unexpected signals are shown in Figure 7.24.

The magnitudes of the unexpected signals in this manoeuvre are significantly smaller than those of the severe manoeuvres, presented in Figures 7.6, 7.11, 7.16, which suggests that the predictor thresholds may be placed at relatively low magnitudes. A second (chicane) manoeuvre is simulated, in which the vehicle is subject to a steady sine-wave road-wheel steering angle signal. A magnitude of 3° is chosen (corresponding to a hand-wheel steering angle of around 45°), which is just below the level which generated oversteer earlier in the chapter. This manoeuvre is presented in Figures 7.25, with the corresponding unexpected signals in Figure 7.26.

The unexpected signals generated by the chicane manoeuvre, whilst being larger than those produced by the lane change, are still significantly smaller than the unexpected signals associated with the severe manoeuvres. Also, where the relatively benign lane change manoeuvre is an everyday situation, the chicane is a more artificial scenario, but as it does not actually produce severe under- or oversteer, its larger unexpected signals should be allowed by the predictor thresholds. The setting of thresholds (and, hence, the potential quality of the prediction) will depend upon the transient vehicle dynamics - as represented by the linear model upon

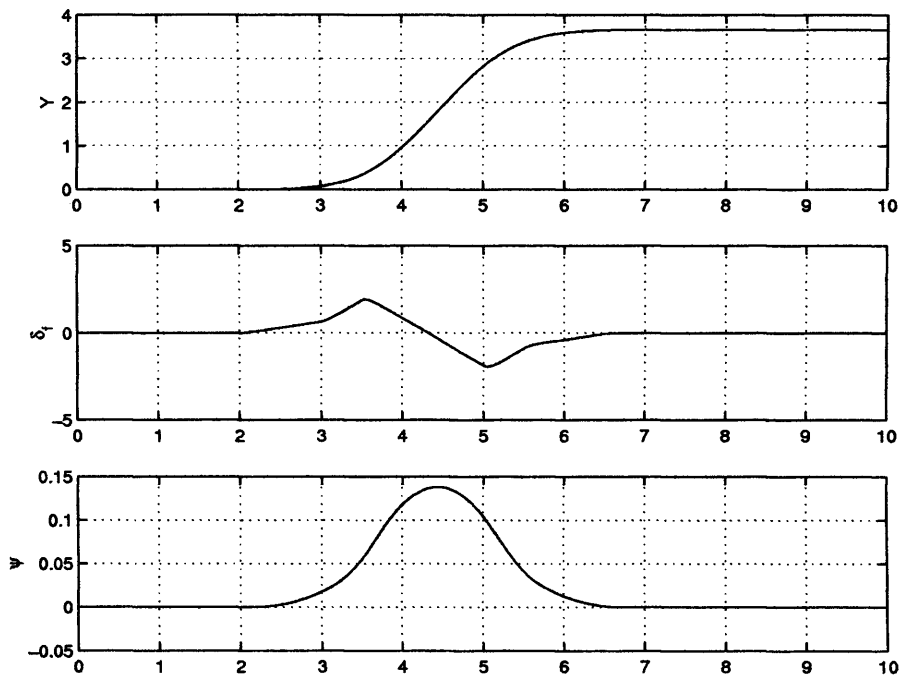


Figure 7.23: Lane change manoeuvre

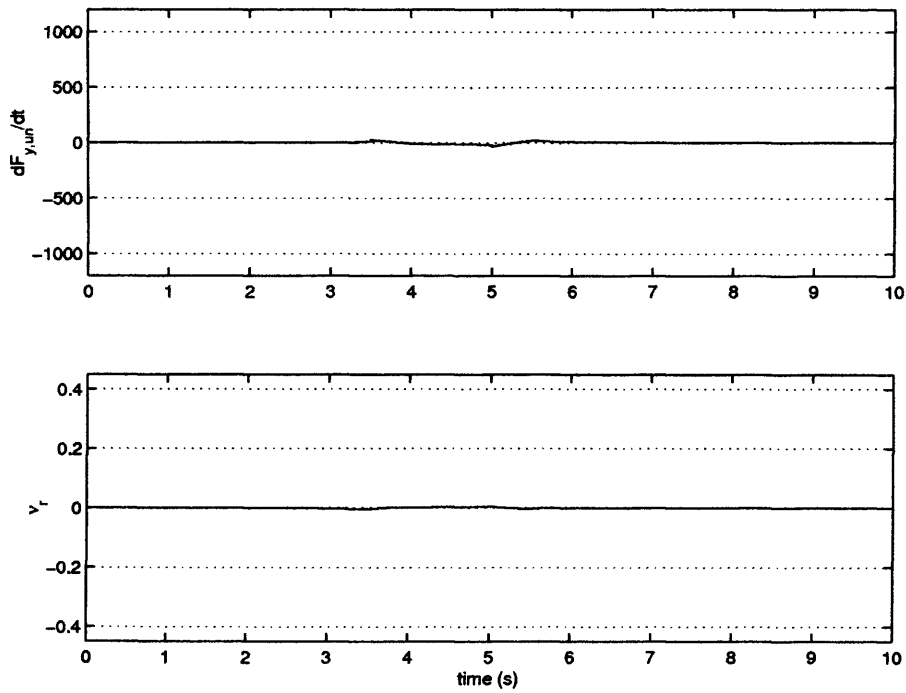


Figure 7.24: Lane change manoeuvre:- reconstructed signals

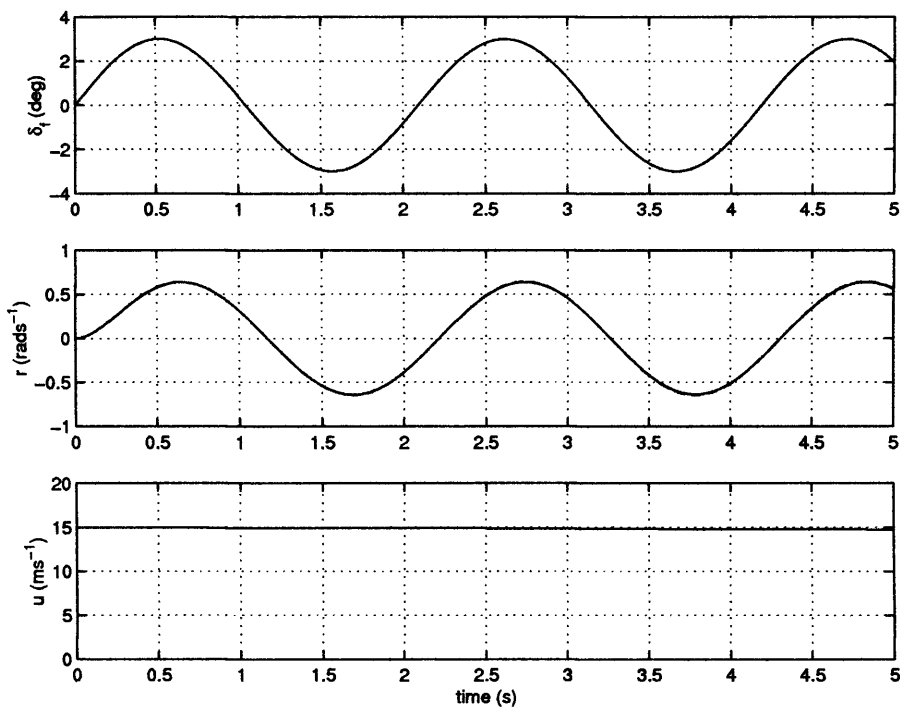


Figure 7.25: Chicane manoeuvre

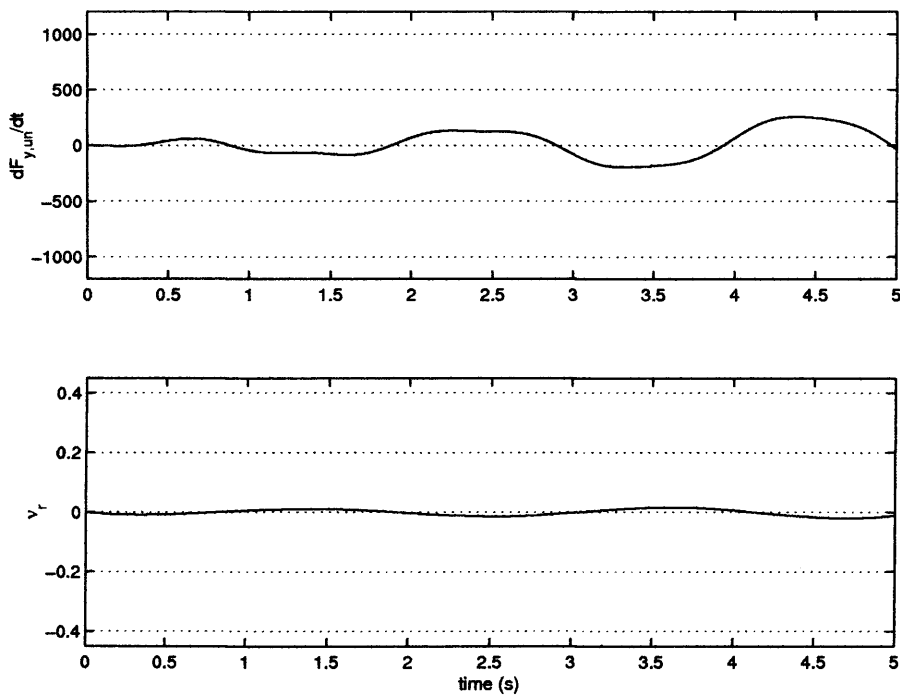


Figure 7.26: Chicane manoeuvre:- reconstructed signals

which the observer is based. Thresholds would, therefore, need to be set for each vehicle, and potentially altered if the load, or other vehicle conditions, changed.

The algorithm chosen to identify the vehicle scenario is given here, and uses the variables t_1 , t_2 and $\Delta t = t_2 - t_1$:

1. When either reconstruction signal crosses a threshold, define $t_1 = t$ to be the crossing time. Isolate whether $\dot{F}_{y,un}$ or \bar{v}_r has triggered the alarm and which side of the threshold has been crossed. For both signals at time t_1 record a reading of '0' (within thresholds), '+' (if the +ve threshold is violated) or '-' (if the -ve threshold is violated).
2. Continue to monitor the two detection signals.

If the other detection signal then crosses a threshold, set $t_2 = t$ as the crossing time and compute $\Delta t = t_2 - t_1$ i.e. the length of time necessary to make the prediction.

Otherwise, if the original signal re-crosses below threshold without the second signal crossing threshold, then reset the algorithm.

In the figures which follow, the upper and lower thresholds are shown by horizontal "dotted" lines. These figures show only the period in time in which the severe manoeuvre is starting to build up eg. Figure 7.28 starts at 1.4s, just before the vehicle starts to understeer.

7.7 Output Measurement Noise

It must be confirmed that the proposed scheme will tolerate reasonable levels of noise in the measured signals. This will have an impact on the size of the switched gains that can be used in the observer. Noise with a standard deviation approximately 5% of the measurement range was added to both output signals, and vehicle manoeuvre simulations were re-performed. It was found that the noise did indeed have a quite significant impact on the quality of the reconstructed signals. In the prediction scheme that will be proposed the undesirable effects of the noise have been minimized by a combination of methods. Firstly, the scalar gains of the sliding mode estimator from Equations (7.18) and (7.19) were reduced to $\rho_r = \rho_a = 10$. The

potential disadvantage of reducing these gains is that it limits the degree of vehicle manoeuvre severity during which the estimator is able to maintain sliding. However, as argued earlier, the purpose of the vehicle scenario scheme is to predict potentially dangerous vehicle scenarios before they build up. Secondly, a low pass filter was applied to the reconstruction signals exiting the observer. This is still in keeping with the notion of the equivalent injection signals $\bar{\nu}_r$ and $\bar{\nu}_a$ as the low frequency components of the switching terms ν_r and ν_a [31, 114]. However, whilst this filter had the capacity to attenuate the noise in these signals, it also produces a small time-delay in the reconstructed signal. A satisfactory trade-off between the requirements for noise reduction - enabling the reconstruction signal to be distinguishable - and without significant reconstruction signal time-delay has been found using a first order filter with time constant $\frac{1}{10}$ s. The effects of these changes can be seen by studying Figure 7.27 which shows the reconstructed \dot{F}_y signal three times in the first plot and the lateral acceleration output estimation error signal in the second plot. The solid lines show the actual signals; the ‘dash-dot’ lines correspond to the reconstruction and output estimation error signals using the decreased gain values; and the ‘dashed’ lines correspond to the signals using decreased gain values and the first order filter. In the second plot, the ‘dash-dot’ and dashed lines are indistinguishable. As can be seen from these plots, the reduction of ρ_r, ρ_a causes the estimator to leave the sliding region only once the thresholds (shown by two ‘horizontal’, ‘dotted’ lines, and defined as $\dot{F}_{y,un} = \pm 1000 N s^{-1}$ and $\nu_r = \pm 0.3$) have been exceeded, and the filter produces only a very minor time-delay. The output estimation error signal plot shows that the decrease in ρ_r, ρ_a and the filter do not produce significant estimation errors until after the thresholds have been breached.

7.7.1 Vehicle Scenario Prediction Simulation Results

The results taken during the simulations are summarized in Table 7.1. The most noticeable feature in the table is that the split- μ braking manoeuvre is the only scenario in which the ν_r reconstruction signal is the first signal to cross the threshold. This, once again, confirms the hypothesis made earlier, that in a split- μ manoeuvre the ‘unexpected’ yaw moment is the first signal to build up, followed by the ‘unexpected’ lateral force.

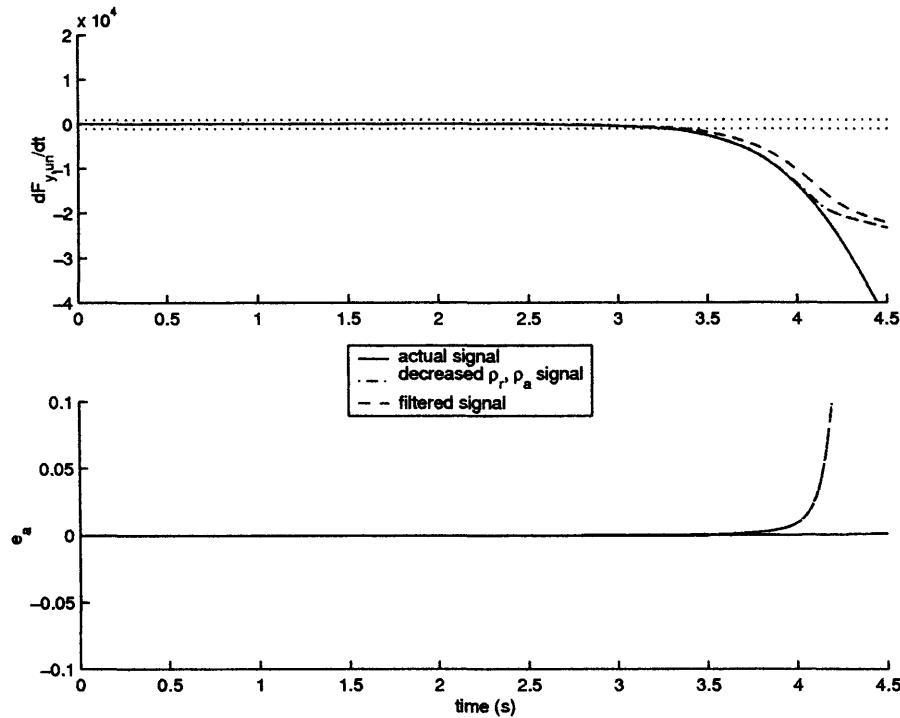


Figure 7.27: Steady-state Oversteer Manoeuvre with decreased ρ , and subsequently filtered

The quantity Δt , in Table 7.1, represents the time between the first *filtered* reconstruction signal crossing a threshold and the point at which a prediction can be made. The time-delay, Δt_f , introduced by the inclusion of the filter must be added to Δt , in order to produce a value for the total time between the time at which the prediction is made. The respective filter time-delays - as witnessed in Figures 7.28-7.32 - are shown in Table 7.2, along with the total time taken for prediction. In Figures 7.28-7.32 the dotted line represents the filtered low gain reconstruction signal whilst the solid line represents the equivalent unfiltered signal.

7.7.2 Discussion of Scenario Prediction Algorithm Results

In the case of the understeer manoeuvre (Figure 7.28), it can be seen, that the first signal to cross its threshold is the \dot{F}_y signal. At this point the algorithm defines $t_1 = 1.65s$, and would rule out a split- μ braking manoeuvre as the \dot{F}_y signal is crossed first. The \dot{v}_r signal then crosses its threshold shortly afterward, defining $t_2 = 1.85s$ and $\Delta t = 0.2s$. At this point the algorithm would deduce that a severe understeer manoeuvre is likely - as both the signal

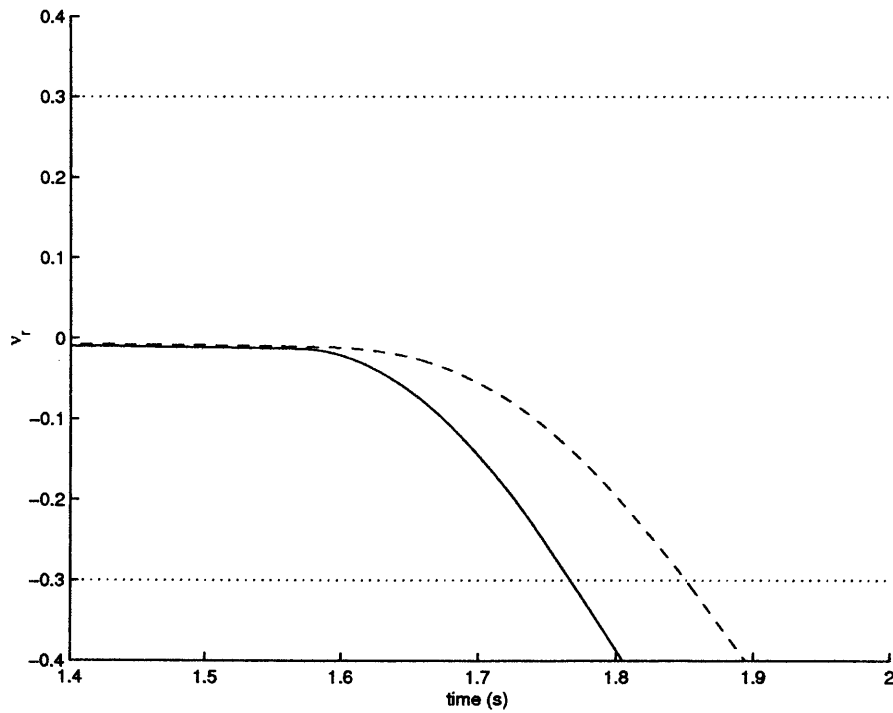
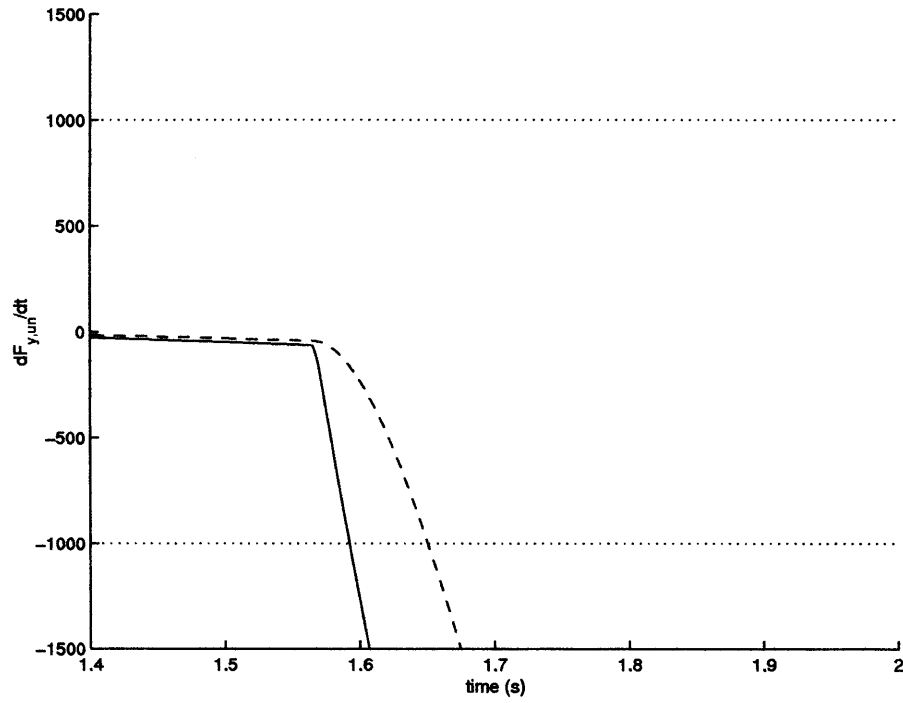


Figure 7.28: Prediction: Understeer Manoeuvre

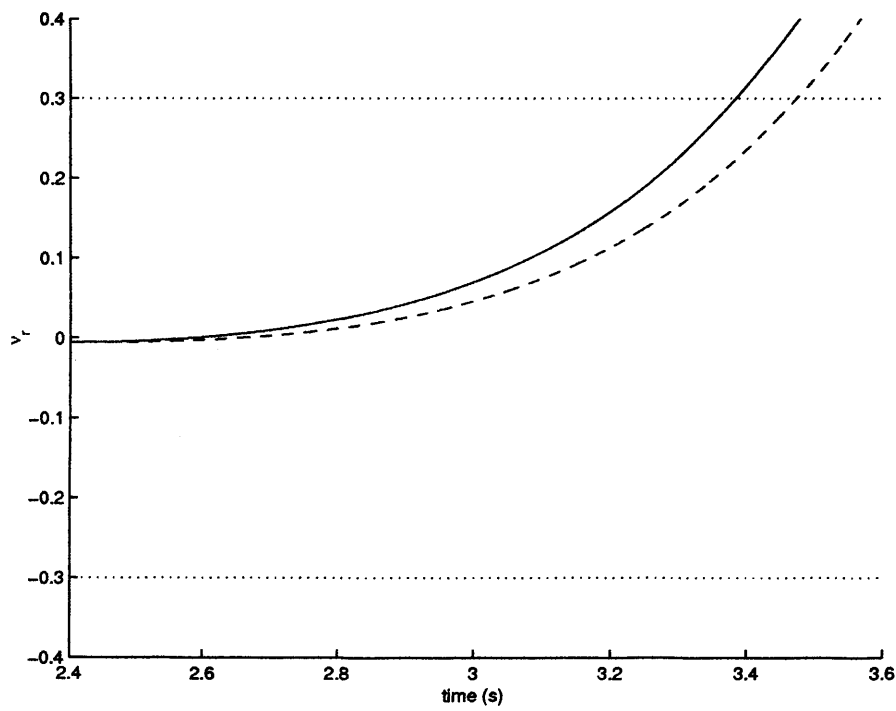
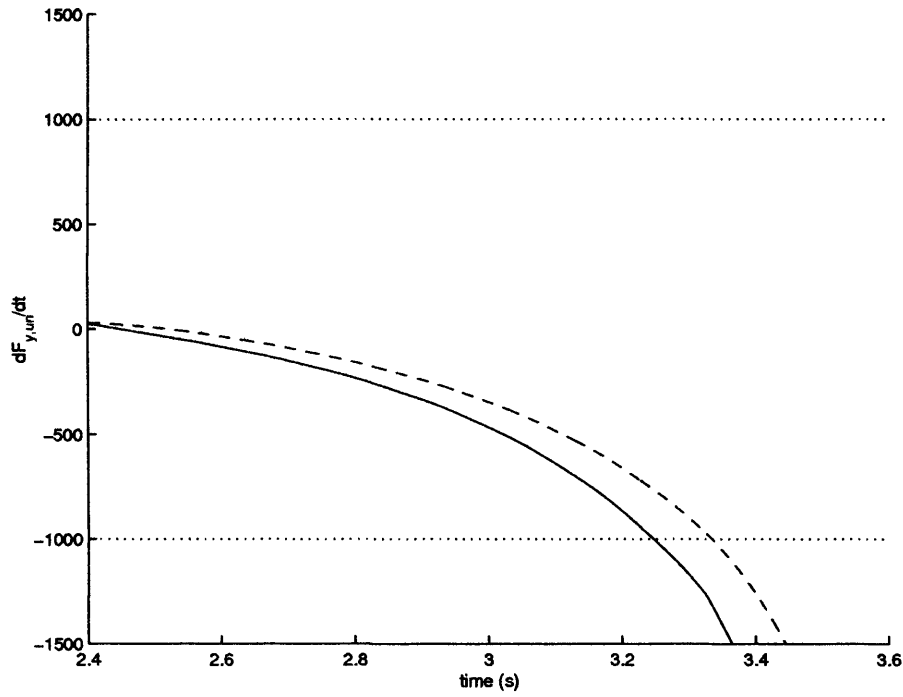


Figure 7.29: Prediction: Steady-state Oversteer Manoeuvre

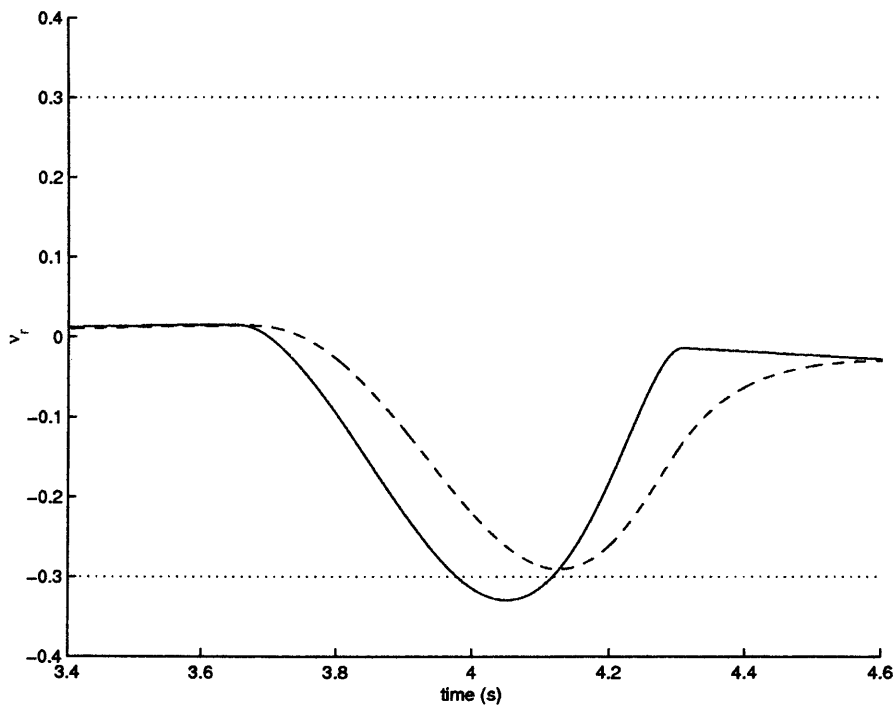
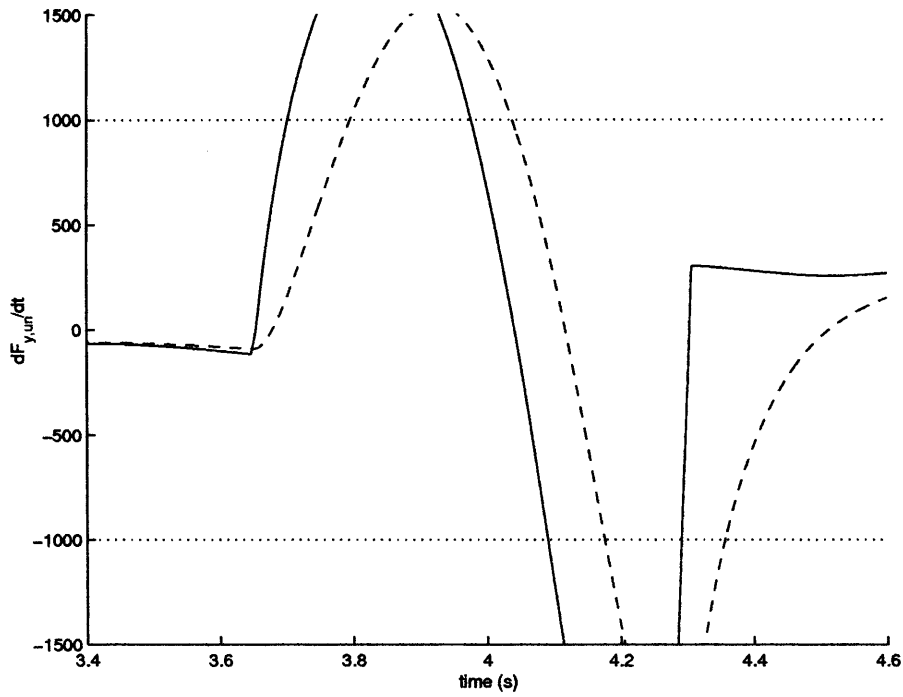


Figure 7.30: Prediction: Further Oversteer Manoeuvre - Region 1

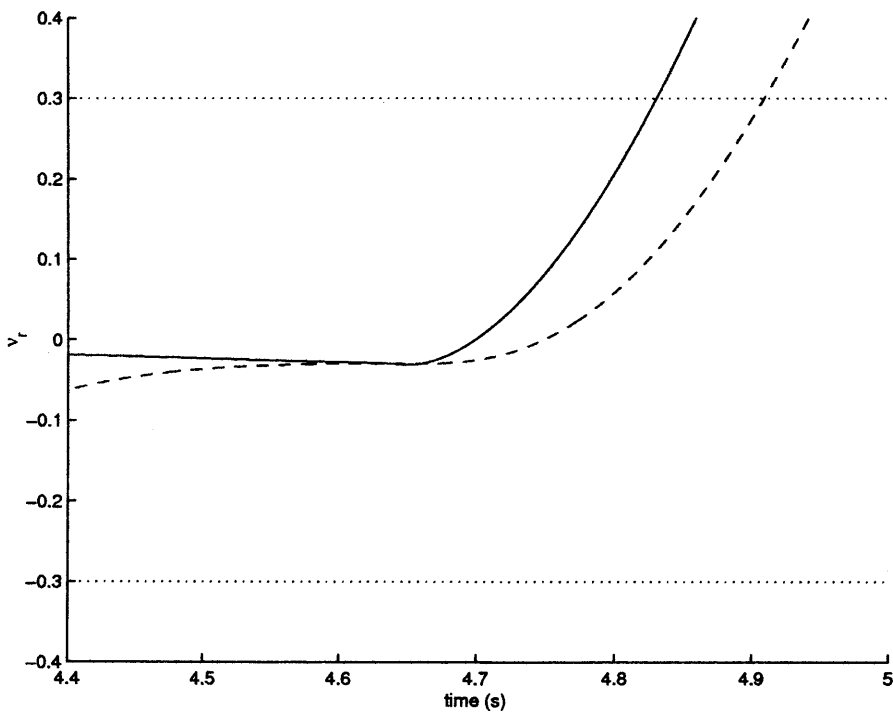
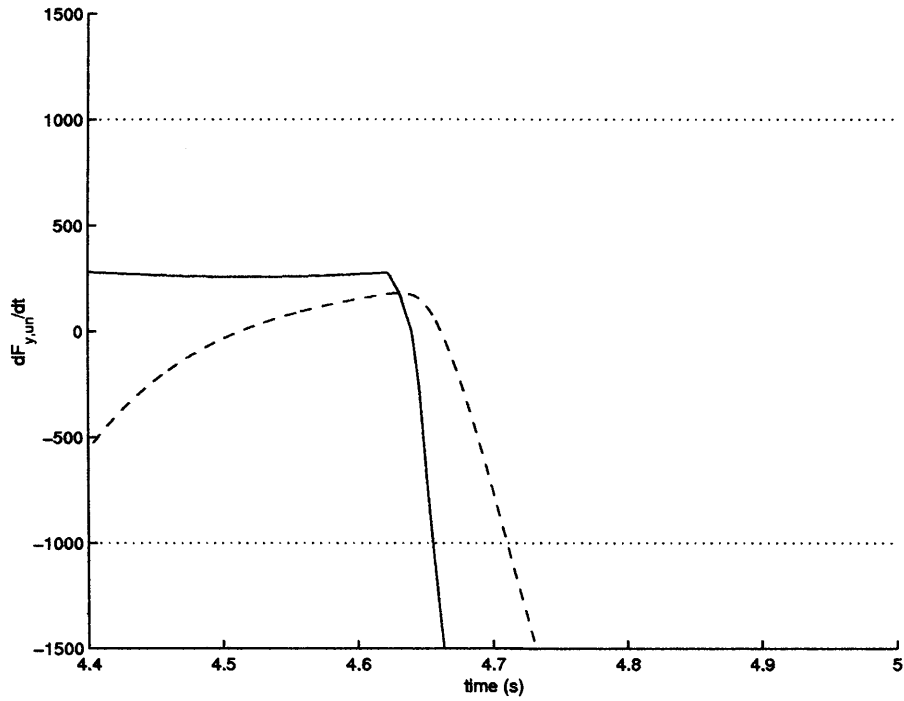


Figure 7.31: Prediction: Further Oversteer Manoeuvre - Region 2

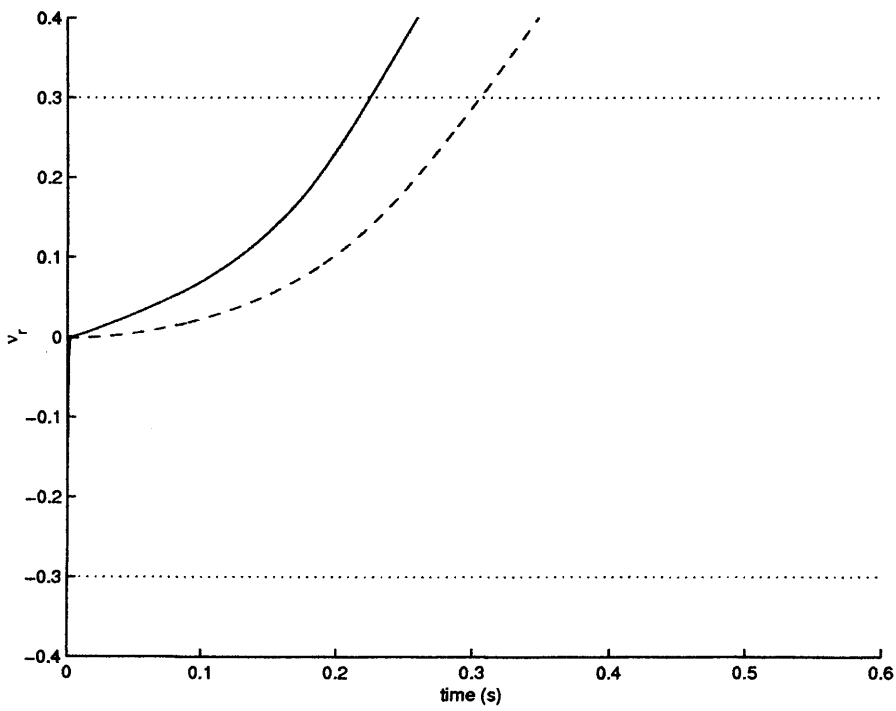
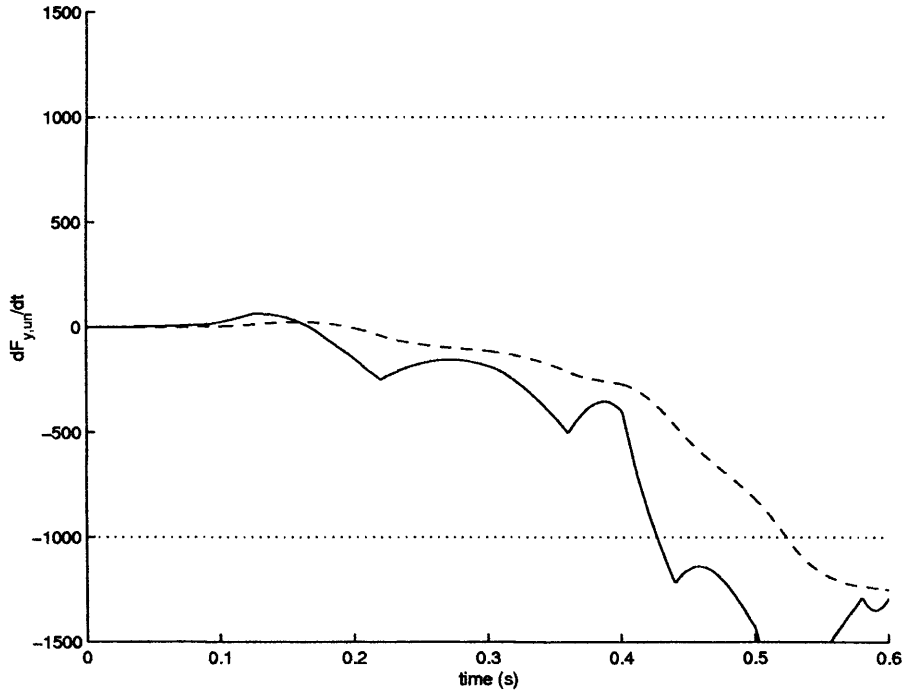


Figure 7.32: Prediction: Split- μ Braking Manoeuvre

Scenario	1 st Reading			2 nd Reading			$\Delta t(s)$
	$t_1(s)$	\dot{F}_y	ν_r	$t_2(s)$	\dot{F}_y	ν_r	
Understeer	1.65	-	0	1.85	-	-	0.20
Steady-State Oversteer	3.34	-	0	3.47	-	+	0.13
Further Oversteer 1	3.80	+	0	N/A	/	/	N/A
Further Oversteer 2	4.71	-	0	4.91	-	+	0.20
Split- μ Braking	0.30	0	+	0.52	-	+	0.22

Table 7.1: Manoeuvre Prediction Readings

Scenario	$\Delta t(s)$	$\Delta t_f(s)$	Total (s)
Understeer	0.20	0.06	0.26
Steady-State Oversteer	0.13	0.09	0.22
Further Oversteer 2	0.20	0.05	0.25
Split- μ Braking	0.22	0.08	0.30

Table 7.2: Prediction Readings continued

thresholds which were crossed had the same sign - and communicate this information to the appropriate controller.

The \dot{F}_y signal is first to cross its threshold for each of the oversteer manoeuvres (Figures 7.29-7.31), which again tells the predictor algorithm that either severe under- or oversteer is likely. In each case the $\bar{\nu}_r$ signal then crosses its threshold, and in each case the two thresholds crossed have opposite signs, which implies an impending severe oversteer manoeuvre.

The final case, the split- μ braking manoeuvre, stands out from those studied as it is the only manoeuvre in which the ν_r signal then crosses its threshold first, followed by the \dot{F}_y signal. Like the oversteer manoeuvres, the thresholds crossed by the two signals in the split- μ case have opposite signs.

7.8 Conclusions

Using Sliding Mode Observer concepts from Chapter 4, an entirely novel vehicle scenario detection and prediction scheme has been presented. The scenario prediction is based upon reconstructing certain signals which would be unexpected in a vehicle behaving in a linear or nearly-linear fashion, and identifying distinctive signatures in these signals in the very early stages of the build-up to a severe vehicle scenario in several manoeuvres.

The method utilizes an algorithm which not only allows the scheme to detect a severe manoeuvre which is taking place, but also to predict likely severe manoeuvres before they become dangerous. Appropriate thresholds have been chosen such that the scheme ignores signal variations of lesser magnitudes which may arise in the course of normal driving. The method was designed to allow for possible output measurement noise.

The new approach to dangerous vehicle scenarios is new, and is simpler than current methods, but identifies potential scenarios extremely early.

The scheme uses a novel sliding mode estimator scheme, specifically designed for the application. The scheme has the flexibility to be retro-fitted to systems already using existing controllers, and could be used as part of a supervisory scheme, optimally engaging other systems.

In the final chapter the work will be summarized. Specific, as well as overarching, conclusions will be drawn. The merit of the work will be discussed, emphasizing once more the particular contributions of the thesis. Also, various aspects of possible and potentially valuable future work will be proposed.

Chapter 8

Conclusions and Future Work

8.1 Summary

In this thesis, a range of work has been presented applying sliding mode ideas to automotive vehicle dynamics applications. In Chapters 5-7, a nonlinear vehicle model, described in Chapter 3, was used in simulation to test the various schemes designed. This nonlinear vehicle model was developed specifically for this work, building upon other models in the literature. The rigid body aspects of the vehicle dynamics of the model was chosen after [40, 78], whilst the tyre forces were developed with reference to [26, 52, 122]. The Anti-lock Braking System, used in the braking manoeuvres, was designed to mimic the control action of an ABS unit, rather than reproduce its actual behaviour.

Chapters 5-7 described the development of schemes using sliding mode ideas for particular vehicle dynamics applications: in Chapter 5, an observer-based sliding mode controller for a harsh split- μ braking manoeuvre; in Chapter 6, a compensator-based sliding mode controller for the same application; and in Chapter 7 a sliding mode scheme designed to predict potentially dangerous vehicle scenarios.

The contributions of this thesis will now be summarized, and possible areas of further work will be suggested.

8.2 Contributions

8.2.1 Observer-based Control Scheme

In Chapter 5, an observer-based sliding mode controller was proposed for stability augmentation control in a vehicle experiencing a harsh split- μ braking manoeuvre. Although the split- μ braking manoeuvre has been addressed in the literature, the methods and approach used in this thesis are novel. The control scheme presented assumes just two measured outputs, the yaw rate and the vehicle lateral deviation, and succeeds in maintaining the driver's desired straight trajectory using only a front road-wheel steering input, despite the disturbance generated by the harsh manoeuvre. In practice, the steering input produced by the control scheme could be realized using either an additional torque to the steering column, provided by an exclusively steer-by-wire system. It is important that, in application, the driver feels no consequence of the control action lest he/she 'fight' the control. In maintaining the driver's intended trajectory, the control scheme could prevent the vehicle veering off the road, or developing excessive yaw rates and yaw angles. The control scheme has been shown to react swiftly, where a driver may react too slowly or even incorrectly, possibly exacerbating the situation. This control scheme has achieved high performance without the need for, or additional expense of, active four-wheel steering.

The control scheme presented requires a minimum of measured signals, using an observer to estimate the remaining states (yaw angle, and a non-physical state formed by an average of yaw rate and vehicle lateral velocity) and avoiding the need for full state feedback. The scheme is designed to be used with emerging vehicle vision systems developed separately for lane detection and path following applications, and has been shown by simulation to perform extremely well under harsh conditions. The controller developed benefits from sliding mode robustness properties, and the validity of the design has been further strengthened by its demonstration, in simulation, to be robust to large parameter variations. Specifically, the control scheme has been shown to cope extremely well in the presence of large changes in tyre stiffness values, which may arise due to circumstances such as incorrect inflation pressures, or fitting incorrect tyres.

8.2.2 Compensator-based Control Scheme

In Chapter 6, the use of a novel compensator-based sliding mode controller, having no observer interpretation, was considered, with only the two measured output signals (yaw rate, and vehicle lateral deviation) available to the controller, again without the requirement of full state feedback. In addition, the controller was produced using a new design methodology, where the four elements of Equation (6.34) are chosen to design a compensator $K(s)$. A compensator-based controller was designed for the split- μ braking manoeuvre, as in Chapter 5, and tested by simulation using the same nonlinear model and robustness tests. Whilst the control scheme did not perform as well as the observer-based controller presented in Chapter 5, particularly in robustness testing and in terms of maintaining closed-loop damping, it has the advantage of being less computationally intensive which can be practically and financially important for implementation.

8.2.3 Vehicle Scenario Prediction Scheme

In Chapter 7, an entirely novel prediction scheme was presented. The potentially dangerous vehicle scenarios which the scheme addresses arise when a vehicle leaves its normal linear or near-linear behaviour, and enters an extremely nonlinear operating region. The severe manoeuvres which have been dealt with in this thesis - understeer, oversteer and harsh split- μ braking - can all cause drivers extreme problems, and, once entered, may lead to collisions. The ability to predict severe vehicle scenarios before they build up, may allow appropriate control action to be selected and applied to prevent any danger arising.

The scheme proposed in this thesis has taken an entirely novel approach to predicting potentially dangerous vehicle scenarios, by describing and identifying distinctive signatures in certain vehicle signals - related to the vehicle lateral force and vehicle yaw moment - which arise unexpectedly in the very early stages of a potentially severe vehicle scenario. By detecting patterns signifying the vehicle scenarios, this approach is simpler than current technologies, whilst identifying potential scenarios extremely early. The novel sliding mode estimator described was designed specifically for this application. The detection scheme benefits from having the flexibility to be retro-fitted to systems with existing controllers and could be used

as part of a supervisory scheme, optimally engaging existing control systems.

8.3 Further Work

The results obtained by the research presented in this thesis open up a number of avenues for possible future work to confirm, extend and build upon that which has already been achieved. Some possible directions of study are proposed here.

8.3.1 Modelling Improvements

In order to make the test simulations more thorough, the nonlinear model could be extended to include greater degrees of freedom. Extensions could include, for example, a vertical component of velocity, roll or pitch rates. Such extra vehicle modelling could give a greater insight into the behaviour of the vehicle, and provide a more stringent test for the schemes developed. A key modelling improvement could be made by including the effects of lateral load transfer, particularly to the results presented in Chapter 7 in which the transient response may have an affect. In Chapter 7, as the prediction occurs quickly, the results would only be significantly affected by 'near instantaneous' load transfer, caused directly by the lateral tyre force development. Whereas, Chapters 5 and 6 might also be affected by suspension induced lateral load transfer.

Also, whilst the current model of the ABS appears to mimic actual ABS operation fairly well, an aspect of real ABS systems which is not seen in the simulation is the cyclic nature of its output. This occurs in the real system as the ABS is continually re-estimating wheel-slip, based on discrete time signals from the wheel velocity sensors. In this respect, the ABS model produces signals which appear a little too smooth and 'clean' to be completely realistic. One way of addressing this could be to discretize the wheel-slip signal from the tyre model before it enters the ABS block. Another reason for the the smoothness of the ABS operation is related to the evenness of the road surface in testing. Currently, the tyre/road friction coefficient, (μ), is either 0.8 or 0.2. On a real road - and even on a test track where the surface may be tiled - the surface would not be so uniform, there would be some variation about the average value.

In order to account for this, a short term plan could include structuring the friction coefficient relative to longitudinal displacement. This should add further realism to the controller testing, and specifically, to the ABS.

8.3.2 Controller Design Issues

From the current results, particularly those presented in Chapter 5, it can be seen that there is little room for improvement in the actual performance. However, other robust controller design approaches, could also be considered.

In the split- μ braking manoeuvre, at the point the vehicle enters the inhomogeneous road surface, the road-wheel steering angle is effectively ramped up by the controller, until it reaches an appropriate angle. In vehicle testing, an experienced driver, accustomed to the situation, will immediately turn the hand-wheel to the appropriate angle, by a learnt reflex, and produce the same effect. In the simulations, the controller, is not prescient of the final road-wheel angle required, so does not ramp smoothly, and overshoots. The addition of a ramped (driver) steer angle could, therefore, be investigated, reproducing the learnt behaviour of the experienced driver. Alternatively, further complexity could be added through the use of some other driver model developed specifically to complement the vehicle model, possibly based on examples from the literature, such as [76].

In the controller designs presented in Chapters 5 and 6, the controllers were designed about a linear model at a fixed operating speed. If the vehicle deviates significantly from these initial conditions, the linear model ceases to be valid. It is self-evident that, in a split- μ braking manoeuvre, the forward speed of the vehicle (monotonically) decreases. Whilst there are no signs from the simulations that this variation causes the controllers any serious problems, for formal analysis the closed-loop system relies on the robustness of the sliding mode controller. With such parameter variations it may be worth investigating the possible value of using a controller design which is dependent on speed, such as LPV approaches.

8.3.3 Scenario Prediction Issues

The area for future work which stands out most keenly for the scenario prediction scheme is to test the system using real vehicle data taken from the test track. This would test the suitability of the thresholds chosen for the algorithm described in Section 7.6, and ensure that the prediction scheme identified the early signs of potentially dangerous scenarios without ‘crying wolf’ during more routine driving manoeuvres. As the scenario prediction can be carried out offline, this scheme would be the simplest, in comparison with the two control schemes, to be tested by implementation on a test vehicle.

Appendix A

Glossary

Ackermann steering angle	The angle whose tangent is the wheelbase divided by the radius of turn.
Bode plot	The logarithm of the magnitude of the transfer function is plotted versus the logarithm of ω , the frequency. The phase, ϕ , of the transfer function is separately plotted versus the logarithm of the frequency.
Braking force	The negative longitudinal force resulting from braking torque application.
Braking force coefficient	The ratio of the braking force to the vertical load.
Braking torque	The negative wheel torque.
Closed-loop feedback control system	A system that uses a measurement of the output and compares it with the desired output.
Compensation	The alteration or adjustment of a control system in order to provide a suitable performance.
Compensator	An additional component or circuit that is inserted into the system to equalize or compensate for the performance deficiency.

Control system	An interconnection of components forming a system configuration that will provide a desired response.
Controllability	A system is said to be completely controllable if, given any initial condition $x(t_0)$, there exists an input function on the finite interval $[t_0, t_1]$ such that $x(t_1) = 0$.
Cornering Stiffness	The negative of the rate of change of lateral force with respect to change in slip angle, usually evaluated at at zero-slip angle.
Damped oscillation	An oscillation in which the amplitude decreases with time.
Disturbance signal	An unwanted input signal that affects the system's output signal.
Driving force	The longitudinal force resulting from driving torque application.
Driving torque	The positive wheel torque.
Error signal	The difference between the desired output and the actual output.
Feedback signal	A measure of the output of the system used as a feedback to the control system.
Free-rolling tyre	A loaded rolling tyre without application of a driving or braking torque.
Hand-wheel steering angle	The angular position of the driver's steering wheel.
Heading angle	The angle between the trace of the vehicle-fixed x -axis and the earth-fixed X -axis.
Lateral force coefficient	The ratio of the lateral force to the vertical load.
Mathematical model	Description of the behaviour of a system using mathematics.
Minimum phase	All the zeroes of a transfer function lie in the left-hand side of the s -plane.
Multivariable control system	A system with more than one input variable and more than one output variable.
Neutral steer line	The set of points in the x - z plane at which external lateral forces applied to the vehicle produce no steady-state yaw rate.

Normal force	The component of the tyre force in the vertical z -direction.
Observability	A linear system is said to be completely observable if the output function $y(t)$ over some interval $[t_0, t_1]$ uniquely determines the initial condition $x(t_0)$.
Open-loop control system	A system that utilizes a device to control a process without using feedback.
Overshoot	The amount the system output response proceeds beyond the desired response.
Plant	The system under control.
Pitch rate	The angular velocity about the y -axis.
Road-wheel steering angle	The angle between the longitudinal axis of the vehicle and the line of intersection of the wheel plane and the road surface.
Robust control	A system that exhibits the desired performance in the presence of significant plant uncertainty.
Roll rate	The angular velocity about the x -axis.
Sideslip angle	The angle between the trace of the vehicle-fixed x -axis and the vehicle velocity vector on the earth-fixed X - Y plane.
Stability	A performance measure of a system. A system is stable if all the poles of the transfer function have negative real parts.
Stable system	A dynamic system with a bounded system response to a bounded input.
State of a system	A set of numbers such that the knowledge of these numbers and the input function will, with the equations describing the dynamics, provide the future state of the system.
State-feedback	When the control signal for the process is a direct function of all the state variables.

Steady-state	The state when periodic (or constant) vehicle responses to periodic (or constant) control and/or disturbances do not change over an arbitrarily long time.
State variables	The set of variables that describe the system.
Static margin	The horizontal distance from the centre of gravity to the neutral steer line divided by the wheelbase. It is positive if the centre of gravity is forward of the neutral steer line.
Steady-state error	The error when the time period is large and the transient response has decayed, leaving a continuous response.
System	An interconnection of element and devices for a desired purpose.
Time-varying system	A system for which one or more parameters may vary with time.
Transient-state	The state when the motion responses, the external forces relative to the vehicle, or the control positions are changing with time.
Tyre contact patch	The area of the tyre in contact with the road surface.
Tyre stiffness	The rate of change of longitudinal force with respect to change in wheel slip, usually evaluated at zero wheel slip.
Trackwidth	The lateral distance between the centres of tyre contact of a pair of wheels.
Tyre forces	The external forces acting on the tyre by the road.
Vehicle lateral acceleration	The component of the vehicle acceleration in the y -direction.
Vehicle lateral force	The sum of the component of the tyre forces acting in the positive direction of the vehicle lateral axis.
Vehicle lateral velocity	The component of the vehicle velocity in the direction of the positive y -direction.

Vehicle longitudinal acceleration	The component of the vehicle acceleration in the x -direction.
Vehicle longitudinal force	The sum of the component of the tyre forces acting in the positive direction of the vehicle longitudinal axis.
Vehicle longitudinal velocity	The component of the vehicle velocity in the direction of the positive x -direction.
Vehicle velocity	The vector expressing the velocity of the centre of gravity of the vehicle relative to the earth-fixed co-ordinate system (X, Y, Z) .
Vertical load	The negative of the normal force.
Wheel heading	The angle between the wheel-plane and the vehicle longitudinal axis.
Wheel slip	The ratio of the wheel slip velocity to the angular velocity of the free-rolling tyre.
Wheel slip velocity	The difference between the wheel angular velocity of the driven or braked wheel and the angular velocity of the free-rolling wheel.
Wheel slip-angle (α)	The angle between the longitudinal axis of the wheel position and the direction of travel of the centre of tyre contact.
Wheelbase	The longitudinal distance between the front and rear axles.
Yaw angle	The angle between the vehicle-fixed x -axis and the earth-fixed X -axis.
Yaw moment	The component of the moment vector tending to rotate the vehicle about the z -axis.
Yaw rate	The angular velocity about the z -axis.

Appendix B

Notation

B.1 Table of Constants

a_0	Nominal front axle distance from the centre of gravity	0.913	m
b_0	Nominal rear axle distance from the centre of gravity	1.730	m
C_{xf}	Front longitudinal tyre stiffness	56635	Nm
C_{xr}	Rear longitudinal tyre stiffness	40000	Nm
$C_{\alpha,f}$	Front lateral tyre stiffness	41825	$Nrad^{-1}$
$C_{\alpha,r}$	Rear lateral tyre stiffness	29540	$Nrad^{-1}$
g	Acceleration due to gravity	9.81	ms^{-2}
$I_{yaw,0}$	Nominal yaw moment of inertia	2550	$kg\ m^2$
M_v	Nominal vehicle mass	1673	kg
x_b	Vehicle boot distance from front axle	2.96	m
x_{fp}	Front passengers distance from front axle	1.24	m
x_{rp}	Rear passengers distance from front axle	1.96	m

B.2 Table of Coefficients

- a Front axle distance from the centre of gravity
- b Rear axle distance from the centre of gravity

C_x	Longitudinal tyre stiffness
C_α	Lateral tyre stiffness
$C_{\alpha f}$	Front lateral cornering stiffness for bicycle model = $2C_{\alpha, f}$
$C_{\alpha r}$	Rear lateral cornering stiffness for bicycle model = $2C_{\alpha, r}$
F_{ni}	Normal force on i^{th} wheel
F_x	Vehicle longitudinal force
F_y	Vehicle lateral force
F_{yf}	Front axle lateral force
F_{yr}	Rear axle lateral force
F_{wxi}	Longitudinal friction force on i^{th} wheel
F_{wyi}	Lateral friction force on i^{th} wheel
I_w	Wheel spin moment of inertia
I_z	Yaw moment of inertia
L_{t1}	Front track width
L_{t2}	Rear track width
M_b	Mass in vehicle boot
M_{fp}	Mass of front passengers
M_{rp}	Mass of rear passengers
m_v	Total vehicle mass
M_z	Yaw Moment
r_b	Vehicle boot radial distance from centre of gravity
r_{fp}	Front passengers radial distance from centre of gravity
r_{rp}	Rear passengers radial distance from centre of gravity
R_t	Wheel radius
T_{bi}	Braking Torque on i^{th} wheel
β	Sideslip angle
μ	Friction force coefficient at road/tyre interface

References

- [1] *Vehicle Dynamics Terminology, SAE J670e*. Society of Automotive Engineers. Warrendale, PA, July, 1976.
- [2] M. Abe. Vehicle dynamics and control for improving handling and active safety: from four-wheel steering to direct yaw moment control. In *Proceedings of the Institute of Mechanical Engineers*, volume 213, pages 87–101, 1999.
- [3] J. Ackermann. Robust decoupling, ideal steering dynamics and yaw stabilization of 4WS cars. *Automatica*, 30:1761–1768, 1994.
- [4] J. Ackermann. Yaw rate and lateral acceleration feedback for four-wheel steering. In *Proceedings of the International Symposium on Advanced Vehicle Control, Tsubuka, Japan*, 1994.
- [5] J. Ackermann. Safer car driving by robust steering control. In *Proceedings of the UKACC International Conference on Control*, page 733, 1996.
- [6] J. Ackermann. Active steering for better safety, handling and comfort. In *AVCS, Amiens, France*, pages 1–9, 1998.
- [7] J. Ackermann and T. Bunte. Yaw disturbance attenuation by robust decoupling of car steering. *Control Engineering Practice*, 5:1131–1136, 1997.
- [8] J. Ackermann and W. Seinel. Robust control for automatic steering. In *Proceedings of the American Control Conference, Green Valley, AZ, USA*, pages 795–800, 1990.
- [9] A. Alleyne. Improved vehicle performance using combined suspension and braking forces. *Vehicle System Dynamics*, 27:235–265, 1997.

- [10] R. Aufrère, R. Chapuis, and F. Chausse. A fast and robust vision based road following algorithm. In *Proceedings of the IEEE Intelligent Vehicles Symposium, Dearborn, MI, USA*, pages 192–197, 2000.
- [11] L. Austin and D. Morrey. Recent advances in antilock braking systems and traction control systems. In *Proceedings of the IMechE*, volume 214, pages 625–629, 2000.
- [12] S.K. Bag, S.K. Spurgeon, and C. Edwards. Output feedback sliding mode design for linear uncertain systems. *Proceedings of IEE, Part D*, 144:209–216, 1997.
- [13] E. Bakker, H.B. Pacejka, and L. Lidner. A new tire model with an application in vehicle dynamics studies. *Society of Automotive Engineers*, 890087:101–113, 1989.
- [14] H. Bauer. *Automotive Handbook, 4th Edition*. Robert Bosch GmgH, Stuttgart (Translation editor in chief: Peter Girling) Distributed by SAE Society of Automotive Engineers, PA, USA, 1996.
- [15] H. Bauer. *ESP Electronic Stability Program*. Robert Bosch GmgH, Stuttgart, 1999.
- [16] J.E. Bernard, L. Segel, and R.E. Wild. Tire shear force generation during combined steering and braking maneuvers. *Society of Automotive Engineers Transactions*, 770852, 1977.
- [17] M. Bertozzi and A. Broggi. GOLD: A parallel real-time stereo vision system for generic obstacle and lane detection. *IEEE Transactions on Image Processing*, 7(1):62–80, 1998.
- [18] M. Bishop. Highways agency information line. Private correspondence. 5th September, 2003.
- [19] V. Boutylin, J. Lepeshko, and V. Ivanov. About interrelation between the tire grip properties and the wheel sliding. *Society of Automotive Engineers*, 013338:81–87, 2001.
- [20] S.P. Boyd, L. El Ghaoui, E. Feron, and V. Balakrishnan. *Linear Matrix Inequalities in Systems and Control Theory*. SIAM: Philadelphia, 1994.
- [21] S.H. Choi and D.W. Cho. Control of wheel slip ratio using sliding mode controller with pulse width modulation. *Vehicle System Dynamics*, 32:267–284, 1999.

- [22] D.A. Crolla. Introduction to Vehicle Dynamics - course notes. School of Mechanical Engineering, University of Leeds. 2001.
- [23] C. Ünsal and P. Kachroo. Sliding mode measurement feedback control for antilock braking systems. *IEEE Transactions on Control Systems Technology*, 7(2):271–81, 1999.
- [24] J.C. Dixon. *Tires, Suspension, and Handling. 2nd Edition*. Society of Automotive Engineers, 1996.
- [25] A. Dreyer and H.-D. Heitzer. Control strategies for active chassis systems with respect to road friction. *Society of Automotive Engineers*, 910660:872–883, 1991.
- [26] H. Dugoff, P.S. Fancher, and L. Segel. An analysis of tire traction properties and their influence on vehicle dynamic performance. *Journal of the Society of Automotive Engineers*, 70377:341–366, 1970.
- [27] C. Edwards and S.K. Spurgeon. On the development of discontinuous observers. *International Journal of Control*, 59:1211–1229, 1994.
- [28] C. Edwards and S.K. Spurgeon. Sliding mode stabilisation of uncertain systems using only output information. *International Journal of Control*, 62:1129–1144, 1995.
- [29] C. Edwards and S.K. Spurgeon. Robust output tracking using a sliding mode controller/observer scheme. *International Journal of Control*, 64:967–983, 1996.
- [30] C. Edwards and S.K. Spurgeon. Sliding mode output tracking with application to a multivariable high temperature furnace problem. *International Journal of Robust and Nonlinear Control*, 7:337–351, 1997.
- [31] C. Edwards and S.K. Spurgeon. *Sliding Mode Control: Theory and Applications*. Taylor & Francis, 1998.
- [32] C. Edwards and S.K. Spurgeon. On the limitations of some variable structure output feedback controller designs. *Automatica*, 36:743–748, 2000.

- [33] C. Edwards, S.K. Spurgeon, and A. Akoachere. Sliding mode output feedback controller design using Linear Matrix Inequalities. *IEEE Transactions on Automatic Control*, AC-46:115–119, 2001.
- [34] C. Edwards, S.K. Spurgeon, and R.G. Hebden. On the design of sliding mode output feedback controllers. *International Journal of Control*, 76(9/10):893–905, 2003.
- [35] C. Edwards, S.K. Spurgeon, and R.J. Patton. Sliding mode observers for fault detection and isolation. *Automatica*, 36:541–553, 2000.
- [36] O.M.E. El-Ghezawi, S.A. Billings, and A.S.I. Zinober. Variable-structure systems and system zeros. *Proceedings of the IEE, Part D*, 130:1–5, 1983.
- [37] R. El-Khazali and R.A. DeCarlo. Variable structure output feedback control: switching surface design. In *Proceedings of the 29th Allerton Conference on Communications, Control and Computing*, pages 430–439, 1991.
- [38] R. El-Khazali and R.A. DeCarlo. Variable structure output feedback control. In *Proceedings of the American Control Conference*, pages 871–875, 1992.
- [39] R. El-Khazali and R.A. DeCarlo. Output feedback variable structure control design using dynamic compensation for linear systems. In *Proceedings of the American Control Conference*, pages 954–958, 1993.
- [40] J.R. Ellis. *Vehicle Handling Dynamics*. Mechanical Engineering Publications Ltd, London, 1994.
- [41] J. Farrelly. Private correspondence. 21st June, 2001.
- [42] B. Fernandez and J.K. Hedrick. Control of multivariable non-linear systems by the sliding mode method. *International Journal of Control*, 46(3):1019–1040, 1987.
- [43] E. Fiala. Seitenkräfte am rollenden luftreifen. *Z. VDI*, 96(29), 1954.
- [44] T. Fujioka and K. Suzuki. Lateral autonomous driving by sliding control. In *Proceedings of the International Symposium on Advanced Vehicle Control, Tsubuka, Japan*, pages 432–437, 1994.

- [45] J.C. Gerdes and J.K. Hedrick. Brake system modelling for simulation and control. *IEEE Transactions of the ASME*, 121:496–503, 1999.
- [46] T.D. Gillespie. *Fundamentals of Vehicle Dynamics*. Society of Automotive Engineers, 1992.
- [47] G. Gim. An analytical model of pneumatic tyres for vehicle dynamic simulations. *International Journal of Vehicle Design*, 1(1), 1990.
- [48] D.N. Godbole and J. Lygeros. Longitudinal control of the lead car of a platoon. *IEEE Transactions on Vehicular Technology*, 43(4):1125–1135, 1994.
- [49] K.B. Goh, S.K. Spurgeon, and N.B. Jones. Fault diagnostics using sliding mode techniques. *Control Engineering Practice*, 10:207–217, 2002.
- [50] R. Gregor, M. Lützel, M. Pellkofer, K.H. Siedersberger, and E.D. Dickmanns. Ems-vision: A perceptual system for autonomous vehicles. In *Proceedings of the IEEE Intelligent Vehicles Symposium, Dearborn, MI, USA*, pages 52–57, 2000.
- [51] J. Guldner, V.I. Utkin, and J. Ackermann. A sliding mode control approach to automatic car steering. In *Proceedings of the American Control Conference, Baltimore, MA*, pages 1969–1973, 1994.
- [52] R. Guntur and S. Sankar. A friction circle concept for Dugoff’s tyre friction model. *International Journal of Vehicle Design*, 1:373–377, 1980.
- [53] J.-O. Hahn, R. Rajamani, and L. Alexander. GPS-based real-time identification of tire-road friction coefficient. *IEEE Transactions on Control Systems Technology*, 10(3):331–343, 2002.
- [54] D. Han, J. Sohn, K. Kim, J. Lee, W. Yoo, B. Lee, and J. Choi. Development and comparative study on tire models in the autodyn7 program. *KSME International Journal*, 14(7):730–736, 2000.

- [55] R.G. Hebden, C. Edwards, and S.K. Spurgeon. An application of sliding mode control to automotive stability on a split- μ manoeuvre. In *Proceedings of the American Control Conference (ACC), Denver, CO, USA*, pages 4359–4364, 2003.
- [56] R.G. Hebden, C. Edwards, and S.K. Spurgeon. Automotive steering control in a split- μ manoeuvre using an observer-based sliding mode controller. *Vehicle System Dynamics*, 41:181–202, 2004.
- [57] R.G. Hebden, C. Edwards, and S.K. Spurgeon. Sliding mode observers for vehicle mode detection. In *Proceedings of the 8th International Workshop on Variable Structure Systems (VSS 04), Spain*, 2004.
- [58] B.S. Heck and A.A. Ferri. Application of output feedback to variable structure systems. *Journal of Guidance Control and Dynamics*, 12:932–935, 1989.
- [59] B.S. Heck, S.V. Yallapragada, and M.K.H. Fan. Numerical methods to design the reaching phase of output feedback variable structure control. *Automatica*, 31:275–279, 1995.
- [60] H. Heisler. *Advanced Vehicle Technology*. Edward Arnold, London, 1989.
- [61] J.-C. Hsu, R.-H. Lin, and E.C. Yeh. Vision-based motion measurement by directly extracting image features for vehicular steering control. In *Proceedings of the Institute of Mechanical Engineers*, volume 211, pages 277–289, 1997.
- [62] J. Huang, G. Lu, and M. Tomizuka. Vehicle lateral control under fault in front and/or rear sensors. California PATH program UCB-ITS-PRR-2000-25, Institute of Transportation Studies, University of California, Berkeley, 2000.
- [63] K. Huh, K. Yi, J. Kim, and D.-I.D. Cho. Monitoring system design for estimating the lateral tire force. In *Proceedings of the American Control Conference (ACC), Anchorage, AK, USA*, pages 875–880, 2002.
- [64] S. Hui and S.H. Žak. Robust output feedback stabilisation of uncertain dynamic systems with bounded controllers. *International Journal of Robust and Nonlinear Control*, 3:115–132, 1993.

- [65] J.Y. Hung, W. Gao, and J.C. Hung. Variable structure control: A survey. *IEEE Transactions on Industrial Electronics*, 40(1):2–21, 1993.
- [66] U. Itkis. *Control Systems of Variable Structure*. Wiley, New York, 1976.
- [67] K. Ito, T. Fujishiro, K. Kanai, and Y. Ochi, 1990.
- [68] C. Kreucher and S Lakshmanan. LANA: A lane extraction algorithm that uses frequency domain features. *IEEE Transactions on Robotics and Automation*, 15(2):343–350, 1999.
- [69] B.H. Kwak and Y.J. Park. Robust vehicle stability controller by multiple sliding mode control. In *Proceedings of 5th International Symposium on Advanced Vehicle Control (AVEC), Ann Arbor, 2000*.
- [70] C.M. Kwan. On variable structure output feedback controllers. *IEEE Transactions on Automatic Control*, 41:1691–1693, 1996.
- [71] C.M. Kwan. Further results on variable output feedback controllers. *IEEE Transactions on Automatic Control*, 46:1505–1508, 2001.
- [72] A.Y. Lee. Design of stability augmentation systems for automotive vehicles. *Journal of Dynamic Systems, Measurement, and Control*, 112:489–495, 1990.
- [73] D.G. Luenberger. An introduction to observers. *IEEE Transactions on Automatic Control*, 16:596–602, 1971.
- [74] P. Lugner. The influence of the structure of automobile models and tyre characteristics on the theoretical results of steady-state and transient vehicle performance. In *Proceedings of the 5th VSD-WND IUAM Symposium, Vienna, Austria*, pages 21–39, 1997.
- [75] C. MacAdam. An optimal preview control for linear systems. *Transactions of the ASME*, 102:188–190, 1980.
- [76] C. MacAdam. Application of an optimal preview control for simulation of closed-loop automobile driving. *IEEE Transactions on Systems, Manufacturing and Cybernetics*, SMC-11(6):393–399, 1981.

- [77] M. Magomedov, V. Alexandrov, and K. Pupkov. Robust adaptive stabilization of moving a car under braking with ABS in control circuit. *Society of Automotive Engineers*, 013187:7–13, 2001.
- [78] W. Manning, D. Crolla, M. Brown, and M. Selby. Coordination of chassis control systems for vehicle motion control. In *Proceedings of 5th International Symposium on Advanced Vehicle Control (AVEC)*, Ann Arbor, 2000.
- [79] W.F. Milliken and D.L. Milliken. *Race Car Vehicle Dynamics*. Society of Automotive Engineers, 1995.
- [80] B.C. Moore. On the flexibility offered by state-feedback in multivariable systems beyond closed-loop eigenvalue assignment. *IEEE Transactions on Automatic Control*, AC-21:689–692, 1976.
- [81] C. Nouillant, X. Moreau, and A. Oustaloup. Hybrid control of a semi-active suspension system. In *Proceedings of the Automotive and Transportation Technology, Congress & Exhibition 1-4, Barcelona, SPAIN*, October 2001.
- [82] K. Ogata. *Modern Control Engineering*. Prentis-Hall International, Englewood Cliffs, New Jersey, USA, 1990.
- [83] H.B. Pacejka. Tyre factors and vehicle handling. *International Journal of Vehicle Design*, 1(1):1–23, 1979.
- [84] H.B. Pacejka and E. Bakker. The magic formula tyre model. *Vehicle System Dynamics*, 21(suppl.):1–18, 1993.
- [85] H.B. Pacejka and I.J.M. Besselink. Magic formula tyre model with transient properties. *Vehicle System Dynamics*, 27(suppl.):234–249, 1997.
- [86] F. Paetzold, U. Franke, and W. v.Seelen. Lane recognition in urban environment using optimal control theory. In *Proceedings of the IEEE Intelligent Vehicles Symposium, Dearborn (MI), USA*, pages 221–226, 2000.

- [87] D.-Y. Park, D.-H. Hwang, K.-C. Lee, J.-W. Jeon, Y.-J. Kim, J.-M. Cho, and J.-S. Joh. Development of HILS system for ABS ECU of commercial vehicles. *Society of Automotive Engineers*, 013186:1–6, 2001.
- [88] Y. Park and I. Jung. Semi-active steering wheel for steer-by-wire system. *Society of Automotive Engineers*, 013306:55–62, 2001.
- [89] H. Pham, J.K. Hedrick, and M. Tomizuka. Autonomous steering and cruise control of automobiles via sliding mode control. In *Proceedings of the International Symposium on Advanced Vehicle Control, Tsubuka, Japan, 1994*.
- [90] A. Piazzzi, C.G. Lo Bianco, M. Bertozzi, A. Fascioli, and A. Broggi. Quintic G^2 -splines for the iterative steering of vision-based autonomous vehicles. *IEEE Transactions on Intelligent Transportation Systems*, 3(2):27–36, 2002.
- [91] M. Plochl and P. Lugner. Braking behaviour of a 4-wheel-steered automobile with an antilock braking system. *Vehicle System Dynamics*, 25:547–558, 1996.
- [92] R. Risack, N. Möhler, and W. Enkelmann. A video-based lane keeping assistant. In *Proceedings of the Intelligent Vehicles Symposium, 2000*.
- [93] P.I. Ro and H. Kim. Four wheel steering system for vehicle handling improvement: a robust model reference control using the sliding mode. In *Proceedings of the Institute of Mechanical Engineers*, volume 210, 1996.
- [94] G. Roppenecker and H. Wallentowitz. Integration of chassis and traction control systems. what is possible - what makes sense - what is under development. *Vehicle System Dynamics*, 22:283–298, 1993.
- [95] E.P. Ryan and M. Corless. Ultimate boundedness and asymptotic stability of a class of uncertain dynamical systems via continuous and discontinuous control. *IMA Journal of Mathematical Control and Information*, 1:223–242, 1984.
- [96] H. Sakai. Theoretical and experimental studies on the dynamic properties of tyres. Part 1: Review of theories of rubber friction. *International Journal of Vehicle Design*, 2(1):78–110, 1981.

- [97] H. Sakai. Theoretical and experimental studies on the dynamic properties of tyres. Part 2: Experimental investigations of rubber friction and deformation of a tyre. *International Journal of Vehicle Design*, 2(2):182–226, 1981.
- [98] H. Sakai. Theoretical and experimental studies on the dynamic properties of tyres. Part 3: Calculation of the six components of force and moment of a tyre. *International Journal of Vehicle Design*, 2(3):335–372, 1981.
- [99] H. Sakai. Theoretical and experimental studies on the dynamic properties of tyres. Part 4: Investigations of the influences of running conditions by calculation and experiment. *International Journal of Vehicle Design*, 3(3):333–375, 1982.
- [100] M.U. Salamci, M.K. Özgören, and S.P. Banks. Sliding mode control with optimal sliding surfaces for missile autopilot design. *Journal of Guidance, Control, and Dynamics*, 23:719–727, 2000.
- [101] M. Salman. Coordinated control of braking and steering. In *ASME Symposium on Advanced Automotive Technologies*, volume 108, pages 69–76, 1990.
- [102] L. Segel. Theoretical prediction and experimental substantiation of the response of the automobile to steering control. *Automobile division, The Institute of Mechanical Engineers*, pages 26–46, 1956.
- [103] P. Setlur, D. Dawson, J. Wagner, and Y. Fang. Nonlinear tracking controller design for steer-by-wire automotive systems. In *Proceedings of the American Control Conference (ACC), Anchorage, AK, USA*, pages 280–285, 2002.
- [104] A. Shimura and K. Yoshida. Non-linear neuro control for active steering for various road conditions. *Society of Automotive Engineers*, 013308:71–75, 2001.
- [105] J.J.E. Slotine. Sliding controller design for nonlinear systems. *International Journal of Control*, 40:421–434, 1984.
- [106] J.J.E. Slotine and W. Li. *Applied Nonlinear Control*. Prentice Hall, Englewood Cliffs NJ, 1991.

- [107] S.K. Spurgeon and R. Davies. A nonlinear control strategy for robust sliding mode performance in the presence of unmatched uncertainty. *International Journal of Control*, 57:1107–1123, 1993.
- [108] A. Steinberg and M.J. Corless. Output feedback stabilisation of uncertain dynamical systems. *IEEE Transactions on Automatic Control*, 30:1025–1027, 1985.
- [109] V.L. Syrmos, C.T. Abdallah, P. Dorato, and K. Grigoriadis. Static output feedback – a survey. *Automatica*, 33:125–137, 1997.
- [110] M. Tomizuka and J.K. Hedrick. Advanced control methods for automotive applications. *Vehicle System Dynamics*, 24:449–469, 1995.
- [111] V. Utkin, J. Guldner, and Shi J. *Sliding Mode Control in Electromechanical Systems*. Taylor & Francis, 1999.
- [112] V.I. Utkin. Variable structure systems with sliding modes. *IEEE Transactions on Automatic Control*, 22:212–222, 1977.
- [113] V.I. Utkin. Principles of identification using sliding regimes. *Soviet Physics Doklady*, 26:271–272, 1981.
- [114] V.I. Utkin. *Sliding Modes in Control Optimization*. Springer-Verlag, Berlin, 1992.
- [115] V.I. Utkin and K.-K.D. Young. Methods for constructing discontinuity planes in multidimensional variable structure systems. *Automation and Remote Control*, 39:1466–1470, 1978.
- [116] B.L. Walcott and S.H. Zak. State observation of nonlinear uncertain dynamical systems. *IEEE Transaction on Automatic Control*, 32:166–170, 1987.
- [117] D. Wang, Z. Guo, and I. Hagiwara. Polytopic dynamics and control for variable suspension system. In *Proceedings of the Automotive and Transportation Technology, Congress & Exhibition 1-4, Barcelona, SPAIN, October 2001*.
- [118] A.B. Will, S. Hui, and S.H. Zak. Sliding mode wheel slip controller for an antilock braking system. *International Journal of Vehicle Design*, 19:523–539, 1999.

- [119] W.M. Wonham. On pole-assignment in multi-input, controllable linear systems. *IEEE Transactions on Automatic Control*, AC-12:660–665, 1967.
- [120] S.-J. Xu and A. Rachid. Sliding mode controller design for linear systems with mismatched uncertainty. In *Proceedings of the 14th World Congress. International Federation of Automatic Control*, volume 8, pages 431–436, 1999.
- [121] J. Yi, L. Alvarez, and R. Horowitz. Adaptive emergency braking control with underestimation of friction coefficient. *IEEE Transactions on Control Systems Technology*, 10(3), 2002.
- [122] S.H. Yu and J.J. Moskwa. A global approach to vehicle control: Coordination of four wheel steering and wheel torques. *ASME Journal of Dynamic Systems Measurement and Control*, 116:659–667, 1994.
- [123] J.R. Zhang, A. Rachid, and S.J. Xu. Robust controller design for automatic steering of vehicles. *Society of Automotive Engineers*, 013323:125–131, 2001.
- [124] J.R. Zhang, A. Rachid, and S.J. Xu. Sliding mode path tracking control for automatic steering of vehicles. *Society of Automotive Engineers*, 013307:63–70, 2001.
- [125] J.R. Zhang, S.J. Xu, and A. Rachid. Path tracking control of vehicles based on lyapunov approach. In *Proceedings of the American Control Conference (ACC), Danvers, MA, USA*, volume 3, pages 2132–2137, 2002.
- [126] K. Zhou, J.C. Doyle, and K. Glover. *Robust and Optimal Control*. Prentice Hall, New Jersey, 1996.